Alma Mater Studiorum - Università di Bologna

DEI - Dipartimento di Ingegneria dell'Energia Elettrica e dell'Informazione

Dottorato di Ricerca in Ingegneria Elettronica, delle Telecomunicazioni e Tecnologie dell'Informazione

XXVI Ciclo

Settore Concorsuale: 09/F2 - Telecomunicazioni

Settore Scientifico Disciplinare: ING-INF/03

From Radio Channel Modeling to a System Level Perspective in Body-Centric Communications

Tesi di:

Ramona Rosini

Coordinatore:

Chiar.mo Prof. Ing. **Alessandro Vanelli-Coralli**

Relatori:

Chiar.mo Prof. Ing. **Roberto Verdone**

Dott. Ing. **Raffaele D'Errico**

Esame anno finale 2014

"A mamma e papà,
che mi hanno insegnato a stare in piedi da sola,
rialzandomi ogni volta che sono caduta."

"A tutte le "500" che ho incontarto sulla strada,
perchè non abbiamo nulla da invidiare alle "Ferrari"."

"...ma tra la partenza e il traguardo,
nel mezzo c'è tutto il resto
e tutto il resto è giorno dopo giorno
e giorno dopo giorno
è silenziosamente costruire,
e costruire è potere e sapere
rinunciare alla perfezione."

["Costruire", N.Fabi]

Table of Contents

Abstract

Body-centric communications are emerging as a new paradigm in the panorama of personal communications. Being concerned with human behaviour, they are suitable for a wide variety of applications. The advances in the miniaturization of portable devices to be placed on or around the body, foster the diffusion of these systems, where the human body is the key element defining communication characteristics.

This thesis investigates the human impact on *body-centric communications* under its distinctive aspects. First of all, the unique propagation environment defined by the body is described through a scenario-based channel modeling approach, according to the communication scenario considered, i.e., *on-* or *on-* to *off-body*. The novelty introduced pertains to the description of radio channel features accounting for multiple sources of variability at the same time. Secondly, the importance of a proper channel characterisation is shown integrating the *on-body* channel model in a system level simulator, allowing a more realistic comparison of different Physical and Medium Access Control layer solutions. Finally, the structure of a comprehensive simulation framework for system performance evaluation is proposed. It aims at merging in one tool, mobility and social features typical of the human being, together with the propagation aspects, in a scenario where multiple users interact sharing space and resources.

List of Acronyms

ACK acknowledgment

AIC Akaike Information Criterion

AFD Average Fade Duration

AP Access Point

B2B body-to-body

BAN Body Area Network

BC Backoff Counter

BER Bit Error Rate

BP Backoff period

BPSK Binary Phase Shift Keying

BSN Body Sensor Network

BT-LE Bluetooth Low-Energy

List of Acronyms

CAP Contention Access Period

CER Chip Error Rate

CFP Contention Free Period

CIR channel impulse response

CM Channel Model

CP Contention Probability

CS Compressed Sensing

CSMA/CA Carrier Sense Multiple Access with Collision Avoidance

CW Continuous Wave

DBPSK Differential Binary Phase Shift Keying

DQPSK Differential Quadrature Phase Shift Keying

DSSS Direct Sequence Spread Spectrum

ECG Electrocardiogram

EEG Electroencephalogram

EMG Electromyogram

GFSK Gaussian Frequency Shift Keying

GMSK Gaussian Minimum Shift Keying

GPRP Generator Pulse Repetition Period

GPRR Generator Pulse Repetition Rate

GTS Granted Time Slot

FFT Fast Fourier Transform

HBC Human Body Communication

IF Intermediate Frequency

IP Integrating Project

ISM Industrial, Scientific, and Medical

LCR Level Crossing Rate

LL Link Layer

LNA Low-Noise Amplifier

LOS Line-of-Sight

LPL Low Power Listening

MAC Medium Access Control layer

MICS Medical Implant Communication Sevice

MIMO Multiple-Input Multiple-Output

MLE maximum likelihood parameter estimation

MPC Multipath component

MSK Minimum Shift Keying

NC Network Coordinator

NET Network layer

NLOS Non Line-of-Sight

O-QPSK Offset Quadrature Phase Shift Keying

PA Power Amplifier

PAN Personal Area Network

PDF Probability Density Function

PER Packet Error Rate

PHY Physical layer

PLCP Physical Layer Convergence Protocol

PLR Packet Loss Rate

PM Wideband Planar Monopole

PRP Pulse Repetition Period

PSDU Physical Service Data Unit

QoS Quality of Service

RC Remote Controller

RF Radio Frequency

Rx receiver

SAR Specific Absorption Rate

SER Symbol Error Rate

SF Superframe

SIR Signal-to-Interference Ratio

SINR Signal-to-Interference-and-Noise Ratio

SIMO Single-Input Multiple-Output

SNR Signal-to-Noise Ratio

TDMA Time Division Multiple Access

TG Task Group

TLM Wideband Top Loaded Monopole

Tx transmitter

UP User Priority

UWB Ultra Wide Band

VNA Vector Network Analizer

WiserBAN Smart miniature low-power microsystem for Body Area Network

WMTS Wireless Medical Telemetry System

WSN Wireless Sensor Network

List of Figures

List of Tables

Introduction

This introduction presents the framework of the thesis that focuses on the paradigm of *body-centric communications*, whose concept is proposed in next sections, along with the motivations supporting the study performed and the research approach followed. Since a significant part of the thesis results were obtained contextually to the European FP7 Integrating Project (IP) "WiserBAN", its structure and main goals are presented hereafter. Finally, the description of the thesis outline and of its main contributions concludes this introduction.

The Ph.D. was performed in the framework of a collaboration between the Department of Electrical, Electronic and Information Engineering "Guglielmo Marconi" (DEI) at the University of Bologna (Italy) and the Department of Systems and Solutions Integration (DSIS) at the "Commissariat á l'Energie Atomique et aux Energies Alternatives", laboratoire d'électronique et de technologies de l'Information (CEA-Leti) in Grenoble (France). The activity was conducted in time sharing between the two host institutions, alternating periods of stay over the three-year Ph.D. term.

Body-Centric Communications: Concept

The general definition of *body-centric communications* applies to all scenarios where at least one of the transmitting/receiving devices is placed *in*, *on*, or *around* the human body, and where the body itself is one of the main actors defining the communication characteristics under different aspects. Being concerned with human behavior, these systems offer an extremely wide range of application possibilities spanning over different aspects of daily life, from medical to entertainment, as well as home automation and localization [1], as it will be presented in Sec. 1.1.1. These few examples show the potentialities of *body-centric communications*, and explain the growing interest in their study, coming from both academia and industry. Moreover, the simultaneous advancement in electronics concerning the design of tiny, long lasting, and portable appliances, along with the increasing need of people to communicate and share information any time and everywhere, foster their widespread diffusion, increasing their socio-economical impact [2].

From a system architecture viewpoint, *body-centric communications* are built around the paradigm of Body Area Networks (BANs) (see Sec. 1.2). These are a particular type of Wireless Sensor Network (WSN) that call for specific technical requirements as detailed in Sec. 1.1.2, where one or more devices are generally located *on* or *around* the human body, or optionally implanted *in* it. These networks are able to collect data coming from the body or from the environment, and send them to a central coordinator node (whether on or outside the body).

According to the nodes position, it is possible to classify *body-centric communications* in three macro categories [3], as shown in Fig. 1:

- ***In-body communications:*** at least one of the transmission ends is placed *inside* the human body. A further subdivision can be made between *in-in*, *in-on*, and *in-off* communications, considering both devices located *in* the body, or just one of them implanted while the other is *on* the body surface or in close *proximity* to it.

- ***On-body communications:*** all communicating devices are located in different positions *on* the surface of the same human body.

- ***On-* to *off-body communications:*** transmissions take place between at least one node located *on* a human body and another one placed *outside* it. The latter being worn by another human subject (*body-to-body (B2B)* case) or placed on an external support acting as a gateway or a router for the transmission (*off-body* case).

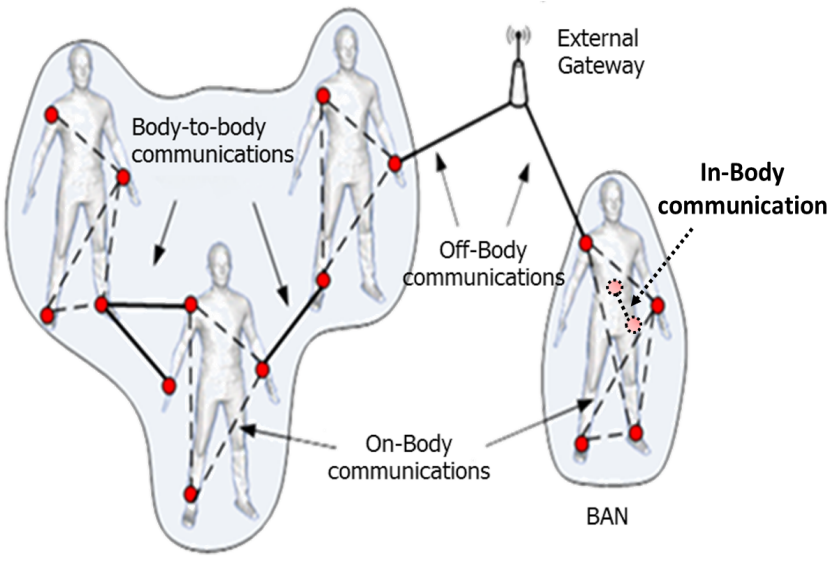

Figure 1: The paradigm of *body-centric communications*.

Among these scenarios, this thesis focuses on the *on-body* and *on-* to *off-body* ones, where in the latter case *off-body* and *B2B* communications are separately investigated. In particular, the *on-* and *off-body* scenarios described above fall within the BAN paradigm, and their system architecture, requirements, and channel characterisation are proposed in the IEEE 802.15.6 standard [4, 5] (see Sec. 1.3.1). *B2B* communications are a relatively new concept, instead, which exploit the presence of multiple BANs in the same environment, opening a novel area of research suitable for a wide range of application possibilities. No specific communication standard is available at present for these kinds of systems, and very few contributions are available in literature investigating related issues (see Sec. 3.1).

Even if *in-body communications* are specifically addressed in the IEEE 802.15.6 standard, they are out of the scope of this work for their peculiarities both at the propagation and requirements levels, since they usually target very specific healthcare applications. Interested readers can find some useful information on the topic in [6, 7].

Problem Statement and Approach

As introduced before, the human body factor is of outmost importance in defining *body-centric communications* characteristics under several aspects. Firstly, tissues dielectric properties, body shape, and movements performed by users determine a unique propagation environment affecting radio channel features and antenna design [8]. Moreover, people mobility and social attitude have to be considered when dealing with upper layer protocols, optimised for *body-centric communications* [9].

The whole protocol stack is hence concerned with the design of reliable systems optimised for these scenarios. Physical layer (PHY) and Medium Access Control

layer (MAC) solutions should be conceived as flexible as possible, to adapt to the specificities of propagation aspects and to the different technical requirements of envisaged applications. Besides, at Network layer (NET), the design of proper routing schemes should present features able to benefit from people movement and from social relationships binding them [10].

To that purpose, this thesis proposes to investigate and characterise the impact of the human presence on *body-centric* systems, accounting for its distinctive aspects, through a multi-layer approach: from radio channel modeling to a system level perspective.

In order to realise efficient protocol solutions optimised for *body-centric communications*, a deep knowledge of the transmission medium and of the related propagation phenomena is needed. This thesis approaches this problem through an experimental modeling of the radio channel based on real-time dynamic acquisitions, focusing on *on-* and *on-* to *off-body* scenarios in the Industrial, Scientific, and Medical (ISM) band at 2.45 GHz. This band is particularly interesting for *body-centric* applications since it is worldwide available and licence-free, and a multiplicity of hand-user devices already operate in this band, employing one or more of the most widespread communication standards like Bluetooth or Zigbee.

Among the models available in literature, most of them addressing *on-body* channels more than *on-* to *off-body* ones, very few are able to properly characterise the time-variant properties arising from the joint effect of body presence and motion. Moreover, antenna impact remains little investigated, with a limited number of contributions [11]. To overcome these limitations, the models proposed in this thesis follow a scenario-dependent approach, which simultaneously accounts for several sources

of channel variability: human body impact in terms of size and tissue properties, antennas and environment effect, users movement, and node on-body position.

The choice of performing a channel modeling based on an experimental approach gives the opportunity for a realistic and detailed characterisation of the main propagation phenomena. The burden due to the heavy cost in terms of time and resources needed to perform measurements is highly rewarded by the degree of precision and accuracy achievable. Even if one can object that experimental results are too tied to the specific investigated scenario, if the data base acquired accounts for different sources of channel variability and it is large enough to perform some consistent statistical analysis (as for the case of the present work), then the model can have a more general applicability.

Implementing channel statistics in a simulation tool gives the opportunity to evaluate and compare the performance of different routing or medium access schemes, in order to choose the optimal solution for the target application. This aspect is of outmost importance also in *body-centric* scenarios, where dedicated protocols are needed to meet different technical requirements in a unique propagation context. A first step in this direction is proposed in this thesis presenting the results obtained from the integration of the previous *on-body* channel modeling in a PHY/MAC simulator. Doing so, system performance is assessed in a more realistic way; environment, human presence and movement, as well as antenna effect, are inherently included in the definition of channel characteristics specific for *on-body* communications.

In the perspective of moving from a radio channel modeling to a more comprehensive system level viewpoint, all distinctive aspects characterising *body-centric communications* should be merged in one single framework, where *on-* and *on-* to *off-body*

transmissions coexist in a specific environment for a target application. To that aim, starting from the work performed on radio channel modeling and PHY/MAC simulation, this thesis presents this framework, in the perspective of realising a modular simulation tool to be used for system performance evaluation. First of all, radio channel features should be considered to account for the effect of the presence of one or more human bodies, moving in close proximity to each other. Related to that, human movement should be properly described, and a model able to reproduce its dynamics and the forces driving it is then needed. Moreover, social aspects of human behavior, defining relationships and corresponding actions, have to be included, leading to a more general *socio-mobility model* that can be exploited to coordinate users transmissions.

Context of the Thesis: the WiserBAN Project

Most of the results presented in this thesis have been obtained in the framework of the large-scale IP project "Smart miniature low-power microsystem for Body Area Network (WiserBAN)" [12], funded by the European Commission under the Seventh Framework Programme [13]. The aim of the project is to create an ultra-miniature and ultra low-power Radio Frequency (RF) micro-system for unobtrusive body-worn and implanted BANs, targeting primarily lifestyle and biomedical applications.

The proposed research concerns BAN communications at 2.45 GHz, with major focus on size and power issues. The final WiserBAN microsystem will be fifty times smaller than today's radio modules, with an improvement in the power consumption level by a factor of 20x. This will be achieved thanks to a novel ad-hoc radio architecture, where antenna miniaturization is a key factor in the definition of device size.

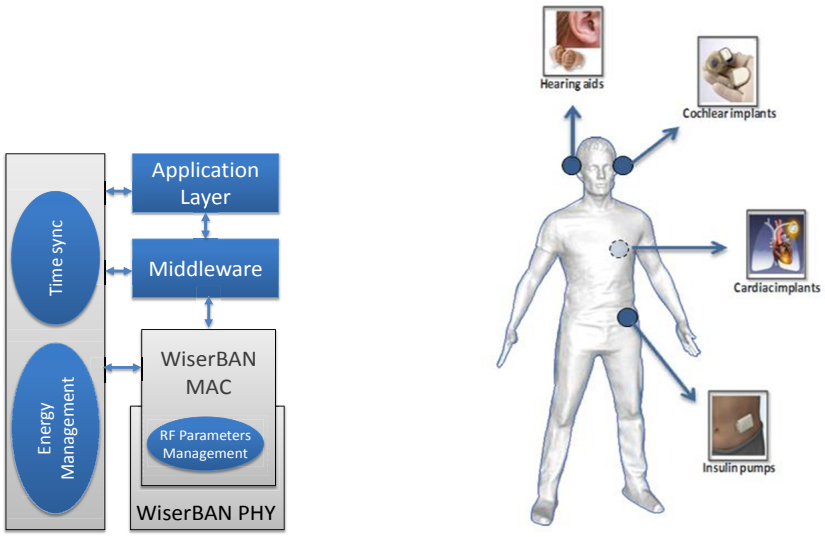

(a) (b)

Figure 2: The WiserBAN project: (a) dedicated protocol stack solution (b) target use- cases.

The development of a dedicated communication protocol stack based on a precise characterisation of the propagation aspects, as the one shown in Fig. 2a, is also one of the major project goals. Flexible and reconfigurable proprietary MAC/PHY solutions have to be designed and optimised for ultra low-power consumption, in compliance with already available standardised architectures used in BAN communications, as described in Sec. 1.3.

At the application level, four industrial-driven wearable and implantable use cases are specifically addressed, representative of the huge potential of BAN for healthcare, bio-medical, and lifestyle applications (see Fig. 2b):

- *Hearing Instruments* and *Cochlear Implants* use-case: wireless connectivity is fundamental to improve performance and comfort of modern hearing systems.

Device miniaturisation and low-power consumption are then important issues to be addressed, while enabling the transmission of different types of traffic, both streaming and non-streaming. Communication between hearing appliances and an external remote unit (e.g., a Remote Controller (RC) or a mobile phone) should be allowed, as well as bidirectional ear-to-ear transmissions.

- *Cardiac Implants* use-case: it concerns people carrying cardiac implants in the context of remote monitoring of patients. Decreasing device power consumption leads to the reduction of battery size and hence of implant dimension, resulting in more comfort for the user. Wireless communication with an external RC should be considered.

- *Insulin Pumps* use-case: a patch insulin pump for medication delivery is applied on the patient's skin, concealed under his clothes. Users interact with the pump using a RC, through a wireless link that should be easily established. Long-lasting batteries, as well as light and comfortable devices, are hence critical aspects to be accounted for.

Beyond these primary reference use-cases, the WiserBAN technology, with its ultra low-power and miniature radio microsystem, may be leveraged in other complementary applicative areas such as ambient intelligence, home automation, entertainment, sport and fitness, motion capture, localization, and other related applications concerning BANs and WSNs in general (see Sec. 1.1.1).

Structure and Contribution of the Thesis

The description of the goals of this thesis and of the approach followed, given in previous sections, highlights the complexity of the investigated topic and the challenges behind it. Very few contributions in literature study *body-centric communications* through such a multi-layer approach, trying to realistically describe the most important features characterising them at different levels.

First of all, Chapter 1 describes more in details the architecture of BANs, which are considered as the central element in any *body-centric* system. Envisaged application fields and related system requirements are presented. Wireless technologies and communication standards suited for these kind of systems, with particular attention to the dedicated IEEE 802.15.6 standard [4], are also discussed in this chapter.

The first step of this multi-layer framework is realised through the characterisation and modeling of the radio channel, based on experimental data sets. After describing the measurements stage, Chapter 2 presents the model for *on-body* channels. Following a scenario-based approach, their time-variant properties are described through the composition of three contributions, namely a *mean channel gain*, a *long-* and a *short-term fading*, each of them accounting for different physical propagation phenomena. With respect to other similar models, different sources of channel variability are here accounted for at the same time. Antenna effect is also investigated for each model component, to show how radiation and polarization characteristics affect radio channel behavior. The outcomes of this work have been presented in a conference paper [11], which was awarded as "Best Student Paper" at Loughborough Antenna and Propagation Conferece (LAPC) 2012.

Similarly, Chapter 3 provides two separate characterisations for *off-body* and *B2B* scenarios, respectively. Each channel power transfer function is described through a distance-dependent model, where a *mean channel gain* and a *short-term fading* component are extracted from experimental channel data. The effect of the body on channel characteristics is also accounted for though an additional *shadowing* contribution. The same scenario-based philosophy presented for the *on-body* case is here considered, representing the main novelty of the proposed models that aim at filling a gap in literature. In particular, the *B2B* contribution is among the few available that proposes a detailed channel characterisation at 2.45 GHz. In the same chapter, the *off-body* model is completed by the investigation of the space-time channel correlation properties. These studies led to the following publications on a journal [14] and in several international conferences [10, 15–17].

Focusing on the *on-body* scenario, Chapter 4 presents the numerical results obtained integrating the channel model described in Chapter 2 in a network simulator. System performance is evaluated in terms of Packet Loss Rate (PLR), average transmission delay, and node energy consumption, with the aim of providing general guidelines for the design of systems optimised for specific application-dependent requirements. Different combinations of PHY solutions and MAC protocols are tested and compared, also highlighting the impact of different antenna types on the overall system behavior. One of the most innovative aspect of this work is that it investigates the effects of realistic channel conditions on the performance of IEEE 802.15.6-based MAC and PHY solutions, operating in an applicative BANs scenario. In order to validate simulation results, a set of on-the-field experiments have been performed using a commercially available IEEE 802.15.4-compliant platforms. The results of this

study have been published in a journal [18] and a conference paper [19].

Finally, Chapter 5 describes the principles behind the implementation of a comprehensive simulation framework for system performance evaluation, combining in one single tool, radio channel models, mobility model, and social features of human behavior. Merging these different aspects characterising *body-centric communications* would be the first step in the design of optimised protocol solutions, tailored for this kind of systems. Both *on-* and *on-* to *off-body communications* are considered in an indoor office scenario, where several people coexist and move according to a socio-mobility model. The latter accounting for the individual working day schedule and for the relationships binding the users. Exploiting social aspects of human mobility could be also useful to allow inter-users coordination in accessing the wireless medium. To the best of author knowledge, there is no such a tool presently available in literature. As originally considered among the goals of the Ph.D. work, the ideas presented in this chapter are the results of the last few months of activity, and they have to be seen as the basis for future reseacrh directions to be pursued.

Chapter 1

Body Area Networks in Body Centric Communications

As already pointed out in the introduction, the core architecture in *body-centric communications* is designed around the concept of BANs, which are thoroughly described in this chapter. After a general overview of the main features of these networks, and of their specificities with respect to generic WSNs, Sec. 1.1 provides an insight on BANs possible applications and on the related system requirements. Sec. 1.2 describes the system architecture, presenting PHY, MAC and NET layer aspects to be considered when designing protocols optimised for *body-centric communications*. The proposed wireless technologies for BANs are detailed in Sec. 1.3, with a particular attention to the recently proposed IEEE 802.15.6 standard [4], which specifically targets short-range, low power, and highly reliable wireless communications for use in close proximity to, or inside, the human body.

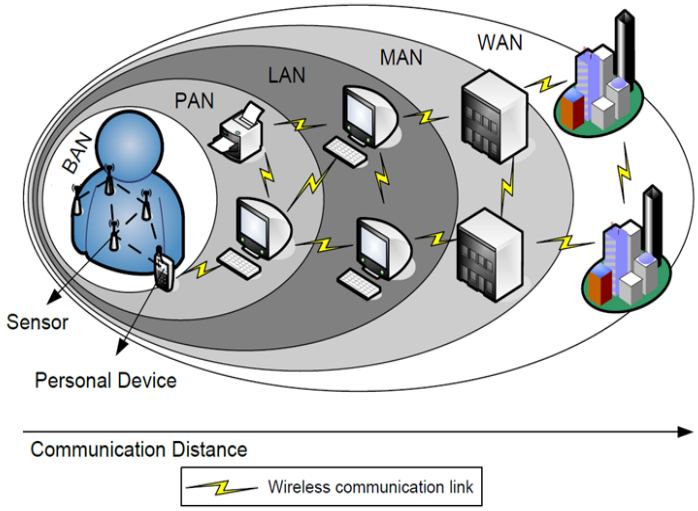

Figure 1.1: Position of BAN in the context of wireless communication networks [22].

1.1 Applications and System Requirements

Advances in microelectronics, wireless communication technologies, and low-power sensors have allowed the widespread diffusion of BANs, also known in literature as Body Sensor Networks (BSNs) [20]. Aiming more at interconnecting one person's wearable devices, BANs complement Personal Area Networks (PANs), the latter referring to a network of wireless peripherals in the environment around the user, whose transmission range can reach up to 10 m [21]. A BAN can be also connected to local and wide area networks using different wired and/or wireless communication technologies, as shown in Fig. 1.1. Some unique aspects distinguish BANs from conventional WSNs, among them one of the most important is the presence of the human body. *On-body* channels, as well as *on-* to *off-body* ones, undergo to specific propagation phenomena, which differ from traditional channel (i.e., distance-dependent models) and have to be properly characterised [23], as it will be shown in Chapters 2 and 3. This

also affects the design of PHY and upper layer communication protocols, where solutions used in generic WSNs result not optimised for *body-centric communications* [24] (see Chapter 4). Furthermore, the intrinsic sociality and mobility of nodes in a BAN, since they are carried by humans, opens other interesting challenges and perspectives. For instance, some interference management schemes should be conceived to operate in densely populated environments [25], or even exploiting the presence of multiple users to create an ad-hoc coordinated "network of people" [26], as in the scenario described in Chapter 5.

1.1.1 Applications

The ability of deploying several wireless nodes on the human body suggests the possibility to use BANs in a wide variety of applications, from healthcare to entertainment up to military and localization ones, just to cite few examples (see Fig. 1.2) [1]. A

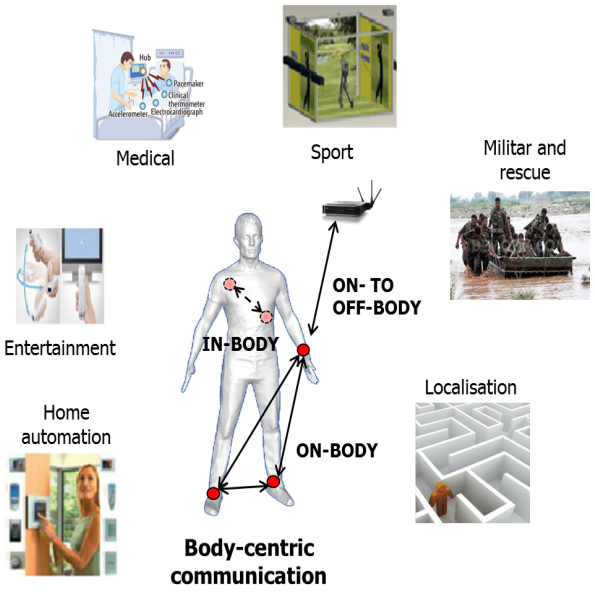

Figure 1.2: Applications for *body-centric communications*.

possible taxonomy of BAN applications is given as follows [27]:

1) *Healthcare*: at a first glance, this could be the most promising field of application for BANs. Several non-intrusive sensors deployed in or on the human body allow the continuous monitoring of vital parameters [24]. Emergency situations that need prompt intervention, such as an heart attack, can be early detected and even foreseen. BANs can be also used to improve the quality of life of hearing and visually impaired people, by means of earing aids or cochlear implants and artificial retina, respectively [28, 29]. A non-exhaustive list of medical applications that can benefit from BAN usage is: Electrocardiogram (ECG), Electroencephalogram (EEG), Electromyogram (EMG), drugs delivery, post operative monitoring, monitoring of vital parameters or body functions, such as temperature, respiration rate, glucose level, oxygen saturation, toxins, blood pressure, etc. [30, 31].

2) *Sport and fitness*: a real-time log of vital parameters like blood pressure, heart beat, blood oximetry, and posture can improve fitness and sport experience [32,33]. In this way users can gather information concerning its sport activity, using them to prevent injuries and to plan future training to improve their performance [34].

3) *Entertainment and gaming*: BANs can bring more realism in the user experience in the field of entertainment. Motion capturing techniques allow the tracking of the position of different body parts by means of a set of gyroscopes and accelerometers wirelessly connected to a central node and worn by the user. The real-time information about motion makes possible for the user the direct employment of his body as a controller in videogames. The film industry takes also advantage of

motion capture techniques in order to realise highly realistic digital movies where actors play the role of non-human subjects [35].

4) *Emergency services*: in the domain of public safety, BANs can be used by firefighters, policemen, or rescue teams [22]. For example, policemen uniforms and firefighters' suits can be equipped with audiovisual, positioning or navigation devices, as well as environmental sensors (e.g., external temperature, carbon monoxide, and carbon dioxide levels), in order to improve their working conditions and safety, and to warn if a life threatening situation is detected [36–38]. Remote viewing techniques and ambient sensing can be extremely beneficial also for guiding rescue operations in post-disaster environments [39].

5) *Military and defence*: new capabilities added by BANs will improve the performance of soldiers engaged in military operations, at both individual and squad levels. At the individual level, a set of sensors can monitor vital parameters and provide information about the surrounding environment in order to avoid threats, whereas information taken at the squad level will make the commander able to better coordinate the squad actions [40]. Spatial localisation techniques and communications between different BANs play an important role in this field, as well as security, in order to prevent sensitive information from being caught by enemies [41].

6) *Industrial*: in the industrial framework, BANs can improve the safety conditions of workers [42], for example monitoring their movements and the surrounding environment in order to prevent the exposure to toxic gasses and radiations, or checking the shocks and vibrations operators are subject to when working with industrial

equipment [43]. Interaction between machines and workers can be improved as well by the information exchange between bodyworn nodes and communication devices embedded in the machines.

7) *Lifestyle applications*: in this last domain several applications can be envisioned, such as emotion detection, ambient intelligence, objects and location tracking, smart keys, identification and authentication [44, 45]. For instance, BANs can be used to monitor people vital signs as a basis to develop systems that adapt the surrounding environment (music type, light level, room temperature) according to the user emotional status [46–48].

1.1.2 System Requirements

The wide variety of possible applications presented in Sec. 1.1.1 lead to an equivalent broad range of different system requirements that has to be met [18]. The most important ones are detailed hereafter according to the classification provided in [49]. Several of these aspects also represent the real challenges that the BAN design has to face, which lead to the conception of specific protocols and system solutions. In particular, energy consumption and coexistence issues are the most critical aspects to deal with [23], considering the reduced size of devices (and of batteries) allowed for bodyworn nodes, and the fact that BANs need to reliably operate also in a crowded environment, where other systems are possibly working using the same frequency band.

More details on some of the following requirements will be given in Sec. 1.3, referring to the specific wireless technology applicable to the BAN paradigm.

1) *Bit rate and Quality of Service (QoS)*: the bit rate requirement varies on a very

broad range, depending on the application and on the type of data to be transmitted. It goes from less than 1 kbps (e.g., temperature monitoring) to 10 Mbps (e.g., video streaming). A list of possible applications with their target bit rates is proposed in [1].

High level of QoS should be guaranteed in medical and military applications, with appropriate error correction and interference-avoidance methods implemented at the PHY and MAC layers to reduce the Bit Error Rate (BER). Other important QoS metrics are: the end-to-end delay, the delay variation, and the capability of providing fast and reliable reaction to emergency situations. Table 1.1 reports a list of QoS requirements and envisaged bit-rates for some example of BAN applications. Furthermore, for this kind of networks, the capability to handle traffic with different priority levels is important [49].

Table 1.1: Bit-rate and QoS requirements for some BAN applications [18].

Application	**Bit-rate**	**Delay**	**BER**
Drug delivery	< 16 kbps	< 250 ms	$< 10^{-10}$
Capsule endoscope	1 Mbps	< 250 ms	$< 10^{-10}$
ECG	192 kbps	< 250 ms	$< 10^{-10}$
EEG	86.4 kbps	< 250 ms	$< 10^{-10}$
EMG	1.536 Mbps	< 250 ms	$< 10^{-10}$
Glucose level monitor	< 1 kbps	< 250 ms	$< 10^{-10}$
Audio streaming	1 Mbps	< 20 ms	$< 10^{-5}$
Video streaming	< 10 Mbps	< 100 ms	$< 10^{-3}$
Voice	50 - 100 kbps	< 100 ms	$< 10^{-3}$

2) *Range and Topology*: the communication range should not be larger than few meters ($3 \div 5$ m) for most of the applications [1]; thus, a simple star topology can

be employed. However, the human body can represent an obstacle itself for the radio propagation, especially for the implanted nodes. In this case, a multi-hop communication must be established, and a relaying technique should be accounted for in order to exploit node spatial diversity, as proposed for example in [50, 51]. The number of nodes forming the BAN ranges from two (e.g., glucose meter) to few hundreds (i.e., motion capture, rehabilitation) and can vary at run time. Therefore, reliable association and disassociation procedures should be considered to allow nodes to join and leave the network as needed by the application [18].

3) *Security*: data security is of primary importance, especially in medical and military applications, and it should be addressed in terms of privacy, confidentiality, authorisation, and integrity [1]. As it will be presented in Sec. 1.3, each standard provides some techniques to deal with security issues. Generally, conventional data encryption mechanisms or authentication process result to be not perfectly suitable for BANs, due to limited processing power, memory, and energy constraints of BAN nodes. Hence, novel lightweight and resource-efficient methods are being developed [52, 53]. A promising solution in this context is the use of biometric identification based mechanisms [54, 55].

4) *Antenna and radio channel*: antenna design can be a very critical issue and research on miniaturisation should lead to quite efficient solutions [56], always considering the proper trade-off between antenna size and its efficiency [57]. Moreover, the presence of the human body could not be neglected since it affects antenna's radiation and polarization characteristics, according to the specific on-body position [11, 58]. Therefore, a good radio channel characterisation is mandatory in order to design antennas able to provide the proper radiation properties. PHY

and MAC protocol design is also affected by radio channel characteristics, whose impact on network performance is described in Chapter 4. A detailed description of channel related issues and two model proposals are given in Chapter 2 and 3 for the *on-* and *on-* to *off-body* scenarios, respectively.

5) *Power Consumption*: the power consumption requirement is very dependent on the nature of the application. However, BAN devices are generally battery-powered and the battery lifetime is required to last up to several years for implants (e.g., at least five years for pacemakers) [59]. Ultra-low power design for radio transceivers is essential, as well as energy-efficient MAC protocols. The latter are commonly achieved decreasing the device duty-cycle, at the expense of end-to-end delay. This allows devices to be in sleep mode (transceiver and CPU shut down) for most of the time, which is an effective solution for applications that require infrequent transmissions. However, a proper trade-off between transmission delay and power consumption should be found. Energy scavenging from body heat [60] or from human movements [61] can be also an option to prolong battery life [62, 63].

6) *Coexistence*: most of the current BAN systems are designed to operate in the license-free ISM band, centered at 2.45 GHz. This is an overcrowded radio band; indeed, Wi-Fi (IEEE 802.11), Bluetooth (IEEE 802.15.1), IEEE 802.15.4/ZigBee, and other communication standards operate in the same spectrum. Considering the need for reliable transmissions, especially in medical applications when an emergency or alarm traffic has to be established, some techniques should be studied and implemented to avoid or reduce interference. A proper evaluation of the real impact of interfering systems on BAN performance, in terms of PLR or transmission delay, is then of outmost importance. Some works that address

this topic are reported in [64–66], which study coexistence aspects between several sources of interference (i.e., systems working according to Wi-Fi standard or IEEE 802.15.4a one) and different PHY solutions for the BANs (i.e., narrowband PHY at 2.45 GHz and IEEE 802.15.6 Ultra Wide Band (UWB)).

Moreover, as specified in [49], in order to reduce or even eliminate possible damaging effect of multiple BANs simultaneous activity, proper techniques of interference rejection should be considered, as proposed in [26, 67–69], just to give some examples. Anyway, the presence of other nearby networks should not be seen just as a potential source of interference, but also as possible relay networks used to forward the information in a non fully connected scenario for delay-tolerant applications [70, 71].

7) *Form Factor*: device size constraints can be stringent; the most critical aspect is to fit the antenna front-end and the battery into a very small case, while providing good radiation property and lifetime. This is true mainly for implantable devices; anyway, for bodyworn nodes, flexibility and stretchability may be even more relevant aspects to consider for the user comfort, especially in sport, fitness, and military applications. For recent advances in stretchable electronics, the interested reader should refer to [72], while [73–75] focus on stretchable antennas and RF circuits.

8) *Signal processing*: as already said, BAN applications are power consumption limited and the radio circuits are often the power-greedy part of the system [76]. However, power efficient signal processing techniques, such as Compressed Sensing

(CS), can help the designer to keep under control the overall system energy consumption. The latter is a technique that allows to sample a sparse analogue signal at a sub-Nyquist rate, saving energy without loosing the information contained in it [77, 78]. CS has been widely used in BAN scenarios; an overview with some application examples can be found in [79].

9) *Safety for the human body*: at the frequencies of interest for BANs, the known health-related effect on human tissues include only heating. The International Commission on Non-Ionizing Radiation Protection (ICNIRP) specifies general restrictions and limits that have to be met to guarantee health safety when the body is exposed to time-varying electromagnetic fields [80]. For the frequency range from 100 kHz to 10 GHz such restrictions are established in terms of Specific Absorption Rate (SAR), which is defined as the mass normalised rate at which RF power is coupled to biological tissues, and it is typically expressed in units of watts per kilogram [W/Kg]. Low-power devices (such as BAN ones), do not radiate enough power for the whole-body SAR to be a concern, while attention has to be paid to the localised SAR, which is measured in specific parts of the body. Therefore, BANs should minimise the localised SAR and comply with international [80] or regional regulations (such as those defined by the European Union for Europe [81] and by the Federal Communications Commission for the USA [82]).

1.2 System Architecture

The requirements presented above highlight the multiplicity and diversity of the aspects to be considered when dealing with the BAN architecture. Some of them have

a stronger impact on the PHY layer, while other affect more the upper layers protocol design. Anyway, flexibility and adaptability are the most challenging goals for any system designer when dealing with these types of networks.

As for the PHY layer, channel modeling is important for the design and the evaluation of the most suitable signalling technique to be adopted. A reliable channel characterisation is needed to support a more effective antenna design and the evaluation and comparison of different PHY and MAC solutions (see Chapter 4). As it will be presented in details in Secs. 2.1 and 3.1, several studies have been performed to characterise the transmission channel, focusing on different radio frequency bands both at narrowband (Medical Implant Communication Sevice (MICS), Wireless Medical Telemetry System (WMTS), ISM) and UWB. More recently, other wireless communication technologies have been studied as possible alternatives to more conventional operating bands, among them: molecular communications [83] or ultrasonic waves [84] for in-body transmissions, and Human Body Communication (HBC) working in the frequency interval between 5 and 50 MHz, which exploits the human body as a communication medium [85, 86]. Results for the channel characterisation show a high variability, also among those referring to the same frequency interval. This underlines the importance of the environment, the movement performed by the user and the specific node position on the definition of channel characteristics [87]. Moreover, antenna design is also affected by the operating environment and the proximity of the user's body, both having a significant impact on device radiation properties. The most suitable antenna design has to be carefully chosen in relation to the target application and considering the limits in terms of device size and radiated power. From the PHY perspective, support for upper layers BAN protocol design gives rise

to a trade-off between transmission distance, data rate and power consumption. Modulation schemes should guarantee the desired data rates while maintaining seamless connectivity in dynamic and interfered environments [24].

At the MAC layer, energy efficiency is one of the most important attributes to be targeted, along with safety, security, QoS provisioning, and reliability. A robust MAC protocol shall consider efficient duty cycling methods to minimise power consumption without compromising QoS in terms of latency and jitter, by controlling the main sources of energy waste (i.e., packet collisions, idle listening, etc.). It shall also be able to cope with topology and density changes induced by nodes moving in and out of the transmission range, due to body movements [1]. Generally, MAC protocols are grouped into contention-based and scheduled-based schemes. In the former case nodes contend for the channel to transmit data. If the channel is busy, the node defers its transmission until it becomes idle. These protocols, such as Carrier Sense Multiple Access with Collision Avoidance (CSMA/CA) or Slotted ALOHA, are scalable, adaptable to traffic fluctuation, and with no strict time synchronization constraints. However, they incur in significant protocol overhead. In scheduled-based approaches, such as the Time Division Multiple Access (TDMA) one, the channel is divided into time slots of fixed or variable duration. These slots are assigned to nodes and each node transmits during its own slot period. Even if these protocols are extremely energy efficient, with low duty cycle and no possibilities for packet collision, or idle listening and overhearing problems, their most significant drawback is the need for frequent synchronization [88]. Other aspects that should be considered at the MAC layer are message prioritization and alarm management capabilities, as well as simple and self-organising network setup [52]. Having said that, accounting

for all these different features calls for a trade-off in system performance, which is the real challenge in MAC protocol design.

Finally, for the sake of completeness, some hints on the NET layer characteristics are given. Being responsible for effective packet delivery from a source to a destination node through a number of relaying nodes, its main tasks is routes discovery, establishment and maintenance [87]. Developing efficient routing protocols for BANs is a non trivial task because of the specific characteristics of the wireless environment on the human body. This makes the solutions adopted in traditional WSNs not suitable ones, due to the stringent constraints in terms of transmitted power, node energy consumption and to frequent node topology reconfiguration due to body movement [88]. To that purpose, the proper network topology is also an important aspect to be studied, since it influences the overall system performance and protocol design. Even if traditionally the star topology is widely proposed for several BAN applications, more recently some studies focus on the assessment of the improvement brought by the introduction of some forms of relaying and node cooperation [50, 51].

Considering this general overview on BAN architecture, next section will describe the choices operated by some standardisation bodies to comply with the technical requirements and system characteristics at the different levels of the protocol stack.

1.3 Wireless Technologies for BANs

This section presents the proposed wireless technologies to be used for BANs. Existing standards, such as IEEE 802.15.4 [89] and Bluetooth Low-Energy (BT-LE) [90], which were originally conceived to operate in more classical WSN scenarios, result not to be able to fulfill all the technical requirements presented in Sec. 1.1.2. Anyway, since

their widespread acceptance and diffusion, being implemented in several personal portable devices, such as smart-phones, PDAs, and laptops, they are still considered practical *de-facto* solutions also for BANs.

Recognising the lack of a proper standard specifically tailored for wireless communications in the vicinity of the human body, in November 2007 the IEEE 802.15 Task Group (TG) 6 was formed to define the PHY and MAC layers characteristic of a communication standard where flexibility is the key word. It aims at supporting the combination of reliability, low power, bit-rate, and non-interference required to broadly address BAN applications [18]. The first draft of the document was released in 2010, while the final version is now available and dates back to February 2012 [4]. Standardisation is an important process since it is the first step in the large-scale diffusion of a communication technology, which become a reference for both vendors and users, and fosters interoperabilty with other operating standards.

Finally, other proprietary or open technologies are briefly reviewed at the end of the section, just to provide a complete picture of the different architectures considered for BANs, even if they target a narrower scope (i.e., some more specific applications).

1.3.1 IEEE 802.15.6 Standard

The first degree of flexibility introduced by this standard is related to the choice of the PHY layer. To meet the wide variety of system requirements coming from the different applications, a unique PHY solution does not seem to be a feasible option, and hence the proposal defines three possible alternatives (see Fig. 1.3):

a) ***Narrowband PHY*** (optional): a compliant device shall be able to support transmission and reception in at least one of the following frequency bands:

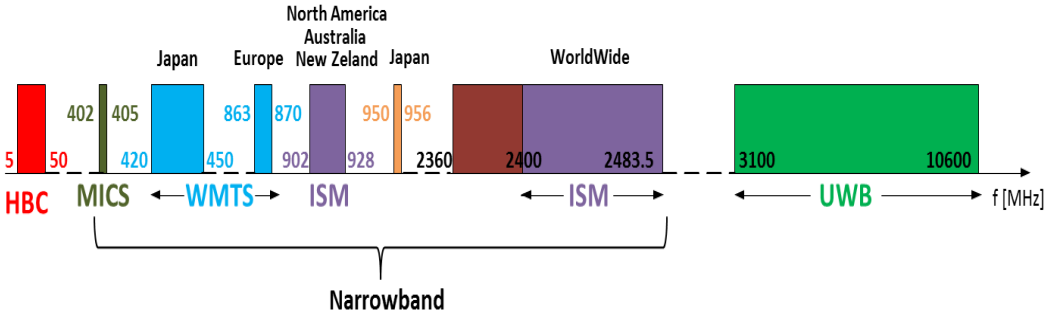

Figure 1.3: Spectrum allocation chart for BAN application in IEEE 802.15.6 standard.

- *402-405 MHz*: MICS band; it is widely accepted although the possible bandwidth is limited;
- *420-450 MHz*: WMTS band; available in Japan;
- *863-870 MHz*: WMTS band; available in Europe;
- *902-928 MHz*: ISM band; it is available to be used without license in North America, Australia and New Zealand;
- *950-956 MHz*: available in Japan;
- *2360-2400 MHz*: this is a newly proposed frequency band to be adopted for BAN applications;
- *2400-2483.5 MHz*: ISM band; it is available worldwide, but there could be issues of coexistence with other standards using the same band.

b) ***UWB PHY***: it is divided into a low (3.25-4.75 GHz) and a high (6.6-10.25 GHz) band, both consisting of operating channels of 500 MHz bandwidth each. UWB PHY is specifically designed to offer robust performance for high quality, low complexity and ultra low power operations, all primary aspects when dealing with BANs, where human safety and coexistence issues are of outmost importance.

Two types of UWB technologies are considered: *impulse radio (IR-UWB)* and *frequency modulation (FM-UWB)*. Two operational modes are also defined: *default* for medical and non-medical applications, and *high quality of service* for high-priority medical applications. Both modes shall support IR-UWB as mandatory PHY, whereas the *default* one also supports FM-UWB as optional.

c) ***HBC PHY***: this PHY solution uses the human body as a communication medium. The band of operation is centerd at 21 MHz with a bandwidth of 5.25 MHz.

Considering that this thesis will focus on systems operating at 2.45 GHz, some more details are provided referring to this PHY solution. For this band, the standard defines seventy-nine channels of 1 MHz bandwidth each, whose center frequency, f_c, is computed according to: $f_c\ [MHz] = 2402 + 1 \cdot n_c$, where $n_c = \{0, \ldots, 78\}$ is the channel number. Four bit-rates are specified, arising from the combined used of different modulation, coding, and spreading factors, according to what presented in Tab. 1.2: As it can be seen, both Differential Binary Phase Shift Keying (DBPSK) and Differential Quadrature Phase Shift Keying (DQPSK) are used to modulate the Physical Service Data Unit (PSDU).

A compliant device shall be capable of transmitting at least -10 dBm EIRP, considering that it should radiate as less power as possible, in order to reduce interference to other systems and limiting radiation exposure to the human body tissues. The maximum transmit power is limited by local regulatory bodies.

The minimum receiver sensitivity in AWGN channels is given referring to a Packet Error Rate (PER) of less than 10% and accounting for a PSDU of 255 bytes; values vary in the interval from -92 dBm to -83 dBm, according to the bit-rate considered

Table 1.2: IEEE 802.15.6 modulation parameters for the 2.45 GHz band [4].

Packet component	**Modulation**	**Symbol rate**	**Code rate**	**Spreading factor**	**Bit rate**
PSDU	$\pi/2$-DBPSK	600 ksymb/s	51/63	4	121.4 kbit/s
PSDU	$\pi/2$-DBPSK	600 ksymb/s	51/63	2	242.9 kbit/s
PSDU	$\pi/2$-DBPSK	600 ksymb/s	51/63	1	485.7 kbit/s
PSDU	$\pi/4$-DQPSK	600 ksymb/s	51/63	1	971.4 kbit/s

in Tab. 1.2 (i.e., from 121.4 kbit/s to 971.4 kbit/s).

Interested reader is referred to [4] for the complete set of specifications applying to the other narrowband frequencies and PHY solutions.

The transmission range considered in the standard is limited to 3 m for *in-* and *on-body* applications and has to be at least 3 m for *on-* to *off-body* communications. The proposed network topology is a star one, with possibility for relaying (2-hop tree structure).

Even if different PHY solutions are presented, just a single MAC protocol is proposed. In order to support different applications and data flow types (i.e., continuous, periodic, non-periodic and burst), each one characterised by specific performance requirements, the MAC protocol should be as flexible as possible, combining both contention-based and contention-free access techniques [91]. The standard also provides several User Priority (UP) values in order to diversify and prioritise node channel access, according to the information they have to transmit (e.g., background

data, video traffic, medical data, or emergency traffic) [27]. A BAN coordinator could decide whether to operate in one of the following three access modes:

a) *Beacon mode with beacon periods (superframes)*: the coordinator establishes a common time base by sending beacon packets that define the beginning of an active beacon period or Superframe (SF). It shall also divide each active SF into applicable access phases ordering them as shown in Fig. 1.4, and defining their duration. The length of any phase may be set to zero, except for the Random Access Phase (RAP) 1, which must have a minimum guaranteed duration. The coordinator may also maintain inactive SF, where it transmits no beacons and provides no access phases [27]. In the Managed Access Period (MAP), the co-

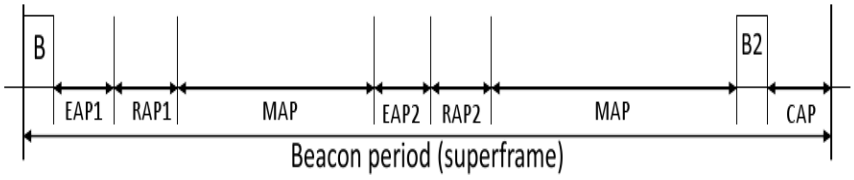

Figure 1.4: IEEE 802.15.6 SF structure for beacon mode access [4].

ordinator may schedule intervals, or send poll or post packets to nodes. A poll is defined as a control frame used to grant nodes an immediate polled allocation (i.e., non-recurring time interval for uplink traffic) or to inform a node of a future poll or post. Whereas a post is a management or data type frame sent by the coordinator to a node to inform of a posted allocation, which is a non recurring time interval that the coordinator grant to itself for downlink traffic exchange. Further details on polled and posted allocation techniques can be found in [4].

In the Exclusive Access Phases (EAPs), used only for the transmission of emergency data, RAP and Contention Access Period (CAP), nodes compete for the medium access using CSMA/CA or Slotted ALOHA techniques. More details on IEEE 802.15.6 version of CSMA/CA and Slotted ALOHA are given in Sec. 4.2.1, where the protocol stack solutions considered in the framework of the WiserBAN project are introduced.

b) *Non-beacon mode with superframes*: in this mode, a coordinator may have only a MAP in any SF, and it may organise the access to the medium as explained above for the MAP phase in the beacon enabled access mode.

c) *Non-beacon mode without superframes*: a coordinator may provide unscheduled allocation intervals. After determining that the next frame exchange will take place in non-beacon mode without SF, a node shall treat any time interval as a portion of EAP or RAP and employ CSMA/CA-based random access to obtain a contended allocation [4].

As it could be seen, the huge variety of channel access techniques proposed in the standard gives a great flexibility to the protocol, but at the same time it is not so immediate for designers to choose the best options for the intended application, and to find the optimal solution.

Security aspects are also accounted for in the standard and they are addressed with nodes choosing among three different security levels. *Level 0:* unsecured communications; it provides no measures for message authenticity and integrity validation, confidentiality and privacy protection. *Level 1:* authentication but not encryption;

messages are transmitted in secured authenticated but not encrypted frames, providing measures for authentication and integrity validation but not confidentiality and privacy protection. *Level 2:* authentication and encryption; it results in the most secure transmission conditions provided by the standard. The security selection sets off a security association between devices for activating a pre-shared master key, or generating a new one. As part of message security, replay protection is also provided [18].

1.3.2 IEEE 802.15.4 Standard

IEEE 802.15.4 wireless technology is a short-range communication system originally intended to provide applications with relaxed throughput and latency requirements in PANs. The key features concern low complexity, low cost, low power consumption, and low data rate transmissions, to be supported by either fixed or moving cheap devices. The IEEE 802.15 TG 4 [92] released a standard focused on the definition of the PHY and MAC layers for the implementation of WSNs [89]. At the upper layers, which are out of the scope of the standard, one of the most used solutions is the ZigBee protocol stack, specified by the industrial consortium ZigBee Alliance [93].

The standard specifies a total of twenty-seven half-duplex channels across three unlicensed frequency bands, whose allocation is detailed hereafter:

- *868 MHz band*: it consists of a single channel covering the band between 868.0 to 868.6 MHz, and it is used just in the European area. A data rate of 20 kbit/s is available, achieved with a Direct Sequence Spread Spectrum (DSSS) Binary Phase Shift Keying (BPSK) modulation scheme.

- *915 MHz band*: it ranges between 902 and 928 MHz, where ten channels with a

data rate of 40 kbit/s are available, implementing again a DSSS BPSK modulation, but with different chip rate. It is used in the North American and Pacific area.

- *2.45 GHz ISM band*: it covers the frequency range from 2400 to 2483.5 MHz, divided into sixteen channels with data rate equal to 250 kbit/s, whose center frequencies, f_c, are defined by $f_c\ [MHz] = 2405 + 5 \cdot (n_c - 11)$, where $n_c = \{11, \ldots, 26\}$ is the channel number [89]. A DSSS Offset Quadrature Phase Shift Keying (O-QPSK) modulation format is employed.

It is possible to notice that very limited bit-rates are allowed with this standard, and this can be an issue for its application in some BAN scenarios where higher data rates are required, such as audio and video streaming.

The lowest value of transmitted power should be as less than or equal to -32 dBm, whereas the maximum limit shall conform to local regulations. Referring to a PER less than 1% for a PSDU of 20 bytes, the minimum receiver sensitivity in the 2.45 GHz band shall be -85 dBm.

At the MAC layer, IEEE 802.15.4 standard defines a protocol based just on a CSMA/CA scheme, which is described in more details in Sec. 4.2.1. The main functions performed by the MAC layer are: association and disassociation, security control, beacon generation and scheduling management, generation of acknowledgment (ACK) frames (if used), and finally, application support for the two network topology possibilities described in the standard, i.e., the star and the peer-to-peer one [27].

The network coordinator can operate in one of two different modes, namely beacon-enabled and non beacon-enabled, which correspond to two different channel access mechanisms. In the former case, a SF is established by the coordinator

by sending a beacon packet. The SF is organized into three parts: a CAP, during which nodes use a slotted CSMA/CA, a Contention Free Period (CFP), containing a number of Granted Time Slots (GTSs) that can be assigned to specific nodes with stringent requirements, and an inactive part. The coordinator may allocate up to seven GTSs, but a sufficient portion of the CAP must remain for contention-based access, which must assume a minimum duration. An example of the SF structure is shown in Fig. 1.5. Interested reader can find more details on SF architecture and the parameter set definition in [89].

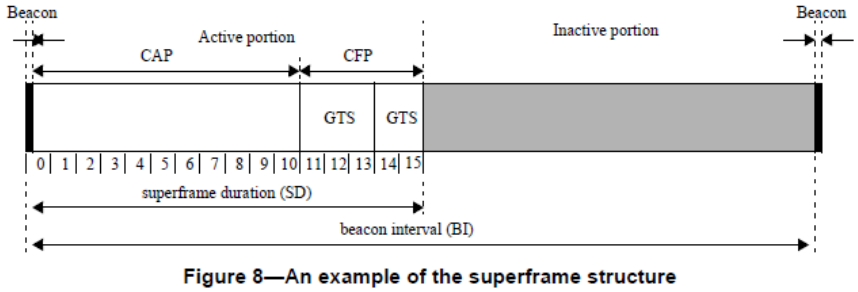

Figure 1.5: Example of IEEE 802.15.4 SF structure [89].

In the non beacon-enabled mode, nodes use an unslotted CSMA/CA protocol to access the channel and transmit their packets and no SF structure is defined.

The description given above refers to IEEE 802.15.4 standard as defined in its 2006 version [89]. During these last years, several amendments have been issued to complement and enhance its applicability. Among these amendments, it is worth mentioning the IEEE802.15.4a [94] and the IEEE 802.15.4e [95]. The former considers two alternative PHYs (UWB and Chirp Spread Spectrum) to support high throughput, ultra low power consumption and high precision ranging and localization, whereas the latter presents new MAC layer features to better support industrial

markets.

The standard also defines an encryption algorithm to be used when cyphering the data to transmit. However, no indication is provided about how the keys have to be managed or what kind of authentication policies have to be applied, which are left to the upper layers. The encryption algorithm used is the Advanced Encryption Standard (AES) with a 128-bit key length, which is not only used to encrypt the information but also to validate the transmitted data. This concept is called data integrity, and it is achieved using a Message Integrity Code (MIC) that is appended to the message [18].

1.3.3 Bluetooth Low Energy and Other Candidate Solutions

Bluetooth wireless technology is a short-range communication system (up to 30 m) intended to replace wires connecting portable and/or fixed electronic devices. The key features of Bluetooth wireless technology are robustness, low power consumption, and low cost [90].

There are two main core configurations of Bluetooth technology systems: Basic Rate (BR), with optional Enhanced Data Rate (EDR), and Low Energy (LE). BR is the "classic" Bluetooth, which allows a bit rate up to 3 Mbps when EDR is used. The LE system includes features aimed at lowering device current consumption, and reducing system cost and complexity as compared to BR/EDR. The BT-LE system is also designed for use cases and applications with lower bit rates and duty cycles. It targets small and cheap devices powered by button-cell batteries, such as wireless sensor devices, for several applications: sports and fitness (sport equipment and

monitoring devices, speedometer, heart rate meter, pedometer), healthcare and illness treatment (weight scale, blood pressure monitor, glucose meter, pulse oximeter), home automation and entertainment (remote controls, home sensors and switches), automotive (tyre pressure monitoring, parking assistant, keyless entry), watch/wrist wearable devices (music players and mobile phones remote controls, proximity detection) [27].

BT-LE specifications regard the whole protocol stack, where only star topologies are considered. Two implementation possibilities are defined: a single-mode (stand-alone), designed for applications requiring low power consumption and small-size devices, and a dual-mode implementation, which is an extension of the classic Bluetooth radio more targeted at mobile phones and PCs.

The frequency band of operation is the 2.45 GHz ISM band, where forty channels of 2 MHz bandwidth each are defined, with center frequency, f_c, defined as: $f_c\,[MHz] = 2402{+}n_c{\cdot}2$ where $n_c = \{0, \ldots, 39\}$ is the channel number. The modulation is Gaussian Frequency Shift Keying (GFSK) with a supported bit rate equal to 1 Mbps. For a transmitter (Tx), the output power level shall be included in the interval between - 20 dBm and + 10 dBm. For a receiver (Rx), the reference sensitivity level is - 70 dBm, defined as the receiver input level for which a BER of 0.1% is achieved.

At the Link Layer (LL), on top of the radio PHY, the channels are allocated into two different types: advertising physical channels and data physical channels. The three advertising channels are used for discovering devices, initiating a connection, and broadcasting data. The remaining data channels are used for communications between connected devices during normal operations. In both cases, channels are subdivided into time units known as events: advertising events and connection events,

respectively [27]. On data channels, the communication is managed by a master node, which defines the timings of transmissions and channel hopping procedures. The functioning of the LL can be described in terms of a state machine with five

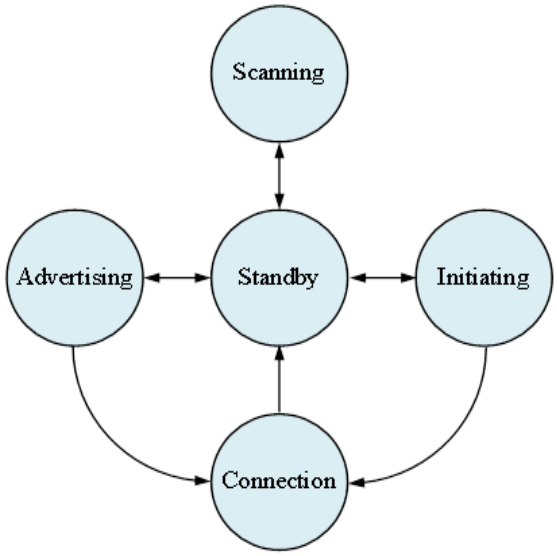

Figure 1.6: Diagram of BT-LE Link Layer State Machine [90].

states, as shown in Fig. 1.6. The *Standby State* is the default one, where no packet transmission or reception is allowed. From the *Standby State* is possible to move to the *Advertising*, *Scanning*, or *Initiating State*, while it can be entered from any other state. A device in the *Advertising State* is known as an advertiser, which transmits advertising packets in advertising events and possibly listens and answers to responses triggered by these packets. In the *Scanning State*, a scanner node listens for advertising packets from advertisers. There are two types of scanning: passive and active. When in passive scanning, just reception and not transmission of packets is allowed. In active scanning, a node should listen for advertising packets and, depending on the advertising type, it may request an advertiser to send additional information. A device in the *Initiating State* is known as an initiator, which listens for

advertising packets from specific devices and responds to these packets to initiate a connection with the other device. Finally, the *Connection State* can be entered either from the *Initiating* or the *Advertising State*. When in *Connection State* nodes can send and/or receive data packets in connection events and they can assume the roles of both master and slave. When entered from the *Initiating State* (i.e., after sending a connection request), the *Connection State* will be in the master role, whereas when entered from the *Advertising State* (i.e., after receiving a connection request), it will be in the slave role.

BT-LE offers various security services for protecting the information exchange between two devices. Most of the supported security services can be expressed in terms of two mutually-exclusive security modes known as *LE security mode 1* and *2*. Encryption and authentication techniques are also implemented using Counter with Cipher Block Chaining-Message Authentication Code Mode and a 128-bit AES block cipher. Some privacy features are also considered: devices hide their real address using randomly generated addresses that change during time. Privacy is then guaranteed since these random addresses can be resolved only knowing the proper key [96].

Since Bluetooth is a well-known and widespread technology, it could be a good option also for BANs. The most recent mobile phones and tablets come with dual-mode Bluetooth radio, and some monitoring devices equipped with BT-LE can already be found on the market (e.g., heart rate belts) [97]. The main drawbacks of BT-LE are the lack of multi-hop communication capabilities and the limited scalability (only star topologies are possible). It operates just at 2.45 GHz, which is actually an overcrowded band already employed by many other communication standards (e.g., Wi-Fi or IEEE802.15.4). Furthermore, both Bluetooth and its low-energy version

often need some user inputs to set up the communication link (e.g; devices pairing phase). This can be very inconvenient in some applications where BAN are employed, such as health monitoring in emergency conditions or rescue operations, where the user is not able to interact with the devices or he/she should be focused on more impelling tasks.

Even if the three standard solutions presented above are the major candidates to be used in BAN scenarios, other proprietary technologies have been proposed to address some more specific applications. Among them ANT [98] is a protocol stack working at 2.45 GHz and designed for sensor networks that require ultra low-power consumption [24]. It features simple design, low latency and a data rate of 1 Mbit/s, employing a TDMA-like adaptive channel access scheme [1]. ANT+ is an open alliance of over 200 member companies that defines health and fitness device profiles and manages network keys, with the aim of bringing a full interoperability among different manufacturer solutions. ANT devices have already been embedded in some products, such as watches, heart rate monitors or pedometers.

Similar to ANT, Sensium [99] also provides a proprietary ultra low-power platform for on-body health and monitoring applications. The network adopts a master-slave architecture, where a bodyworn slave node periodically sends data to a central master node, enabling remote monitoring of patients status. To reduce energy consumption, only single-hop communications are allowed and nodes are in standby state except when they transmit some data, which happens just in scheduled time slots [87].

Zarlink, now Microsemi [100], developed an ultra low-power RF transceiver (ZL70101) to be used in medical and implantable applications for reliable wireless communications. It is extremely low-power consuming, supporting also a deep-sleep

operational mode that can be interrupted by a specially coded message. Zarlink devices have already been used in the implementation of a camera capsule that can be swallowed by patients in order to transmit images from inside the human body [87].

Some other suitable proprietary technologies are for instance: Z-Wave [101] and Insteon [102] for home automation application, or RuBee [103] for operations in the Low Frequency band. Interested reader is referred to the cited websites.

1.4 Conclusions

This chapter proposes a detailed description of different aspects related to BANs, which are presented as the basic element in *body-centric communications*. Starting from a taxonomy of possible application areas, the requirements that BAN system design have to meet are commented in details. The wide variety of applications, which lead to a heterogeneous set of technical aspects to be accounted for, demand for robust and flexible protocols at both PHY and MAC layers. Finally, the wireless technologies considered for BAN communications are described, highlighting the importance of the definition of a specific standard to foster the widespread diffusion of these networks. Anyway, above all the regulations, standardisation processes and market laws, a careful attention should be paid to the final user (i.e., a patient, an impaired person or a general consumer), who has to perceive the real benefits and lifestyle improvements of using such a technology, and hence promoting its development.

Chapter 2

Radio Channel Modeling for On-Body Communications

This chapter proposes an experimental *on-body* channel model at 2.45 GHz. Some of the most relevant contributions available in literature, dealing with the same topic, are detailed in Sec. 2.1, highlighting the most interesting outcomes they present.

For the acquisition of the experimental channel data, a dedicated test-bed is set up, which is detailed in Sec. 2.2, along with the measurements scenarios considered. A specific section (Sec. 2.2.3) is devoted to the description of the radiation and propagation characteristics of the two antenna types employed for the acquisitions.

The proposed model characterises the *on-body* channel power transfer function as composed by a *mean channel gain* and *fading* contributions, which are described in Secs. 2.3.1 and 2.3.2, respectively. An additional subdivision between *long-* and *short-term fading* is considered, to account for different propagation phenomena occurring in the BAN context.

2.1 Related Works

Studying the influence of the body proximity on antennas radiation characteristics [104,105], or investigating the physical principles behind the propagation of radio waves on the human body [106], has attracted researchers interest since late 90s. The propagation mechanisms on and around the human body are very specific, mainly combining free space propagation, diffractions (creeping waves), and reflections from the environment, resulting in peculiar channels as compared to more classical ones, such as indoor or urban [107]. These preliminary works served as a basis for the first investigations on *on-body* channels characterisation, which date back to 2002 and 2003 [108, 109].

Since then, several studies have been performed and contributions come from different European and non-European institutions. Among them, some works of notable importance are provided by ETH Zurich (Switzerland) [110], IMEC (Netherlands), ULB and UCL (Belgium) [111–113], the University of Birmingham and Queen Mary University of London (United Kingdom) [3,114] and the Queen's University of Belfast (United Kingdom) [115,116]. Worldwide, other works come from NICTA (Australia) or NICT (Japan) [117–119], just to mention few examples.

The approaches to channel modeling can be classified into analytical and experimental-based. In the former case, theoretical description of electromagnetic phenomena is used to describe specific aspects of the propagation on the human body, such as the effect of tissue properties on antenna patterns. Examples of such models can be found in [120,121], where Maxwell's equations are directly solved considering waves propagating on the human body, the latter modeled as as an infinite

lossy cylinder. The models derived are validated through the comparison with some experimental data. Another interesting study is presented in [122], where creeping waves theory is used in the prediction of surface waves attenuation on curved surfaces (i.e., human head and waist) [123]. The mathematical soundness of this kind of models is unquestionable, anyway they are extremely demanding in terms of computational cost, especially if the effect of the body movement or the environment has to be considered. To that purpose, experimental model can naturally include these aspects while performing measurements, leading to more realistic models that account at the same time for different sources of channel variability. The price to pay is a cost in terms of time taken to perform measurements and the technical equipment needed. Since the model presented in this chapter belongs to the latter class, the rest of this section will focus just on this kind of modeling approach, surveying some of the most notable contributions proposed in literature based on experimental data.

Considering the wide range of channel characterisations available, a detailed description of each of them would not be useful, resulting in a confused list of modeling approaches and statistical parameters. Similarly to what is proposed in [124], a more functional description comes from the discussion of the proposed models sorting them according to the propagation aspect they mainly focus on, with a further classification according to the investigated frequency band, whether narrowband or UWB. Even if IEEE 802.15.6 standard consider HBC communications as one of the envisaged PHY layer for BAN, channel models referring to that band are not considered in this overview, due to the specific propagation mechanisms characterising it. Interested reader can find some useful insights on that topic in [125, 126].

As a general comment, it will be shown how results coming from different institution and different measurements are widely dispersed, even when referring to similar controlled environment, as an anechoic chamber. Reasons to that are manifold; first of all, it points out a lack of standardised measurements procedures and data analysis. Secondly, it underlines the strong dependency of the *on-body* channel on multiple sources of variability, such as population, body posture, and movements. Finally, the statistical approach used seems to be not wide enough to offer a model of general applicability, not just related to the specific investigated scenario [127]. Moreover, the homogenisation and the comparison of the different models is made difficult by the fact that antenna effect can be hardly de-embedded from the measured channel data [128]. Indeed, antenna/body interaction strictly depends on the specific on-body node position. The same applies to the energy absorbed by the body, which is also related to antenna's total efficiency. For some antenna types the effect of the body proximity can be minimised by shielding them from the body with ground planes. However, the orientation of the on-body device, which has an effect on the antenna gain and on its polarization, is difficult to measure with accuracy. Therefore, antennas are considered to be an integral part of the channel model [129]. One of the first contribution aiming at studying antenna decoupling possibilities in *on-body* channels is presented in [130].

Distance or Link Dependent Phenomena

A large part of the works focusing on the characterisation of *on-body* channels attempts to model the expected path-loss as a function of the distance separating Tx and Rx, and hence to determine the path-loss exponent through a best-fitting of the

experimental data [124].

In this direction, the first model that has to be mentioned is the one proposed in the IEEE 802.15.6 channel model document [5], under the name of CM3. It is actually a collection of three models characterising the radio channel at different frequencies (i.e., 400, 600, 900 MHz, and 2.45 GHz), plus a dedicated one for the UWB. While the first two narrowband sub-models are certainly distance-dependent, accounting just for static measurements, the last one goes more in the direction of a *scenario-based* approach, as it will be better described further in this section.

Other contributions proposing a distance-dependent path loss model can be found in [129,131–133] for the narrowband channel in static conditions, and in [111,134–137] for the UWB in both static and dynamic scenarios. Results show a very wide variation of the extracted path-loss exponents for both narrowband and UWB, even within similar environment and measurements conditions. This suggests the idea that this modeling approach is poor, and that node location and environment play a more important role in channel characterisation, than Tx/Rx distance [124]. Moreover, according to the specific node relative position, path-loss values can be significantly affected by the body posture and by the movement performed.

To account for all these sources of channel variability, a scenario-based approach seems more appropriate, as previously introduced in the 802.15.6 model, but very few works in literature provide contributions in this direction. Some examples are proposed in [138–141]. In these cases, for a given operating frequency, a scenario is defined not just by the node position, but also by the environment and by the movement performed. This latter aspect allows to account for the time-varying channel characteristics, improving static approaches that tend to generate less realistic

and possibly misleading models. Since this thesis proposes a scenario-based *on-body* channel characterisation, some more details on the contributions following a similar approach are reported hereafter.

In particular, in [142] narrowband quasi-static measurements (i.e., a sequence of static acquisition emulating the evolution of body posture while moving) at 2.45 GHz are performed in anechoic chamber, to highlight the effect of body posture. A log-normal distribution of the variation of the path-gain around its mean value is proved, without any separation between short- and long-term statistics. A similar pseudo-dynamic measurements method is used for UWB investigations in [112, 143, 144], to reproduce human walking and arm movement. Improvements to these models are proposed in [140], where measurements are performed at 2.45 GHz for different types of movements in an indoor environment, considering several node positions and antennas types. Short- and long-term fading are separated by averaging channel data over a sliding temporal window. Their values results to be well modeled by a Rice and a log-normal distribution, respectively. More details on works focusing on the characterisation of short-term propagation phenomena will be given further in this section.

Authors in [141, 145] propose a statistical characterisation of the short-term fading for indoor and outdoor environment at 2.45 GHz using a Nakagami distribution. Nodes are placed in different on-body positions. When the user is stationary, very little fading is observed and Nakagami-m parameters are always $\gg 1$. Compared to this, the m parameter is found to significantly decrease in mobile conditions, showing that motion acts to increase the diffuse on-body component experienced by body-worn devices. On-body fading is also found to increase when the user moves from

anechoic to multipath conditions [141]. The same group of authors performed similar investigations in the frequency band at 868 MHz [115].

Measurements by NICT investigate the channel at 4.5 GHz [146, 147] for different node positions. The scenarios measured in anechoic chamber are: standing position, walking on the spot, and up-down movement. The authors propose three different distributions of the relative path-gain: normal or log-normal ones seem the best solutions for static or quasi-static scenarios, while the Weibull distribution can be employed for larger movements.

Another notable work has been carried out by NICTA in [138] focusing on two frequencies relevant for BAN applications: 820 MHz and 2.36 GHz. The human subject was asked to perform three different actions: standing still, walking and running on the spot. The analysis carried out for several antenna positions shows that a unique statistic is not suitable for describing all the scenarios for the three movements, also highlighting the dependency on the specific frequency. Despite the fact that different statistical behaviors are considered according to the scenario, these results were integrated in the final IEEE 802.15.6 channel model [5] merging all the scenarios [107].

Finally, one of the latest scenario-based *on-body* channel models is the one proposed in [139]. Results refer to several on-body node positions, and measurements where performed both UWB and narrowband al 2.45 GHz, in indoor and anechoic environment for dynamic scenarios. An analysis of mean channel gain, long- and short-term fading, and shadowing correlation is presented with emphasis on the differences given by the human body variability and the movement conditions. Starting from this work, the characterisation proposed in this thesis describes the channel

model as composed by three contributions, each one accounting for specific propagation phenomena such as body movements and Multipath component (MPC) fading environment. With respect to similar model available in literature, the proposed one comprehensively accounts for several sources of channel variability as the node position, the human subject, the environment considered and the time-variability brought by users movement. Moreover, antenna effect on channel characteristics in also investigated, repeating measurements with two different types of devices. The aim is not to define the overall best performing antenna for *on-body* applications, as proposed by other works [114, 140], but to assess how different radiation and polarization features affect channel characteristics, with a particular focus on the impact on each channel model component. First- and second-order statistic are also provided; results similar to those proposed in [141] are found to describe the short-term fading. Nakagami distribution is here replaced by a Rice one, which was found to provide an extremely good fit to the experimental data (comparable to the former), while assuring easiness of use and implementation.

Small-scale Phenomena

As briefly introduced above for the scenario-based approaches, literature proposes a wide range of first-order small-scale statistical descriptions both at narrowband and UWB, particularly focusing on indoor environment, where the MPC contribution is more important. Authors of [124] present an useful summary of the most considered fitting distributions, among them the most commonly used are the lognormal, followed by the Nakagami and the Ricean one. Each of these statistical descriptions is related to a physical propagation scenario leading to a specific fading environment, which

can be more or less adapted to the BAN case. For example, the Rice distribution describes a fading signal where a main dominant propagation path predominates over the scattered MPC within one single cluster of multipath waves. On the opposite, the Rayleigh statistic considers the case where there is no such dominant component, and the propagation takes place mainly due to the combination of the secondary paths arising from reflections and diffractions on the surroundings. Generally, Rayleigh distribution results to be a good fit in classical mobile radio channels, when the different multipaths are additive in the linear domain according to the central limit theorem. This is not the case for the BAN context, where fading is not well modeled by this distribution and the best fitting is often provided by the lognormal one, especially in the UWB [8, 111, 148]. This is reasonable considering that BAN channels, particularly those with large bandwidths, contain a large number of factors that contribute to the attenuation of the transmitted signal (i.e., body presence, environment, user movement), which are additive in the log-domain, indeed [124].

Apart from the lognormal distribution, other statistics properly modeling narrowband fading channels are the gamma one, followed by the Weibull [117, 138]. In particular, the use of a gamma distribution shows how BAN fading channels are often dominated by a shadowing effect [149]. For its ease of use and manipulation, Nakagami statistic is also considered to describe the *on-body* small-scale fading, and it often results in a good fitting [115, 141]. Even if it was extracted from on-the-field measurements and no theoretical derivation was originally provided, authors in [150] propose a physical model for these type of fading channels, where the signal can be seen as composed of a cluster of multipath waves with no dominant components within any cluster, which can be the case in a general BAN scenario.

Given this general overview, it is worth mentioning that each of the proposed statistical description provides its own parametrisation to describe *on-body* small-scale phenomena. This lead to a great dispersion of the results and the choice of the most appropriate solution is extremely hard for any designer.

To complete the channel characterisation, several of the discussed models also investigate important second-order statistics, such as the Average Fade Duration (AFD) and Level Crossing Rate (LCR) [8, 138, 140, 145, 151]. Results show again a high degree of variability since these parameters are highly dependent on channel dynamics, as defined by rate and amount of body movement according to the node position.

Finally, even if not specifically addressed in this thesis, time and space correlation aspects for *on-body* channels should be at least mentioned. Both these parameters give important information for system design, and some works in literature focus on their investigation.

Time correlation can be evaluated through the channel autocorrelation and it is used to determine its coherence time, helping in the definition of the proper packet length or in the estimation of the time interval during which a successful transmission is possible according to channel conditions [152–154].

As for the space correlation, it is defined as the cross-correlation level between different *on-body* links [8, 155, 156]. Its evaluation can be helpful in defining the cooperation possibilities among nodes of the same BAN, as suggested in [50, 51], highlighting whether they are experiencing similar channel conditions and if they are suitable to be used as communication relays in the case where the direct link is temporarily unavailable.

2.2 *On-Body* Channel Measurement Campaign

To study the time-variant characteristics of the *on-body* radio channel, a specific measurement test-bed is set up to operate in the time-domain. Several node positions on the human body are accounted for and acquisitions are repeated in various measurement conditions, combining different environments and movements performed by the user. Two sets of antennas are used, to highlight the impact of their polarization and radiation characteristics on the time-variant components of the radio channel.

2.2.1 Channel Measurement Test-bed

As already pointed out in Sec.2.1, radio links performance are strongly affected by the body presence and by its movement; hence, catching the time-variant features of the BAN channel is of primal importance for a realistic characterisation. The dedicated test-bed set up to allow the dynamic acquisition of channel data is shown in Fig. 2.1.

The transmitting side is mainly composed of a Picosecond Pulse Lab [157] pulse step generator, connected to a Power Amplifier (PA) through two impulse forming filters, the latter allowing to fit the desired pulse shape into the bandwidth from 2 up to 9 GHz. The PA delivers +37 dB gain (± 3 dB) in the frequency band of interest, and it is connected to the Tx antenna. More details on the radiation characteristics of the antennas employed in the measurements are given in Sec. 2.2.3.

At the receiving side, four antennas are connected to as many Low-Noise Amplifiers (LNAs), each one delivering +42 dB gain (± 2 dB) in the frequency band of interest. It is worth noting that LNAs should be placed just after the Rx antennas front-end, in order to reduce the global noise figure as much as possible. To

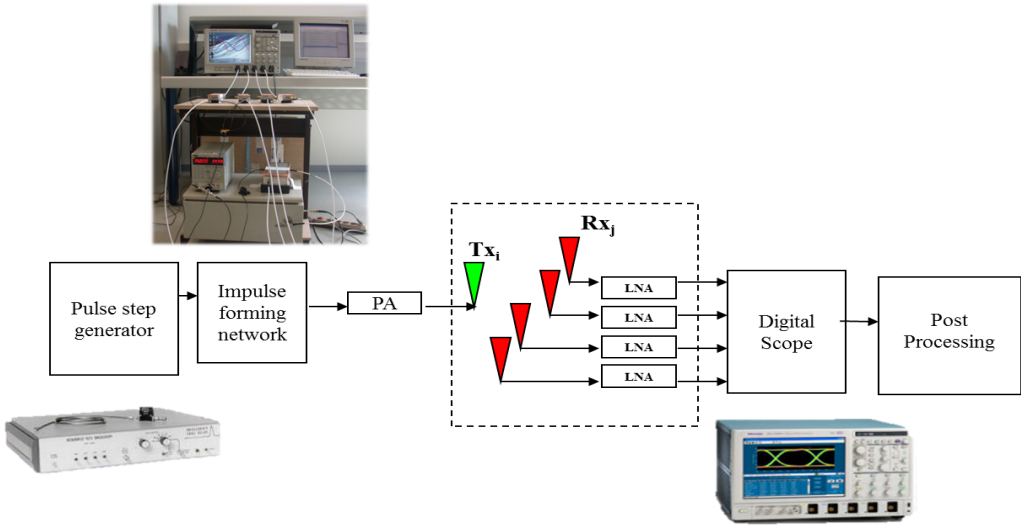

Figure 2.1: Measurements test-bed for *on-body* channel investigations.

complete the receiving side, a wideband digital oscilloscope by Tektronix [158] allows to sound up to four channels at the same time, collecting four channel impulse responses (CIRs), $h_{i,j}(t,\tau)$. Each of them corresponds to a different on-body link composed by the i-th Tx and the j-th Rx. Connectors and RF cables complete the test-bed description. It is worth saying that cables can potentially affect the quality of the measurements, considering their proximity with both the Tx and Rx devices and the positioning on the subject's body. No detailed characterisation of their possible effects was performed, but some countermeasures were adopted to limit their impact on the acquisitions. First of all, cables were connected as to be orthogonally oriented with respect to antenna's main polarization and ferrite beads were placed close to the antenna/cable junction to prevent harmful interferences. Moreover, cables were tightly placed on the human body using some velcro strips to hold them in the same position, avoiding inconvenient displacements during dynamic acquisitions.

Given the complex set-up described above, a calibration procedure is needed in

order to extract just the channel behavior. This was practically realised by deconvoluting the effects of the different elements composing the test-bed chain out of the acquired data, thanks to a preliminary end-to-end calibration measurements. Anyway, the effect of the antenna, which can be hardly deembedded from the acquisitions, is part of the model.

The oscilloscope works with a time window of 200 ns and a sampling rate of 12.5 Giga Sample per Second (corresponding to a time resolution of 80 ps), resulting in a total number of 2500 recorded points per CIR. The duration of each acquisition, T_{obs}, is set to 3 s, which is considered to be enough for an user to perform an entire movement cycle, whether walking or bending (as it will be described in more details in Sec. 2.2.2). The number of acquired CIRs per channel, N_p, is equal to 22500, which is the maximum available at the oscilloscope. However, in order to deal with high Signal-to-Noise Ratio (SNR) signals, some averaging procedures are needed in the post-processing phase. To chose the most suitable averaging factor, N_{Avg}, some empirical tests were realised to quantify the test-bed noise floor reduction as the averaging factor increases. Considering that some preliminary tests showed channel attenuations up to -70 dB for the considered *on-body* scenario, the N_{Avg} values is set to 150. This results in a noise floor of approximately -95dB, which is considered enough to achieve high SNR signals. Given the choice made for the averaging parameter, the total number of CIRs to be used for the channel characterisation is then given by: $N = N_p/N_{Avg} = 22500/150 = 150$. The corresponding time interval between two consecutive CIRs is defined as: $\delta_{t,CIR} = T_{obs}/N_{Avg} = 3s/150 = 20$ ms, which is a a good trade-off between signal dynamic and channel variability over time (i.e., the channel can be considered stationary over $\delta_{t,CIR}$, assuming an average human speed

in common activities in the range between 0.5 and 2 m/s).

In the perspective of investigating the time-variant properties of the BAN channel, the set-up described is extremely interesting since it allows gathering the signals coming from different antenna positions while the subject in moving. This being representative of realistic applications, where multiple on-body sensors co-exists in the same BAN and send data to a central coordinator node.

2.2.2 Measurement Scenarios

To evaluate the impact of different on-body node positions on the definition of channel characteristics, the four receiving antennas (Rx_j with $j = 1, 2, 3, 4$) are located at the same time on the user's right and left hand, right thigh and left ear. The Tx_i ($i = 1, 2, 3$) is placed alternatively on the right ear, on the chest and on the left hip of the same subject, as shown in Fig. 2.2 [11]. It is worth noting that the distinction between Tx and Rx is done in relation to the specific measurement set-up considered, but given channel reciprocity these definitions can be inverted. All the acquisitions are performed both in anechoic premises and in a (4.6×6.6) m^2 indoor office equipped with some standard furniture. In the anechoic chamber a catwalk of 3 m, realised by solid RF absorber, is placed to allow human movements. Anyway, the presence of some portions of uncovered metallic floor makes the environment not perfectly anechoic.

In order to account for the variability brought to the channel by differences in human body shape and tissues properties, four human subjects are involved in the measurements. Their main physical characteristics are summarized in Tab. 2.1.

To be able to reproduce the same antenna emplacement on the different subjects,

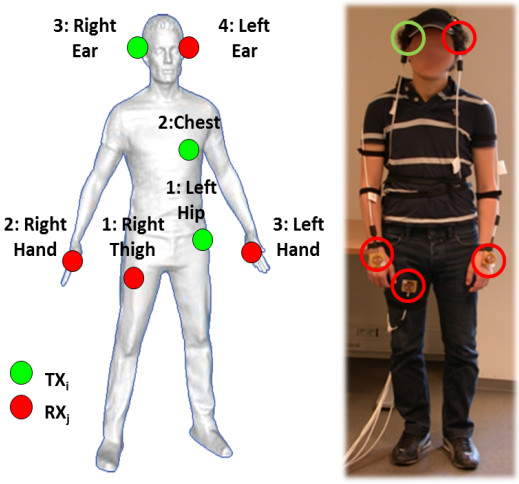

Figure 2.2: Node emplacement for *on-body* measurements.

some reference points are adopted for each node location.

For every Tx$_i$ position, each subject performs different actions:

- two acquisitions while walking over a distance of 3 m. Considering the duration of each acquisition $T_{obs} = 3$ s (see Sec. 2.2.1), this results in an average walking speed of approximately 1 m/s;
- two acquisitions while standing up and sitting down on a chair (i.e., bending). Given some mechanical constraints on the antenna connector, this movement is not performed for the Tx located on the left hip;
- two acquisitions while standing still. These measurements are performed just in the anechoic chamber, therefore the only source of channel time-variability is related to the human breathing and not to a specific movement.

Considering all the acquisitions performed, the total amount of CIRs available for the post-processing is in the order of 5×10^3 per Tx position per environment, which

Table 2.1: Physical characteristics of human subjects involved in *on-body* channel measurements.

	Weight [Kg]	**Height [cm]**	**Sex**
Sub A	63	169	M
Sub B	45	160	F
Sub C	74	175	M
Sub D	61	170	F

is considered a consistent data base to extract a statistical characterisation for the radio channel.

2.2.3 Antennas

In order to study the antenna effect on radio channel, all the experiments described above are repeated with two sets of antennas with different characteristics: Wideband Planar Monopoles (PMs) and TLMs (see Fig. 2.3). Antennas free-space properties are reported hereafter for the sake of completeness, along with the realised gain elevation patterns in Fig. 2.4, showing a more important cross-polarization component for PMs than for TLMs (red curve in Fig. 2.4a). As a matter of fact, antennas radiation characteristics result to be influenced by the presence of the human body according to their location and related tissue properties. However, the aim of this work is not to de-embed the antenna from the radio channel, but to investigate how radio channel model is differently affected by a specific antenna type in the BAN context [11].

PM is a 25x35x0.8 mm^3 wideband notch antenna with integrated balun, characterised by 70% total efficiency at 2.45 GHz in free space. It is worth noting that

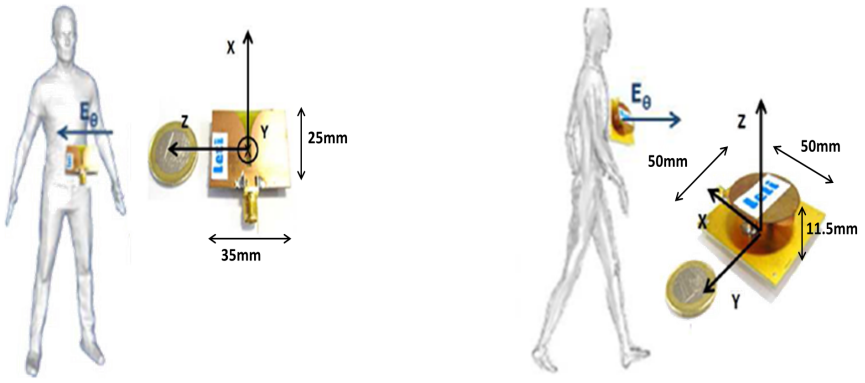

(a) (b)

Figure 2.3: Antennas for *on-body* measurements: (a) PM and its orientation with respect to the body surface; (b) TLM and its orientation with respect to the body surface.

antenna efficiency is generally reduced by the proximity to the human body, in particular for devices not presenting a ground plane in their layout, as in the PM case. To limit this effect, a 5 mm thick dielectric foam was used to space these antennas from the body surface. It was verified that devices impedance properties were kept almost unchanged even when mounted on the user's body, except for an expected deformation of the radiation pattern. As shown in Fig. 2.3a, positioning these antennas parallel to the body surface results in PMs main polarization tangentially oriented with respect to it.

TLM is based on a wire-patch monopole design [159] fed by a strip-line within the antenna ground plane, whose dimensions are 50x50x11.5 mm^3. It presents 70% total efficiency from 2.36 up to 5 GHz even when placed on-body, thanks to the presence of a ground plane reducing body influence. TLMs, which presents a good monopolar behavior, were actually designed to result into a normal polarization with respect to the body surface (Fig. 2.3b).

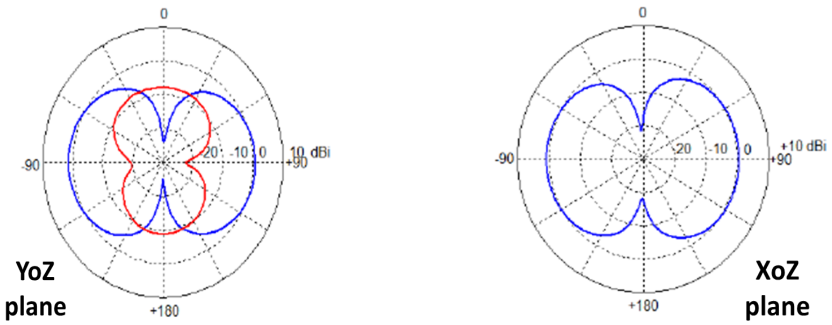

(a) (b)

Figure 2.4: Antennas for *on-body* measurements: (a) realised gain pattern in the air for PM (YoZ plane); (b) realised gain pattern in the air (XoZ plane) for TLM. In gain pattern charts: co-polarization (blue line), cross-polarization (red line).

Even if a deep study of antenna/body interaction is out of the scope of the present work, it was verified that antennas impedance matchings were maintained even when on-body, as shown in Fig. 2.5. It can be seen how the reflection coefficients for both antennas (PMs on the left (a) and TLMs on the right (b)) lie below the threshold of -7 dB in the frequency band of interest, in particular at 2.45 GHz. As expected, placing the antennas on the body (dashed curves) results just in a shift of the resonant frequencies with respect to the free space case (continuous curves), but no important mismatching effects have been observed. Each color in the figures refers to one antenna sample, and on-body measurements were obtained placing the devices on a standardised phantom [160].

2.3 On-Body Channel Modeling

Realistic model for the *on-body* radio channel should properly account for the different sources of variability affecting it. More than the physical distance separating the ends

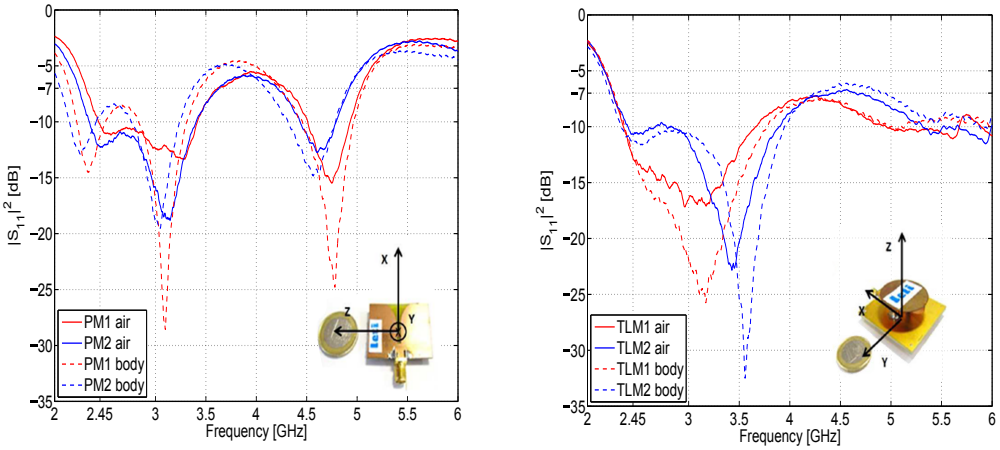

(a) (b)

Figure 2.5: Antenna's reflection coefficients: PMs (a) and TLMs (b). Free space (continuous curves) and on-body (dashed curves) characterisation, each color (blue and red) referring to one sample of the antenna type considered.

of the communication link, important factors having an impact on the definition of channel characteristics are:

- *Human factor*: it accounts for the heterogeneity brought by human bodies in terms of shape, tissue dielectric properties, and the way in which each human subject moves.

- *Environment factor*: it refers to the variability introduced by the specific environment considered, whether indoor, outdoor, or anechoic.

- *Antenna factor*: antennas with different radiation and polarization characteristics may have a different impact on the transmission channel; indeed, they can result more or less adapted to the specific propagation environment realised by the human body surface.

- *Movement factor*: time-variant characteristics of the *on-body* links are strongly

affected by the type of movement performed by the user. Dynamic acquisitions are then required to account for this type of channel variability.

To consider the effect of all these variables, a *scenario-based* approach is used for channel modeling, where a scenario $\mathcal{S}$ is defined by the Tx/Rx position on-the body, the human subject, the environment, the antenna type, and the movement performed.

For every scenario $\mathcal{S}$ (i.e., for each link under investigation in every measurement condition considered), the time-dependent channel power transfer function, $P_{i,j}(t)$, is evaluated by averaging the modulus of the channel transfer function, $H_{i,j}(t,f)$, over the band of interest B (in this case $B = 10MHz$):

$$P_{i,j}(t) = \frac{1}{B}\int_B |H_{i,j}(t,f)|^2 df = G_{i,j} * S_{i,j}(t) * F_{i,j}(t). \tag{2.3.1}$$

$G_{i,j}$ represents the *mean channel gain*, $S_{i,j}(t)$ is the *long-term fading* or *shadowing*, mainly due to the masking effect of the human body and to its movement. $F_{i,j}(t)$ is the *short-term fading* that accounts for the effect of the MPCs arising from reflections and diffractions from the environment or from the body itself [8].

It has to be specified that, even if the acquisitions are performed wideband according to the test-bed described in Sec. 2.2.1, the channel model and the results that are presented in this section refer just to the frequency range centered at $f = 2.45$ GHz in the ISM band.

An example of the acquisition performed is shown in Fig. 2.6, which presents the evolution over time of $P_{i,j}(t)$ in dB (dashed curves) while the subject is walking in indoor environment. Each color refers to one of the on-body link, considering the Tx placed on the user's left hip.

The comparison between Fig. 2.6 and Fig. 2.7 (the latter is equivalent to the former but referring to a static case, where the subject is standing still in the anechoic

chamber), highlights how the node position and the movement performed affect the dynamic evolution of $P_{i,j}(t)$. This effect is particularly evident when focusing on the slow-varying component of the power transfer function, $S_{i,j}(t)$ (continuous curves). It represents the *shadowing* impact of the body that dynamically masks the direct communication link according to the subject movement. For example, following the trend of the continuous blue curve (hip/right hand link) in Fig. 2.6, it is possible to retrace the swinging movement of the arm during the walk. The dips of the curve refer to the moments where the arm is behind the subject's torso, i.e., the body completely shadows the communication, resulting in strong channel attenuations. On the opposite, *shadowing* phenomena are quite moderate in static conditions (Fig. 2.7) where no movement is performed, and the slight variations of channel $P_{i,j}(t)$ are due to the breathing of the user [18].

More details on channel model components, and the effect of antenna radiation characteristics on each of them are given in next sections.

2.3.1 Mean Channel Gain

For a given channel transfer function, $H_{i,j}(t, f)$, the total power, $G_{i,j}$, also referred to as *mean channel gain*, is evaluated as:

$$G_{i,j} = \frac{1}{T_{obs} \cdot B} \int_0^{T_{obs}} \int_B |H_{i,j}(t, f)|^2 df dt; \tag{2.3.2}$$

where $T_{obs} = 3$ s, i.e., the duration of each acquisition. The *mean channel gain* is a key parameter to determine the SNR level (averaged over *long-* and *short-term fading*) that a wireless system can achieve. The averaging operation over B in Eq. 2.3.2 implies that the dielectric constants of the materials, and all propagation phenomena related with them, do not depend on the frequency at least for the bandwidth

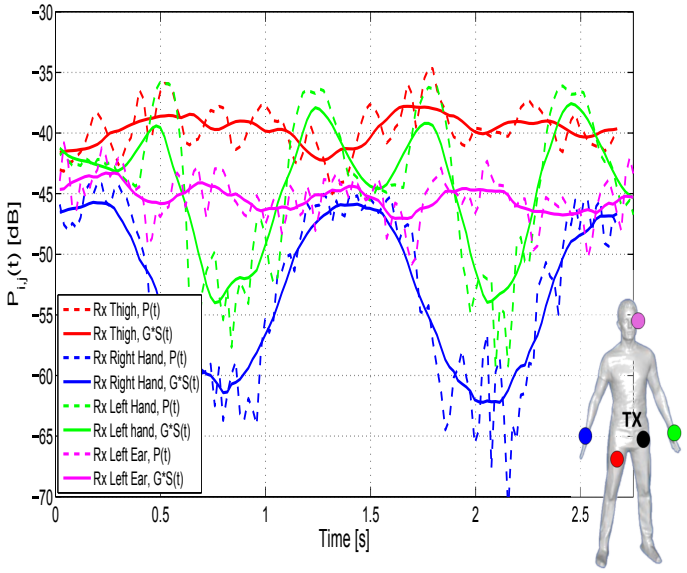

Figure 2.6: *On-body* channel power transfer functions: Tx on left hip, TLM antennas, indoor, walking.

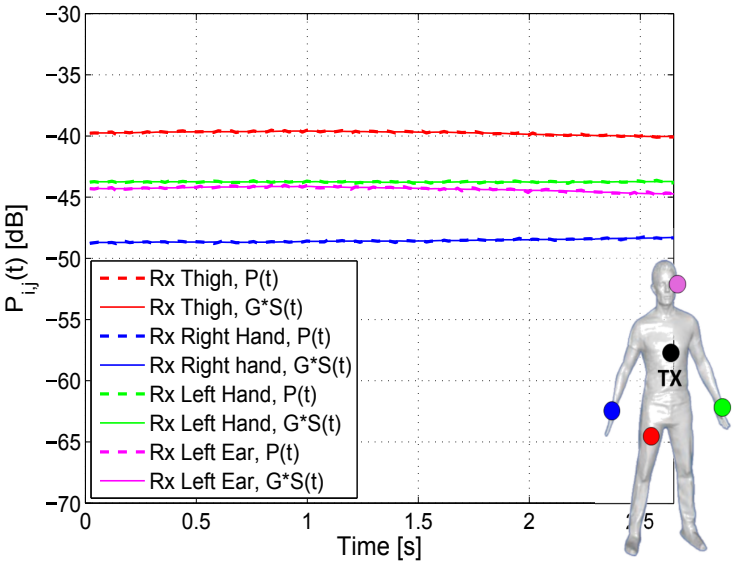

Figure 2.7: *On-body* channel power transfer functions: Tx on chest, TLM antennas, anechoic, standing still.

Table 2.2: $G_{i,j}$ values - Tx on Right Ear - Anechoic Chamber

	Rxs	Planar Monopole		Top Loaded Monopole	
		μ_0 [dB]	σ_0 [dB]	μ_0 [dB]	σ_0 [dB]
Walking	**Right Thigh**	-72.53	5.96	-55.13	3.29
	Right Hand	-64.61	4.49	-53.82	3.92
	Left Hand	-74.89	2.63	-66.59	4.98
	Left Ear	-58.54	6.05	-35.81	0.82
Bending	**Right Thigh**	-72.27	3.58	-56.77	2.99
	Right Hand	-61.83	5.41	-54.20	2.97
	Left Hand	-73.82	3.26	-61.52	3.62
	Left Ear	-57.41	8.28	-36.33	1.56
Standing	**Right Thigh**	-76.22	3.05	-53.82	1.99
	Right Hand	-67.77	2.47	-49.92	2.47
	Left Hand	-78.83	2.05	-66.87	3.43
	Left Ear	-68.02	4.12	-33.69	0.81

considered.

Tabs. 2.2 and 2.3 list the results for $G_{i,j}$ in dB, given through its mean (μ_0) and standard deviation (σ_0), according to the specific measurement scenario $\mathcal{S}$. The analysis is performed gathering the *mean channel gain* values of all subjects, so that σ_0 accounts for the heterogeneity brought by the human bodies in terms of shape, tissue dielectric properties and small variations of the nodes position.

Even if these results refer to the case for the Tx on the ear, they are useful in drawing some general considerations on the differences in antenna behavior, which also apply to the other investigated Tx positions. The complete set of results, which are not reported here for the sake of briefness, can be found in Appendix A. First of

Table 2.3: $G_{i,j}$ values - Tx on Right Ear - Indoor

	Rxs	Planar Monopole		Top Loaded Monopole	
		μ_0 [dB]	σ_0 [dB]	μ_0 [dB]	σ_0 [dB]
Walking	**Right Thigh**	-67.01	2.77	-57.57	1.84
	Right Hand	-59.18	2.27	-53.31	3.19
	Left Hand	-65.67	4.63	-57.57	0.91
	Left Ear	-54.67	4.73	-37.01	2.00
Bending	**Right Thigh**	-65.93	4.41	-57.78	2.56
	Right Hand	-61.22	2.50	-55.18	1.95
	Left Hand	-64.79	3.63	-58.00	1.52
	Left Ear	-55.44	6.33	-36.43	2.08

all, PMs generally present smaller values of $G_{i,j}$ as compared to TLMs (see Fig. 2.8). This can be explained considering that tangentially polarized antennas, as PMs are, do not help creeping waves propagation on the body, resulting in larger channel attenuations [161]. As a consequence, this effect is even more evident for the links with a strong on-body propagation component, such as chest/thigh, hip/thigh or ear/ear (see Tabs. 2.2 and 2.3).

Moreover, the two antennas show a different behavior according to the environment considered. Indeed, PMs present larger *mean channel gains* in indoor than in anechoic, while TLMs show similar $G_{i,j}$ values in both environments, with anechoic results just few dBs smaller than those in indoor. For the links considerably masked by the human body (such as right ear/left hand), this effect is even more stressed, with $G_{i,j}$ values up to 10 dB larger in indoor than in anechoic premises when PMs are used. This is reasonable considering that in the anechoic chamber the propagation is mainly due to creeping waves traveling on the body, whereas in indoor the presence of

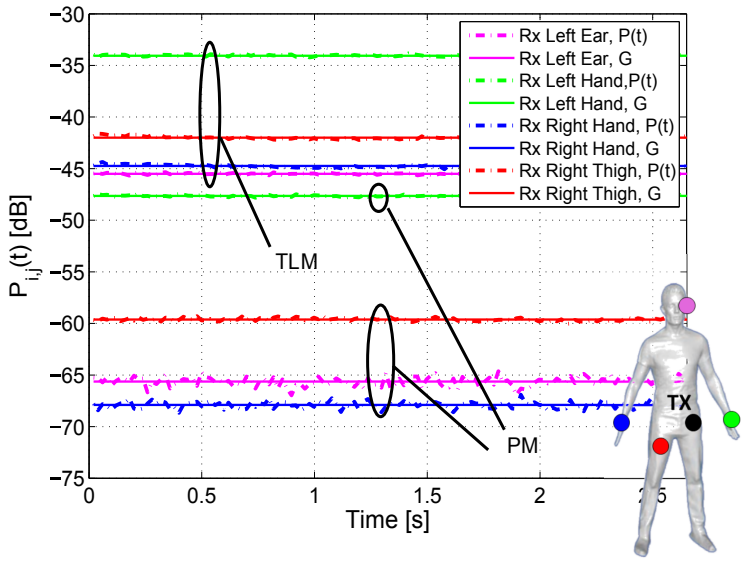

Figure 2.8: Comparison of $G_{i,j}$ values for the two antennas types: TLM and PM. Tx on left hip, anechoic chamber, standing still.

a more significant MPC leads to an additional energy contribution (i.e., larger *mean channel gains*). Antennas with normal polarization with respect to the body surface enhance on-body creeping waves diffusion, and hence the difference between the $G_{i,j}$ values in indoor and anechoic is less significant for TLM, as compared to PMs.

Finally, PMs present larger values of σ_0 with respect to those found for TLMs, probably indicating that the former are more influenced by the body presence, due the lack of a ground plane in the antenna design that can help in the reduction of the human body impact on channel variability.

2.3.2 Long- and short-term fading

The power transfer function, $P_{i,j}(t)$, can be also decomposed in a *long-term fading*, also known as *shadowing*, $S_{i,j}(t)$, and a *short-term* one, $F_{i,j}(t)$, as highlighted in Eq. 2.3.1.

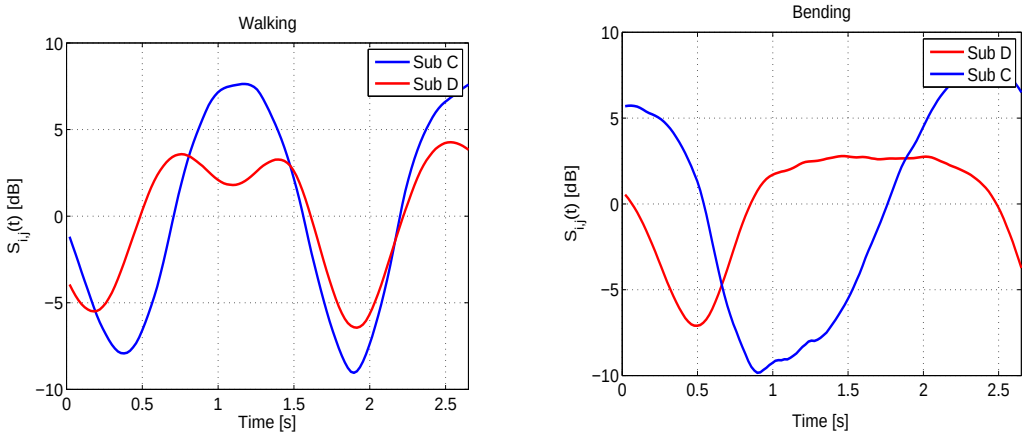

(a) (b)

Figure 2.9: *Shadowing* trends for two subjects performing two types of movements: walking (a) and bending (b). Tx chest, Rx left hand.

In classical wireless systems, the *long-term fading* normally accounts for the shadowing effect of some obstacles that obstruct the direct link between nodes. For the specific case of BANs in *on-body communications*, the definition of *shadowing* describes the condition where the human body itself acts as an obstacle to the main direct transmission path, which evolves according to the movement performed as presented in Fig. 2.6. This effect is particularly evident when one of the antennas is placed on a limb (hand or leg). The specific type of action, and the way in which each user performs it, affect the *shadowing* characteristics, as shown in Fig. 2.9 that compares $S_{i,j}(t)$ trends for two subjects (subjects C and D in Tab. 2.1) and two movements (walking in Fig. 2.9a and bending in Fig. 2.9b).

$S_{i,j}(t)$ is evaluated for each scenario $\mathcal{S}$, gathering the data of the whole population of human subjects. A low-pass filter, which is practically realised by averaging the recorded channel data over a sliding temporal window of 320 ms, is used to extract the *shadowing* contribution. The window size is empirically determined to allow the

extraction of smooth *shadowing* curves, able to accurately follow the slow variations of $P_{i,j}(t)$. It is kept unchanged for every subject, and it is chosen as to present the best compromise between the accuracy in the shadowing extraction and the variances in walking styles or average speeds of the test subjects.

Shadowing values in dB are statistically described by a normal distribution, $S_{i,j}(t) \backsim \mathcal{N}(0, \sigma_S)$, where the standard deviation σ_S accounts for the slow variations of $P_{i,j}(t)$ due to the body shadowing effect. As an example, Tab. 2.4 lists the σ_S values considering the Tx placed on user's chest. Results referring to the other Tx positions are reported in Appendix A.

Generally, PMs present larger values of σ_S as compared to those found for TLMs, meaning that they are more affected by the shadowing effect of the body and by its movement. Indeed, normally polarized antennas, helping creeping waves propagation around the body, present a dominant main path that overcomes the secondary paths generated by reflections on the body, resulting in a smaller *long-term fading* contribution.

Furthermore, the *shadowing* effect is generally less important in the indoor environment, since the propagation occurs also by reflections on the surrounding environment. This somehow mitigates the masking effect of the human body, resulting in smaller σ_S values than in the anechoic chamber.

Fig. 2.10 presents the evolution over time of the slow-varying component of $P_{i,j}(t)$ for the chest/left hand (circle marker) and hip/left hand links (triangle marker) for both the antenna types: in blue the PMs and in red the TLMs. Focusing on the

Table 2.4: σ_S values in dB - Tx on Chest

	Rxs	Anechoic		Indoor	
		PM	TLM	PM	TLM
Walking	Right Thigh	3.20	1.07	1.82	1.40
	Right Hand	4.34	3.46	2.99	2.57
	Left Hand	4.33	3.67	4.21	1.97
	Left Ear	0.97	1.06	1.96	1.50
Bending	Right Thigh	4.09	2.01	3.14	3.22
	Right Hand	3.13	2.15	4.42	3.85
	Left Hand	5.25	2.57	4.93	2.83
	Left Ear	1.15	1.12	2.39	0.90

curves referring to the chest/left hand link, both antennas types present approximately the same trend, with some slight differences possibly due to movement repetition mismatches. On the opposite, for the hip/left hand link, antennas behavior is completely different, up to the condition where PMs present better performance than TLMs. This comparison highlights the importance assumed by the node position on the definition of channel characteristics, jointly with the specifities of the radiating device.

As for the *short-term fading*, $F_{i,j}(t)$, it accounts for the effect of the MPC arising from reflections and diffractions on the human body and/or on the surrounding environment. Fig. 2.11 shows that $F_{i,j}(t)$ linear envelope values is well modeled by a Rice distribution, which is defined by its K-factor according to the expression: $K = \nu_F^2/(2 \cdot \sigma_F^2)$, where ν_F and σ_F are the non-centrality and scale parameters of Rice distribution, and K represents the ratio between the power associated to the direct path and the contribution coming from the MPC.

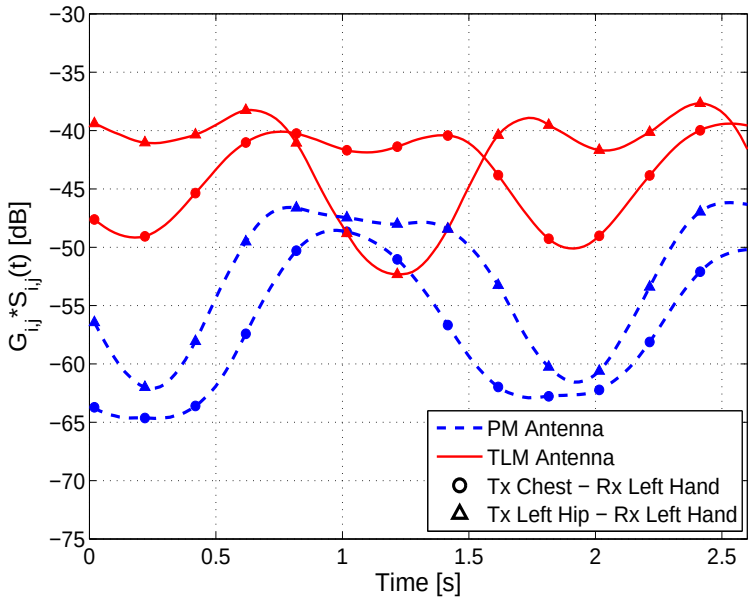

Figure 2.10: Slow-varying component of $P_{i,j}(t)$ for chest/left hand (circle marker) and hip/left hand (triangle marker) link. Blue curves refer to PM case, red ones to TLM.

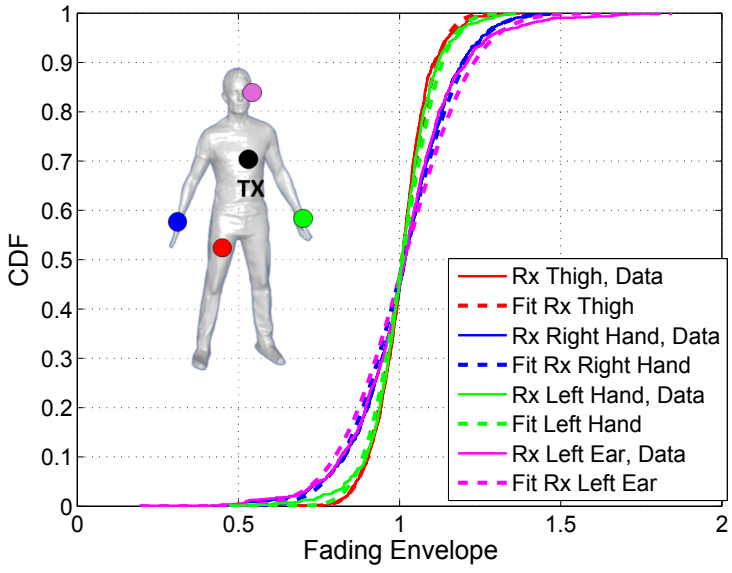

Figure 2.11: Cumulative Distribution Function of *short-term fading* amplitude: Tx on chest, indoor, TLM, walking.

Tab. 2.5 lists the results obtained based upon the Akaike Information Criterion (AIC) [162] applied to the experimental data for the case where the Tx is on user's chest when both antennas are used. LCR values in Hz, given with respect to a 0 dB threshold, are also reported. TLMs present larger K-factors as compared to PMs, meaning that the channel experiences smaller amplitude fading episodes. Higher K-factors are due to the presence of a main propagation path with stronger energy contribution, which confirms the hypothesis of an on-body creeping wave component enhanced by the use of TLMs. This difference is particularly relevant for the chest/thigh and chest/ear links, where the propagation happens mostly by diffraction on the body surface, and dissimilarities in antenna behavior are even more stressed. This trend is confirmed by the LCR, with larger values for PMs than for TLMs, meaning a more important and more frequent *short-term fading* contribution in the former case.

Table 2.5: Fast Fading Statistics - Tx on Chest - Indoor

	Rxs	**Planar Monopole**		**Top Loaded Monopole**	
		K	**LCR [Hz]**	**K**	**LCR [Hz]**
Walking	**Right Thigh**	3.03	9.06	69.75	5.56
	Right Hand	3.29	8.81	21.97	6.31
	Left Hand	5.87	8.06	54.67	5.81
	Left Ear	5.98	6.98	17.34	7.02
Bending	**Right Thigh**	9.84	5.60	34.08	4.09
	Right Hand	16.34	5.30	36.49	5.14
	Left Hand	15.86	5.47	45.72	4.60
	Left Ear	9.19	5.93	78.28	6.06

2.4 Conclusions

On-body radio channel characteristics are modelled starting from an experimental data base. Dynamic channel measurements were performed at 2.45 GHz in indoor and anechoic environments, employing two sets of antennas with different radiation features.

As a general consideration, the specific node position plays a central role in the definition of time-variant characteristics of the radio channel, in accordance with the movement performed by the user. This motivates the choice of pursuing a scenario-based approach for channel modeling, more than presenting it as a simple function of the distance between nodes.

The differences in antenna behavior are studied for each model component. As expected, antennas with normal polarization results in larger *mean channel gains*, as compared to tangentially oriented ones, since their radiation characteristics enhance creeping waves diffusion around the body, reducing the corresponding attenuation level.

The *fading* contribution is further modelled by two components, a *long-* and a *short-term* one, to account for different propagation phenomena. On one hand, the *long-term fading*, also known as *shadowing*, describes the masking effect exerted by the human body while obstructing the direct communication path according to the movement performed. On the other hand, the *short-term fading* accounts for the MPC arising from reflections and diffractions on the surrounding environment or on the body. The comparison of antennas behavior is particularly interesting for these two model components; indeed, normally polarized devices result to better counteract the

body masking effect, presenting smaller values for the *shadowing* standard deviation. They also show a weaker *short-term fading* contribution, witnessed by larger K-factor of the Rice distribution describing it.

Finally, to complete the characterisation of the *on-body* channel, its space and time correlation properties should be also investigated. Contributions available in literature on this topic are proposed in [8, 152, 155], but they usually do not consider several sources of channel variability, lacking in general applicability of the results. To fill this gap, some investigations have been recently performed by the author of this thesis in collaboration with the ICTEAM - Universitè Catholique de Louvain (UCL) and other collegues at CEA-Leti, studying space correlation properties of the *shadowing* component at 4.2 GHz. A comparison of the results obtained from two measurement campaigns (the one described in Sec.2.2.2 and a similar one performed at UCL) is part of the work. The preliminary outcomes available at the moment of writing are not reported here for the sake of soundness, more details can be found in [163].

Chapter 3

Radio Channel Modeling for On- to Off-Body Communications

Radio channel characterisation for *on-* to *off-body communications* is the focus of this chapter, proposing two separate experimental models describing the *off-body* and the *B2B* scenario, respectively. After a detailed insight on the most relevant related works available in literature (Sec. 3.1), the common frequency-domain test-bed used in the two measurement campaigns is described in Sec. 3.2.

Off-body channel is characterised in Sec. 3.3, describing each model component in which the power transfer function is structured. In particular, the *mean channel gain* contribution is detailed in Sec. 3.3.1, whereas Sec. 3.3.2 deals with the *short-term fading*. The shadowing effect of the body is also accounted for and it is referred to as *long-term fading*, which is described in Sec. 3.3.3. To complete the *off-body* channel description, its *space* and *time* correlation properties are presented in Sec. 3.3.4.

As for the *B2B* channel model proposed in Sec. 3.4, the description of the *mean channel gain* and of the *short-term fading* is given in Secs. 3.4.1 and 3.4.2, respectively, focusing on the specificities brought by the different investigated measurement scenarios. Finally, the *body shadowing* effect is analysed in Sec. 3.4.3.

3.1 Related Works

Even if *on-body communications* is a quite well investigated topic, *on-* to *off-body* scenarios have been just more recently approached by the research community. A more limited number of contributions is available in literature, and a large part of them is devoted to *off-body* scenarios, more than *B2B* ones.

Since dedicated investigations are needed to characterise the *off-body* and *B2B* radio channels, related works are presented in separate sections to highlight the distinctive studying approaches followed in these two cases.

Off-Body Communications

The emerging interest in *off-body* communications is witnessed by a dedicated channel characterisation available in the IEEE 802.15.6 channel model document [5]. The final version was released in 2010, and it focuses on the description of the propagation aspects for BANs in different communication scenarios. In particular, CM4 addresses the body surface to external scenario, presenting a path loss model for different operating bands (900 MHz, 2.45 GHz and lower UWB), extracted from some experimental measurements performed in indoor environment in static conditions. Details of the measurement set up, derivation and data analysis can be found in [164]. First and second order statistics of the recorded data are provided to complete channel characterisation.

One of the first contributions to the narrowband channel modeling for *off-body* communications is proposed by Ziri-Castro *et al.* in [165, 166]. The authors present a comparison between simulations and measured data in the 5.2 GHz band, for two

indoor scenarios. The measurements involved one fixed Tx and one Rx placed on the hip of a subject walking towards (Line-of-Sight (LOS)) and away (Non Line-of-Sight (NLOS)) the Tx, whereas the simulations were performed using a 3D image-based propagation prediction technique. First and second order small-scale fading statistics result to be well modelled by a Rayleigh or a lognormal distribution, according to the environment and measurement condition considered. The same group of authors also investigate the impact of the body presence on channel characteristics. Results presented in [167] show a reduction of the received power of approximately 10 dB due to the blocking effect of the body, which shadows the direct communication path between Tx and Rx. Considering more than one human subject at a time, they also found that the dynamic range and standard deviation of the received signals increase with the number of users. Densely populated environments and human effect on *off-body* links are the focus of other two papers [168, 169], where the authors perform measurements in the UWB at 5.8 GHz. Channels time delay parameters and cross-correlation coefficients between two co-located antennas are also provided, in order to assess the impact of using multiple antenna techniques to reduce users influence on radio channel.

Other experimental models investigating different frequency bands are available in literature. One of the most notable work is realised by Cotton *et al.* focusing on the 868 MHz band [170–172]. Dynamic acquisitions are performed considering several on-body node positions, different environments (i.e., anechoic chamber, open office, and hallway), and LOS and NLOS conditions. Data analysis highlights the importance of node position and body movement on the definition of channel characteristics. Nakagami distribution provides the optimum fit for the majority of the investigated

channels; indeed, differently from other distributions like Rice or Rayleigh, it does not assume scattered components of equal amplitude. Second-ordered statistics, as LCR and AFD, are also given. The cross-correlation level between the fading experienced at different body locations is also evaluated in [173]. The low values found suggest the idea that a spatial diversity combining scheme can significantly improve the overall system performance. This aspects is thoroughly investigated in [174], where authors show the real advantages of using receiver diversity techniques operating in Nakagami fading channels.

Similar experiments are presented in [175], authors perform a measurement campaign collecting real-time channel responses at the carrier frequencies of 820 MHz and 2.36 GHz. They consider a subject equipped with two antennas and standing still in front of an external node, just changing its orientation or performing a walk towards the outer device. Different statistics are compared to find the one that best describes the received signal amplitude. Overall, the lognormal distribution provides the most reliable fit for both the considered bands. A new parameter called channel variation factor is introduced as a measure of channel stability over time. *Off-body* channels turn out to be quite stable, more at 820 MHz than at 2.36 GHz, showing a coherence time of the order of tens of milliseconds, with on-body node position playing a significant role in the channel temporal stability features.

Another interesting frequency band envisaged for BAN applications is the ISM at 2.45 GHz, which is also the focus of the channel model presented in this work. Among the contributions available (e.g., [176,177]), one of the most exhaustive study is performed by Cotton *et al.* in [178]. Starting from an experimental data base acquired in anechoic premises, considering different movements performed by an user

with one bodyworn antenna, the authors model the channel path loss through a classical log-distance expression. When in NLOS conditions, two additional terms are considered to account for the shadowing effect of the body and for the fading caused by small movements, which results into long- and short-term signal variation, respectively. In the same frequency band, works by Van Torre *et al.* [179–182] investigate the Multiple-Input Multiple-Output (MIMO) communication possibilities to improve *off-body* channels reliability and system performance, while evaluating shadowing and fading correlation.

With respect to the models presented above, the one proposed in this thesis (see Sec. 3.3) gives a more general characterisation of the radio channel at 2.45 GHz, accounting for different sources of variability. In particular, the impact of the node position and of the environment is jointly studied. Static measurements are used as a benchmark for the dynamic ones. Similarly as presented in [178], a short- and a long-term fading contributions are extracted from the experimental data, but they are statistically characterised not just according to the measurements conditions (i.e., LOS or NLOS), but also according to the antenna type considered, highlighting the importance of their radiation characteristics on channel behavior. The *body shadowing* effect is also described as a function of the body orientation. Moreover, to the best of author knowledge, *space* and *time* correlation characteristics are jointly studied for the first time at 2.45 GHz in dynamic conditions, comparing the results for the two antennas.

Even if not directly comparable with the work proposed in this chapter, some studies have been performed to characterise the *off-body* UWB channel. UWB is one of the proposed IEEE 802.15.6 standard technology to be used in *body-centric*

communications, considering the great advantages it can bring in terms of multipath fading reduction, high data rates, and decreasing of the operative power. Goulianos *et al.* [183–186] propose a multi-slope dual breakpoint model, obtained from the study of propagation mechanisms around the body (creeping waves) combined with the traditional distance-dependent path loss equation. Based on measured data in anechoic environment, statistical channel parameters are extracted as a function of the distance between the user and the Tx, and of the body orientation. Power delay profile and time dispersion analysis are also performed. Other significant works in the UWB can be found in [187, 188] or in [189–191], where the importance of the node location, the specific environment and the device relative position (whether LOS or NLOS) play a fundamental role in the definition of radio channel modeling.

As a final comment, some interesting works have been recently published dealing with the investigation on *off-body* channels at 60 GHz for short-range indoor communications. The wide availability of spectrum around this frequency and the high data-rate achievable make it a promising alternative also for *body-centric* applications. Interested readers can refer to [192–194] for a more detailed insight on this topic.

B2B Communications

As for the *B2B* radio channel, only a limited number of contributions are available in literature, and just few of them propose a precise channel characterisation. For example, in [195, 196] Cotton *et al.* statistically describe just the small-scale fading observed in dynamic conditions, using a k-μ distribution. Results are obtained from the analysis of experimental data collected in indoor premises at 2.45 GHz, while users performed some random walking movements simulating fire rescue operations.

Second-order parameters are provided to complete channel description. Considering the low cross correlations values found and comparable mean signal levels of received signals, the idea of using spatial diversity to improve channel performance is also proposed.

Similar considerations on diversity are presented in [197, 198], even if measurements are carried out wideband at the carrier frequency of 5.5 GHz in indoor environment. Starting from the classical distance-dependent path loss model, the authors highlight how the body shadowing is a prominent factor in *B2B* communications considering an additional lognormal variable accounting for its effect. Generally, path loss exponents result to be smaller than 2 in indoor.

Another work [199] focuses on the comparison of indoor channel characteristics at 2.45 GHz and 5.8 GHz. Few node positions are investigated and random movements are performed by the users during the acquisitions. Short- and long-term fading components of the path gain envelope are separated, and they are independently described by a Rice and a gamma (or a lognormal) distribution, respectively. Second-order statistics are also provided, with smaller AFD and larger LCR at 5.8 GHz than at 2.45 GHz.

Focusing just on the ISM band at 2.45 GHz, the works in [200] and [2] investigate the outdoor channel, performing several dynamic acquisitions in different communication conditions. The model is given in terms of log-distance path loss, body shadowing and small scale fading, but just few node positions are accounted for. Indoor small-scale fading at the same frequency is statistically characterised in [201], where authors demonstrate the high impact of local operating environment on channel characteristics when in LOS conditions.

An UWB channel characterisation can be found, for example, in [202]. Authors provide a characterisation for the path loss in static conditions and for different subject orientations, showing that it is strongly related to the node on-body position as well as to the subject relative orientation.

The model proposed in this thesis (see Sec. 3.4) aims at providing a general framework to characterise the most important feature of the *B2B* channel. The novelty introduced lies in the fact that several sources of variability are taken into account, and their impact is properly highlighted for each of the model component. Similarly to what proposed in [200], the channel power transfer function is described by a mean channel gain and a fading contribution, the latter being further decomposed in a short- and a long-term component. Different node positions are investigated and two antennas are used in the measurements to account for their effect on channel behavior. Several dynamic communication scenarios are reproduced to broaden the application possibilities of the proposed model, considering that a specific movement leads to peculiar time-variant channel characteristics. To the best of author's knowledge, for the first time in literature the body shadowing effect is described as a function of the body orientation through a gaussian mixture distribution.

Other works study the *B2B* radio channel from a different perspective. For example, works in [70, 203–205] deal with the characterisation of inter-user interference brought by nearby BANs in terms of Signal-to-Interference Ratio (SIR), which can highly impact system transmission reliability. All these studies show the importance of body presence and its orientation in the definition of inter-body channel characteristics. In particular, in [205] authors propose a solution to mitigate the interference problem using a fixed network infrastructure to monitor those BANs that are more

likely to interfere with each other. Another solution is also suggested in [68], where diversity brought by MIMO technique is exploited not only for interference rejection, but also to increase channel capacity. The same topic is also discussed in [206], where the impact of two antenna designs on channel capacity is compared and discussed.

3.2 *On-* to *Off-Body* Channel Measurement Campaigns

As for the characterisation of the *off-body* and *B2B* channels, some preliminary tests pointed out the occurrence of significant attenuations in channel gains, with fading episodes possibly yielding to very low link budgets, up to -100 dB. This phenomenon is particularly evident when the communication takes place in NLOS conditions, i.e., when a receiving antenna is masked from the transmitting one by the human body. For this reason, the use of an oscilloscope to perform channel measurements would not be useful, due to the limited signal dynamic of this device. Hence, a more specific test-bed is set up to overcome this problem.

3.2.1 Channel Measurement Test-bed

The solution adopted is common to both the *off-body* and the *B2B* measurement campaigns; differences are stated where needed. As shown in Fig. 3.1, the frequency-domain test-bed is mainly composed by a Rohde&Schwarz ZVA24 4-port Vector Network Analizer (VNA) [207]. It operates in Continuous Wave (CW) mode at the frequency $f_0 = 2.45$ GHz, allowing the simultaneous acquisition of the S-matrix parameters, one for each link composed by the i-th Tx and the j-th Rx. The observation

time T_{obs} is set to 5 s in the *off-body* case and 10 s in the *B2B* one, with a common sampling rate of 2 ms. This resolution is considered to be appropriate in order to follow the dynamic variations of channels due to body movements, given an expected average human speed in common activities in the range between 0.5 and 2 m/s. A total number of sampled points per acquisition $N_p = 2501$ is available for each link in the *off-body* scenario, whereas for the *B2B* case N_p is equal to 5001. For both measurement campaigns, Tx power is set to +18 dBm (the maximum available at the VNA), considering an Intermediate Frequency (IF) bandwidth of 1KHz. To complete

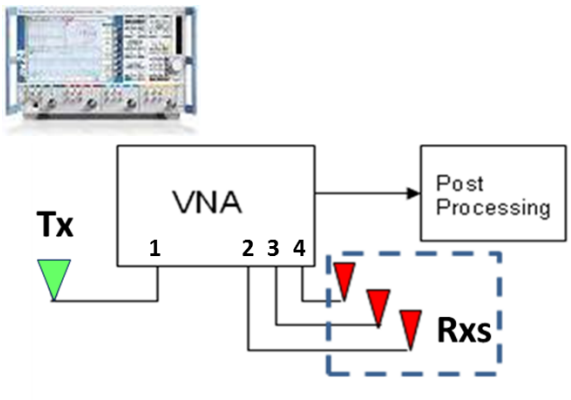

Figure 3.1: Measurements test-bed for *on-* to *off-body* channel investigations.

the test-bed description, low attenuation RF cables and antennas are also part of the set up. Since the same sets of antennas used in the *on-body* measurement campaign are also considered for these acquisitions, the reader is referred to Sec. 2.2.3 for more details on their radiation characteristics. As for the RF cables, their effect is deconvoluted directly from the acquired channel data through a proper configuration of the calibration VNA settings. As in the *on-body* measurement campaign, also in this case their impact is reduced by connecting them as to be orthogonally oriented with respect to antennas main polarization, and the use of ferrite beads helps in preventing

possible damaging interferences.

3.2.2 *Off-Body* Measurement Scenarios

As discussed in the Introduction, *off-body* scenarios refer to the case where the communication takes place between at least one device placed on a human body and another one outside it, generally static, acting as a gateway or a router to other communication systems (e.g., a Wi-Fi Access Point (AP) to connect to the Internet).

To characterise these type of channels, the experimental test-bed described above is used in a 1:3 configuration, with one transmitting and three receiving devices (see Fig. 3.1). In this way, three channel transfer functions are simultaneously recorded, each one referring to one of the available (i, j) links. Fig. 3.2 shows the nodes emplacement considered: the external Tx is mounted on top of a 1.2 m high mast (i.e., at chest level), whereas Rxs are placed on different on-body positions on a male subject (1.8 m tall and 73 kg in weight). In particular, Rx1 is on the left hip, Rx2 on the chest and Rx3 on the right ear position, the latter hosted in a side pocket of a hat worn by the subject.

Nodes positions are chosen having in mind possible medical and non medical applications; for example nodes on the ears emulate device emplacement for cochlear implants or general hearing instruments to be used in gaming or video streaming applications. Hand positions, instead, could be a possible location for a smart phone or a PDA [208], as well as being representative of a smart watch or an item tracking device carried around by an user.

Measurements are performed both in anechoic chamber and in an indoor laboratory, the latter equipped with some technical furniture.

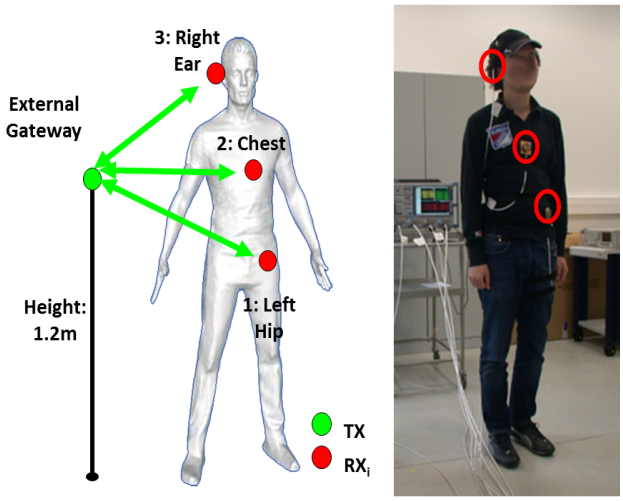

Figure 3.2: Node emplacement for *off-body* measurements.

In order to characterise different aspects of the radio channels, four scenarios are investigated as shown in Fig. 3.3:

I. Experiments are performed while the subject stands still at fixed distances d from the Tx, from 1 m up to 4 m far from it, with steps of $\Delta d = 2\lambda$ (i.e., 25 cm at 2.45 GHz). Acquisitions are repeated while the user alternatively faces the Tx (LOS case), or turning his back to it, in a way that his body shadows the direct communication link between the on-body devices and the external one (NLOS case).

II. The subject performs ten walking cycles over a distance of 3 m, from $d = 1$ m up to $d = 4$ m from the Tx. In the first 5 experiments he walks towards the external device (LOS), whereas in the other 5 he walks away from it (NLOS).

III. Acquisitions are realised for different body orientation α, where α is the relative angle set up between the front side of the body and the external Tx. Considering

the user standing at $d = 2$ m from the outer device, measurements are repeated for every $\Delta\alpha = 45°$ completing a clock-wise rotation, from LOS ($\alpha = 0°$) to NLOS ($\alpha = 180°$) before returning to a LOS condition.

IV. The user performs some continuous clock-wise rotations at different distances d from the gateway: 2, 3, and 4 m, respectively. Acquisitions are repeated 3 times at every d, considering an average angular speed of $70°/s$ ($360°/T_{obs}$).

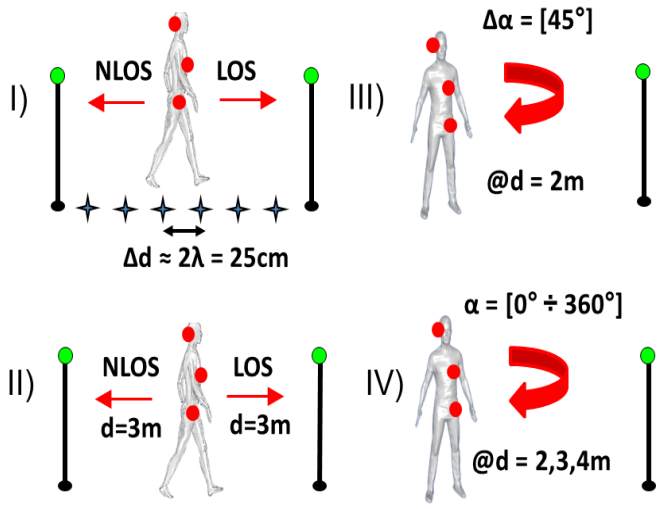

Figure 3.3: Measurement scenarios for *off-body* channel investigations.

Considering the set of acquisitions performed, the number of sampled points per link is in the order of 10^3 for scenarios *I* and *III*, and in the order of 10^4 for scenarios *II* and *IV*, both in anechoic and indoor. This is considered as a consistent data base to extract a statistical characterisation of the radio channel.

3.2.3 *B2B* Measurement Scenarios

B2B communications take place when the devices involved are placed at least on two different human bodies, free to move around. The same frequency-domain test-bed described for the *off-body* case is used here, but nodes emplacement and measurement scenarios should be properly adapted.

Four human subjects, sorted by couple and with different physical characteristics (same as in Tab. 2.1), are involved in the measurements. Every couple is composed of one subject, *subA*, wearing all the Rxs, whereas the other one, *subB*, hosts the Tx, which is placed in one out of three possible positions, as shown in Fig. 3.4. Rxs are connected to three VNA's ports and they are located at the same time on the left ear (hosted in a side pocket of a hat worn by the subject), on the chest, and on the right hip on *subA*'s body. The Tx is placed alternatively on *subB*'s left thigh, right hip, or right hand. Measurements are performed just in a furnished (15x13) m^2 room.

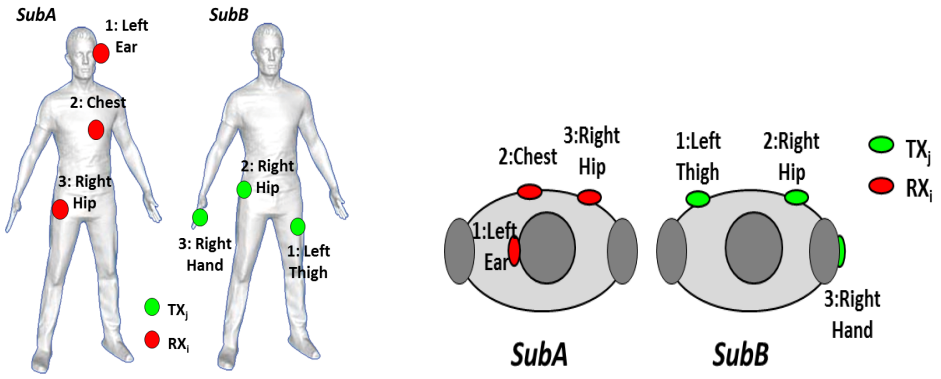

(a) (b)

Figure 3.4: Nodes emplacement for B2B channel measurements: front (a) and top (b) view.

Four scenarios are investigated in order to account for different users positions and movements, as shown in Fig. 3.5:

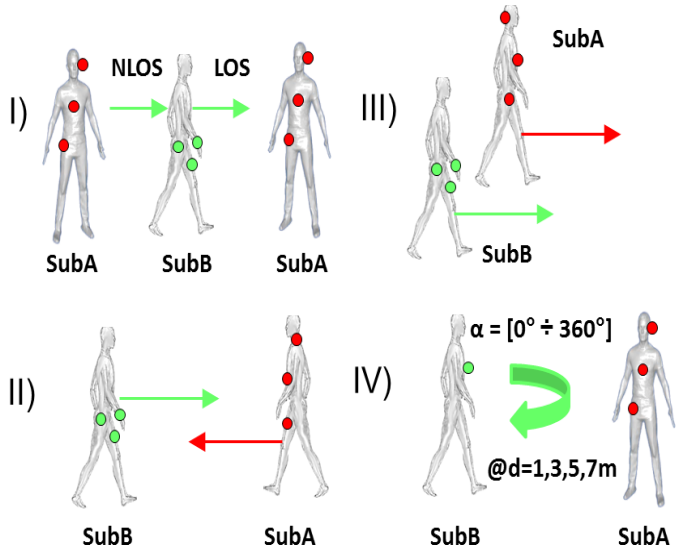

Figure 3.5: Measurement scenarios for *B2B* channels investigations.

I. Walking: *subB* performs some walking cycles forwards and backwards *subA*, who is standing still at one end of the room. Hereafter, the former case will be referred to as LOS, considering that no obstacle shadows the direct link between the two subjects, whereas the latter will be defined as NLOS, because *subB*'s body completely masks the main communication path while walking away from *subA*. The distance covered by *subB* is 8 m and acquisitions are repeated four times per couple, twice in LOS and twice in NLOS.

II. Opposite Walk - from LOS to NLOS: starting from opposite ends of the room at a distance $d = 8$ m, *subA* and *subB* walk one towards the other, meeting approximately in the middle of the path. They continue their movement walking away from each other, until they reach the position formerly occupied by the

other subject. In that way, an initial LOS condition gradually turns into a NLOS one, merging in just one scenario the two that are separately investigated in measurements set *I*. Acquisitions are repeated four times per couple.

III. Parallel Walk - walking side by side: *subA* and *subB* stand one next to the other separated by 40 cm, walking in parallel over a distance of 8 m. Acquisitions are repeated four times per couple. Mutual position of users is shown in Fig. 3.4b, from a top-view perspective.

IV. Rotation: *subB* performs some rotations in front of *subA*, moving from $\alpha = 0°$ (LOS) to $\alpha = 180°$ (NLOS), before returning to a LOS condition. α is defined as the angle between the front sides of the two subjects' bodies. Experiments are repeated four times per couple at different distances d from *subA*: 1, 3, 5, and 7 m, respectively. For this set of acquisitions the Tx is placed only on the chest on *subB*'s body.

For every investigated scenario, more than 360.000 measured channel responses are acquired, which are considered to be a sufficient base for statistical analysis and channel modeling.

3.3 *Off-Body* Channel Modeling

The proposed *off-body* experimental channel model describes each power transfer function in dB, $P_{i,j}(d, \alpha)$, according to the following expression:

$$P_{i,j}(d, \alpha) = |H_{i,j}(t, f_0)|^2 = G_{i,j}(d, \alpha) + F_{i,j}(d, \alpha); \quad [\text{dB}] \tag{3.3.1}$$

where d is the distance separating the external Tx and the user, while angle α

describes the orientation of the front side of the subject with resect to the gateway. $H_{i,j}(t, f_0)$ is the channel transfer function given by the sampled S-matrix parameters acquired for each (i, j)-th link by the VNA working at $f_0 = 2.45$ GHz.

$G_{i,j}(d, \alpha)$ represents the *mean channel gain*, whereas $F_{i,j}(d, \alpha)$ is defined as the *short-term fading* component, a random variable accounting for the MPCs originating from the environment or from the body itself.

A *long-term fading* contribution, $S_{i,j}(d, \alpha)$, can be also extracted from the channel power transfer function, following the slow variations of $G_{i,j}(d, \alpha)$ over its mean value according to:

$$G_{i,j}(d, \alpha) = \overline{G_{i,j}(d)} + S_{i,j}(d, \alpha); \quad [\text{dB}] \tag{3.3.2}$$

where $\overline{G_{i,j}(d)}$ is defined as $\overline{G_{i,j}(d)} =< G_{i,j}(d, \alpha) >_\alpha$ and it represents the average over α of the *mean channel gain*.

$S_{i,j}(d, \alpha)$ is referred to also as *shadowing*, since it accounts for the masking effect of the body on the direct communication path between devices, given its orientation according to the movement performed.

Next sections describe each model component according to the specific scenario, and showing the impact of movement, node position, and antenna type on the definition of channel characteristics. In this case, the scenario $\mathcal{S}$ is defined by the Tx/Rx position, the environment considered, the antenna used, and the movement performed.

From here on, subscripts *(i,j)* will be omitted for the sake of readability, implying that the analysis is performed for each possible combination of the i-th Rx and the Tx (as shown in Fig. 3.2), and the underlying reciprocity of the radio channel.

3.3.1 Mean Channel Gain

Starting from the measurement set I described in Sec. 3.2.2, the *mean channel gain*, $G(d, \alpha)$, is characterised through a Root Mean Square Error (RMSE) fitting of the experimental data. The distance-dependent *mean channel gain* can be expressed as:

$$G(d, \alpha) = G_0(d_0, \alpha) - 10 \cdot n(\alpha) \cdot \log_{10}(d/d_0); \quad [\text{dB}] \tag{3.3.3}$$

where $G_0(d_0, \alpha)$ is the mean channel gain evaluated at the reference distance $d_0 = 1$ m, whereas $n(\alpha)$ is defined as the path loss exponent.

Fig. 3.6 presents an example of the analysis performed in LOS conditions for TLM antennas. It is shown the good agreement between the log-distance fits (i.e., the continuous curves) and the experimental data represented by the vertical sets of crosses, acquired at each d. Each color refers to a specific on-body node position. It can be noticed that the dispersion of the recorded samples at a specific d is very limited, since measurements are performed in anechoic chamber and the only source of channel variability is related to the breathing movement of the subject.

Tabs. 3.1 and 3.2 list the values obtained for the two antennas types in every scenario $\mathcal{S}$. As shown, the distance-based modeling approach presented through Eq. 3.3.3 is used both in LOS ($\alpha = 0°$) and NLOS ($\alpha = 180°$). Anyway, since the limited distance interval considered in the experiments (i.e., approximately 3 m), the NLOS case results more in an attempted modeling of the *mean channel gain* variation over distance, and it should be considered less significative than the one in LOS.

First of all, it should be mentioned that anechoic chamber measurements allows to reproduce the ideal free space conditions. Hence, the path loss exponent should be ideally equal to $n_0 = -2$, whatever the orientation and the antenna emplacement

Table 3.1: *Mean Channel Gain* Characterisation for Planar Monopoles

	Anechoic Chamber				**Indoor**			
	LOS		**NLOS**		**LOS**		**NLOS**	
	$n(0°)$	$G_0(d_0, 0°)$	$n(180°)$	$G_0(d_0, 180°)$	$n(0°)$	$G_0(d_0, 0°)$	$n(180°)$	$G_0(d_0, 180°)$
Rx Right Ear	-2.2	-63.48	-2.2	-51.69	-1.47	-50.24	-0.69	-53.43
Rx Chest	-1.99	-41.75	-1.8	-72.46	-2	-38.92	-0.4	-62.62
Rx Left Hip	-1.61	-50.11	-0.9	-69.09	-2	-51.94	-0.1	-68.78

Table 3.2: *Mean Channel Gain* Characterisation for Top Loaded Monopoles

	Anechoic Chamber				**Indoor**			
	LOS		**NLOS**		**LOS**		**NLOS**	
	$n(0°)$	$G_0(d_0, 0°)$	$n(180°)$	$G_0(d_0, 180°)$	$n(0°)$	$G_0(d_0, 0°)$	$n(180°)$	$G_0(d_0, 180°)$
Rx Right Ear	-2.18	-45.14	-2.07	-45.82	-1.62	-45.7	-2.96	-46.03
Rx Chest	-2.44	-49.11	0	-71.42	-1.37	-54.71	0	-66.33
Rx Left Hip	-1.83	-43.99	0	-66.48	-1.99	-47.67	-0.59	-61.33

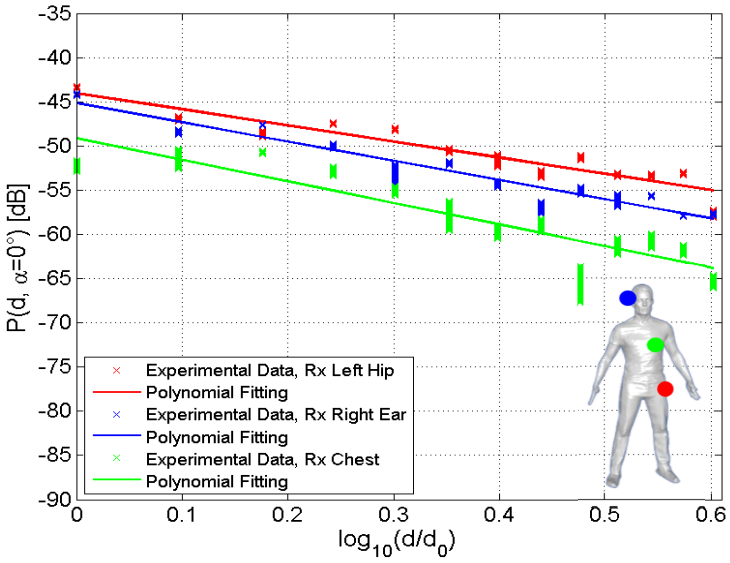

Figure 3.6: Polynomial fitting of $G(d, \alpha)$ to the experimental data. Anechoic chamber, LOS, TLMs.

considered. This is the case for the anechoic results shown in Tabs. 3.1 and 3.2, which present $n(\alpha)$ values close to -2, except for just few scenarios. These exceptions can be explained considering that results obtained in anechoic chamber are strictly dependent on the way measurements are performed, and on the fact that a real human subject was used during the process. Moreover, the on-body antenna exact orientation with respect to the off-body one is somehow affected from the subject's behaviour, who cannot naturally stand a precise orientation from one measured spot to the other. Therefore, the real measured antenna angle could involuntarily change over the desired value, and recorded path loss values can be affected by this measurement methodology.

This effect is particular evident when the on-body antenna is oriented towards the off-body one in the zero of its radiation pattern, and a strong masking effect by the body is present, such as in TLM NLOS chest and hip scenarios (see Tab. 3.2). In

these cases, very small involuntary variations of the subject orientation can change the angle seen by the antenna, with a consequent variation of the path loss around its mean value due to the variation of the radiation pattern itself in that angle range. The direct consequence is that, over the distance covered by the measurements, the path loss is quite constant, which results into a path loss exponent close to 0.

Similar considerations can be done for the PM LOS scenario for the hip position (see Tab. 3.1). In this case, antenna's off- and on-body polarizations are not aligned, and measurements account for the cross-polarization of the on-body antenna at different distances, whose pattern can strongly change over the angle range around the main propagation direction.

It has to be noticed that if acquisitions were performed on a rigid human phantom automatically displaced and rotated in anechoic chamber, measurements would have resulted into a sum of three contributions: the on-body antenna gain pattern in the angle and polarization considered, the free space attenuation ($n_0 = -2$), and the off-body antenna gain pattern in the angle and polarization considered. However, the aim of this work was not to measure the on-body antenna radiation pattern, as it could has been done with a human phantom and precise antenna measurement premises, respecting the far field conditions considering the body size. The objective of anechoic chamber measurements was here to model the *off-body* channel (over a limited distance range), in a scenario whose characteristics could be close to an open-field outdoor environment, and quite different from the indoor one, to be used for system performance evaluation.

As for the indoor LOS case, the environment significantly affects channel characteristics due to an additional energy contribution coming from the secondary MPCs,

the latter arising from reflections or diffractions from the environment. As shown in Fig. 3.7, irrespective from the antenna type (PMs on the left and TLMs on the right), indoor data are largely dispersed as compared to those in Fig. 3.6, resulting in a higher variability of $n(\alpha)$ values around n_0 (see Tabs. 3.1 and 3.2).

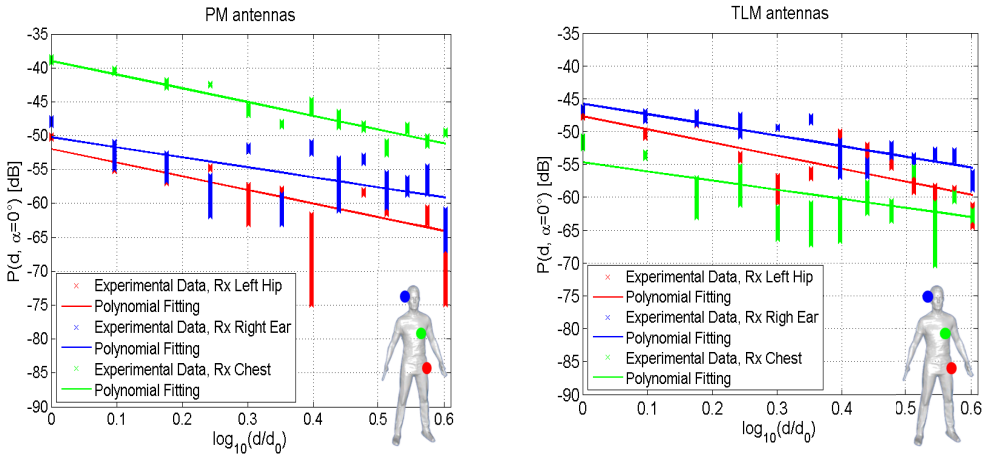

(a) (b)

Figure 3.7: Polynomial fitting of $G(d, \alpha)$ to the experimental data. Indoor, LOS: a) PMs, b) TLMs

The comparison of Fig. 3.7a and Fig. 3.7b also highlights the importance of antennas polarization characteristics on channel behavior. Considering the node on the chest (i.e., green curves), when TLMs are used they show a null radiation path in the main propagation direction towards the external Tx, which is placed exactly at the same level (see Sec. 3.2.2). This results in a larger dispersion of the data and in smaller *mean channel gains* with respect to the values for PMs. Indeed, the latter present a non-null radiation pattern in the same direction, instead. Similar consideration, but with exchanged antennas roles, applies for the ear node. In this case, PMs (not TLMs) show a radiating zero-direction in the main propagation path.

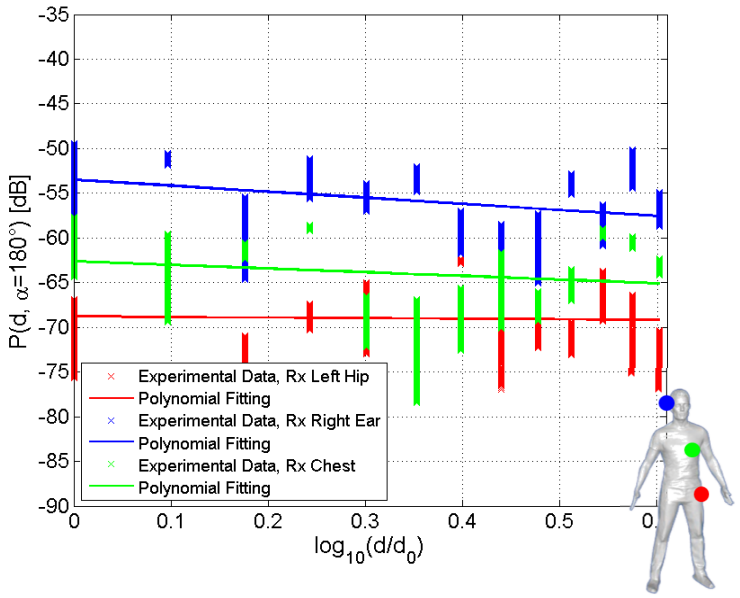

Figure 3.8: Polynomial fitting of $G(d, \alpha)$ to the experimental data. Indoor, NLOS, PMs.

As for the NLOS case, it presents a significant dispersion of channel data, up to 10-12 dB in indoor, as shown in Fig. 3.8. Differently from the classical indoor channel model [209], in *body-centric communications* the NLOS condition corresponds to the case where the human body completely masks the direct communication link between devices. The propagation happens thanks to the combination of two components: a main direct path travelling in free space (i.e., from the user's body to the *off-body* node), plus a creeping waves contribution propagating around the body surface [161] to reach the masked device, overcoming the shadowing effect of the body. This description applies to the case where propagation happens in free space conditions, and the body presence is the main factor affecting channel characteristics and propagation mechanisms in NLOS. Considering that measurements are taken also in indoor, an additional component shall be considered to account for the multipath effect that arises

from reflections and diffractions from the surroundings (walls, objects, furniture, etc.) and from the body itself. Hence, the more important secondary MPCs contribution in NLOS results in a stronger channel variability, as compared to the LOS case. As a consequence, $n(\alpha)$ values result quite small, typically around 0, as shown in Tabs. 3.1 and 3.2. This means that, at least for the distances considered in the experiments, the additional randomness brought by secondary paths contribution globally reduces the distance dependence of the *mean channel gain* (see Fig. 3.8). Moreover, it shall be considered that the subject's body proximity can affect antenna's radiation pattern, causing distortions that possibly affect propagation phenomena, especially when in NLOS. These considerations do not apply for the ear node, which presents $n(180°)$ values significantly different from 0. Indeed, for this position the NLOS condition does not correspond to a complete shadowing by the body, but just to an inversion from one side of the head to the opposite (i.e., from right in LOS to left in NLOS). It is also interesting to notice that the same node presents $n(0°) \neq n(180°)$ when in indoor, highlighting the different impact of the environment on channel characteristics; indeed, LOS and NLOS corresponds to specific source of multipath interference (opposite sides of the room). This is not the case for the anechoic chamber, where similar $n(\alpha)$ values are found (see Tabs. 3.1 and 3.2).

The body effect is also witnessed by the significant decreasing of $G_0(d_0, \alpha)$ values (up to 31 dB in anechoic), when the user moves from LOS to NLOS. This phenomenon is observed both in anechoic and in indoor, but less evident in the latter case due to the more important secondary MPC contribution, mitigating this effect.

Results presented in Tabs. 3.1 and 3.2 show also that the specific node position and the antenna type play an important role in the definition of channel characteristics.

In particular, for a node placed on the user's chest or hip, TLMs present a null radiation path in the LOS communication direction, which results in large channel attenuations. This is not the case for a node placed on the ear, where TLMs show a non-null radiation pattern both in LOS and NLOS, explaining also why $G_0(d_0, \alpha)$ assumes similar values in these two conditions (see Tab. 3.2).

On the contrary, PMs present a null radiation pattern in LOS when the antenna is located on the ear and a non-null one for the other two investigated positions. This results in opposite trends for the $G_0(d_0, \alpha)$ values, with respect to what is obtained using TLMs.

From the results presented, it is very difficult to state which is the most suitable antenna type to be used in *off-body* communications. Indeed, their behaviour in terms of *mean channel gain* is too related to the combination of radiation characteristics, on-body node position, and subject orientation. Anyway, normally polarized antennas generally show to be less affected by the presence of the human body, and the passage from a visibility to a non-visibility condition (i.e., from LOS to NLOS) is less sharp than with tangentially oriented devices.

3.3.2 *Short-term* Fading

The *short-term fading*, $F(d, \alpha)$, is extracted from measurement set *II* described in Sec. 3.2.2. Fig. 3.9 shows the good agreement between these dynamic acquisitions and the fit for the *mean channel gain* extracted as described in the previous section.

As presented in Fig. 3.10 for the NLOS case, the overall best fit to the linear envelope of $F(d, \alpha)$ is given by a Nakagami distribution. The choice is based upon the maximized log likelihood derived from the maximum likelihood parameter estimation

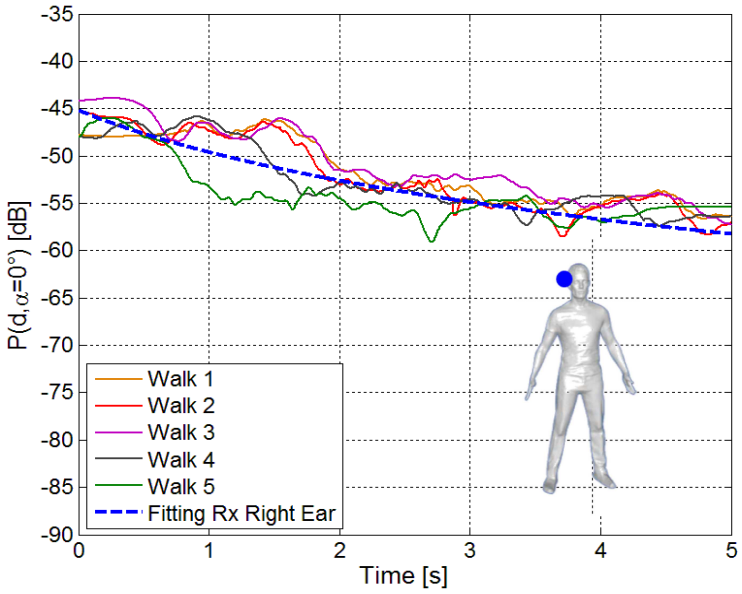

Figure 3.9: Comparison between the fit for $G(d, \alpha)$ and dynamic acquisitions. Rx Right Ear, Anechoic Chamber, LOS, TLMs.

(MLE) applied to the experimental data. Nakagami statistic is defined through a shape (μ) and spread (ω) parameter, whose values are listed in Tab. 3.3 for all possible scenarios $\mathcal{S}$, along with the LCR values in Hz, the latter defined as the average rate at which the small-scale fading falls below the 0 dB level (i.e., a fading episode).

For both antennas, moving from anechoic to indoor results in a more significant secondary MPCs, due to the influence of the surrounding environment. As a consequence, Nakagami *short-term fading* statistics shows smaller values of μ. Same considerations also apply when moving from LOS to NLOS conditions, where the main propagation path is reduced by the shadowing effect of the human body. To confirm this, the fading rate results sensibly higher in indoor than in anechoic or in NLOS than in LOS (see Tab. 3.3).

$F(d, \alpha)$ values for the ear link differ from the other ones since both in LOS and NLOS case the node is not shadowed by the body, but it corresponds to a reciprocal

Table 3.3: Fading Statistics for *off-body* channels

		Planar Monopoles						Top Loaded Monopoles					
		LOS - (α=0°)			NLOS - (α=180°)			LOS - (α=0°)			NLOS - (α=180°)		
	Rxs	μ	ω	LCR $[Hz]$	μ	ω	LCR $[Hz]$	μ	ω	LCR $[Hz]$	μ	ω	LCR $[Hz]$
Anechoic	Right Ear	1.04	0.66	2	7.62	1.66	0.75	5.83	1.34	1.3	9.96	1.14	2.35
	Chest	12.02	1.52	0.5	1.42	2.02	7.7	2.74	1.08	1.05	1.15	1.88	1.75
	Left Hip	11.43	1.04	1.35	5.28	2.12	0.8	4.68	0.81	1.5	0.82	0.8	2.1
Indoor	Right Ear	2.11	0.98	4.3	1.24	2.09	4.55	2.15	0.76	3.4	1.46	2.1	4.15
	Chest	5.48	0.73	1.65	0.81	1.12	5.35	1.28	1.45	3.2	1.02	1.79	6.25
	Left Hip	2.61	2.06	2.75	0.92	1.91	6.25	1.46	1.49	3.3	1.02	1.22	5.95

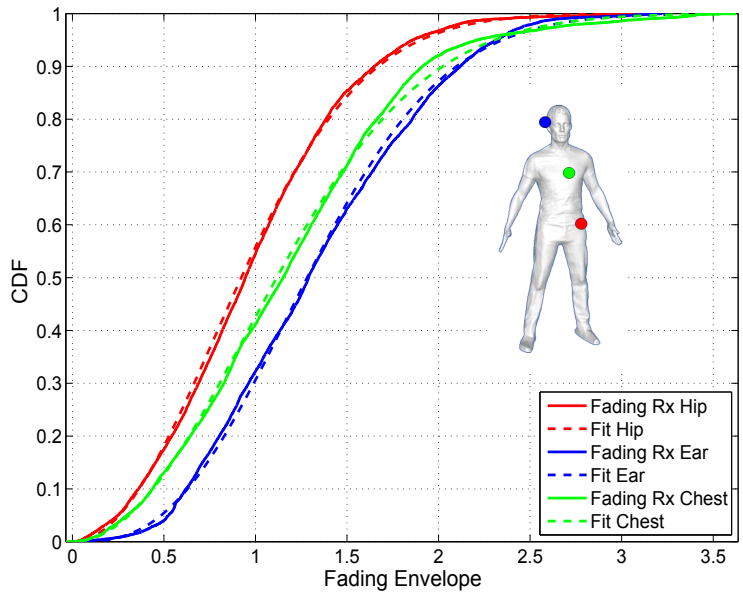

Figure 3.10: Cumulative Distribution Function of $F(d, \alpha)$ linear envelope. Indoor, NLOS, TLMs.

position on the head side (i.e., right and left side, respectively).

3.3.3 Body Shadowing Effect

The last channel model component that has to be studied is the *long-term fading* $S(d, \alpha)$ (see Eq. 3.3.2) also known as *body shadowing*. Starting from the data acquired in measurements set *III* (Sec. 3.2.2), Fig. 3.11 shows the evolution over α of the *body shadowing* effect for PM (left) and TLM (right) antennas, where the vertical sets of crosses represent the channel data acquired at every α. Each color refers to a specific on-body node position, and the dashed lines connect the mean values of each group of acquisitions. Comparing Fig. 3.11a and Fig. 3.11b, highlights the different behaviors of antenna type, according to the specifities of their radiation patterns.

The *body shadowing* effect is given at each α as the variation of $P(d, \alpha)$ data

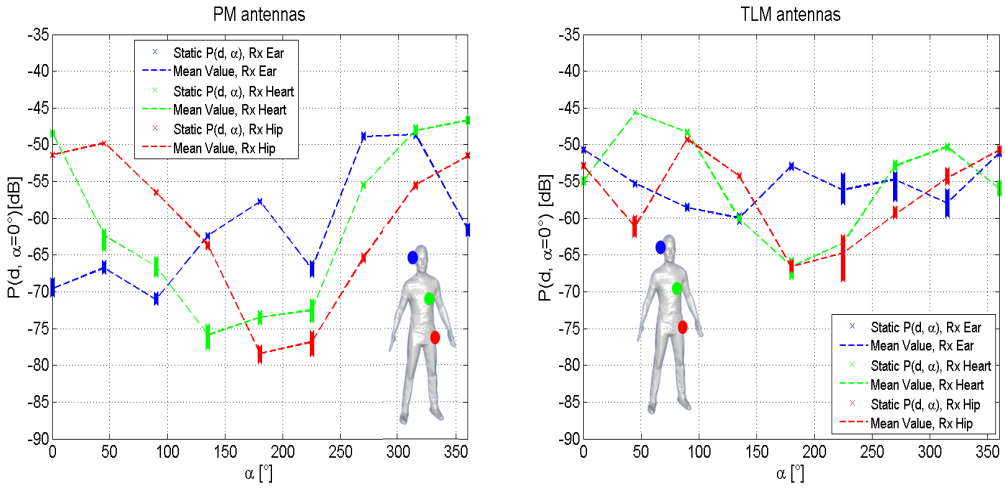

(a) (b)

Figure 3.11: *Body shadowing* evolution over α for different on-body node positions in anechoic chamber: a) PM, b) TLM.

with respects to the reference ones for $\alpha = 0°$. It is characterised by its maximum, mean, and standard deviation values expressed in dB, normalised to the reference. Tab. 3.4 lists the results obtained with both antennas considering the node placed on subject's chest. Similar values are also found for the other links and in anechoic conditions, but they are not reported here for the sake of briefness (see Appendix B).

Table 3.4: *Body Shadowing* Effect Characterisation in dB - Rx Chest - Indoor

		0°	**45°**	**90°**	**135°**	**180°**	**225°**	**270°**	**315°**
Max	**TLM**	-	10.15	8.34	-1.03	-0.66	0.77	8.03	9.21
	PM	-	-2.4	-9.41	-25.68	-23.33	-15.84	-20.81	-11.57
Mean	**TLM**	-	11.41	9.88	0.84	0.41	2.48	9.8	10.74
	PM	-	-2.77	-9.5	-27.34	-24.99	-17.03	-22.77	-12.4
Std	**TLM**	1.79	0.61	0.86	0.46	1	0.41	0.55	0.71
	PM	0.2	0.49	0.28	1.6	1.39	0.81	1.3	1.03

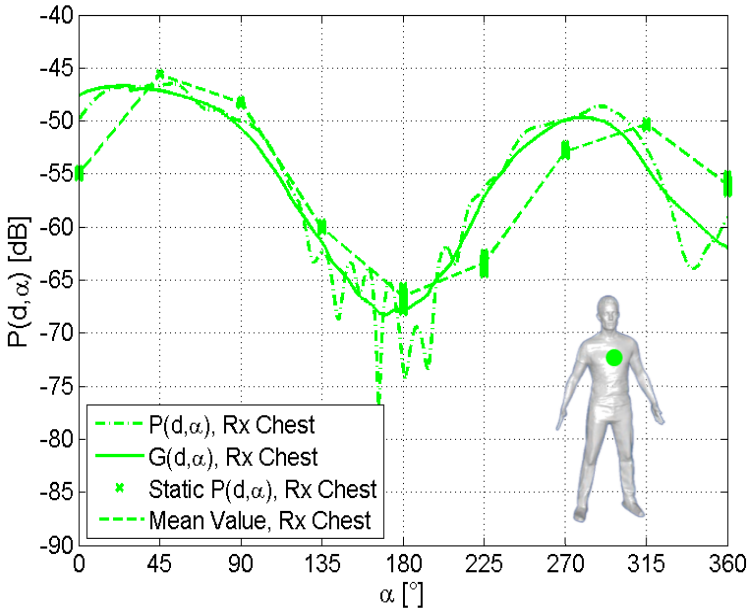

Figure 3.12: Dynamic vs. static acquisitions: *body shadowing* effect evolution over α. Rx on chest, anechoic chamber, TLM.

Comparing PMs and TLMs results confirms their different behavior in terms of *body shadowing* evolution over α. The shadowing effect of the body can be also extracted from the dynamic acquisitions of set *IV* (Sec. 3.2.2). Fig. 3.12 presents an example of the analysis performed for the chest link in anechoic chamber using TLMs. In this case, the *body shadowing* component embedded in the *mean channel gain* (continuous curve) is extracted by averaging the dynamic recorded data (dashed-dotted line) over a sliding temporal windows of 800 ms, which is found appropriate in order to follow channel slow variations considering an average angular speed of $70°/s$ (see Sec. 3.2.2). The dashed line represents again the mean value of the equivalent set of static acquisitions (vertical sets of crosses), whose values are listed in Tab. 3.4. The dashed and continuous curves result to follow a similar trend despite the possible loss of synchronism while performing the dynamic rotation, confirming the consistence and

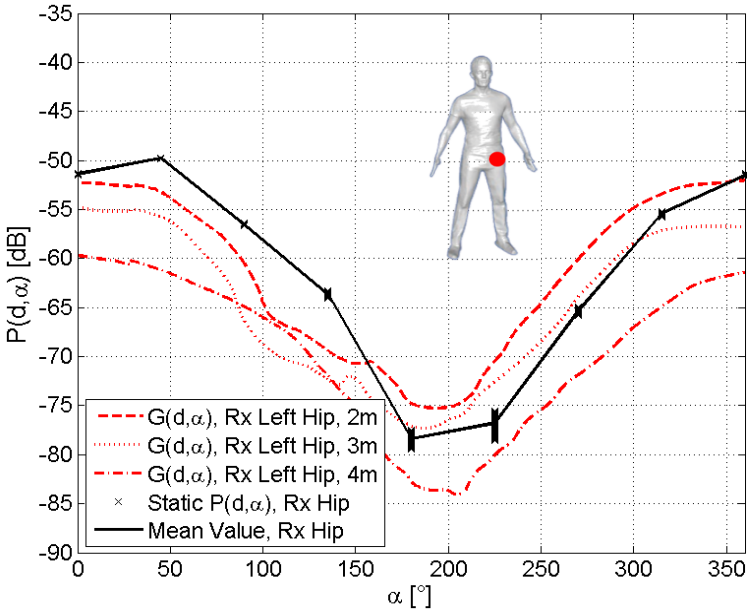

Figure 3.13: *Body shadowing* evolution over *alpha* at different distances between Tx and Rx. Rx on Hip, anechoic chamber, TLM.

reliability of the measured data set. Rotation cycles are also performed at different distances d, respectively 2, 3 and 4 m far from the Tx. Fig. 3.13 shows that the trends of the *body shadowing* over the angle α result almost unchanged, no matter the distance at which the movement is realised. This means that the body effect does not depend significantly on the distance between Tx and Rx (at least for the ones considered in the experiments), but more on the subject orientation α. Moreover, the variation of the *mean channel gain* as a function of d, which results from the comparison of the curves with different lines in Fig. 3.13, appears to be in good agreement with the results presented in Sec. 3.3.1 and listed in Tabs. 3.1 and 3.2, which refers just to the cases $\alpha = 0°$ and $\alpha = 180°$.

3.3.4 Space-time Correlation Properties

To complete the *off-body* channel characterisation, links correlation properties in the *space* and *time* domain are also investigated. The model proposed in Sec. 3.3 and the results presented in the following ones are used as a starting point for the study of correlation aspects. Only the data acquired through measurements sets *II* and *IV* (see Sec 3.2.2) are taken into account, since they refer to the dynamic acquisitions, where correlation properties can be highlighted.

3.3.4.1 Space Correlation

Space correlation between link *(i-j)* and link *(i-k)* aims at describing the relationship existing between these two *off-body* channels, where i refers to the external device, whereas j and k are two of the possible on-body positions. Investigating this kind of correlation properties is extremely important, for example in the study of cooperation opportunities among nodes in a BAN. When the quality of a communication link is too low to achieve the expected performance, one possibility is to complete the transmission hopping to another channel that presents more favorable characteristics. Evaluating the correlation level of two links undergoing different propagation conditions (for example due to the different node position) is then a good indicator for the best alternative channel.

The *space* correlation $\rho_{j,k}^{(i)}$ is evaluated as the cross-correlation between the channel power transfer functions $P_{i,j}(d,\alpha)$ and $P_{i,k}(d,\alpha)$, according to:

$$\rho_{j,k}^{(i)} = \frac{\mathbb{E}\Big[(P_{i,j} - \mathbb{E}\left[P_{i,j}\right])(P_{i,k} - \mathbb{E}\left[P_{i,k}\right])\Big]}{\sqrt{\mathbb{E}\Big[P_{i,j}^2 - \mathbb{E}^2\left[P_{i,j}\right]\Big]\mathbb{E}\Big[P_{i,k}^2 - \mathbb{E}^2\left[P_{i,k}\right]\Big]}}, \tag{3.3.4}$$

where $P_{i,j}(d,\alpha)$ (or equivalently $P_{i,k}(d,\alpha)$) is derived from Eq. 3.3.1 for the *(i-j)* and *(i-k)* link, respectively. Dependency on d and α are omitted for the sake of readability. Considering the three on-body node positions as described in Sec. 3.2.2, the possible links combinations (j/k), whose cross-correlation is investigated, are: hip/chest, hip/ear, and chest/ear, respectively. Tab. 3.5 presents the values found for the two antenna designs and in both environments, while the subject performed a walking movement both in LOS and NLOS conditions. Generally, the cross-correlation results to be stronger in anechoic chamber than in indoor for both antenna types and body orientations (i.e., LOS and NLOS). This can be explained considering that in indoor the secondary MPC contribution to the channel power transfer function is far more important. The additional randomness brought by these secondary paths, arising from reflections and diffractions from the environment, results in practically uncorrelated links, no matter the antenna used or the subject's orientation. Moreover, the weak correlation in indoor makes the comparison between antenna designs and between LOS/NLOS conditions not really significant, because the differences in the $\rho_{j,k}^{(i)}$ values are not so stressed. For this reason, from here on only the results referring

Table 3.5: *Space* Correlation - $\rho_{j,k}^{(i)}$ - Walking scenario

		Anechoich		**Indoor**	
		LOS	**NLOS**	**LOS**	**NLOS**
PM	**hip/chest**	0.02	0.15	0.25	-0.04
	hip/ear	-0.02	0.54	-0.06	-0.02
	chest/ear	0.52	0.15	0.02	-0.02
TLM	**hip/chest**	0.07	0.47	-0.09	0.05
	hip/ear	0.31	-0.31	0.28	-0.08
	heart/ear	0.08	-0.37	-0.08	-0.03

to the anechoic case are considered.

In particular, Figs. 3.14 and 3.15 show the $\rho_{j,k}^{(i)}$ values obtained in LOS and NLOS conditions, respectively, considering the subject walking in anechoic environment. Each figure compares the results for PM (blue) and TLM (red) antennas. First of all, it can be noticed that the cross-correlation tends to increase for both antennas when moving from LOS to NLOS. In the former case, channel conditions strongly depend on the specific antenna type used and on the on-body position, and $\rho_{j,k}^{(i)}$ values results smaller, in modulus, than in NLOS. Indeed, in the latter condition the human body shadows the direct communication between the Tx and the Rx, which results in stronger cross-correlations because the dependency of channel characteristics on the specific node position is reduced by the body presence.

Secondly, focusing on the NLOS cross-correlation between the hip and the chest links, an interesting observation arises comparing the two antennas. According to their position on the body (i.e., hip and chest), when the subject is in NLOS both devices are completely masked from the external node by the user's body. To overcome the *body shadowing* effect, communication takes place not only through a direct propagation path traveling in the free space (from the user's body to the outer device), but also thanks to an on-body component realised by creeping waves propagating on its surface. To that purpose, TLMs normal polarization enhance the latter propagation mechanisms, resulting in a stronger free space component, and hence in larger $\rho_{j,k}^{(i)}$ values, as compared to PMs.

The hip/chest correlation shows interesting results also when analysing the data referring to the dynamic rotations (measurements set *IV* in Sec. 3.2.2). In this case, cross-correlation is computed accounting just for the *long-term fading* component.

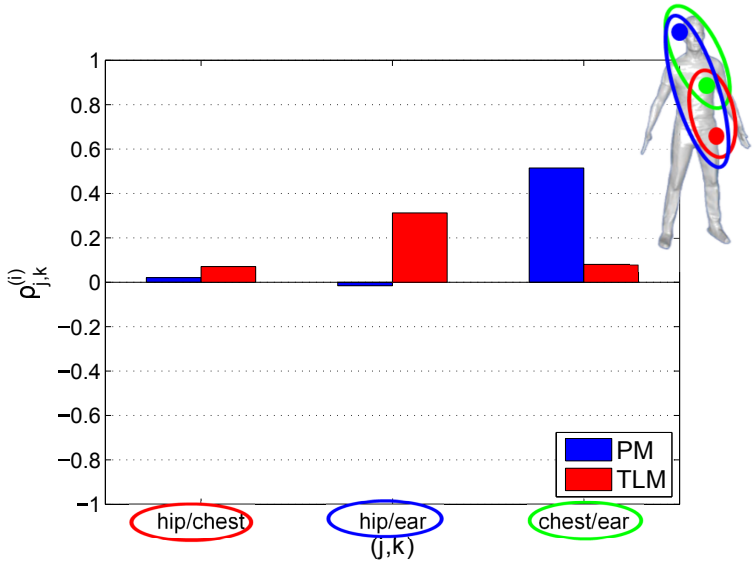

Figure 3.14: $\rho^{(i)}_{j,k}$ values for PMs (blue) and TLMs (red). Walking, anechoic chamber, LOS.

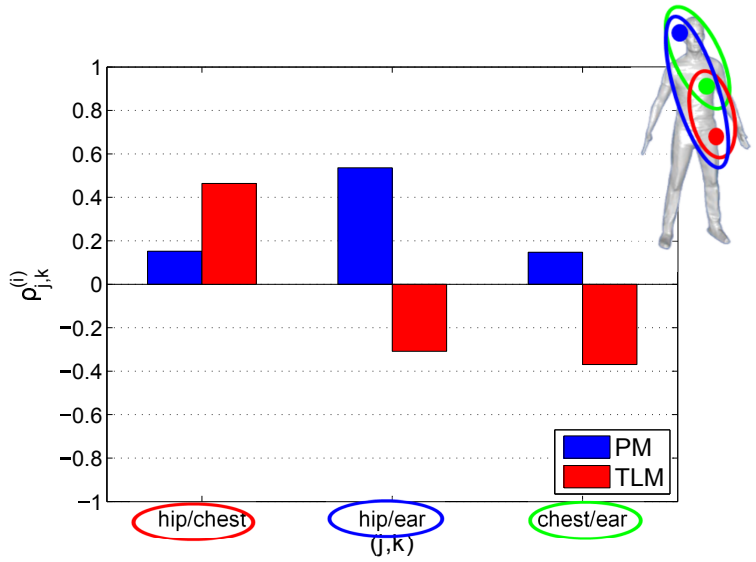

Figure 3.15: $\rho^{(i)}_{j,k}$ values for PMs (blue) and TLMs (red). Walking, anechoic chamber, NLOS.

Eq. 3.3.4 is used also in this case, but considering $S_{i,j}(d,\alpha)$ instead of $P_{i,j}(d,\alpha)$ according to:

$$\rho_{j,k}^{(i)} = \frac{\mathbb{E}\Big[(S_{i,j} - \mathbb{E}\left[S_{i,j}\right])(S_{i,k} - \mathbb{E}\left[S_{i,k}\right])\Big]}{\sqrt{\mathbb{E}\Big[S_{i,j}^2 - \mathbb{E}^2\left[S_{i,j}\right]\Big]\mathbb{E}\Big[S_{i,k}^2 - \mathbb{E}^2\left[S_{i,k}\right]\Big]}}. \tag{3.3.5}$$

Fig. 3.16 compares the cross-correlation values obtained for PM (blue) and TLM (red) antennas, when rotations are performed in anechoic chamber. It could be noticed that, especially for TLMs, the hip/chest links present larger correlation values, as compared to the other possible combinations (i.e., hip/ear and chest/ear). This is due to the fact that in the former case the nodes are placed on the same side of the user's trunk (hip and chest on the subject's front side), resulting to be influenced by the body almost in the same way. Hence, their correlation is stronger with respect to the links that involve one node placed on the ear, whose position is less affected by the human presence. Same considerations apply to the indoor case, but the corresponding graph is not reported here for the sake of briefness.

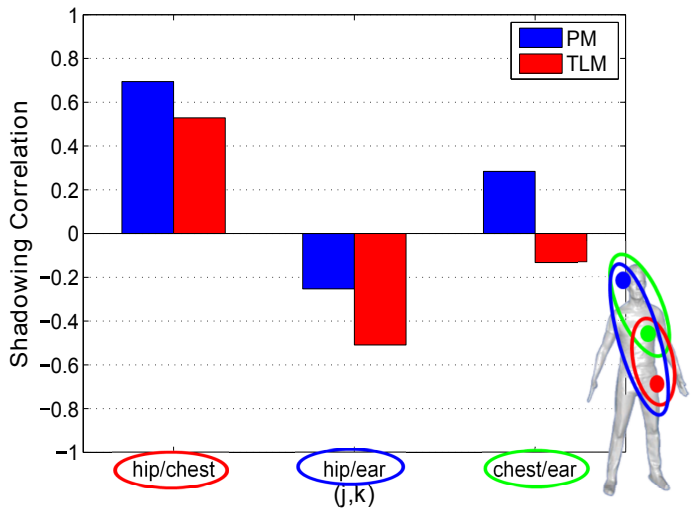

Figure 3.16: *Long-term fading* correlation values for PMs (blue) and TLMs (red). Rotation, anechoic chamber.

3.3.4.2 Time Correlation

Investigating the *time* correlation of each *off-body* link *(i-j)* means analysing its stability and its coherence over time. This indication is highly important also at a system level, in order to design upper layer protocols that exploit channel temporal characteristics and not just passively experiencing its randomness and variability.

Time correlation is evaluated through the normalised autocorrelation function of *(i-j)* link, $R_{j,j}^{(i)}(\Delta t)$, defined as:

$$R_{j,j}^{(i)}(\Delta t) = \frac{\mathbb{E}\left[H_{i,j}(t, f_0) \cdot H_{i,j}(t + \Delta t, f_0)^*\right]}{\mathbb{E}\left[|H_{i,j}(t, f_0)|^2\right]}; \tag{3.3.6}$$

where $\mathbb{E}[\cdot]$ represents the mean operator applied to the channel complex transfer function $H_{i,j}(t, f_0)$, and $*$ acts as the conjugate operator. Accounting for the complex value of $H_{i,j}(t, f_0)$ results in an additional informative contribution given by the phase of the channel transfer function, and not just by its magnitude as in previous works available in literature [210].

An example of the results obtained is reported in Fig. 3.17, which presents the evolution over Δt of $|R_{j,j}^{(i)}(\Delta t)|$ obtained for TLM antennas when walking in indoor, for LOS and NLOS cases. The comparison allows to notice that moving from LOS to NLOS conditions results in a faster decorrelation of the channel, due to the more important secondary MPCs contribution. The additional randomness introduced by the multipath component results in a channel that is less stable over time, and curves in Fig. 3.17b present a steepest decrease and a non-smooth evolution over Δt, as compared to the LOS case. Same considerations also apply for PMs, and in both cases no significant differences between the three channels under investigation can be pointed out.

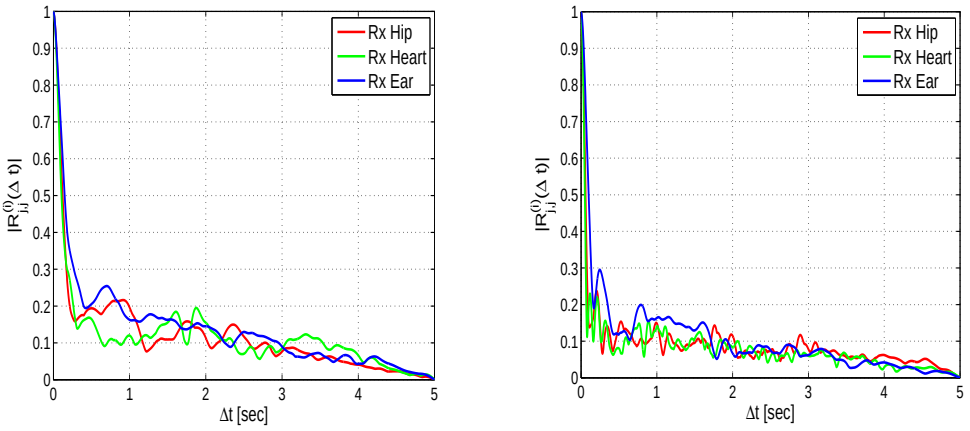

(a) (b)

Figure 3.17: $|R_{j,j}^{(i)}(\Delta t)|$ in LOS (a) and NLOS (b) conditions. Walking, indoor, TLMs.

$|R_{j,j}^{(i)}(\Delta t)|$ values are computed also in the anechoic case, for all possible scenarios $\mathcal{S}$. The comparison of results for the two environments highlights how the curves referring to the anechoic case have a smoother evolution over Δt, as compared to the indoor ones. This is mainly due to the presence of a less important secondary MPC contribution, which results in channels that decorrelate for larger values of Δt. The correlation times at 50%, $T_{c,0.5}$, are presented in Fig. 3.18 for the chest link; similar results are available also for the other channels but they are not reported here for the sake of briefness. Generally, it is possible to observe that $T_{c,0.5}$ does not exceed 150 ms when in LOS and 100 ms when in NLOS conditions. The correlation results to be bigger than 100 ms in anechoic premises, whereas in indoor it assumes smaller values, confirming what previously stated just observing $|R_{j,j}^{(i)}(\Delta t)|$ evolution over Δt.

Time correlation properties, as well as *space* ones, are also affected by the antenna type according to their specific radiation and polarization characteristics. In particular, TLMs normal polarization helps to better counteract the *body shadowing* effect

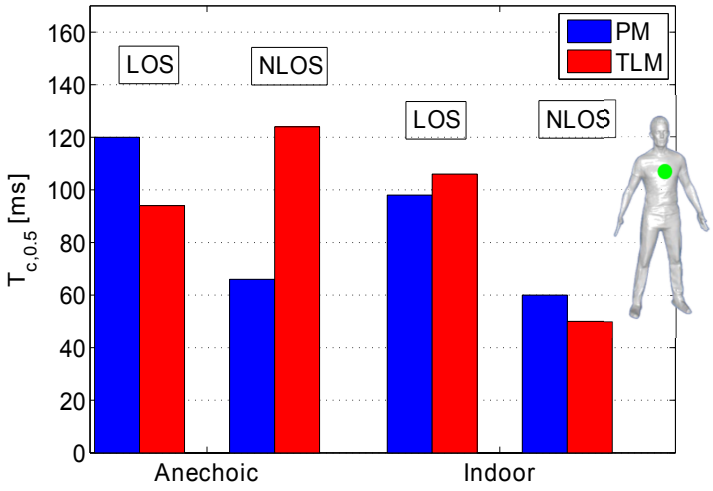

Figure 3.18: $T_{c,0.5}$ values for PM (blue) and TLM (red) antennas, in LOS and NLOS conditions. Rx on chest, walking, anechoic chamber and indoor.

in NLOS conditions. This affects not only the *mean channel gain* values, but also the statistics of the *short-term fading* and consequently the *time* correlation properties. Hence, TLMs autocorrelation functions generally present a smoother trend as compared to PMs ones.

3.4 *B2B* Channel Modeling

Starting from the $H_{i,j}(t, f_0)$ data acquired through the experiments presented in Sec. 3.2.3, the proposed *B2B* channel model describes each channel power transfer function in dB, $P_{i,j}(d, \alpha)$, as composed by a *mean channel gain*, $G_{i,j}(d, \alpha)$, plus a *short-term fading*, $F_{i,j}(d, \alpha)$, component. Eq. 3.3.1, used for *off-body* communications, also applies to the *B2B* scenario, and it is reported here for the sake of clarity:

$$P_{i,j}(d, \alpha) = |H_{i,j}(t, f_0)|^2 = G_{i,j}(d, \alpha) + F_{i,j}(d, \alpha). \quad \text{[dB]} \tag{3.4.1}$$

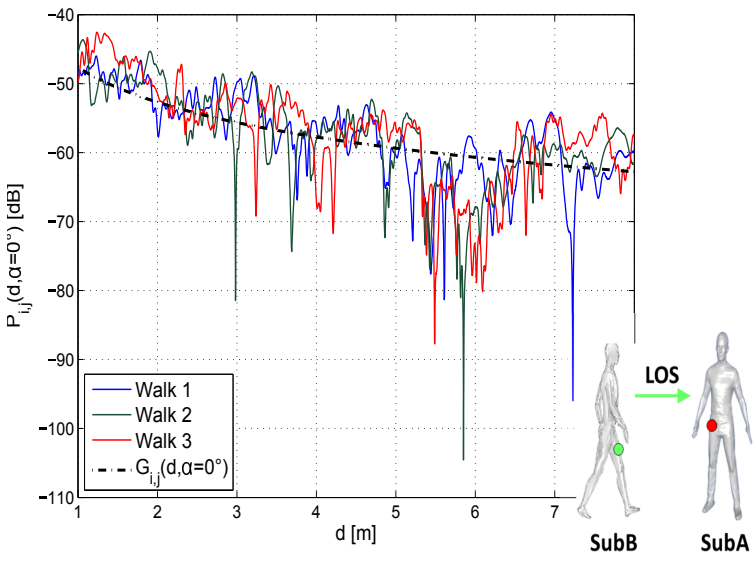

Figure 3.19: *Mean channel gain* extraction for the thigh/hip link in LOS conditions, PM antennas.

In this case, d is the distance separating the front sides of the two subjects, and α is the angle describing their mutual orientation. As usual, from here on subscripts *(i,j)* will be omitted for the sake of readability, implying that the analysis is performed for each possible combination of the *i-th* Rx and the *j-th* Tx, as shown in Fig. 3.4.

A *long-term fading* component, $S_{i,j}(d,\alpha)$, can be also extracted from the channel power transfer function, following the slow variations of $G_{i,j}(d,\alpha)$ over its mean value. The *mean channel gain* can be then expressed as:

$$G_{i,j}(d,\alpha) = \overline{G_{i,j}(d)} + S_{i,j}(d,\alpha); \quad [\text{dB}] \tag{3.4.2}$$

where $\overline{G_{i,j}(d)}$ is defined as $\overline{G(d)_{i,j}} = < G_{i,j}(d,\alpha) >_\alpha$ and it represents the average over the angle α of the *mean channel gain*. $S_{i,j}(d,\alpha)$ is also referred to as the *body shadowing* component, representing the masking effect of the body on the *B2B* radio channel. Next sections describe each model component, characterising them ac-

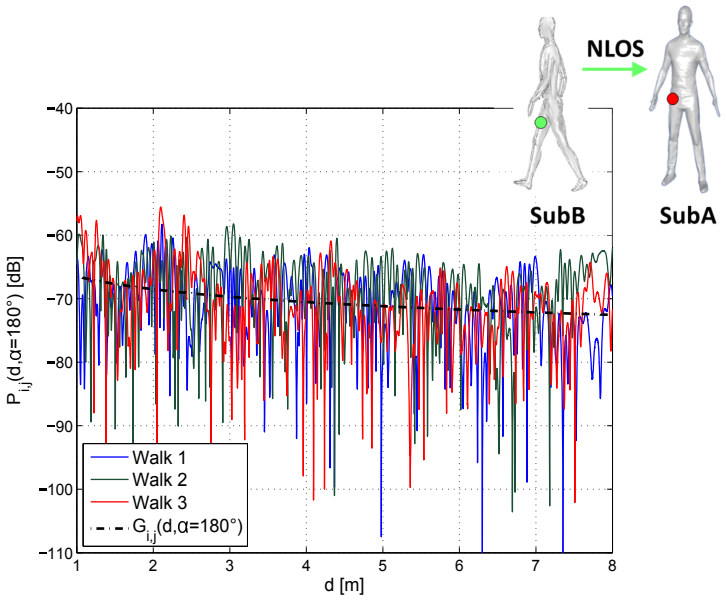

Figure 3.20: *Mean channel gain* extraction for the thigh/hip link in NLOS conditions, PM antennas.

cording to the measurements scenario considered and showing the impact of human motion and of antenna radiation properties on *B2B* channels. The dependency of each term on d and α is explained case by case. Considering that all acquisitions are performed just in indoor premises, in the *B2B* case a scenario $\mathcal{S}$ is defined by the Tx position on *subB* body, the Rx location on *subA* body, the couple of users involved, the antenna type, and the movement performed.

3.4.1 Mean Channel Gain

Scenario I: Walking

Starting from measurement set I (see Sec. 3.2.3), the *mean channel gain*, $G(d, \alpha)$, is characterised through a RMSE fitting of the acquired data. An example is proposed in Figs. 3.19 and 3.20, for PMs in LOS ($\alpha = 0°$) and NLOS ($\alpha = 180°$) conditions.

The dash-dotted line represents the polynomial fitting of the continuous curves, each of them representing the power transfer function acquired for a specific walking cycle.

Even if these examples refer to the thigh/hip link, comparing these two figures is helpful in understanding how important the impact of the body is on channel characteristics. Indeed, the NLOS case (Fig. 3.20) presents a more evident fading effect, with deeper (up to -40 dB below the mean value) and more frequent fading episodes, as compared to the LOS scenario shown in Fig. 3.19. This can be explained considering that in NLOS the entire body of one subject ($subB$) shadows the LOS path between Tx and Rx. Propagation occurs then mainly by reflections and diffractions from the body and/or from the surroundings, leading to a more important *short-term fading* contribution due to the MPCs and to the absence of a dominant direct path. More details on the *short-term fading* characterisation are given in Sec. 3.4.2.

The polynomial fitting of the experimental data allows the description of $G(d, \alpha)$ according to the following equation:

$$G(d, \alpha) = G_0(d_0, \alpha) - 10 \cdot n(\alpha) \cdot \log_{10}(d/d_0); \quad [\text{dB}] \tag{3.4.3}$$

where $G_0(d_0, \alpha)$ represents the mean channel gain evaluated at the reference distance $d_0 = 1$ m, whereas $n(\alpha)$ is defined as the path loss exponent.

Tabs. 3.6 and 3.7 report the values obtained using PMs and TLMs antennas, for all the investigated links. As shown, the distance-based modeling approach presented through Eq. 3.4.3 is used both in LOS and NLOS conditions. Anyway, since the limited distance interval considered in the experiments (i.e., approximately 8 m), the NLOS case results more in an attempted modeling of the *mean channel gain* variation over distance, and it should be considered less significative than the one in LOS. Given the important contribution of reflections coming from the environment

to the overall channel gain, which is maybe more important as d increases, $n(\alpha)$ values could have been even larger at larger distances. It can be noticed that generally the path loss exponents significantly decrease when switching from LOS to NLOS conditions, meaning that in the latter case the *mean channel gain* is little dependent on distance, resulting in a non-dominant component in the modeling of NLOS scenarios, indeed. Even if this is true for both antennas, this trend is more stressed when PMs are considered. This is due to their radiation and polarization characteristics that, differently from TLMs, do not enhance the creeping waves component on the body, arising to overcome its masking effect on the direct communication path. Indeed, TLMs' normal polarization can improve waves propagation around the body surface [161], which results into a stronger free-space component from one body to the other, even when in conditions of devices non-direct visibility (i.e., NLOS). The considerations on propagation mechanisms in NLOS conditions done for the *off-body* scenario can be extended to the *B2B* case; readers are referred to Sec. 3.3.1 for more details.

As for $G_0(d_0, \alpha)$, it gives an estimation of the additional attenuation brought by the body shadowing to the radio channel. When *subB* moves from LOS to NLOS condition, the *mean channel gain* tends to decrease, with a variation that depends on the node position and on the antenna type: up to 29 dB for PMs and 12 dB for TLM. This difference is in line with antennas radiation and polarization characteristics, with TLMs resulting to be less affected by the body presence.

Finally, TLMs generally show larger values of $G_0(d_0, \alpha)$, with respect to those for PMs, but this is not true for two specific links, i.e., hip/hip and hip/hand, when in LOS condition. In these cases, both the Tx and the Rx antennas are placed

Table 3.6: Walking - $G(d, \alpha)$ - Planar Monopoles - Indoor

	Txs	Right Hip			Left Thigh			Right Hand		
	Rxs	**Left Ear**	**Chest**	**Right Hip**	**Left Ear**	**Chest**	**Right Hip**	**Left Ear**	**Chest**	**Right Hip**
LOS	$\boldsymbol{n}(\mathbf{0°})$	1.14	1.14	3.33	0.75	1.00	1.68	0.69	0.74	2.80
	$\boldsymbol{G_0(1m, 0°)}$ $[dB]$	-56.80	-54.02	-37.88	-58.33	-57.67	-47.64	-57.60	-51.30	-36.10
NLOS	$\boldsymbol{n}(\mathbf{180°})$	0.80	0.67	1.15	0.82	0.46	0.67	1.07	0.72	1.17
	$\boldsymbol{G_0(1m, 180°)}$ $[dB]$	-70.59	-70.77	-66.33	-67.53	-70.30	-66.50	-64.38	-63.46	-58.80

Table 3.7: Walking - $G(d, \alpha)$ - Top Loaded Monopoles - Indoor

	Txs	Right Hip			Left Thigh			Right Hand		
	Rxs	**Left Ear**	**Chest**	**Right Hip**	**Left Ear**	**Chest**	**Right Hip**	**Left Ear**	**Chest**	**Right Hip**
LOS	$\boldsymbol{n}(\mathbf{0°})$	0.95	2.19	1.70	1.33	2.57	1.99	1.20	2.46	1.86
	$\boldsymbol{G_0(1m, 0°)}$ $[dB]$	-52.97	-44.85	-46.89	-52.90	-41.67	-47.10	-48.34	-43.70	-45.20
NLOS	$\boldsymbol{n}(\mathbf{180°})$	0.77	1.64	1.47	0.92	1.99	1.28	0.70	1.91	1.01
	$\boldsymbol{G_0(1m, 180°)}$ $[dB]$	-60.30	-56.10	-55.47	-59.76	-53.86	-56.77	-58.06	-52.46	-56.53

approximately at the same level on the users' bodies, and they present a null radiation pattern in the LOS direction when TLMs are used. This results in higher losses, as compared to the case with PMs, since the latter are characterised by a non-null radiation path in the same direction, instead.

Scenario II: Opposite Walk

Measurements set *II* (see Sec. 3.2.3) mixes in one single scenario both *LOS* and NLOS conditions, including a *transition zone* that takes place when the two subjects approach, meeting and crossing each other in the middle of the path, and then continuing their walk in opposite directions. The proposed model aims at characterising

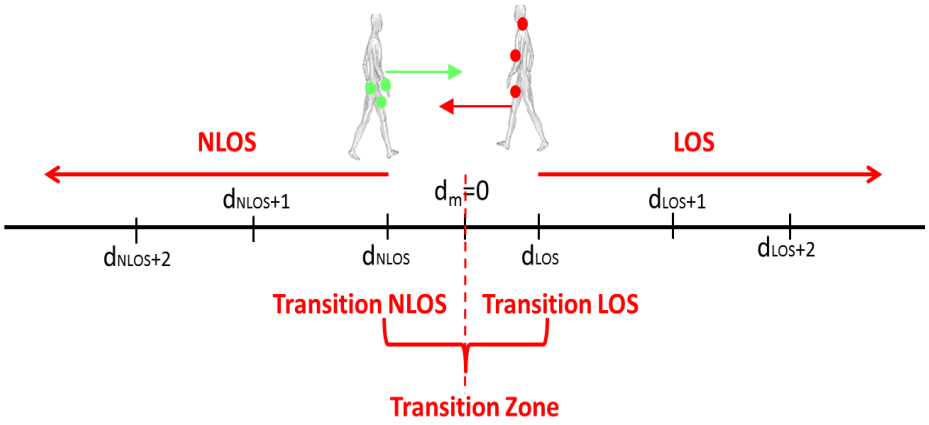

Figure 3.21: Propagation zone in Opposite Walking scenario: LOS, NLOS and Transition Zone.

the evolution of the channel power transfer function according to the propagation conditions realised (see Figs. 3.22 and 3.21), namely *LOS, NLOS* and *transition zone*. It describes the *mean channel gain* in dB, for each *(i,j)*-th link, as a function of the distance d separating the users and of their mutual orientation α. For each zone

$G(d, \alpha)$ can be described according to the log-distance dependent expression as:

$$G(d,\alpha) = \begin{cases} G_0(d_{LOS}, 0°) - 10 \cdot n_{LOS}(0°) \cdot \log_{10}(d/d_{LOS}) \\ \qquad\qquad \text{if } d \geq d_{LOS},\ \textit{LOS}, \\ G_0(d_{LOS}, 0°) - 10 \cdot n_{TR} \cdot \log_{10}[(d_{LOS} + |d - d_{LOS}|)/d_{LOS}] \\ \qquad\qquad \text{if } 0 \leq d < d_{LOS},\ \textit{transition LOS}, \\ G_0(d_{LOS}, 0°) - 10 \cdot n_{TR} \cdot \log_{10}[(d_{LOS} + (d + d_{LOS}))/d_{LOS}] \\ \qquad\qquad \text{if } 0 < d < d_{NLOS},\ \textit{transition NLOS}, \\ G_0(d_{NLOS}, 180°) - 10 \cdot n_{NLOS}(180°) \cdot \log_{10}(d/d_{NLOS}) \\ \qquad\qquad \text{if } d \geq d_{NLOS},\ \textit{NLOS}. \end{cases} \tag{3.4.4}$$

d_{LOS} and d_{NLOS} represent the values of d identifying the beginning of the LOS and the NLOS parts, defining in that way the length of the *transition zone*. As shown in Fig. 3.21 for the hip/chest link when TLMs are used, the *transition zone* describes the slope of the channel power transfer function due to the passage from a face-to-face condition (LOS at d_{LOS}) to a back-to-back one (NLOS at d_{NLOS}). The two subjects meet approximately at half way, which is conventionally fixed at $d_m = d_{LOS} - d_{NLOS} =$ 0 m, so that $d_{LOS} = d_{NLOS}$.

In Eq. 3.4.4, n_{LOS}, n_{NLOS} and n_{TR} are defined as the path loss exponents describing the evolution over d of the *mean channel gain*, each one referring to one of the propagation zone: LOS, NLOS and *transition zone*, respectively. It has to be noticed that n_{TR} does not present α dependence, considering that, for this specific scenario, the definition of the angle between the two users' bodies loses its significance in the *transition zone*.

A polynomial fitting of the data subset describing the slope of $P(d, \alpha)$ is performed

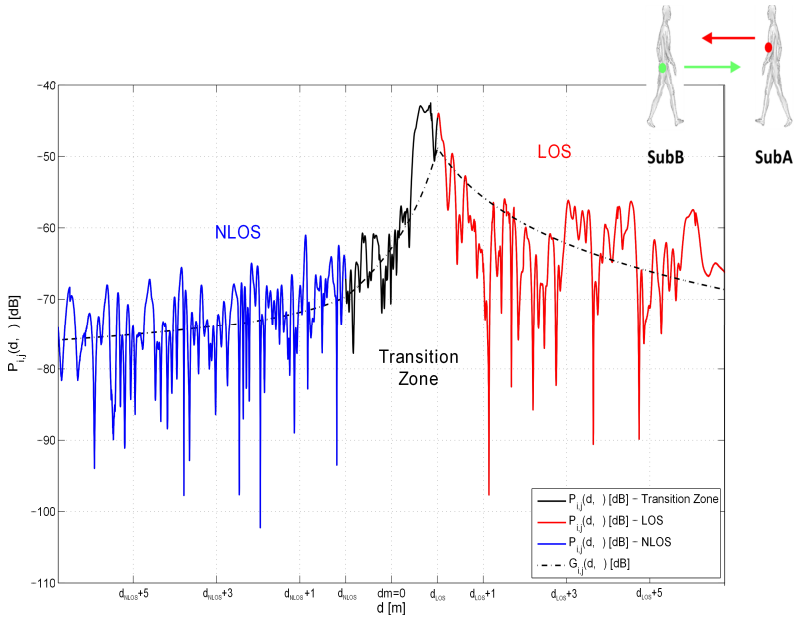

Figure 3.22: *Mean channel gain* extraction for the hip/chest link, opposite walking. LOS, NLOS and transition zone, TLM antennas.

to allow the extraction of the values for d_{LOS} and d_{NLOS}. A good approximation of the *transition zone* is given by a third degree polynomial, whose maximum and minimum values happen at the reference distances defined as the starting point of LOS and NLOS conditions, respectively (i.e., d_{LOS} and d_{NLOS}).

A best fitting of the experimental data (RMSE fit) allowed the characterisation of the *mean channel gain* in terms of path loss exponents (i.e., n_{LOS}, n_{NLOS}, and n_{TR}) and of *mean channel gains*, (i.e., $G_0(d_{LOS}, 0°)$, $G_0(d_{NLOS}, 180°)$), according to Eq. 3.4.4.

As a matter of example, Tab. 3.8 lists the results for the characterisation of *LOS* and *NLOS* zones in terms of $G_0(d_{LOS}, 0°)$, $G_0(d_{NLOS}, 180°)$, $n_{LOS}(0°)$ and $n_{NLOS}(180°)$, for the Tx placed on user's thigh. Analysis is performed for all possible *(i,j)*-th link, but results are not shown here for the sake of briefness, interested reader

Table 3.8: Mean Channel Gain Characterisation - Opposite Walk LOS/NLOS - Tx Left Thigh

		Planar Monopole			**Top Loaded Monopole**		
	Rxs	**L. Ear**	**Chest**	**R. Hip**	**L. Ear**	**Chest**	**R. Hip**
LOS	$\boldsymbol{n_{LOS}(0°)}$	1.19	1.31	1.62	1.33	2.47	2.00
	$\boldsymbol{G_0(d_{LOS}, 0°)}$ $\boldsymbol{[dB]}$	-60.64	-57.30	-54.68	-55.56	-47.45	-49.24
NLOS	$\boldsymbol{n_{NLOS}(180°)}$	0.91	0.34	0.32	0.55	0.60	0.49
	$\boldsymbol{G_0(d_{NLOS}, 180°)}$ $\boldsymbol{[dB]}$	-69.40	-78.77	-77.86	-63.21	-69.00	-68.61
	$\boldsymbol{\Delta G_0}$	8.79	21.48	23.18	7.66	21.55	19.37

can find the complete set of values in Appendix C. Values in the table are obtained as the average of the fitting parameters extracted from each measurements performed.

It is interesting to notice that LOS values presented in Tab. 3.8 are quite similar to those in Tabs. 3.6 and 3.7, which refer to acquisition set *I* (see Sec. 3.2.3). Differences can be attributed to possible non-synchronism and slightly dissimilarities in performing the two types of measurements. Anyway, this good agreement confirms the accuracy of the results obtained and it suggests the idea to merge the results referring to scenario *I* and *II*, in order to create a larger data base for a more precise channel characterisation.

Conversely, *NLOS* values are not directly comparable with those obtained from the previous measurement set, since in the current scenario (i.e., *opposite walking*) the NLOS case refers to the condition where two bodies mask the direct communication link, and hence *mean channel gains* and path loss exponents assume smaller values.

To quantify the impact of the two human bodies on the channel, Tab. 3.8 lists

the values of ΔG_0 for both antennas types, which is defined as the difference between the *mean channel gains* at d_{NLOS} and d_{LOS} according to: $\Delta G_0 = G_0(d_{LOS}, 0°)$-$G_0(d_{NLOS}, 180°)$. It can be noticed that this parameter is extremely dependent on the node emplacement; antenna on the ear presents smaller values of ΔG_0 with respects to the other on-body locations, confirming that this position is less affected by the body presence. Indeed, for the ear node, NLOS correspond to an inversion of its position (from left to right side of the head) and not to a complete obstruction of the body.

Tab. 3.9 presents the parameters for the characterisation of the *transition zone* for all *(i,j)*-th links, using both antenna types. It is possible to observe that d_{LOS} and d_{NLOS} generally assume values around 1 m, no matter the link considered and the antenna used, meaning that the *transition zone* covers approximately 2 m (i.e., 1 m before the meeting point at d_m and 1 m after). It has to be considered that slight variations in the effective walking speed of the users may affect the value for these parameters. As for the results concerning the path loss exponent, n_{TR} assumes smaller values for the links where one node is placed on the ear, as compared to those obtained for the other channels. This is in line with the consideration that nodes on the head are less affected by the body presence, and hence the passage from LOS to NLOS condition, described by the *transition zone*, is less sharper and more related to the physical distance between users. From Tab. 3.9 it is not possible to highlight any significant difference in the results for the two antenna types. The effect of specificities of their radiation characteristics is less stressed and somehow reduced in the *transition* part. The extreme user proximity in that zone makes it difficult to separate in the channel model the body effect from the distance dependence, and

Table 3.9: Mean Channel Gain Characterisation - Transition LOS/Transition NLOS

Tx	**Rxs**	**Planar Monopole**		**Top Loaded Monopole**	
		n_{TR}	d_{LOS} $[m]$ = d_{NLOS} $[m]$	n_{TR}	d_{LOS} $[m]$ = d_{NLOS} $[m]$
R. Hip	**Left Ear**	2.50	1.25	2.85	1.32
	Chest	5.33	1.04	4.54	1.28
	Right Hip	5.83	1.13	4.44	1.27
L. Thigh	**Left Ear**	1.83	1.26	1.60	1.27
	Chest	4.50	1.36	4.51	1.35
	Right Hip	4.85	1.42	4.06	1.25
R. Hand	**Left Ear**	2.13	1.04	2.03	0.74
	Chest	4.04	1.50	3.37	1.24
	Right Hip	3.48	1.15	3.53	1.30

corresponding propagation mechanisms (i.e., on-body creeping waves and free-space path) are then less distinguishable in antennas behavior.

***Scenario III*: Parallel Walk**

For this specific scenario where the two subjects are walking in parallel side by side (see Sec. 3.2.3), the definition of bodies orientation α and of distance d, as considered in previous paragraphs, lose its inner significance. In this case, the most useful description is the one given as a function of time t, which allows to characterise the dynamic properties of the *B2B* channel due to the subjects movement. Starting from Eq. 3.4.1 and considering the subject walking at a constant average speed $v = 0.8$ m/s, so that $D = v \cdot T_{obs} = 0.8[m/s] \cdot 10[s] = 8$ m, where D is the distance covered by the users, it is then possible to describe the (i,j)-th channel power transfer function

expressed in dB as:

$$P(t) = G(t) + F(t). \quad [\text{dB}] \tag{3.4.5}$$

The distance dependence is here replaced by the temporal one and α is omitted because it does not apply to the specific scenario and it is constant throughout the experiment (see Figs. 3.4b and 3.5). The *mean channel gain*, $G(t)$, is defined as the slow-varying part of the power transfer function, and it can be extracted applying a sliding temporal window w to the recorded channel data. For example, Fig. 3.23 shows the evolution over time of $P(t)$ for the hip/hip channel, comparing the values obtained with PMs (dashed red curve) and with TLMs (dashed blue curve). Trends for the *mean channel gain* are shown by the continuous curves; they are obtained considering a sliding window of 500 ms, which is found to be appropriate in order to follow the slow channel variations due to the walking movement at speed v.

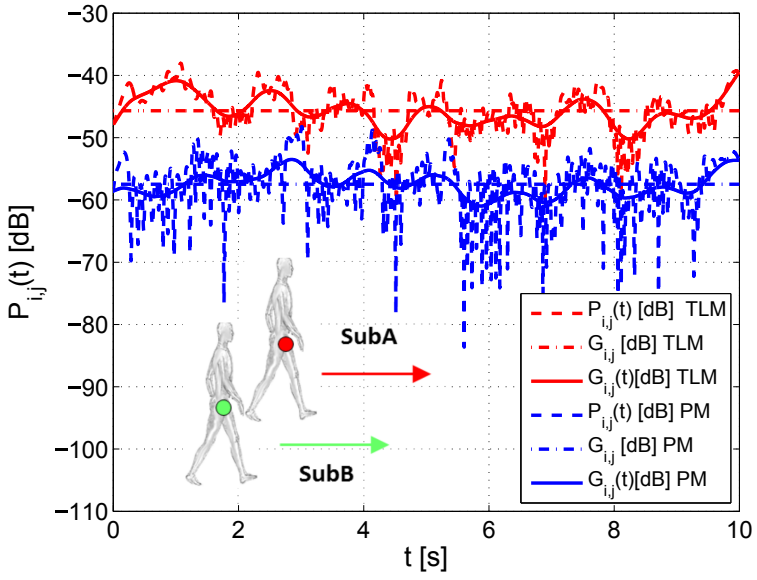

Figure 3.23: $P(t)$ evolution over time for the hip/hip link: PMs (blue curves) and TLMs (red curves), walking side by side.

According to Eq. 3.4.2, the *mean channel gain* is described by two separate contributions; and for this specific scenario it can be expressed as:

$$G(t) = \overline{G} + S(t). \quad [\text{dB}] \tag{3.4.6}$$

$\overline{G} =< G(t) >_t$ represents the average over time of $G(t)$, and it is characterised by its standard deviation σ_G. It is computed gathering the acquisitions performed with the two pairs of subjects, accounting in that way for the heterogeneity of human bodies in terms of shape, tissues dielectric properties and local micro-variations of nodes emplacement. $S(t)$ is the *shadowing* contribution describing the slow variations of the *mean channel gain* around its mean value $\overline{G}$. It is statistically described by a normal distribution $\mathcal{N}(0, \sigma_S)$, where σ_S in dB accounts for the impact of bodies movements shadowing the direct link between nodes while walking. This is shown for example in Fig. 3.23, where the oscillatory trend of the continuous curves represents the effect of users' arms swinging while walking, which cyclically masks the communication between devices located on both subjects' hip.

Even if this set of measurements allowed the characterisation of $S(t)$, a deeper insight on the *body shadowing* contribution will be given in Sec. 3.4.3, where it is characterised considering different body orientations α.

Tab. 3.10 reports the values obtained for all *(i,j)*-th links and for both antenna types. It should be noticed that, even if these results refer to one specific measurement scenario and environment, some general considerations can be drawn anyway.

Generally, PMs present smaller $\overline{G}$ values as compared to those obtained with TLMs, no matter the Tx position considered. This is in line with antennas polarization and radiation characteristics, similarly as in the walking scenario. Indeed, considering the two subjects walking side by side, communication takes place not just

Table 3.10: Walking side by side - Mean Channel Gain Characterisation: $\overline{G}$ $[dB]$ and $S(t)$ $[dB]$

	Txs	**Right Hip**			**Left Thigh**			**Right Hand**		
	Rxs	**Left Ear**	**Chest**	**Right Hip**	**Left Ear**	**Chest**	**Right Hip**	**Left Ear**	**Chest**	**Right Hip**
PM	$\overline{G}$ $[dB]$	-71.41	-68.86	-63.32	-69.84	-68.36	-61.56	-66.29	-64.88	-59.95
	σ_G $[dB]$	1.22	4.42	5.69	1.61	0.72	1.25	2.64	1.28	1.45
	σ_S $[dB]$	2.05	2.57	2.25	2.39	2.04	4.63	2.20	2.09	2.76
TLM	$\overline{G}$ $[dB]$	-56.66	-51.34	-47.66	-60.28	-50.64	-44.73	-59.65	-54.79	-51.68
	σ_G $[dB]$	0.61	0.78	2.09	2.08	1.46	2.19	0.51	0.44	1.78
	σ_S $[dB]$	1.79	1.84	0.75	1.93	3.10	2.03	2.07	3.56	3.77

Table 3.11: Fast Fading Statistics - Walking - Tx on Left Thigh

	Rxs	**Planar Monopoles**					**Top Loaded Monopoles**				
		ν	σ	K	$LCR[Hz]$	$AFD[ms]$	ν	σ	K	$LCR[Hz]$	$AFD[ms]$
LOS	**Left Ear**	0.79	0.72	0.60	2.80	190	0.0006	0.97	0	4.49	120
	Chest	0.93	0.58	1.29	2.60	200	0.71	0.78	0.41	3.60	150
	Right Hip	0.91	0.60	1.15	2.23	240	0.59	0.85	0.24	4.46	120
NLOS	**Left Ear**	0.001	0.93	0	6.66	80	0.001	0.96	0	7.06	70
	Chest	0.0003	0.93	0	6.71	90	0.001	0.97	0	5.14	110
	Right Hip	0.001	0.96	0	6.80	80	0.001	0.93	0	6.63	80

through a free-space path traveling from one subject to the other, but also thanks to a creeping waves contribution propagating on both bodies [161]. TLMs, helping on-body waves diffraction, result in smaller channel attenuations than in PM case. Moreover, when PMs are placed on the hip, thigh or chest positions on one subject, they present a null radiation pattern in the main LOS direction towards nodes placed in the same positions but on the other subject. This is not the case for TLMs, and so the difference in antennas behavior is even more evident for these links than for those involving one node placed on the ear, with a variation in $\overline{G}$ values up to 18 dB (i.e., thigh/chest link).

Finally, TLM antennas usually present smaller σ_G than PMs, meaning that the variability due to antenna/body interaction is reduced by the presence of the ground plane in TLMs' layout. Moreover, PMs result to be more affected by the masking effect of the body, presenting larger variations of the *shadowing* component (i.e., larger σ_S.). Indeed, PM's tangential polarization do not enhance on-body waves propagation, corresponding to a more important channel variability brought by the *body shadowing* effect while moving.

3.4.2 Short-term Fading

Scenario I: Walking Scenario

As shown in Eq. 3.4.2, the *short-term fading* component, $F(d, \alpha)$, is extracted from data set I (see Sec. 3.2.3) subtracting the *mean channel gain* $G(d, \alpha)$ from the corresponding channel power transfer function.

The statistical analysis performed shows that the linear envelope of $F(d, \alpha)$ is well modeled by a Rice distribution, which is defined by its K-factor (see Sec. 2.3.2).

Tab. 3.11 lists the results obtained based upon the maximized log likelihood derived from the MLE applied to the experimental data, for the case where the Tx is placed on *subB*'s thigh, in all possible measurements conditions. LCR values expressed in Hz and AFD ones in ms are also reported, where the former is defined as the average rate at which the small-scale fading falls below the 0 dB level (i.e., a fading episode), while the latter represents the average duration of the fades with respect to the same threshold. Similar values are obtained for the other two Tx positions, interest reader can find the complete set of results in Appendix C.

When moving from LOS to NLOS, the user's completely shadows the main direct path, and propagation is realised mainly by the secondary MPCs due to reflections and diffractions from the environment and partially from the body itself. The more important secondary MPCs contribution, overcoming the main dominant path weakened by the *body shadowing* effect, directly affects also the *short-term fading* statistics. Indeed, the NLOS K-factors values are generally lower than in the LOS case for both antenna types, often tending to zero. Hence, the Rice distribution can be well approximated by a Rayleigh one, confirming the presence of a more significant secondary MPCs over the direct one. For similar reason, the NLOS case also presents much more frequent fading episodes (up to 7 times per second) than in LOS.

An interesting consideration comes from the comparison of antenna behavior in LOS condition, with TLMs presenting smaller K-factors as compared to PMs. Considering antennas polarization characteristics, when one subject walks towards the other, TLMs show a null radiation pattern in the LOS direction, both at the Rx and at the Tx side (except for the case where a node is placed on the ear). This in not true for PM antennas, which present a non null radiation pattern in the same

Table 3.12: Fast Fading Statistics - Parallel Walking - Tx on Right Hip

	Rxs	$\boldsymbol{\nu}$	$\boldsymbol{\sigma}$	$\boldsymbol{K}$	$\boldsymbol{LCR[Hz]}$	$\boldsymbol{AFD[ms]}$
PM	**Left Ear**	0.82	0.70	0.69	7.53	72
	Chest	0.92	0.59	1.22	9.43	60
	Right Hip	0.97	0.51	1.81	9.05	60
TLM	**Left Ear**	0.98	0.45	2.37	8.35	65
	Chest	1	0.34	4.33	5.65	91
	Right Hip	1	0.32	4.88	5.50	93

direction, and hence the main direct propagation path results stronger than in TLM case, with larger K values. For the same reason, PMs show smaller LCR values in LOS condition, as well as longer fading periods (see Tab. 3.11).

***Scenario III*: Parallel Walk**

As in the previous scenario, $F(t)$ is computed according to Eq. 3.4.5, subtracting the *mean channel gain* $G(t)$ from the corresponding $P(t)$.

Results show that the linear envelope of the *short-term fading* can be statistically described by a Rice distribution. Fig. 3.24 shows an example of the good fitting to the experimental data for the case where the Tx is placed on the hand and PM antennas are considered; each color referring to a specific Rx position.

Tab. 3.12 reports the values obtained for the statistical characterisation of Rice distribution (ν, σ and K) as well as the LCR and AFD values, for the case where the Tx is placed on the hip and for both antenna types. The reader is referred to Appendix C for results referring to the other Tx positions. It is possible to notice that generally PMs present sensibly smaller K values with respect to those obtained with TLMs. Indeed, when the two subjects are walking side by side, PM antennas

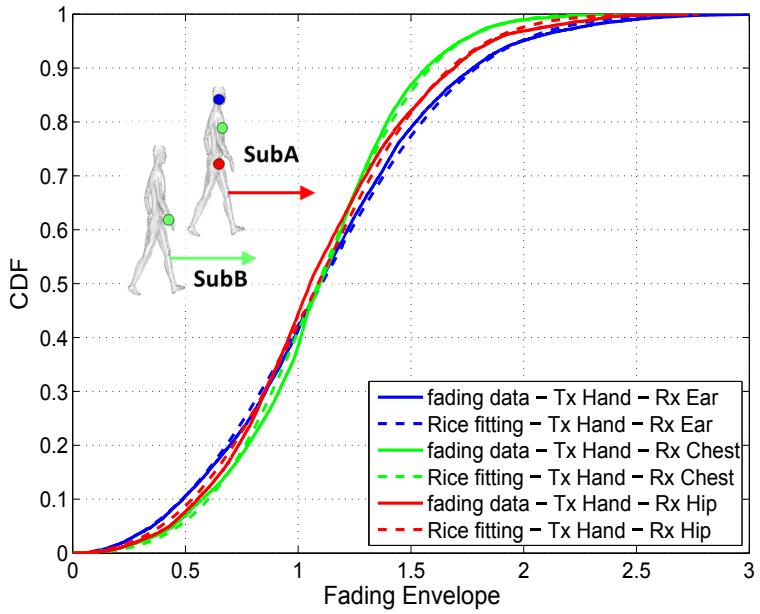

Figure 3.24: Cumulative Distribution Function of *short-term fading* amplitude. Tx on right hand, PM, walking side by side.

show a null radiation pattern in the main direct propagation path, both at Rx and Tx, which is not the case for TLMs. For this reason, the two antennas experience a different *short-term fading*, with TLM presenting a more important dominant path component traveling from one body to the other, which results in larger K factors. This difference in antennas behaviors is also witnessed by LCR and Δt values, as shown in Tab.3.12, with PMs presenting more frequent and shorter fading episodes.

Anyway, it is worth noting that both antennas types show K values larger than zero, meaning that they experience a main dominant propagation component that overcomes the secondary paths generated by reflections and diffractions on the bodies (or on the environment) while moving.

3.4.3 Body Shadowing Effect

Starting from measurements set *IV* (see Sec. 3.2.3) and considering Eq. 3.4.2, the *mean channel gain* is extracted applying a sliding temporal window w to the recorded samples of $P(d, \alpha)$, in order to follow its slow-variations over the angle α. Curves in Fig. 3.25 show an example of the results obtained for the chest/chest link when PM antennas are used, each color referring to acquisition at different d. *Mean channel gains*, $G(d, \alpha)$ (continuous curves) are extracted from $P(d, \alpha)$ values (dashed curves) considering $w = 1.5$ s. It can be noticed that, even if $G(d, \alpha)$ follows the same trend

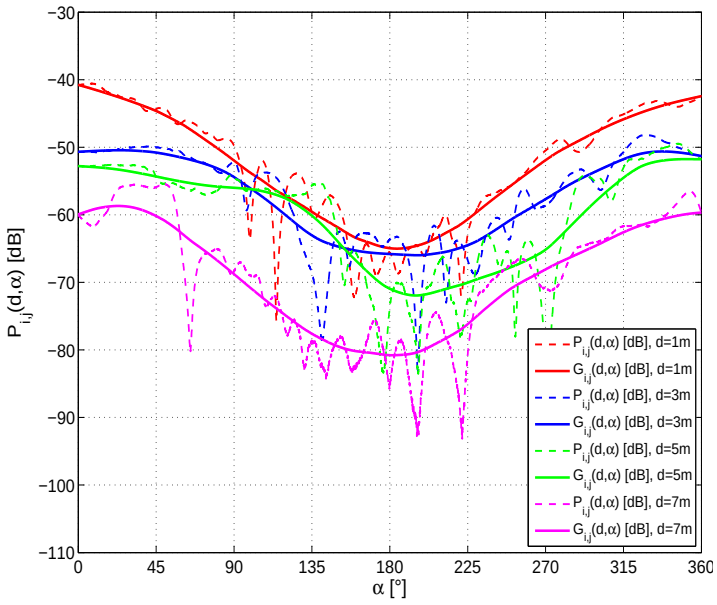

Figure 3.25: Body shadowing trends for the chest/chest link at different d, PMs, rotation.

independently on the distance, it presents different fade depth. This can be explained considering that acquisitions are performed in indoor and at each d corresponds a specific source of multipath interference, which results into different shadowing dips.

As presented in Eq. 3.4.2 the *body shadowing* effect, $S(d, \alpha)$, can be extracted for

Table 3.13: $\Delta S(d)$ $[dB]$ for different distances d - Rotation - Tx Chest

Rxs	$\boldsymbol{d = 1m}$		$\boldsymbol{d = 3m}$		$\boldsymbol{d = 5m}$		$\boldsymbol{d = 7m}$	
	PM	**TLM**	**PM**	**TLM**	**PM**	**TLM**	**PM**	**TLM**
Left Ear	17.89	18.30	15.05	12.64	14.07	14.51	11.79	12.41
Chest	23.07	13.47	17.27	11.89	18.02	13.92	19.93	14.46
Right Hip	21.78	16.81	15.53	14.05	17.61	12.09	16.36	13.63

each d, as the variation of $G(d, \alpha)$ around its average over the angle α $\overline{G(d)}$. In that way, $S(d, \alpha)$ accounts for the effect of the body that masks the direct communication path, as the user changes its orientation α over time during the rotation. It is described through its *maximum variation range* $\Delta S(d)$ according to:

$$\Delta S(d) = \mathbb{E}\Big[\max(S(d,\alpha)) - \min(S(d,\alpha))\Big]. \quad [\text{dB}] \tag{3.4.7}$$

$\max(S(d, \alpha))$ and $\min(S(d, \alpha))$ are computed for every single channel acquisition, and the mean operator is applied gathering all measurements performed at a specific d. Results for both antennas types are reported in Tab. 3.13. Even if the *maximum variation range* results to be strictly dependent on the specific link and antenna type considered, generally PMs present larger $\Delta S(d)$ values, with respect to those found for TLMs. Indeed, the latter are less affected by *body shadowing*, as already discussed in Secs. 3.4.1 and 3.4.2, resulting in smaller values of $\Delta S(d)$. A statistical characterisation of the *body shadowing*, $S(\alpha)$, is performed gathering all the acquisitions, regardless of the distance d where the measurements are realised. Bars in Figs. 3.26 and 3.27 present an example of the empirical Probability Density Function (PDF) of $S(\alpha)$ for the chest/chest link for PM and TLM antennas, respectively. Both PDFs show a peculiar two-lobe configuration, symmetric around the

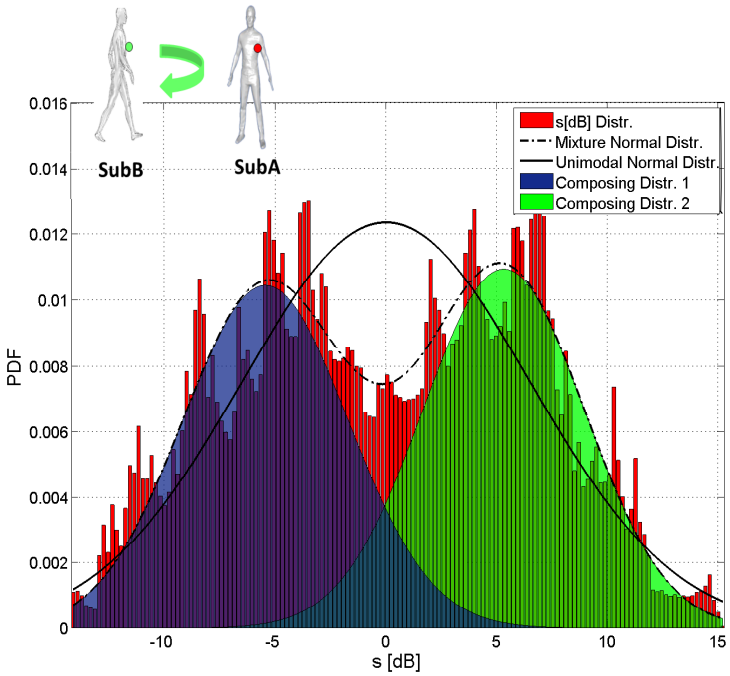

Figure 3.26: Mixture Probability Density Function of s for the chest/chest link, PMs.

mean value, which can be modeled through a *mixture distribution* composed by two one-dimensional normal distributions, as shown in Figs. 3.26 and 3.27 by the light colored areas. Each composing distribution is defined by its mean value μ_i and standard deviation σ_i, $i = 1, 2$. Considering $s \in S(\alpha)$ as the *body shadowing* values expressed in dB, the resulting mixture PDF, $p_S(s)$, (dashed curve in Figs. 3.26 and 3.27) can be expressed as the weighted combination of the individual composing PDFs $p_i(s)$, according to:

$$p_S(s) = \sum_{i=1}^{2} w_i \cdot p_i(s); \tag{3.4.8}$$

where w_i are the non-negative weights assigned to each $p_i(s)$. More details on mixture modeling can be found in [211]. Tab. 3.14 lists the values describing each composing distribution for both antenna cases.

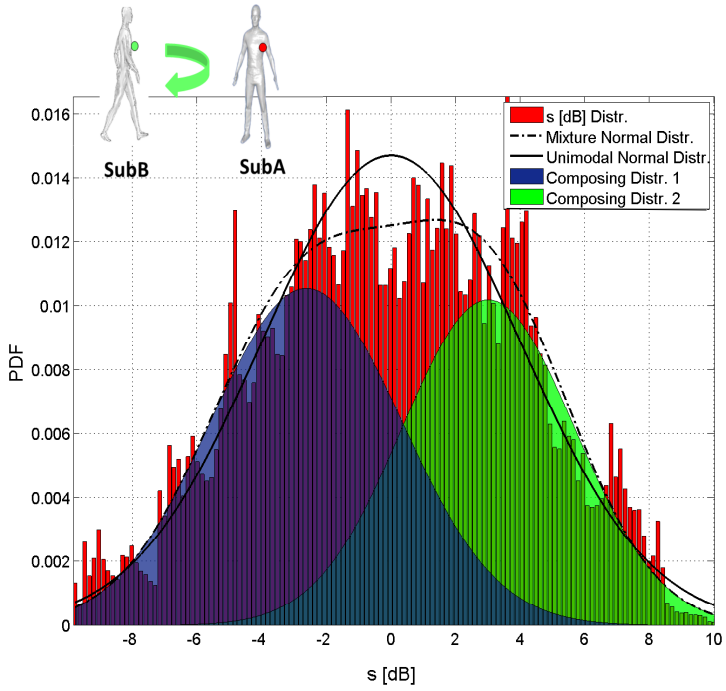

Figure 3.27: Mixture Probability Density Function of s for the *chest/chest* link, TLMs.

The physical meaning of the two-lobe configuration can be explained considering the particular movement performed by the user. Indeed, during a rotation the body stands for most of the time (i.e., for a wide span of the full circle) in intermediate positions between the mutual directions of maximum and zero of Tx/Rx antenna radiation patterns, which correspond to a maximum and a minimum of $S(\alpha)$. As a consequence, a large part of the *shadowing* values result to be in between its mean, i.e., 0 dB, and its extreme values, i.e., $\max(S(\alpha))$ and $\min(S(\alpha))$. In other words, each composing distribution $p_i(s)$ models the subset of values that the *shadowing* assumes while approaching or moving away from antennas' mutual max or zero direction, defining in that way a *"visibility"* or *"non visibility"* area, respectively. Values close to 0 dB are assumed few times during rotation, instead, acting as a sort of "breaking

Table 3.14: Mixture Distribution Parameters - Rotation - Tx Chest

	Planar Monopole			Top Loaded Monopole		
	Rx Left Ear	**Rx Chest**	**Rx Right Hip**	**Rx Left Ear**	**Rx Chest**	**Rx Right Hip**
$\mu_1[dB]$	-0.97	-5.28	-5.01	-3.01	-2.87	-1.59
$\mu_2[dB]$	0.87	5.45	4.79	1.42	2.79	4.72
$\sigma_1[dB]$	4.52	3.83	3.79	4.57	2.86	3.64
$\sigma_2[dB]$	5.10	3.58	4.04	3.42	2.74	2.16
w_1	0.47	0.51	0.49	0.32	0.49	0.75
w_2	0.53	0.49	0.51	0.68	0.51	0.25

point" separating the two composing distributions.

This effect can be eventually mapped on the full circle, dividing the angles α related to $S(\alpha)$ values belonging to one distribution or to the other. However, it has to be noticed that antennas' mutual max and zero directions strongly depend on their specific radiation pattern and on the on-body position, and they could evolve during time according to the movement performed by the user. A precise evaluation of these directions is out of the scope of the present work, but reader can find a related work on simulating how antennas position and radiation characteristics evolve during a walk in [212]. Depending on the specific node location and on the antenna considered, the two-lobe configuration can be more or less stressed. For example, the chest/chest link presents symmetric mean values with approximately same standard deviation and equal weight (see Tab. 3.14), resulting in a bimodal distribution, which is more evident in PMs case than in TLMs one (see Figs. 3.26 and 3.27). Similar considerations apply to the chest/hip link when PMs are considered.

Generally, TLMs present a less important bimodal configuration as compared to PMs. Indeed, the latter are more affected by the *body shadowing*, resulting in sharper

transition between the *"visibility"* and *"non-visibility"* areas, and composing distributions lobes are hence more defined than in TLM case. This trend can be also highlighted comparing Figs. 3.26 and 3.27, where the continuous black curves represent the unimodal gaussian distribution approximating the *body shadowing* values. TLM antenna presents an unimodal distribution very close to the resulting gaussian mixture one (dash-dotted line) as compared to the PM case. This is mainly related to antennas radiation characteristics that in the TLM case result into a less pronounced two-lobe configuration, which can be possibly described by a simple gaussian distribution, even if it introduces a loss in modeling precision.

Due to the particular position of the node on the ear, the mixture distribution for this link almost loses its bimodal features, for both antennas types. The two $p_i(s)$ present closer mean values (not necessarily symmetric) and large standard deviations, in a way that they almost superpose (see Tab. 3.14). This is due to the fact that the body impact is less important in the ear case, since this position is less masked by the body while rotating. *Shadowing* dips result then moderately deep, and the largest part of $S(\alpha)$ values varies around its mean value. A good description can be given by a simple gaussian distribution, even if it introduces a loss in modeling precision with respect to the use of a mixture distribution.

3.5 Conclusions

An experimental dynamic channel model for *on-* to *off-body communications* is proposed for the 2.45 GHz band, accounting for different measurement conditions (i.e., environments and movements performed) and antennas.

Experimental results show that the *mean channel gain* is strongly dependent on

the specific on-body node location and on the antenna type. In particular, normally polarized antennas yield to smaller attenuation in NLOS conditions, with respect to tangentially oriented ones, thanks to the higher creeping waves diffraction around the body. Moreover, it is shown how the specific movement results into different effects on channel time-variant characteristics. This aspects was considered by proposing a channel model adapted to the investigated scenario.

The statistical description of the *short-term fading* envelope highlights how the secondary MPCs arising from reflections and diffractions from the environment and from the body become more important in NLOS than in LOS conditions. Indeed, in the former case, the human body acts as an obstacle to the main direct communication path, which is weakened by the user's shadowing effect, and secondary paths are then more significant.

The *body shadowing* effect is extracted following the slow variation of the channel power transfer function, as a function of the subject orientation. According to the node position, the body masking effect can be more or less stressed, which results in different *shadowing* trends as the user moves. Generally, antennas with normal polarization help to better counteract the body masking effect, even if this consideration strictly depend on the movement performed and on the mutual position of the subjects.

Off-body channels *space* and *time* correlation properties were also evaluated, to study the relationship between fading effects of different link, and their stability over time. Correlation parameters also depend on node position and on antenna type.

The proposed models, jointly with the *on-body* one presented in Chapter 2, are derived in order to be able to account for the most important dynamic characteristics

related to the body movement and to the environment considered. Network simulation studies can take advantage of the implementation of these models, allowing the evaluation of system performance considering realistic radio channel conditions. An example of the potential of the work performed is shown firstly in Chapter 4, focusing just on the *on-body* scenario, and subsequently in Chapter 5, merging *on-* to *off-body* communications with human mobility and sociality aspects.

Chapter 4

How the Radio Channel Affects System Level Performance

This chapter presents the results obtained from an extensive simulation campaign aimed at assessing and comparing the performance of different MAC protocols suitable for *on-body* communications. Simulations are conducted integrating real-time channel data to account for realistic propagation aspects and their impact on system level performance. A general overview of the MAC schemes available in literature, specifically addressing *on-body* scenarios, is given in Sec. 4.1, with a particular focus to those simulating IEEE 802.15.6-based solutions. Sec. 4.2 presents in details the WiserBAN protocol solutions and reference scenario, explaining how the propagation aspects are considered and included in the simulations. Finally, numerical results for system PLR, node transmission delay and energy consumption are provided in Sec. 4.3; considerations on the impact of a proper channel description on network performance and a comparison of the different protocol solutions is also provided.

4.1 Related Works

Studies on the optimal MAC protocol solution to be used in the BAN context have drawn the attention of many research groups, and a wide variety of proposals are available in the literature of recent years. As already pointed out in Sec. 1.2, the two most important attributes of a good MAC protocol are the energy efficiency and the QoS provisioning capability [88]; therefore, all the proposed solutions aim at minimising the device energy consumption while assuring adequate system performance, for example in terms of transmission delay or jitter.

Several works in literature overviews the MAC proposals for BAN, among them [88, 213–217] are the most complete and general ones, to the best of author's knowledge. They provide a taxonomy of MAC protocols according to the type of access scheme they employ (whether TDMA- [213], contention- [218, 219], or contention/schedule-based [220]) and a description of the energy-efficient techniques they implement, such as Low Power Listening (LPL) [221–223], context and traffic awareness [224–226], or wake-up strategies [227, 228], etc.

The general picture that can be drawn from these surveys is that many of the available contributions refer to the study of the applicability of existing WSN protocols to the BAN scenario [87]. A particular emphasis is given to IEEE 802.15.4 standard [229], which is often used as term of comparison with newly proposed protocols, such as in [225, 230–234]. Potential improvement and optimisation of existing protocols are also proposed in [235, 236].

Other than the IEEE 802.15.6 MAC solution, very few contributions are specifically designed for BANs. Among them, some examples that deserve a more detailed

description are the following:

- *Controlling Access with Distributed slot Assignment (CICADA)* [237]: it is a low energy protocol designed for multi-hop, mobile BANs. It aims at supporting high-rate data traffic with reduced delays (i.e., all sensors send data frequently instead of buffering them locally).

- *BSNMAC* [235]: it is a dedicated ultra-low-power MAC protocol for star topology networks. BSNMAC is compatible with the IEEE 802.15.4 solution, and it accommodates unique requirements of the sensors in BANs. By exploiting feedback information from distributed sensors in the network, BSNMAC adjusts protocol parameters dynamically to achieve best energy conservation on energy-critical sensors.

- *Hybrid MAC (H-MAC)* [238]: it is a TDMA-based MAC protocol, which aims at improving energy efficiency by exploiting heartbeat rhythm information to perform time synchronization. It is achieved following the naturally synchronized heart rhythm extracted from ECG data, without the need to receive periodic timing information from a central coordinator node, and thus reducing energy costs due to time synchronization tasks [87].

- *BAN Adaptive TDMA MAC (BATMAC) [239]*: it is a protocol based on an adaptation of IEEE 802.15.4 SF structure, which automatically detects the shadowing effect of the human body on the channel, in order to accordingly change the parameters of the SF and to use relay node when necessary. Latency outage probability is reduced at the expense of a reasonable increase in the power consumption of the relaying nodes.

As a concluding consideration arising from the literature, the first step in the selection of the best performing MAC protocol is certainly related to the type of channel access it is preferable, whether contention-based or contention-free. These two macro-categories cover almost the totality of proposed solutions, with possible merging of the two resulting in hybrid protocols. Their characteristics and the performance they lead to are diametrically opposite in terms of energy consumption, scalability, transmission delay, synchronization requirements and traffic level they can handle. Hence, the final choice should be the one that provides the best trade-off between the different requirements the application demands to the system designer.

The work proposed in this chapter, which targets the WiserBAN use cases and the related reference scenario presented in Sec. 4.2, does not propose a new MAC access scheme, rather it evaluates and compares via simulation three contention-based protocols among those already available in literature: the Slotted ALOHA and two versions of the CSMA/CA. Algorithms performance are given in terms of PLR, average transmission delay and node energy consumption.

With respect to the studies presented above and to other similar ones, the novelty introduced by this thesis is twofold. First of all, two of the simulated access schemes (Slotted ALOHA and one of the CSMA/CA protocols) are those proposed in the IEEE 802.15.6 standard. Moreover, one of the PHY solution considered in the simulations is compliant with the narrowband one working at 2.45 GHz, as described in the IEEE 802.15.6 document [240,241]. Very few studies can be currently found in the literature regarding this communication protocol, all of them accounting anyway for simplified assumptions regarding BANs architecture. Among them, [242] gives an overview of the different MAC mechanisms proposed in the standard, describing their pros and

cons. In [243] a simple analysis of theoretical throughput and delay limits is carried out, considering an ideal channel with no transmission errors and the different IEEE 802.15.6 frequency bands and bit-rates. [244] extends the work in [243], comparing theoretical limits with simulations for networks with increasing number of nodes. An analytical model to examine the energy lifetime performance of periodic scheduled allocations is presented in [245]. Performance analysis based on a Markov chain model for CSMA/CA can be found in [246] and [247], which study networks in saturated and unsaturated conditions, respectively [27]. Authors in [248] propose an evaluation of the IEEE 802.15.6 CSMA/CA performance, given in term of PLR, delay and throughput, considering two different simplified channel models. Results are also compared to those referring to the simulation of IEEE 802.15.4 CSMA/CA algorithm, and they highlight the importance of choosing a proper channel model to account for the impact of realistic propagation conditions at the system level. This issue was already investigated in [249], along with impact of the PHY layer characterisation in simulation, which call for a trade-off between soundness and computational cost.

Starting from these last considerations, the second innovative aspects of the present chapter refers to the fact that simulations are conduced integrating real-time channel data acquired through an ad-hoc measurement campaign. To the best of author knowledge, this is one of the very few works in literature that investigate the effects of realistic channels on IEEE 802.15.6-based MAC protocol performance for BANs. A similar study was performed by authors in [250], they evaluate the impact of Rice fading channels on IEEE 802.15.6 MAC scheme working in non-saturation regime; the results obtained through an analytical Markov chain model are then validated via simulations. The channel model they consider does not account for

the impact of body movement, which is embedded in the channel data used in the work presented in this thesis, instead. The dynamic aspects of channel modeling are accounted for in other two works [251, 252], aiming at assessing MAC protocols and localization algorithm performance in the BAN context, but they refer to the solutions proposed in the IEEE 802.15.4 standard.

4.2 The WiserBAN PHY/MAC Solutions

4.2.1 WiserBAN Protocol Solutions

As already presented in the Introduction, the WiserBAN project aims at developing a dedicated protocol stack, targeting some specific use cases, as shown in Fig. 2a. In particular, at the PHY layer three different modulation schemes are accounted for, as possible solutions to be implemented:

- *PHY 1*: IEEE 802.15.4-compliant PHY; it adopts a Minimum Shift Keying (MSK) modulation with spreading, resulting in a bit-rate of 250 kbit/s;
- *PHY 2*: it is derived from *PHY 1* removing the spreading; just MSK modulation is used with a bit-rate of 2 Mbit/s;
- *PHY 3*: Bluetooth Low Energy-compliant PHY, which uses a Gaussian Minimum Shift Keying (GMSK) modulation, with a bit-rate of 1 Mbit/s.

As for the MAC layer, one of its main functions consists in the management of node access to the radio resource, when more than one device (other than the Network Coordinator (NC)) are part of the network. This task is practically realised by the NC through the establishment and the maintenance of a SF, whose length

(T_{SF}) is defined as the time interval between two consecutive beacon packets (see Fig. 4.1). The SF may be structured in an *active* and an *inactive* part; during the latter, nodes can go into stand-by state to reduce their power consumption. As shown in Fig. 4.1, the WiserBAN SF active portion is divided into several parts, adapting the IEEE 802.15.4 [89], IEEE 802.15.6 [4], and BATMAC [239] proposals:

- *Beacon portion*: reserved for the transmission of the beacon by the NC. It contains network management information;
- *Indicators portion*: where nodes have reserved mini-slots to send an ACK to the NC, in case the beacon is correctly received;
- *CFP*: where nodes access the radio channel through a TDMA-based scheme. A certain number of time slot is allocated to nodes with more stringent application requirements;
- *CAP*: where nodes compete for the access to the channel, according to the CSMA/CA or Slotted ALOHA algorithm;
- *ACK portion*: mini-slots are assigned to the nodes to communicate if data exchange during the current SF were successful or not.

T_{SF}, as well as the duration of the single part composing the SF, can be tuned according to the specific requirement demanded by the application. The CAP portion has to be always present in the SF, at least to handle slots requests. If no other traffic needs to be managed in it, its duration T_{CAP} is set to the minimum possible value.

The MAC protocol solutions that WiserBAN considers for adoption in the CAP part are three: the CSMA/CA in the two versions proposed in the IEEE 802.15.4 and

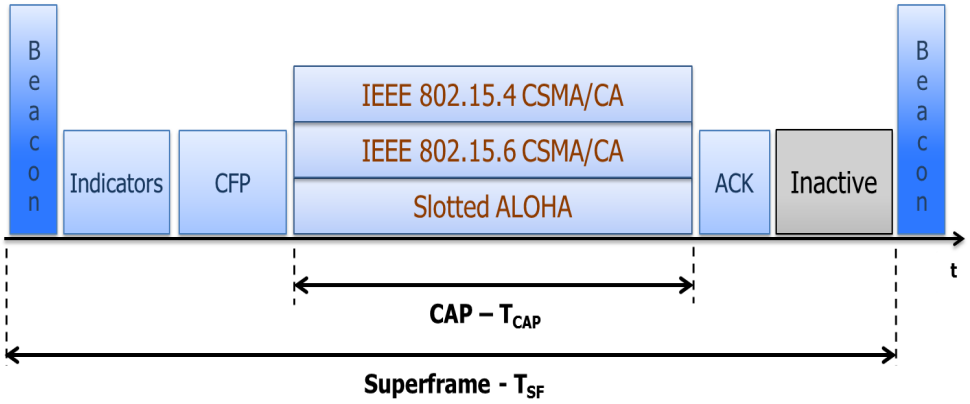

Figure 4.1: WiserBAN reference SF structure [27].

802.15.6 standard, and the Slotted ALOHA algorithm as defined in IEEE 802.15.6 (see Fig. 4.1).

1. *IEEE 802.15.4 CSMA/CA Algorithm*: It is implemented using units of time called Backoff periods (BPs) with a duration of 320 μs. For each transmission attempt, every node in the network should maintain three variables, namely NB, CW, and BE. NB, is the number of times the algorithm is required to backoff while attempting the current transmission; it is initialized to 0 and it can assume a maximum value of $\mathrm{NB}_{\mathrm{max}}$. CW is the contention window length, whose initial value is equal to 2. It defines the number of BPs where no activity on the channel should be detected before a new transmission can start. BE is the backoff exponent related to the number of BPs a node shall wait before attempting again to sense the channel. It varies between $\mathrm{BE}_{\mathrm{min}}$ (initial value) and $\mathrm{BE}_{\mathrm{max}}$. Once a node receives a beacon from the NC, it delays any activity (backoff state) for a number of BPs randomly drawn in the range $[0 \div 2^{\mathrm{BE}-1}]$. After this delay, channel sensing is performed for one BP. If the channel is sensed as busy, CW is reset to 2, while NB and BE are increased by 1, ensuring

that BE $\leq$ BE_{max}. If NB $\leq$ NB_{max} the node should return in backoff state and wait for another random interval of time. If the channel is assessed as idle, instead, CW is decremented by 1. If CW$<$ 0, the node waits for another BP and then it sounds again the channel state, acting accordingly to what explained before (busy or idle state). The algorithm ends whether with the data transmission for $CW = 0$ or with a failure, when NB $\geq$ NB_{max}, meaning that the node does not succeed in accessing the channel in a maximum number of attempts.

2. *IEEE 802.15.6 CSMA/CA Algorithm*: In this case the time is divided into slots of 125 μs. When a node has data to be sent, it randomly chooses a Backoff Counter (BC) in the interval $[1 \div \text{CW(UP)}]$, where $\text{CW(UP)} \in [\text{CW(UP)}_{\text{min}} \div \text{CW(UP)}_{\text{max}}]$. The values of $\text{CW(UP)}_{\text{min}}$ and $\text{CW(UP)}_{\text{max}}$ depend on the user traffic priority (UP); larger CW values for data with less stringent requirements. If the channel has been sensed as idle for a Short Inter Frame Spacing ($pSIFS = 50\mu s$), the node decrements its BC by one for each idle slot that follows. Once the BC has reached zero, the node can transmit its frame. The CW is doubled every two failures, ensuring that it does not become larger than $\text{CW[UP]}_{\text{max}}$. If the channel is found busy, the BC is locked until the channel becomes idle again for *pSIFS* [19].

3. *IEEE 802.15.6 Slotted ALOHA Algorithm*: Time is divided into slots, whose duration depends on the length of the frames that have to be transmitted. Each node wishing to perform a transmission obtains a contended allocation in the current ALOHA slot if $z \leq \text{CP[UP]}$, where z is a random value in the interval $[0 \div 1]$, newly drawn for every attempt. CP(UP) is the Contention Probability,

set according to the result of the last contended allocation, and whose value depends on the UP (smaller for lower priority data). If the node did not obtain any contended allocation previously or succeeded in the last contended allocation it had obtained, it shall set the CP(UP) to its maximum value, which depends on the user priority. If the node transmitted a frame requiring no ACK or the ACK was received at the end of its last contended allocation, it shall keep the CP unchanged. If the node failed in the last contended allocation it had obtained, it shall halve the CP(UP) value every two failed attempts, ensuring that it does not become smaller than $\mathrm{CP(UP)}_{\mathrm{min}}$ [208].

4.2.2 Reference Scenario and Simulation Settings

As for the evaluation and comparison of the different MAC protocols and PHY solutions presented in Sec. 4.2.1, the reference network topology considered in simulations is a star one. In particular, it is composed of four nodes transmitting data to the NC. Each end-device is placed in a specific on-body position according to the four WiserBAN use-cases, as described in the Introduction (see Fig. 2b). Nodes on the ear refers to the hearing aids or to the cochlear implant application, the node on the chest is related to the cardiac implant use-case, while the device on the hip accounts for the insulin pump application [208]. As for the NC, it acts as the Remote Controller (RC) node as described in Sec. , and it is considered to be placed in three different positions, each one corresponding to an investigated sub-scenario (see Fig. 4.2). Sub-scenarios A and B are the cases when the RC is held in the left and right hand, respectively; whereas in sub-scenario C the RC is considered to be placed at the thigh level, emulating a device hosted in a pocket.

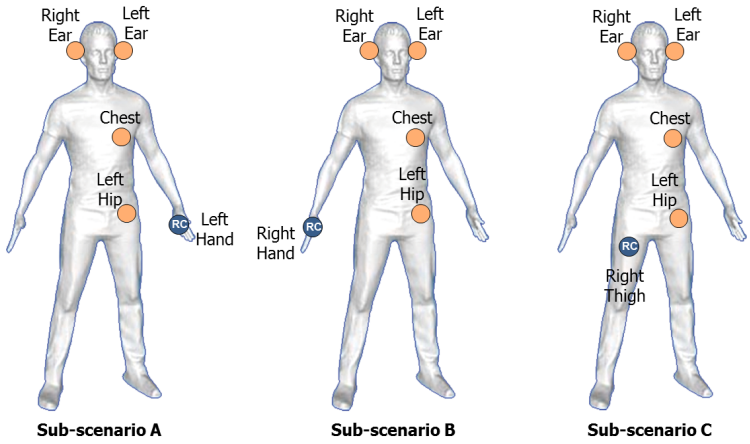

Figure 4.2: WiserBAN simulated sub-scenarios and related nodes position [27].

As for the movement and posture, both walking and standing conditions are accounted for. Note that the investigated node positions are consistent with those considered during the *on-body* measurement campaign described in Sec. 2.2.2 (see Fig. 2.2). This allows the direct integration of the measured channel data in the simulator, which lead to a more realistic performance evaluation and comparison of the different PHY and MAC protocol solutions. In particular, two sets of measurements are used in simulations: the first one are the data acquired in anechoic chamber while the test subject stood still for the duration of the experiment; the second one refers to the indoor acquisition while the subject was walking (see Sec. 2.2.2). Considering that measurements refer to the use of two different kind of antennas, namely TLM and PM (see Sec. 2.2.3), simulations are performed including both data sets. This allow to draw some interesting consideration on how antenna radiation and polarization characteristics affect the system performance. It should be noticed that, for the specific measurement campaign performed, the whole mesh network needed to completely simulate the channel access scheme is not covered by the acquisitions.

To overcame this problem, the non-measured links are statistically described using some previous available models or characterised by the acquired channel data of a symmetric link [253].

To perform the simulation campaign, two platforms are used: the first one, available at UniBO, allows the investigation of the performance of the two CSMA/CA algorithms, while Slotted ALOHA protocol is implemented over another simulation tool realised at CEA-Leti; both institutions are partner within the WiserBAN consortium. For a fair comparison of the results, common scenarios, channel data, and packet capture models (see Sec. 4.2.3) are implemented in both simulators. Only the CAP portion of the SF is considered for data transmission, and no CFP is accounted for in simulations (see Fig. 4.1).

A simplified query-based traffic model is taken as a reference: upon reception of a query from the NC asking for data, at the beginning of every SF each node generates one packet of equal size. If a node does not succeed in correctly sending its packet before the next query (i.e., before the end of the current SF), the packet is considered as lost. It is also assumed that ACK packets do not collide. According to this, packets can be lost due to *connectivity* (the end-device could not reach the NC), *collisions* (a maximum number of retransmissions is set), and due to the *end of the SF*.

100 000 SFs are simulated, meaning 100 000 packets to be transmitted by each node to the NC. The parameters set used for the different channel access algorithms are: $CW_{min} = 8$ and $CW_{max} = 16$, for 802.15.6 CSMA/CA, while for 802.15.4 CSMA/CA $NB_{max} = 4$ and the other MAC parameters are set to the standard default values [89]; finally, $CP_{min} = 1/8$ and $CP_{max} = 1/4$ for Slotted ALOHA. Other relevant PHY and MAC simulation parameters are listed in Tab. 4.1.

System performance are evaluated in terms of:

a) Packet Loss Rate (PLR); averaged on all the links composing the network. It is computed as the ratio between the number of packets lost and the total number of generated packets. A loss due to *connectivity* or *collision* issues is assessed according to the packet capture model, as described in more details in Sec. 4.2.3 according to the specific PHY solution considered;

b) average delay; which is the average interval of time between the beginning of the SF and the correct reception of the packet at the NC;

c) average energy consumption; which represents the average energy consumed by a node to send its packet in the SF.

4.2.3 Packet Capture Model

This section illustrates how the packet capture phenomenon is modeled in the simulators. The model takes into account the fact that packets can overlap totally or partially. To better clarify the latter condition, a graphical example is shown in Fig. 4.3.

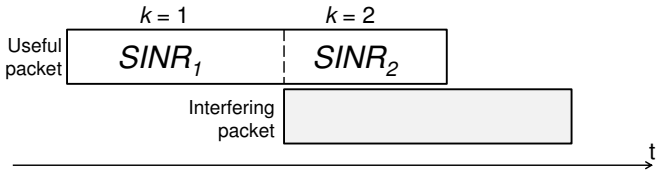

Figure 4.3: Example of packets partial overlap. [27]

For a given packet of interest sent by a node, several Signal-to-Interference-and-Noise Ratio (SINR) values can be computed, depending on current variations of

Table 4.1: Simulation parameters for WiserBAN scenario. [27]

Parameter	Value	
Noise power, P_n	PHY 1	- 102 dBm
	PHY 2	- 102 dBm
	PHY 3	- 104 dBm
Transmit power, P_T	0 dBm	
Receiver sensitivity	PHY 1	- 96 dBm
	PHY 2	- 87 dBm
	PHY 3	- 90 dBm
Coordinator antenna efficiency, η_C	- 3 dB	
End-device antenna efficiency, η_{ED}	- 15 dB	
Current consumption, transceiver on	10 mA	
Current consumption, stand-by	100 nA	
Supply voltage	1.2 V	
PHY header + preamble	112 bits	
MAC header + FCS	9 bytes	
Maximum number of retransmissions	3	
CAP duration, T_{CAP}	37 ms	

interference level. Therefore, for every packet portion k (see Fig. 4.3 for an example), we have:

$$\mathrm{SINR}_k = \frac{P_R}{P_n + P_I}, \tag{4.2.1}$$

where P_R is the useful received power, P_n is the noise power (see Tab. 4.1), and P_I is the interfering power.

P_R can be expressed as:

$$P_R = P_T \cdot |H_u|^2 \cdot \eta_{NC} \cdot \eta_{ED}, \tag{4.2.2}$$

considering P_T as the power transmitted by the node, and $|H_u|^2$ as the channel transfer

function of the useful link at a given observation time, which is directly taken from the measured channel data. η_{NC} and η_{ED} are the antenna factors that take into account antenna efficiency at the NC and at the end-device when placed on the human body (see Tab. 4.1). These correction factors are used to consider the efficiency reduction due to the miniaturisation effect, according to the physical limitation of small antennas [57].

P_I is evaluated through:

$$P_I = \sum_m P_T \cdot |H_m|^2 \cdot b_{k_m} \cdot \eta_{NC} \cdot \eta_{ED_m}, \tag{4.2.3}$$

where $|H_m|^2$ is the on-body channel gain for the m-th interfering link and b_{k_m} is a boolean variable indicating if the m-th interferer is present during the packet portion k (in the example of Fig. 4.3, $b_{1_1} = 0$ and $b_{2_1} = 1$). Also in this case, η_{NC} and η_{ED_m} accounts for the antennas efficiency at the NC and at the m-th interferer, respectively.

For each computed SINR value, the BER or the Symbol Error Rate (SER) for each portion k is calculated in a different way for every PHY, in order to derive the PER according to the following:

$$\text{PER} = \begin{cases} 1 - \prod_{k=1}^{N} (1 - \text{SER}_k)^{N_{\text{s}_k}} & \text{for PHY 1} \\ \\ 1 - \prod_{k=1}^{N} (1 - \text{BER}_k)^{N_{\text{b}_k}} & \text{for PHY 2, 3} \end{cases} \tag{4.2.4}$$

where N is the number of packet portions ($N = 2$ in the example of Fig. 4.3) and N_{b_k} (N_{s_k}) is the number of bits (symbols) in the portion k.

SER and BER values are estimated as reported below, according to the PHY Layer considered, and the packet reception decision is then based on the PER calculated as in Eq. 4.2.4. Considering x as a uniformly distributed random variable in $[0 \div 1]$,

drawn for each packet, if $x \geq$ PER the packet is correctly received, otherwise the packet is lost [27].

PHY 1

In this case the SER has to be computed:

$$\mathrm{SER}_k = \sum_{n=1}^{32} \binom{32}{n} \mathrm{CER}_k^n \left(1 - \mathrm{CER}_k\right)^{32-n} \cdot P_s(n), \tag{4.2.5}$$

where $P_s(n)$ is the symbol error probability when n chips are not correctly received (values are taken from [254]) and CER is the Chip Error Rate. The expression of the CER as a function of the SINR is evaluated here through the formula $\mathrm{CER}_k = \frac{1}{2} e^{-(\mathrm{SINR}_k)^{0.66}}$. The latter has been obtained through the comparison between experimental derivations of [255] and the PER expression found in [254], and minimum least square fitting.

PHY 2

Without spreading, the expression given above (PHY 1) for the CER applies in this case to the BER, owing to the absence of any sort of bit aggregation to form multi-level symbols:

$$\mathrm{BER}_k = \frac{1}{2} e^{-(\mathrm{SINR}_k)^{0.66}}. \tag{4.2.6}$$

PHY 3

The following expression, empirically derived for Bluetooth Low Energy PHY [256], is used:

$$\mathrm{BER}_k = \frac{1}{2} e^{-(\mathrm{SINR}_k)^{0.7}}. \tag{4.2.7}$$

4.3 System Level Performance Evaluation

This section presents the numerical results obtained from the different simulation campaign realised. For each PHY Layer proposed in the WiserBAN framework, simulations are performed to evaluate the performance of the three channel access schemes presented above. Realistic channel conditions are considered, integrating the real-time channel data acquired from the *on-body* measurements campaign described in Sec. 2.2.2. Comparison on the effect of the antenna radiation and polarization specifities on the system performance are also reported. Outcomes are presented in separate sections according to the system performance parameter analysed; on one hand the system PLR and on the other hand the transmission delay and the average node consumption. Finally, numerical results are validated through some additional measurements performed with on-the-shelf devices IEEE 802.15.4-compatible.

4.3.1 Packet Loss Rate

Firstly, an interesting comparison can be made between the PLR results referring to the standing and walking measurement scenarios. Results coming from the acquisitions performed in anechoic chamber, while the subject is standing, can be considered as a benchmark for those referring to the other sets of measurements, i.e., with the user walking in indoor. Indeed, the former case allows the evaluation just of the effect of the human body on the system performance, since in anechoic premises the effect of the surrounding environment is negligible and no movement is actually performed. On the contrary, in the latter case the channel, and hence the overall system, is strongly affect by the specific environment and by the mobility of the user.

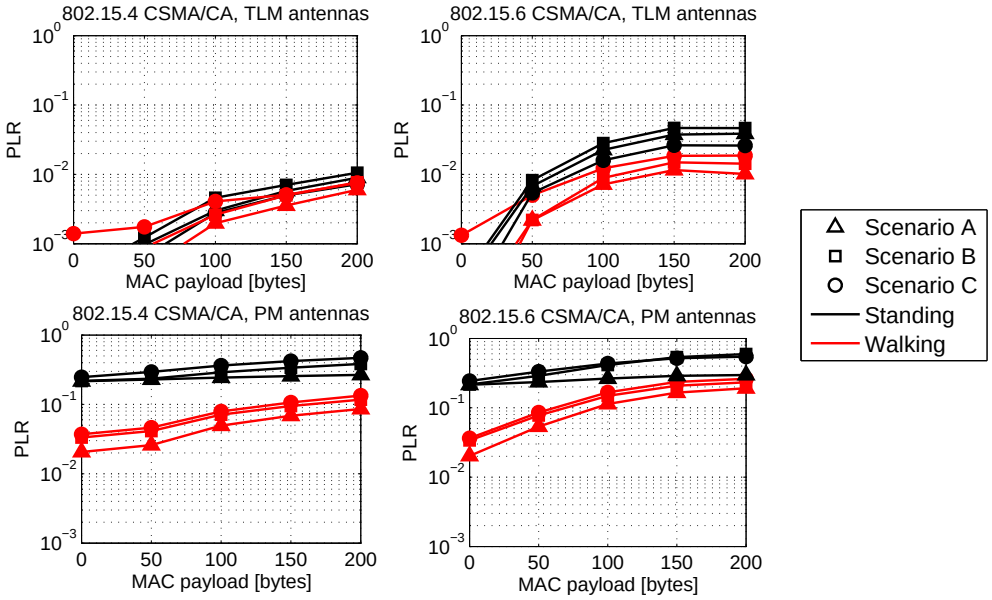

Figure 4.4: Comparison of the PLR for standing (black curves) and walking (red curves) scenarios using CSMA/CA algorithms, considering PHY3. TLMs (upper graphs), PMs (lower graphs).

An example of the results obtained is proposed in Fig. 4.4, where the PLR is given as a function of the MAC payload. Comparing the walking (red curves) and the standing (black curves) scenarios, when PHY3 is accounted for. Each symbols refers to one of the simulated sub-scenarios (i.e., A, B, or C in Fig. 4.2). Irrespective of the channel access scheme (whether CSMA/CA 802.15.4 or 802.15.6) and of the antenna type (TLM or PM) considered, performance for the standing scenario are generally worse than those obtained for the walking one. This is due to the fact that when a person is still, if a link shows some connectivity issues (i.e., the received power is lower than the receiver sensitivity), this condition will never change for the entire duration of the simulations. Conversely, when a subject walks, the PLR values are obtained averaging over different values of the channel power transfer function, corresponding to different relative node positions, evolving in time according to the

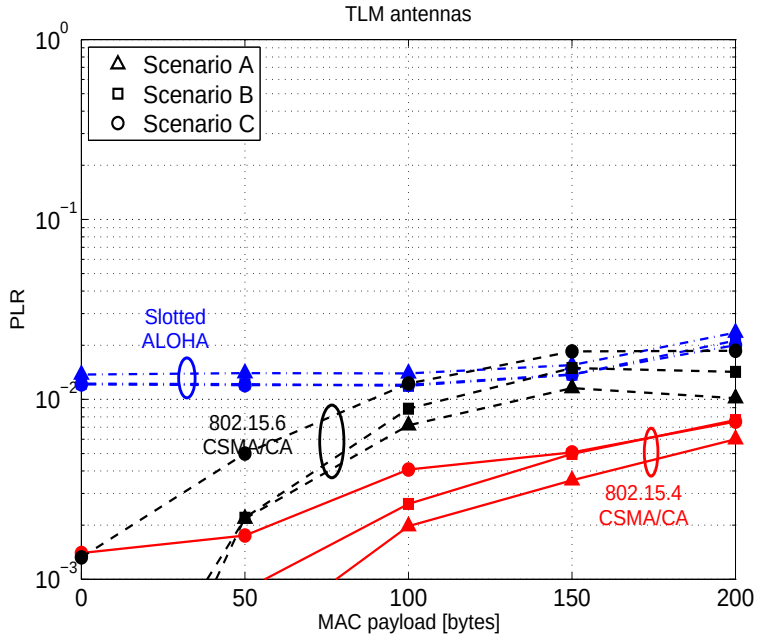

Figure 4.5: Comparison of PLR values for different channel access protocols, PHY3, TLM antennas, walking.

walking movement. This time-varying trend for the channel data globally leads to an overall lower PLR.

This phenomenon is particularly evident for PM antennas (lower graphs in Fig. 4.4), which are not able to achieve an acceptable PLR level, often presenting values higher than 10^{-1}. This is in line with what already pointed out in Sec. 2.3. Indeed, PMs tangential polarization does not help creeping waves propagation on the body, resulting in transmission channels, and hence in system performance, which are more affected by bad link conditions, as could be the case for the standing scenario. A more precise evaluation of the different effects that the antenna type exerts on system performance can be done looking at Figs. 4.5 and 4.6, which show the PLR values obtained with TLMs and PMs, respectively, comparing the different channel access schemes when PHY3 is considered . In both cases, it can be noticed that the

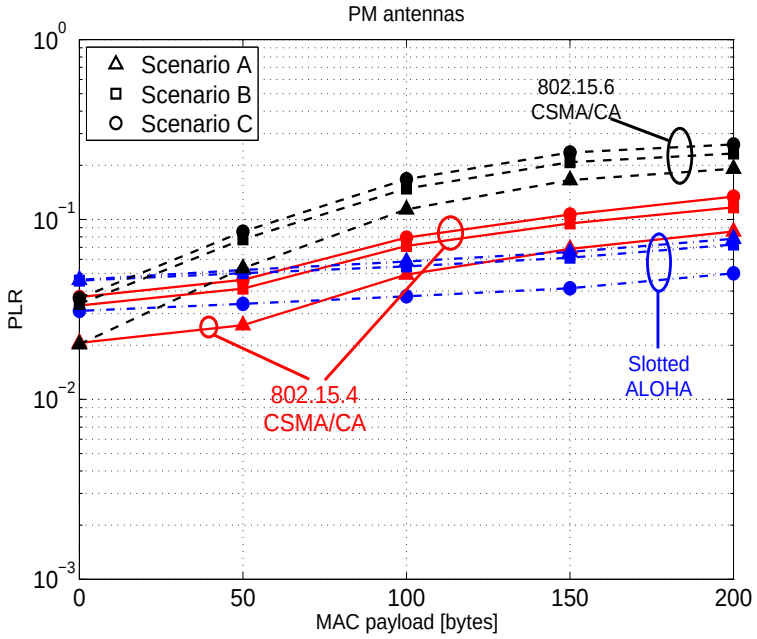

Figure 4.6: Comparison of PLR values for different channel access protocols, PHY3, PM antennas, walking.

differences between the three investigated sub-scenarios, each one represented by a different marker in the figures, are almost negligible. Generally, PMs present worse PLR values than those related to the use of TLMs. This confirms what was expected from the channel measurements; indeed, for their particular propagation and radiation characteristics, PM antennas present lower *on-body* channel gains (see Sec. 2.3.1), as compared to TLMs, which results in a higher attenuations leading to connectivity problems [11]. This effect is confirmed in Fig. 4.7, where each curve represents a possible cause for the loss of the packet, considering the 802.15.6 CSMA/CA algorithm for sub-scenario A. It is possible to notice that 2% of losses are due to connectivity problems when PMs are used (figure above); whereas, in the TLM case (figure below), a generic packet is lost mainly because of collisions or the maximum number of retransmissions is reached, and no problems related to high path losses are present at

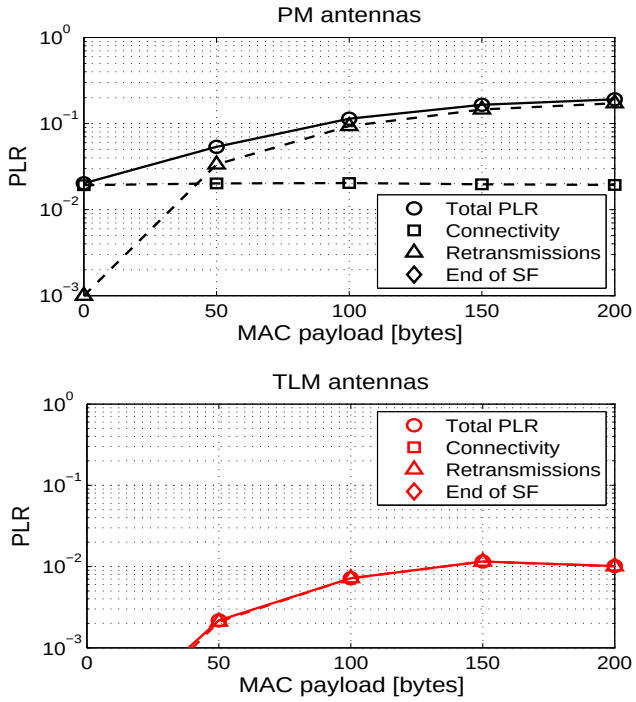

Figure 4.7: PLR causes for IEEE 802.15.6 CSMA/CA algorithm, PM (above) and TLM (below), PHY3, sub-scenario A, walking.

all [19]. Similar consideration also apply for the other two proposed access schemes, but they are not reported here for the sake of conciseness. As a general consideration, it is difficult to choose the overall best performing channel access scheme in terms of PLR, as it is strictly dependent on the antenna used and the underlying PHY. For the PHY3 example in Figs. 4.5 and 4.6, 802.15.4 CSMA/CA slightly outperforms 802.15.6 algorithm; for instance, this is not true for PHY1, as it is shown in Fig. 4.8a when TLMs are accounted for (similar trends are obtained for PMs). Indeed, this latter PHY is characterised by the lowest bit-rate among the ones considered (i.e., 250 kbit/s), which leads to longer time needed to transmit a packet over the channel. In this case, the 802.15.4 CSMA/CA scheme leads to a higher number of packet lost than 802.15.6 algorithm does, since the channel is often found busy. Indeed, the

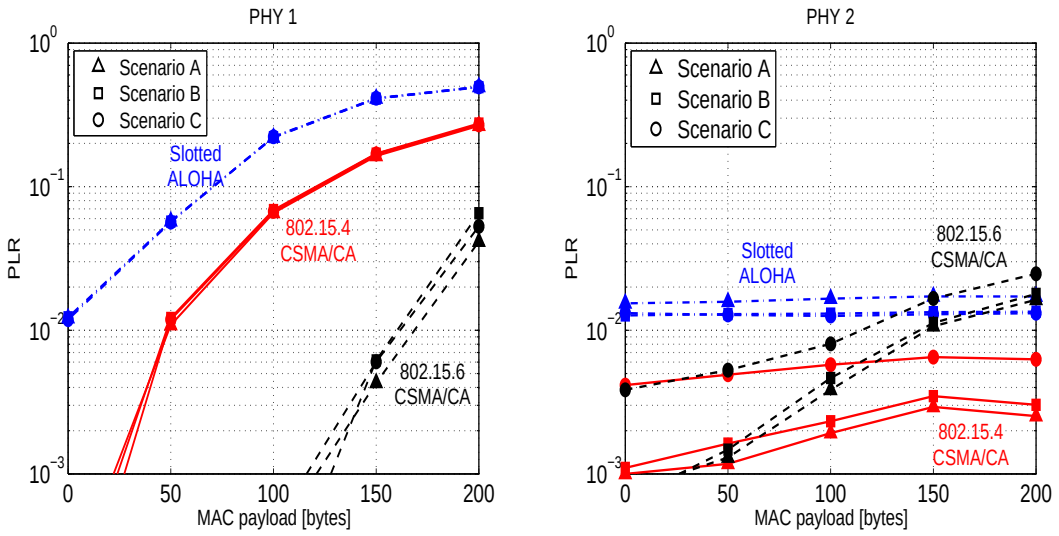

(a) (b)

Figure 4.8: Comparison of PLR values for different channel access protocols, PHY1 (a) and PHY2 (b), TLM antennas, walking.

former algorithm considers a maximum number of possible backoff, which is not the case for the 802.15.6 one. Packets are discarded when the current number of backoffs is grater than the maximum allowed, as shown in Fig. 4.9a, where the PLR are separately presented just for sub-scenario A [27].

As for the PHY2 (see Fig. 4.8b and Fig. 4.9b), PLR values comparable with those found with PHY3 are obtained, and similar considerations can be drawn. The higher bit rate of these two PHYs leads to better system performance than when PHY1 is considered, even when long packet payloads are sent. Generally speaking, Slotted ALOHA protocol presents the worst performance in terms of PLR, irrespective of the PHY and antenna considered.

Another set of simulations is performed considering an antenna efficiency reduction of -35 dB for the device located on the chest position, in order to simulate system

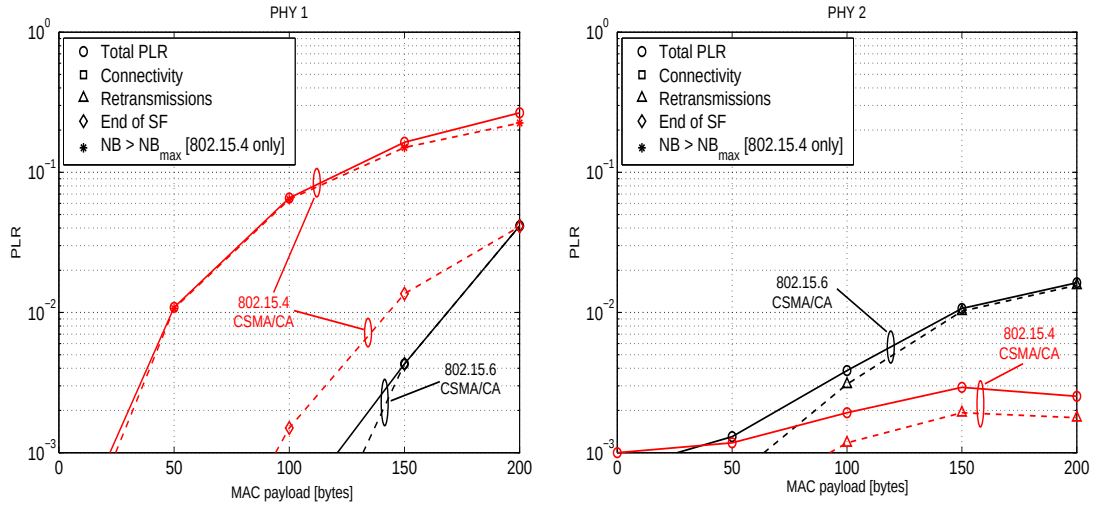

(a) (b)

Figure 4.9: PLR causes for IEEE 802.15.6 CSMA/CA (black) and IEEE 802.15.4 CSMA/CA (red) algorithms, with PHY1 (a) and PHY2 (b), TLM antennas, sub-scenario A, walking.

performance of the cardiac implant application (see Introduction), which has to account for an additional *in-body* channel attenuation (i.e., propagation from the heart to the body surface). This particular value is set considering a typical efficiency for an implanted antenna [123], assuming that its radiation pattern is not modified with respect to the case when the node is placed on-body, but just an efficiency reduction is considered [257].

Fig. 4.10 shows the values of PLR obtained using 802.15.4 CSMA/CA with TLMs in sub-scenario A for PHY3, each curve referring to a specific node position. The degradation of the performance is evident for the chest link when considering the efficiency reduction (dashed line with squares), if compared to the case where it is not taken into account (continuous line). In the former situation, in fact, the implanted

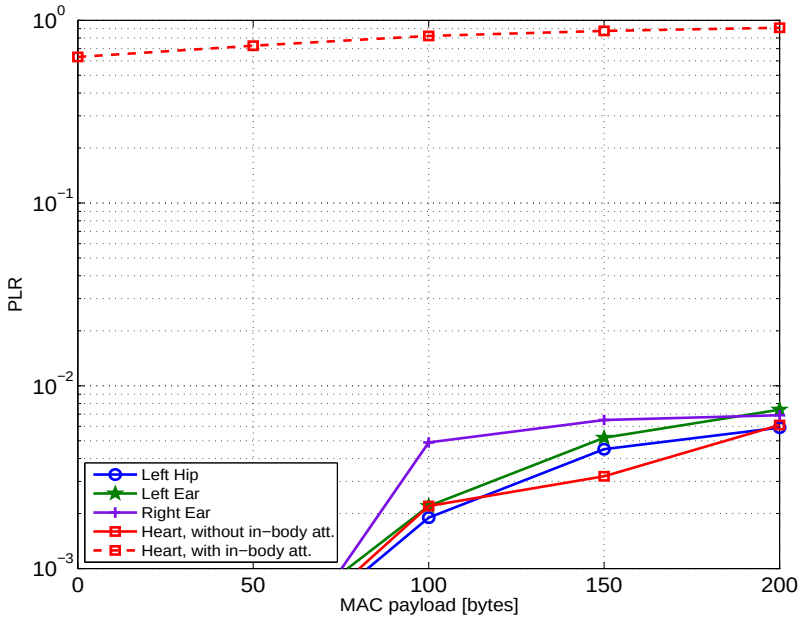

Figure 4.10: PLR per node position for IEEE 802.15.4 CSMA/CA algorithm, PHY 3, TLM antennas, with and without additional in-body heart attenuation.

device would not be able to directly reach the coordinator node in most of the cases.

In order to evaluate how the end-device antenna efficiency, η_{ED}, affects the system performance, some additional simulations are performed varying the value of η_{ED} from -15 dB (i.e., the value considered in previous simulations) up to -21 dB, with a resolution of 2 dB. NC antenna efficiency, η_C , is kept to -3 dB, as in Tab. 4.1. As expected, the PLR increases as the efficiency decreases, since the received power results to be lower, causing connectivity problems (see Fig. 4.11 for 802.15.6 CSMA/CA). It is important to remark that antenna miniaturisation leads to smaller efficiency values, and hence Fig. 4.11 is useful in the definition a proper trade-off between network performance and antenna size, considering how the size issue is of primary importance in the BAN context.

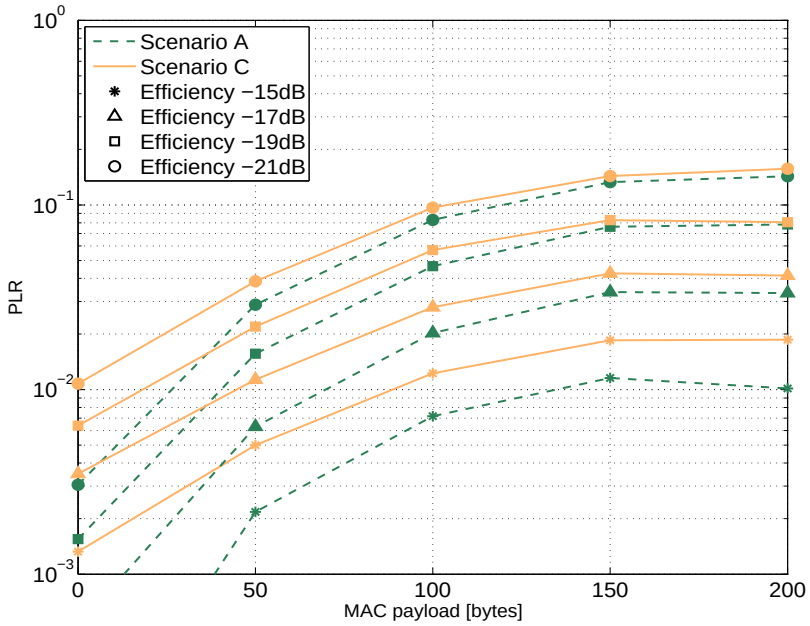

Figure 4.11: PLR for IEEE 802.15.6 CSMA/CA algorithm, PHY3, TLM antennas with varying end-device efficiency, η_{ED}.

4.3.2 Delay and Energy Consumption

As for the delay performance evaluation, Fig. 4.12 shows the results obtained with TLMs comparing the three channel access scheme when the PHY1 is considered. It is possible to notice that there are no significant difference among the three simulated sub-scenarios, and that IEEE 802.15.6 CSMA/CA algorithm presents the lowest delay values, irrespective of the packet payload. This last consideration applies also to the other PHYs under investigation, leading to the conclusion that CSMA/CA protocol in the 802.15.6 standard version is the best performing one, at least from the average transmission delay viewpoint.

Similar trends as the ones in Fig. 4.12 are also found when considering channel data measured with PMs. Delay values in the latter case are just slightly larger than

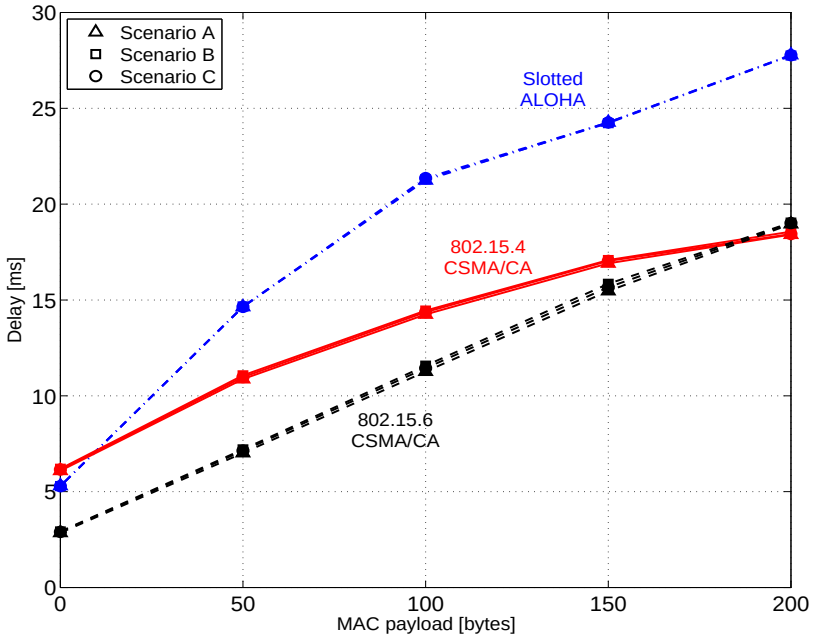

Figure 4.12: Comparison of average delay for the different channel access protocols, PHY1, TLM antennas, walking.

those with TLMs, confirming that worse channel conditions arising from the use of PMs, lead to more important connectivity problems, which actually results in longer time to complete the packet transmission (i.e., more retransmission needed).

As for the comparison of the three PHY solutions, as expected lower delay values are achieved when higher bit-rates are considered, so that focusing on a specific channel access scheme, PHY1 presents larger transmission delays as compared to the other two PHY options, both characterised by higher bit-rates.

The average energy consumed by a node to complete its transmission is also investigated. Considering the values listed in Tab. 4.1 for the current consumption and the supply voltage, Fig. 4.13 compare the values obtained for the different access schemes given as a function of the packet payload. PHY2 is considered, along

with TLM antennas. Results do not change significantly for the three different sub-scenarios and, generally, Slotted ALOHA protocol is the less consuming among the three under investigation. This is due to the lack of backoff and sensing operations in Slotted ALOHA, with respect to the CSMA/CA solutions. Also in this case, when the bit-rate is higher (PHY2 and PHY3) less energy is consumed, since the time needed to send a packet is lower, as well as the time spent with the transceiver on [27]. Energy consumption values are then much higher with PHY1 than those presented in Fig. 4.13, instead. As for the antennas comparison, again PMs show worse performance than those obtained with TLMs, in accordance to what previously highlighted about channel characteristics when tangentially polarized antennas are used (see Sec. 2.3.1).

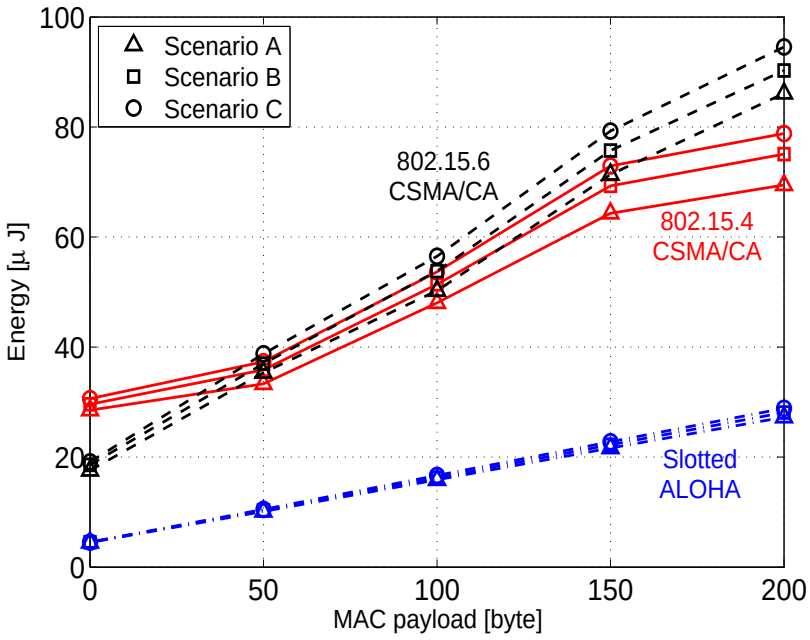

Figure 4.13: Comparison of average energy consumption for the different channel access protocols, PHY2, TLM antennas, walking.

4.3.3 Validation of Numerical Results

In order to validate the simulation results, a set of on-the-field experiments have been performed. The Texas Instruments CC2530 platform is used [258]. The chip contains an IEEE 802.15.4-compliant transceiver (i.e., equivalent to the proposed PHY1), working in the 2.45 GHz band. The access to the channel is managed through the SF shown in Fig. 4.1 not considering the CFP portion, and using the 802.15.4 CSMA/CA protocol in the CAP part.

As in the case of simulations, experiments are performed placing five CC2530 devices (one NC and four end-devices) on a human subject, according to the simulated sub-scenario B (see Fig. 4.2). The NC, located on the right hand, periodically sends beacon packets and waits for replies from devices, which use the CAP portion to access the channel. As for the packet dimensions, the beacon size is equal to 20 bytes, whereas the data packets size is equal to 17 bytes (including PHY and MAC headers), plus the MAC payload (different payload size are considered). For a fair comparison with simulations, the device transmit power is set equal to -22 dBm, instead of 0 dBm (see Tab. 4.1), to compensate the different antennas efficiency. Acquisitions are performed in an indoor environment, while the human subject performed several walking cycles, using alternately monopole antennas with normal or tangential polarization with respect to the body surface. Numerical results, in terms of PLR and average delay, are computed by averaging over 10 000 packets transmitted by each end-device towards the NC.

Fig. 4.14 shows the PLR as a function of the packet payload comparing simulation (dashed curved) and experimental (continuous curve) values achieved considering PHY1 and 802.15.4 CSMA/CA (see Sec. 4.3.1). The good agreement of the curves

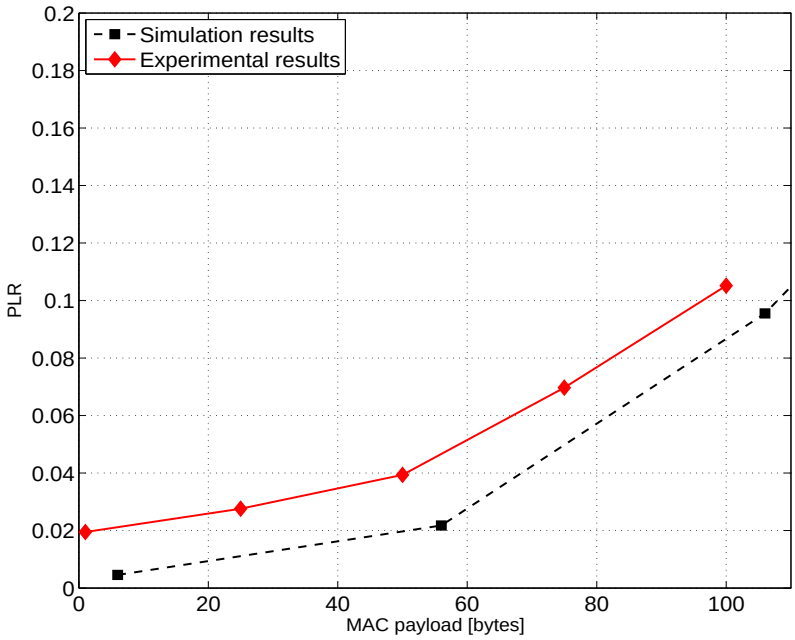

Figure 4.14: Comparison of simulated and experimental values of PLR for 802.15.4 CSMA/CA, PHY1, PM antennas, sub-scenario B, walking.

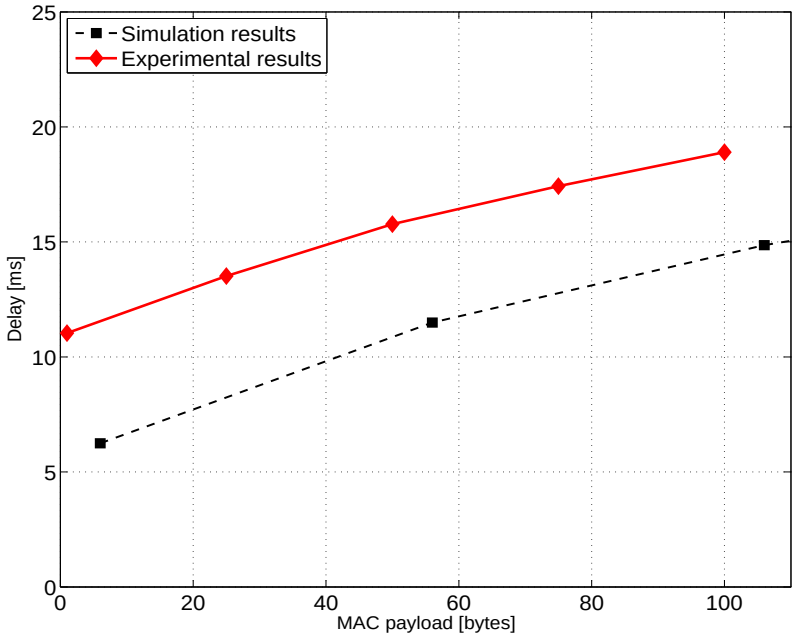

Figure 4.15: Comparison of simulated and experimental values of average delay for 802.15.4 CSMA/CA, PHY1, PM antennas, sub-scenario B, walking.

confirms the reliability of the numerical results obtained, and the slight differences in their trends can be explained considering how differently the connectivity can affect system performance. Indeed, the antennas used in the experiments and in the measurements (see Sec. 2.2.3) present different radiation characteristics, even if the polarization is the same. Moreover, it is worth noting that the size of the hardware platform affects the antenna radiation pattern. Same considerations can be done for the exact node emplacement and the environment considered in the two cases.

Finally, Fig. 4.15 compare the simulated (dashed curve) and measured (continuous line) average delay as a function of the packet payload. Also in this case, the curves follow similar trends. A constant shift of approximately 5 ms between the curves is observed, which can be due to the hardware inner data processing delays, which are not taken into account in simulations.

4.4 Conclusions

The performance of a BAN at the MAC layer are evaluated in terms of PLR, average transmission delay and node energy consumption, comparing different random access schemes for three possible PHY solutions. Simulations are performed considering a node on-body deployment that emulates some target applications, as the one proposed by the WiserBAN project. The impact of the propagation aspects on system level performance is accounted for integrating into the simulator some experimental channel data. The latter coming from an ad-hoc dynamic measurement campaign aimed at characterising the *on-body* communication channel for two antenna type with different polarizations. In this way, the results obtained are representative of

more realistic conditions, considering a proper channel characterisation when evaluating and comparing different protocols for system design. To that purpose, the results presented demonstrate that a single optimal solution, able to fulfil all possible requirements demanded by the application, seems not feasible. Depending on the target performance metric, on the PHY layer considered, on the movement performed, and on the antenna used, the overall best performing MAC may change. Therefore, protocols should be designed as flexible as possible to adapt to different communication conditions and application possibilities, and the outcomes resulting from the presented simulation campaign can guide their design.

As a general consideration, CSMA/CA access schemes are the most suitable solutions when the PLR is the key requirement to be met. Anyway, they show higher energy consumption level with respect to the Slotted ALOHA protocols, which are more useful when power constraint is the primary issue. Moreover, results show that the performance achieved with PM antennas are generally worse than those obtained with TLMs. This confirms the importance of integrating a realistic channel characterisation into simulations, accounting for the antennas effect according to their radiation characteristics. Finally, analysis on the impact of antenna efficiency (in or on-body) on the PLR demonstrate the need to identify a proper trade-off between system performance and antenna dimensions.

Some experiments performed using commercially available devices validate the simulation results obtained in terms of PLR and average packet transmission delay, also confirming the reliability of the implemented channel characterisation.

Chapter 5

Towards a System Level Perspective in Body-Centric Communications

This chapter presents the description of the work started in the last few months before the end of the Ph.D., which aims at integrating in only one general framework different aspects related to *body-centric communications*: from radio channel modeling to a system level perspective.

The final goal is to realise a modular simulation tool (see Sec. 5.2) to be used for the performance evaluation of complex systems, where people are the main actors and the communication takes place between nodes on the same body (*on-body communication*), or between a node carried by an user and others outside it, whether an external gateway or another human subject (*on-* to *off-body communications*). Each module of the proposed platform is devoted to the description of different aspects of the communication system. Starting from the definition of a reference scenario, given in Sec. 5.1, the first step is to properly describe how people move in the simulation area and the types of interactions established among users or between users and environment. This is achieved through the implementation of a mobility model, as

described in Sec. 5.2.1, which has to account not just for single user mobility, but also for social relationships binding them. Moreover, the environment where communication takes place has to be accounted for, since people tend to adapt their movement and the paths they follow according to the location they are in.

The outputs of the mobility block defines the position and the orientation of the users with respect to other subjects or to the environment. At a given simulation instant, it is then possible to characterise the propagation channel set up between different nodes (see Sec. 5.2.2), exploiting the models provided in Chapters 2 and 3 according to the communication type considered (i.e., *on-* or *on-* to *off-body*).

The last module is the one devoted to the system performance evaluation, and it is described in Sec. 5.2.3. Similarly to what presented in Chapter 4, the channel characterisation coming from the previous block is used as input to compute different system metrics such as: SNR, SINR, and PER, if focusing of PHY layer performance, or PLR, transmission delay, and throughput, if upper layer aspects are accounted for.

This work is the natural extension and completion of the one proposed in Chapter 4, where just *on-body* communications are considered. All the studies presented in this thesis are here used and implemented not as stand alone investigations, but as founding elements of a more general framework to approach the study of *body-centric communications*. Numerical results are not provided here, considering the early stage of the research at the moment of writing, but the paradigm of the work and the different blocks composing the simulation platform, are described in details.

5.1 Reference Scenario

Before describing the structure of the simulation platform, the reference scenario is presented, as shown in Fig. 5.1. It consists in an indoor office environment where several users (e.g., employees) share the same space during a working day, moving around according to their activity-schedule or to accomplish a temporary task. Social relationships between people, the working hierarchy, and the personnel structure also influence the type and timing of movements. For instance, employees working in the same team are more likely to spend some time together during meetings or exchanging opinions and ideas; similarly, colleagues sharing common interests or being friends tend to have lunch or a coffee together. In this kind of scenario, it is easy to figure out the importance assumed by communications. Considering each user equipped with one or more nodes composing a personal BAN, transmissions of some kind of information could take place either between on-body nodes or between devices carried around by different users. Furthermore, people may need to send or receive data from the outside world, needing to be connected to an external fixed device, such as an AP, acting as a bridge to the Internet, for example. In this way, all the communication channels characterised in this thesis are accounted for, and the proposed channel models can be used to describe channel conditions once the user's movement, position and distance from the intended Tx/Rx are defined.

Since the environment is crowded and transmissions could take place simultaneously sharing the same spectral resources, the access to the common medium should be controlled employing some channel access techniques. At the *intra-BAN* level (i.e., *on-body communications*) both contention- or scheduled-based algorithms should be

Figure 5.1: Indoor office reference scenario for system level perform evaluation in complex environment.

employed at the MAC layer, as seen in Sec. 4.1, to reduce system failures while keeping good QoS. Performance should be evaluated choosing the most appropriate metrics to compare different protocol solutions, according to the application type. As for the *inter-BAN* (i.e., *B2B*) viewpoint, one possible solution is to define a coordinated approach to multi-user communications, where the nodes belonging to different BANs agree on a common strategy to optimise their own transmissions in the perspective of enhancing overall system performance. The best strategy could take advantage from the knowledge of social relationships between users, their interests and daily routines.

The scenario described is representative of the different topics investigated throughout the Ph.D., and whose results have been presented in this thesis. It can be considered as a illustrative application environment where the distinguish aspects of *body-centric communications* are merged in one general picture. People mobility and

sociality are the new elements to be considered for a practical description of human behavior, and to evaluate system performance in dynamic and realistic context [259]. It is worth mentioning that the specific interest for indoor environment is twofold: on one hand, it is related to the fact that channel measurements were performed in such premises, and proposed channel models account for its effects. On the other hand, there is a lack of works in literature dealing with indoor mobility models, in particular for office scenarios that offer several possibilities for socio-mobility investigations, instead. This should not be considered as niche application, but as the starting point for future studies targeting a broader scope.

5.2 Simulator Structure

In order to be able to reproduce the scenario described above, a simulation platform has been conceived, whose structure is presented in Fig. 5.2. Its architecture consists mainly of three parts, each one characterised by a specific color in the block-diagram. The first part (purple colored) is devoted to the definition of the simulation parameters, such as the number of users and the type of social interactions between them, the duration of the simulation, etc. These parameters can be customized by the system designer, to create the target simulation environment. Moreover, this part accounts also for the description of people movement, according to their schedule, relationships and the local environment previously defined.

The second block (light-blue colored) deals with the channel characterisation. A specific channel model is implemented for each type of communication considered, to provide a description in terms of channel transfer function, $H_{i,j}(f, t_k)$, at the operating frequency f and for each simulation instant t_k.

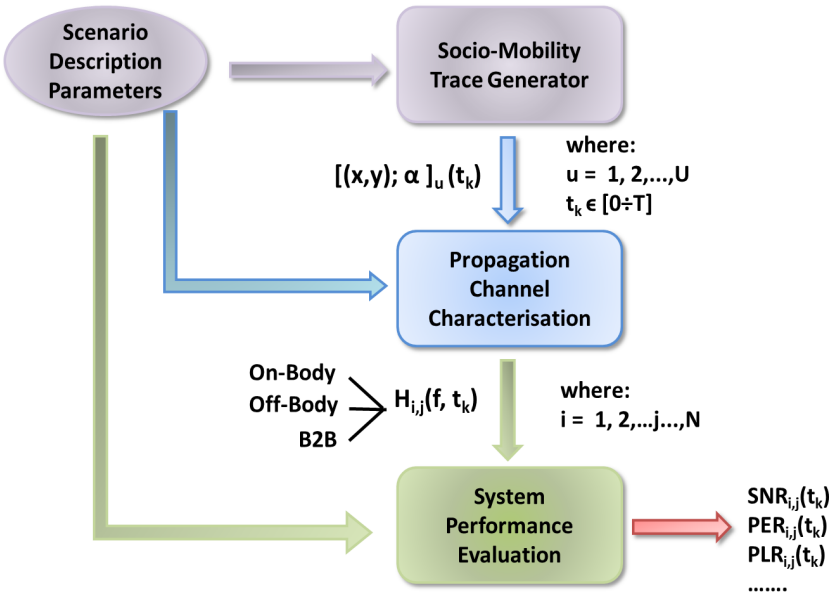

Figure 5.2: Simulation platform block-diagram for multi-BAN system performance evaluation.

Finally, considering all the information coming from the previous blocks, the last one (light-green colored) is used to evaluate system performance, both at the PHY or MAC level. This allows to draw some general considerations on the applicability and usefulness of the proposed protocols; comparison between different communication strategies are also possible.

Next sections provides more details on the different parts of the simulation platform, highlighting their most important features and how they are interconnected.

5.2.1 Indoor Socio-Mobility Aspects

This first part aims at defining the simulation context and how users moves around. It is structured in two blocks: the first one provides the second block with the set of parameters needed to describe the scenario, while the latter is in charge of generating

the daily activity schedule and describing people movement.

The system designer shall customize the parameter set he/she needs to properly account for the different features of the simulation context, however a common subset should include the followings:

- *number of users*: it defines how many users U are considered in the scenario;
- *number on nodes*: it represents the total number of simulated nodes, N. The i-th ($i \in N$) device can be placed either on the human body of a generic user $u \in U$ or acting as an infrastructured node located somewhere in the environment;
- *simulation duration*: its value, T, defines the time interval to be simulated, (i.e., some specific hours or the whole working day);
- *operating frequency*: it is the values of the frequency f defining the system working band.
- *environment description*: some indications describing the scene where the action take place is needed. At a macro level, room dimensions, doors, stairs, corridors, etc. should be defined to reproduce a realistic indoor environment. Including details on furniture positions or generic obstacles provide a deeper level of precision.

The second block has now all information needed to define, for each user $u \in U$, a schedule of the activities to be performed during the simulation time T. This last aspect is the one that has been mainly investigated in the ending part of the Ph.D., and it has already been implemented in MATLAB code. Starting from an idea similar to the one presented in [260], the proposed activity-schedule generation

consists in defining different categories of workers, such as *secretary*, *general manager*, or *employee*, each of them characterised by a set of working activities he/she can do. For example, a *secretary* can *have a phone call* or *collect a print* but can not *participate a board meeting*, which is exclusive to the *general manager*. Each activity is classified as *scheduled* or *random*; the scheduled ones, such as a *meeting* or *coming to work* are those with the highest priority and are the first to be generated. They can be performed with a certain probability at a given time of the day, according to the role assumed by the user. For instance, an *employee* has a higher probability of *coming to work* between 8 a.m. and 9 a.m., while a *general manager* can be more flexible and can have a non-zero probability of arriving at work also after 9 a.m. Once all the scheduled activities are generated, specifying a start time and a duration, the rest of the simulation time is used to perform the so called *random* actions. Between one scheduled task and the following one, each user can do a sequence of *random* activities, among those available for his/her role, passing from one to the other using a state machine (i.e., one state for each *random* activity) with different transition probabilities. Example of such type of task are: *working at the workspace*, *taking a coffee*, or *collecting a print*. Their generation is then subordinated to the *schedule* activity one. Possibility of not coming to work and leaving before the end of the day are also accounted for. The flow-chart of the daily activity of a generic user u is presented in Fig. 5.3. In this way it is possible to recreate a realistic office situation where people assume specific roles and perform different tasks, following an agenda that drives the daily activity [261].

Social aspects of human behavior, which have not been included yet, have also to be accounted for, while generating the user activity schedule. In this perspective,

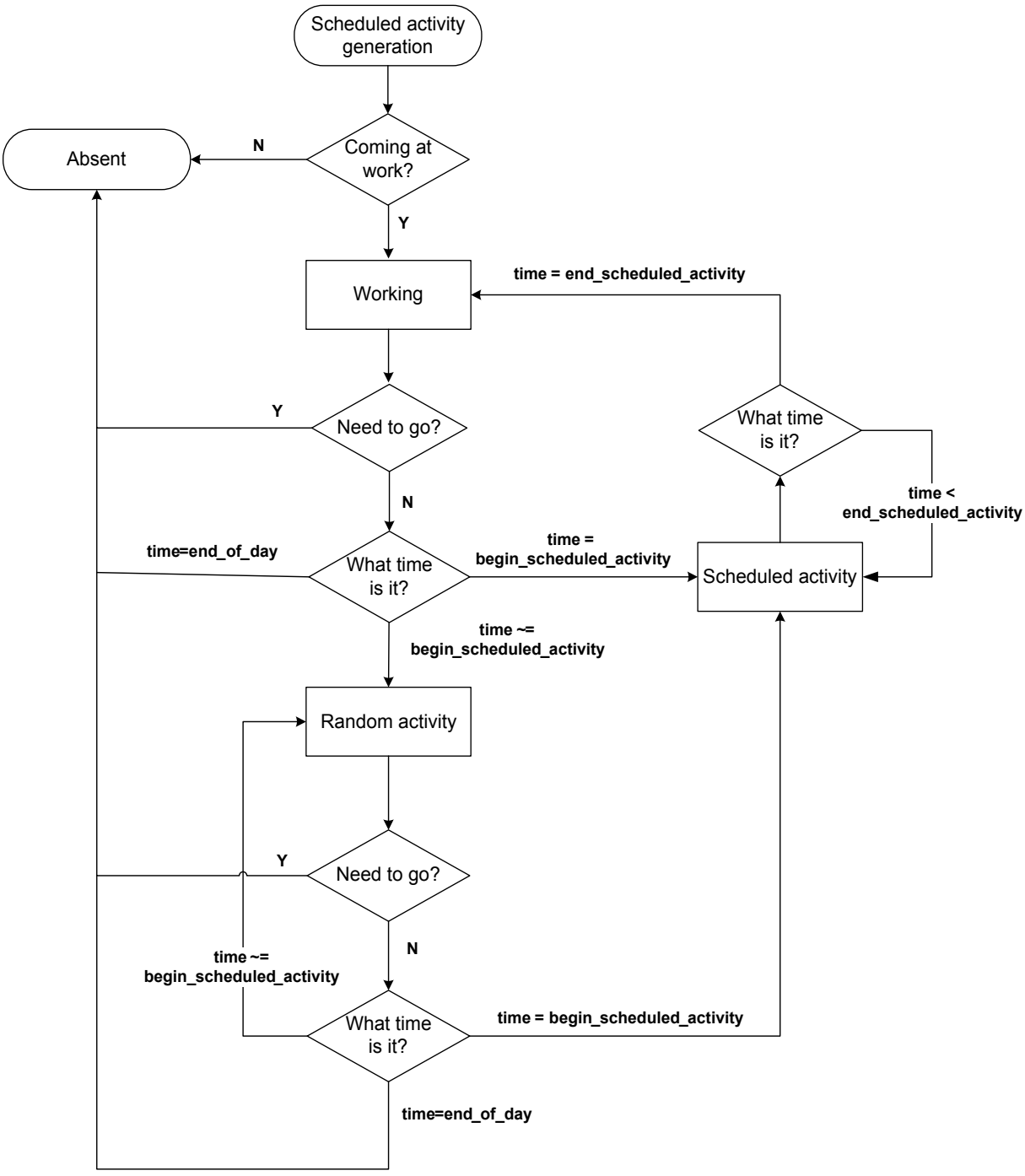

Figure 5.3: Flow-chart of the daily activity of a generic user u in the simulated scenario.

one possibility would be for example to create a graph of the relationships existing between people, similarly to what proposed in [262]. The set of possible relationships include, but is not limited to: *colleagues*; when two or more users share the same office, *working group*; when two or more users are part of the same working team, or *friend*; when two or more users are bonded by friendship. Of course this has an effect on the activity schedule design, since friends will have a higher probability of taking a coffee together, while colleagues share the same space for a longer time during the day. Finally, members of the same working team have to participate to the group meetings, which is a *scheduled* activity, and hence their agenda should include a common time and place to actually meet. As it will be discussed further in this chapter (see Sec. 5.2.3), catching people sociality is of outmost importance to give realism to the simulation scenario, moreover it can be used to improve overall system performance reducing inter-network interference or even exploiting people intercontacts possibilities to forward delay-tolerant data [263, 264].

Finally, considering that each activity occurs in a specific location, performing a task means also moving towards the place where the activity is supposed to take place. Several efforts have been performed by researchers in recent years to model human movement in the most realistic way, studying its main characteristics [265–268]. Anyway, just few of them focus on indoor scenarios, where environmental constraints play a fundamental role in the definition of propagation features and of the movement directions followed by the user. More details on channel characterisation will be provided in next section. As for the definition of the movement directions, the impact of the environment results in the limitation of possible movements, e.g., people can not walk through walls but they enter rooms using doors. A limited

number of contributions in literature propose mobility models that account for such environmental constraints [269–271]; among them, the most suitable one that could be used in the office reference scenario seems to be the *Obstacle Mobility Model* proposed by Jardosh *et al.* in [272, 273]. It enables the inclusion of obstacles in the description of the scenario (i.e., furniture, walls, etc.), specifying the placement coordinates of polygons of different shape and dimensions within the simulation area. Then, pathways followed by the user to move around are obtained using the Voronoi Diagram of obstacle corners, possibility of entering rooms is clearly allowed. Among all possible path generated by the diagram, the shortest path routing policy is applied, meaning that the user moves to its destination following the shortest route. The speed at which people walks is drawn at random from a set of possible values defined by the system designer. It is worth to be notices that obstacle can also represent to other people moving in the same area, in order not to make users crash into each other while walking. Interested reader can find a deeper insight on this mobility model in [272, 273]. Using this mobility model jointly with the daily activity schedule described before, it is then possible to evaluate the location of each user u in the area at every simulation instant $t_k \in T$. The output values of this block of the simulation platform are the spatial coordinates (x, y) and the angle α, defining the actual position and orientation of people with respect to a reference point.

5.2.2 Channel Modeling Aspects

The outputs of the previous block are used as inputs for the channel characterisation part, where channel models like the ones proposed in Chapters 2 and 3 are implemented. For every simulation instant t_k, the definition of the absolute position (x, y)

and orientation α of each user u allows to determine the relative distance and direction with respect to other human subjects or infrastructured devices. Considering the operating frequency f, as defined in the simulation parameter setting (see Sec. 5.2.1), all information needed by the models to characterise the channel transfer function $H_{i,j}(f, t_k)$ is now available. For *on-body* links, the channel is described not as a function of the distance between nodes, but according to their specific position on the body and to the movement performed by the user.

The output of this block can be imagined as a matrix, each column accounting for a simulation instant t_k, while each row refers to one of the available communication links composed by the couple of nodes (i, j). Values of the matrix represent link attenuations computed starting from the channel transfer function $H_{i,j}(f, t_k)$ according to the model equations. If node i and node j are located on the same human body, then an *on-body* channel model is used, as the one proposed in Chapter 2; whereas if they are placed on two different users or one acts as an external gateway, channels are described by a *B2B* or *off-body* model (see Chapters 3). Zero value entries are found when there is no established connection between two nodes, which implies that they are not in the respective transmission range at time t_k. This raises the question about which is the most appropriate criterion to define the device transmission range. One option, the most intuitive one, is to describe a circumference centered at each node, with the radius set according to the receiver sensitivity. Nodes outside the area described by this circumference are not considered as potential communication ends, and the matrix attenuation value is then zero. Other smarter definitions of the transmission range can be also conceived, keeping in mind that it should be a trade-off solution between accuracy and computational cost.

Generally, any propagation model should be representative of the environment where transmissions take place, tuning its parameter accordingly. In particular, for the reference scenario, $H_{i,j}(f, t_k)$ values should account for:

- *materials properties*: indoor propagation considers the presence of an important multipath contribution due to possible reflections and diffractions on walls, objects, or more generally on any kind of surface, including the human body. Different materials are characterised by specific dielectric properties that result in a unique multipath interference scenario that affects overall channel behaviour. Moreover, if nodes (i, j) are located in two different rooms, additional attenuations should be considered to account for the impact of the walls or obstacles separating them. To that purpose, as an initial approximation, the attenuation to be accounted for when the communication ends are located in separated rooms can be considered as infinite.

- *location size*: for similar reasons, rooms size where transmissions take place also plays an important role in the definition of propagation aspects. Indeed, it can result in more or less dense multipath environments.

- *human presence*: it should be considered not just at an individual level, as already pointed out, but also as a densely populated context. The presence of more than one human body in the same space also affects channel characteristics, for example shadowing the communication links or acting as possible sources of waves reflection. Modelling this kind of effect should be then a primal aspects to be considered. Some examples of available works performed in

this direction can be found in [274] starting from a set of measurement performed at 60 GHz and in [275], where the authors propose a knife-edges model to determine the loss introduced by a person in the UWB.

Experimental models, such as those proposed in Chapters 2 and 3, naturally embed these features since measurements are performed in a real indoor environment and with real human subjects. Of course, not all the possible existing environments or people configurations are accounted for by any channel characterisation. The scenario description provided by the first simulator block (see Sec. 5.2.1) should be used as input to the channel modeling part, in order to choose the most appropriate model to be implemented. Possible approximations to the target scenario should be known in order to consider their effect when evaluating system performance.

One final remark regards which model components have to be considered to properly characterise the channel. As already explained, channel models are given as composed of different terms; specifically, a *mean channel gain*, a *long-* and a *short-term fading*. Each of them accounts for a specific propagation phenomena and it is described by a different statistics. In a scenario like the one considered above, there could be situations in which the communication conditions do not vary for a long time interval, for example when employees are in a meeting or at the working desk they tend not to move frequently, and hence channel conditions remain quite stable. In these cases the communication link can be described just through the mean channel gain and the long-term fading components, which account for the body presence effect and for the distance between nodes (or the node position if referring to *on-body* channels). Simulation time resolution can be quite large until some significative

activity is detected, such as user movements, which changes the communication context. One such event shall trigger a more refined simulation over time (i.e., at least as large as the channel coherence time), and short-term fading should be included for channels characterisation, since it accounts for MPCs coming from reflections on the body while moving or from the environment, which has a strong impact on channel behavior while subjects move in both *on-* and *on-* to *off-* communications. The idea behind this description is to have a time-adaptive simulation platform that tunes its simulation time according to the scenario considered, the latter evolving with respect to the users motion and needs. Again, the definition of triggering events shall be done in order not to miss significative changes in channel conditions, while not overloading the simulation tool to the expense of the computational cost [249].

5.2.3 Evaluation of System Performance

Considering the inputs coming from the other parts of the simulation platform, this last block allows the evaluation of system performance. Different metrics can be extracted according to the type of considerations the designer is interested in. If focusing on the PHY layer performance, SNR values can be computed at the link level to allow the evaluation of the BER and the PER, according to packet capture model considered. Different solutions can be implemented and compared to find the optimal one for the reference scenario. On top of this, MAC protocols behavior can be also assessed in terms of PLR, transmission delay and jitter, throughput (both at the link or at the system level), or device energy consumption, just to cite few examples. According to the target application, the network designer shall focus on one or more of these performance metrics, trying to optimise them to fulfill system

requirements.

At the MAC level different channel access techniques can be compared, similarly to what presented in Chapter 4. Considering the multi-BANs scenario described in Sec. 5.1, the possibility to let each network working independently from the other, just focusing on the optimisation of the performance of each single network, leads to a large number of packet collisions and information losses. Traditional access schemes, such as CSMA/CA or a TDMA-based approach, can take advantage from some form of coordination to improve overall system conditions. Coordination may take place at two different levels, namely intra- and inter-BAN [26], both aiming at maximizing system performance, providing high QoS by reducing inter-BAN interferences. For example, BAN coordinator nodes could find an agreement on their afferent nodes transmission schedule, exploiting information related to users sociality and movements [276, 277]. For instance, knowing if people tend to meet frequently or if they share the same space for a long period of time, could give some hints to improve resource scheduling algorithms.

Scheduling and adaptive-scheduling techniques have been widely studied in literature for different types of wireless communication system (e.g., cellular networks, WSNs, etc.) [278–280], and BANs offer new challenges mostly related to the network topology (which varies according to the movement of the users), and to device energy constraints. Cooperative scheduling and interference mitigation techniques remain very little investigated in the BAN context, with just few recent contributions available [26, 276, 277, 281–283], mainly dealing with power control and game theory approaches. A large field of action for new researches to be performed is hence opened, especially thinking about merging in a unique algorithm aspects related to

channel access management, mobility and sociality.

5.3 Conclusions

This chapter presents a detailed description of a simulator platform targeting system performance evaluation in *body-centric communication* for an indoor office environment. Even if no numerical results are provided, the vision of the future activity that will be performed during next year is clearly presented, showing the level of detail reached during this preliminary study phase.

The proposed work highlights how the different aspects studied during this Ph.D., and presented in this thesis, can be merged into one single tool for the evaluation of system level performance, accounting for realistic features of the propagation channel and user socio-mobility. Some aspects have already been investigated, such as those concerning the daily activity schedule generation or the channel characterisation. Some others have been more recently approached, and just some proposals on how to face this issues are proposed. For instance, the *obstacle mobility model* has been considered as one of the options to describe human mobility pattern, but has not been implemented, yet.

The level of detail and realism in the description of the envisaged system has a strong impact on the computational cost and on the soundness and reliability of the results. Since these aspects demand for opposite requirements, a proper trade-off shall be found. Approximation issues will be faced during the working process; anyway, one of the problem that the author is already aware of, is that the considered channel model does not account for a densely populated environment (since measurements were performed with just one subject, or two in B2B scenario). This could have some

impact on channel behavior description and on final results on system performance. Anyway, since no other measurements campaigns were possible before the end of the Ph.D., this can be considered an interesting future working perspective.

To the best of author knowledge, no simulation tool is available in literature focusing on different aspects related to *body-centric communication*, jointly accounting for propagation, mobility and sociality features. This works aims at preparing the ground to realise such a simulation platform, to foster studies on *body-centric applications* proving a reliable tool for system designers.

Conclusions

The general topic investigated in this thesis is related to *body-centric communications*, which are characterised by the human presence that defines their distinctive communication characteristics among other wireless systems. In particular, it has been shown how the body represents a unique propagation environment susceptible to different sources of channel variability, mainly related to the human factor. A precise characterisation of the propagation aspects is then of outmost importance for the design of Physical (PHY) or upper-layer solutions optimised for *body-centric communications*. On top of that, merging mobility and social features of human behaviour with channel modeling will provide more realism to system performance evaluation. Protocols could benefit from these additional information to improve overall system quality. In order to address all these different aspects, this thesis proposes a multi-layer approach: from radio channel modeling to a system level perspective.

The first part of the work has focused on an experimental channel modeling at 2.45 GHz for different communication scenarios: *on-*, *off-*, and *body-to-body (B2B)*. While the first two fall within the Body Area Network (BAN) scope, as defined by the IEEE 802.15.6 standard, the latter is an emerging paradigm just recently investigated

by the research community. The three proposed models follow a similar scenario-based approach for the characterisation of the propagation aspects. Starting from real-time dynamic measurements, radio channels are described accounting simultaneously for different factors: human mobility, node emplacement, body physical characteristics and environment effect. Moreover, antenna impact is accounted for, repeating all the acquisitions with two sets of devices with different radiating properties. Each channel power transfer function is given as composed by three contributions: a *mean channel gain*, a *long-* and a *short-term fading*, which account for different propagation phenomena. In particular, the second one, also known as *body shadowing*, describes the masking effect of the human body on radio channel, considering its orientation and the movement performed. As for the *short-term fading*, it accounts for the secondary Multipaths contribution (MPC) arising from reflections or diffractions from the body or from the environment.

For each model component first- and/or second-order statistics have been provided in every considered scenario and for different antenna designs. It has been shown how the specific node position and antenna's radiation and polarization characteristics play a fundamental role in the definition of channel behaviour, according to the movement performed and to the user's orientation. This justifies the use of a scenario-based approach, more than modeling the channel just as a function of the distance between nodes or users. As a general statement, normally polarized antennas lead to smaller on-body attenuations and they better counteract *body shadowing* effect, since they enhance creeping waves diffusion on the human body. This consideration can vary according to the node position, the movement and the communication scenario considered.

Space and *time* correlation properties, which have been investigated mainly for the *off-body* scenario, need to be studied to complete any channel characterisation. They are left as future research to be performed, since they can provide useful information to system designers as for the channel coherence time and cooperation possibilities between nodes. Another open issue left from the proposed B2B model, is the characterisation of the channel behaviour in a densely populated environment, where several BANs move together in the same environment. This condition is representative of several applicative scenarios, and its modeling would provide important hints as for systems coexistence aspects.

Accounting for a precise characterisation of the channel features is an added value when performing network simulation studies. In this direction, this thesis has presented the results obtained simulating different Medium Access Control (MAC) and PHY layer solutions targeting a primary BAN application. As novel contribution, two of the MAC schemes are those considered by the IEEE 802.15.6 standard. The implementation in the simulator of the *on-body* channel model proposed in this thesis allows a more precise evaluation and comparison of these algorithms, accounting for realistic channel conditions and for the antenna effect. It has been shown that a single optimal solution seems not feasible, but generally Carrier Sense Multiple Access with Collision Avoidance (CSMA/CA) algorithms are more appropriate solutions when Packet Loss Rate is the key requirement to be met, whereas Slotted ALOHA is more suitable when energy constraints are the primary issues. Protocols should be designed as flexible as possible to adapt to different communication conditions and applications, and the outcomes of the presented simulation campaign can guide their design.

As possible future research directions, more protocols could be implemented and compared, targeting other emerging BAN applications and communication scenarios, such as the *off-* and *body-to-body* ones. In this direction, the last part of this thesis has proposed a comprehensive simulation framework for system performance evaluation. People are the main actors in the reference scenario considered, and communications take place between nodes on the same body, or between bodyworn devices and outer ones, whether carried by another human subject or acting as external gateways. This work extends the one just focusing on PHY/MAC performance evaluations, merging features related to channel modeling, mobility, and social attitude of the human being. In particular, the latter aspects could be described through a joint socio-mobility model, to add realism to the investigated scenario (i.e., indoor office environment). System designers could benefit from it improving classical channel access schemes with some node coordination techniques based on socio-mobility information. The aim is to maximize overall system performance, both at an intra- or inter-BAN level, dealing with multi-BANs coexistence issues. This research area is extremely new, and it opens a wide range of investigation possibilities to be explored. Even if no numerical results have been presented, the envisaged simulation tool has been described in all of its composing parts, highlighting how the studies performed throughout the Ph.D. can be used as founding elements of a more general framework for system design in *body-centric communications*.

Two are the main achievements presented in this thesis; on one hand the *B2B* channel modeling activity, representing a novel and thorough contribution to a topic which remains little investigated. On the other hand, the PHY/MAC performance evaluation, which accounts for a detailed description of realistic propagation features.

This work is the result of the activity performed by the author, but the collaboration and support of the colleagues at UniBO and CEA-Leti has been always fruitful and constructive. In particular the author wants to acknowledge Mickael Maman, Kawtar Belmkaddem, Alessandro Di Paolo, Julien Keignart, Christophe Delaveaud, and Lionel Rudant at CEA-Leti, for their help in the measurements, as well as Flavia Martelli, Chiara Buratti, and Riccardo Cavallari at UniBO, for their work and contribution to the simulation platform for system performance evaluation.

Appendix A

On-Body Channel Model Parameters

Table A.1: $G_{i,j}$ values - Tx on Chest - Indoor

	Rxs	**Planar Monopole**		**Top Loaded Monopole**	
		μ_0 [dB]	σ_0 [dB]	μ_0 [dB]	σ_0 [dB]
Walking	**Right Thigh**	-62.72	2.41	-38.65	1.15
	Right Hand	-60.15	5.79	-49.47	1.20
	Left Hand	-58.35	1.50	-42.97	3.19
	Left Ear	-60.48	3.50	-46.82	4.57
Bending	**Right Thigh**	-58.02	3.61	-41.04	1.44
	Right Hand	-56.06	4.89	-47.73	4.60
	Left Hand	-56.21	3.53	-43.02	2.76
	Left Ear	-59.13	4,47	-43.47	1.98

Table A.2: $G_{i,j}$ values - Tx on Left Hip - Indoor

	Rxs	**Planar Monopole**		**Top Loaded Monopole**	
		μ_0 [dB]	σ_0 [dB]	μ_0 [dB]	σ_0 [dB]
Walking	**Right Thigh**	-60.77	4.89	-38.40	1.17
	Right Hand	-61.69	6.90	-53.09	2.89
	Left Hand	-49.62	2.95	-40.74	4.32
	Left Ear	-64.26	3.30	-48.30	2.69

Table A.3: $G_{i,j}$ values - Tx on Chest - Anechoic Chamber

	Rxs	**Planar Monopole**		**Top Loaded Monopole**	
		μ_0 [dB]	σ_0 [dB]	μ_0 [dB]	σ_0 [dB]
Walking	**Right Thigh**	-66.77	3.35	-38.45	1.06
	Right Hand	-63.87	6	-47.07	2.16
	Left Hand	-60.42	4.35	-43.86	2.46
	Left Ear	-61.06	5.18	-48.62	3.62
Bending	**Right Thigh**	-63.96	5.36	-39.45	1.59
	Right Hand	-58.41	2	-46.54	2.46
	Left Hand	-54.62	3.07	-43.52	2.35
	Left Ear	-63.07	2.72	-48.34	2.43
Standing	**Right Thigh**	-68.34	4.92	-38.75	0.92
	Right Hand	-66.25	6.17	-46.58	1.69
	Left Hand	-62.43	2.36	-42.12	1.87
	Left Ear	-60.96	2.27	-45.01	1.36

Table A.4: $G_{i,j}$ values - Tx on Left Hip - Anechoic Chamber

	Rxs	**Planar Monopole**		**Top Loaded Monopole**	
		μ_0 [dB]	σ_0 [dB]	μ_0 [dB]	σ_0 [dB]
Walking	**Right Thigh**	-63.85	2.40	-38.78	2.06
	Right Hand	-67.54	7.50	-52.09	4.58
	Left Hand	-50.38	1.08	-40.32	3.17
	Left Ear	-68.45	5.40	-47.24	2.02
Standing	**Right Thigh**	-61.17	1.06	-42.78	2.26
	Right Hand	-68.97	1.29	-48.35	4.80
	Left Hand	-47.59	2.40	-34.522	1.37
	Left Ear	-69.77	3.63	-46.77	1.46

Table A.5: σ_S values in dB - Tx on Left Hip

	Rxs	Anechoic		Indoor	
		PM	TLM	PM	TLM
Walking	Right Thigh	3.46	1.43	3.05	1.01
	Right Hand	6.07	4.05	3.76	3.98
	Left Hand	7.17	3.73	7.22	3.45
	Left Ear	3.40	1.35	2.38	2.79

Table A.6: σ_S values in dB - Tx on Right Ear

	Rxs	Anechoic		Indoor	
		PM	TLM	PM	TLM
Walking	Right Thigh	2.91	4.06	2.23	3.17
	Right Hand	2.42	2.25	2.58	2.89
	Left Hand	6.40	2.53	2.37	1.72
	Left Ear	0.67	0.12	2.15	0.67
Bending	Right Thigh	3.94	2.89	2.21	2.08
	Right Hand	3.11	3.82	2.71	2.08
	Left Hand	3.82	6.73	2.43	2.19
	Left Ear	0.71	0.20	1.75	0.59

Appendix B

Off-Body Channel Model Parameters

Table B.1: *Body Shadowing* Characterisation in dB - Rx Hip - Indoor

		0°	**45°**	**90°**	**135°**	**180°**	**225°**	**270°**	**315°**
Max	**TLM**	-	0.03	5.10	7.18	-11.58	-8.88	2.15	6.46
	PM	-	3.98	-0.34	-9.86	-13.38	-12.40	-12.35	-3.68
Mean	**TLM**	-	1.26	5.99	9.00	-13.26	-9.75	3.62	7.52
	PM	-	3.97	-0.16	-10.20	-16.70	-15.20	-15.50	-6.23
Std	**TLM**	1.27	0.48	0.60	0.10	2.45	1.60	0.50	0.72
	PM	0.19	0.22	0.11	0.41	2.47	2.34	1.62	2.06

Table B.2: *Body Shadowing* Characterisation in dB - Rx Ear - Indoor

		0°	**45°**	**90°**	**135°**	**180°**	**225°**	**270°**	**315°**
Max	**TLM**	-	-0.91	-6.75	-9.31	-3.47	-9.04	-4.45	-10.33
	PM	-	-7.12	-3.26	-2.97	-2.50	2.60	9.63	9.07
Mean	**TLM**	-	0.33	-7.28	-8.68	-4.89	-8.79	-3.36	-13.17
	PM	-	-8.73	-4.58	-2.80	-3.65	1.12	9.53	9.14
Std	**TLM**	1.21	0.36	1.53	0.93	1.68	0.80	0.35	3.39
	PM	0.22	1.70	1.22	0.18	0.86	1.43	0.61	0.27

Table B.3: *Body Shadowing* Characterisation in dB - Rx Chest - Anechoic

		0°	**45°**	**90°**	**135°**	**180°**	**225°**	**270°**	**315°**
Max	**TLM**	-	9.06	6.53	-5.06	-10.99	-7.89	2.33	4.52
	PM	-	-13.48	-17.30	-26.41	-24.55	-23.00	-7.06	0.70
Mean	**TLM**	-	9.38	6.68	-5.12	-11.56	-8.43	2.10	4.70
	PM	-	-13.92	-18.11	-27.49	-25.06	-24.09	-7.06	0.34
Std	**TLM**	0.18	0.03	0.11	0.17	0.61	0.48	0.25	0.14
	PM	0.14	0.39	0.60	0.66	0.38	0.65	0.11	0.33

Table B.4: *Body Shadowing* Characterisation in dB - Rx Hip - Anechoic

		0°	**45°**	**90°**	**135°**	**180°**	**225°**	**270°**	**315°**
Max	**TLM**	-	-7.13	3.54	-1.43	-13.23	-9.87	-5.93	-0.71
	PM	-	1.56	-5.10	-12.00	-26.30	-24.30	-13.70	-3.89
Mean	**TLM**	-	-8.38	3.59	-1.43	-13.75	-11.86	-6.62	-1.68
	PM	-	1.61	-5.17	-12.30	-27.00	-25.40	-14.00	-4.09
Std	**TLM**	0.09	0.67	0.10	0.06	0.28	1.86	0.32	0.54
	PM	0.03	0.03	0.08	0.19	0.37	0.65	0.21	0.13

Table B.5: *Body Shadowing* Characterisation in dB - Rx Ear - Anechoic

		0°	**45°**	**90°**	**135°**	**180°**	**225°**	**270°**	**315°**
Max	**TLM**	-	-4.60	-7.74	-9.02	-2.12	-3.56	-3.37	-5.71
	PM	-	2.37	-1.96	6.18	10.80	2.42	19.84	20.06
Mean	**TLM**	-	-4.65	-7.95	-9.32	-2.28	-5.51	-4.09	-7.29
	PM	-	2.83	-1.49	7.19	11.87	2.68	20.66	20.94
Std	**TLM**	0.10	0.09	0.12	0.23	0.20	1.24	0.88	0.96
	PM	0.43	0.24	0.24	0.07	0.05	0.43	0.14	0.17

Appendix C

B2B Channel Model Parameters

Table C.1: Mean Channel Gain - Opposite Walk LOS/NLOS - Tx Right Hip

		Planar Monopole			**Top Loaded Monopole**		
	Rxs	**L. Ear**	**Chest**	**R. Hip**	**L. Ear**	**Chest**	**R. Hip**
LOS	$\boldsymbol{n_{LOS}(0°)}$	1.24	0.95	1.38	1.38	2.35	2.00
	$\boldsymbol{G_0(d_{LOS}, 0°)}$ $\boldsymbol{[dB]}$	-62.52	-57.52	-55.70	-51.85	-47.17	-47.12
NLOS	$\boldsymbol{n_{NLOS}(180°)}$	0.49	0.23	0.28	0.38	0.77	0.61
	$\boldsymbol{G_0(d_{NLOS}, 180°)}$ $\boldsymbol{[dB]}$	-74.44	-82.97	-83.57	-64.09	-68.87	-68.33
	$\boldsymbol{\Delta G_0}$	11.95	25.45	27.87	13.53	21.70	21.20

Table C.2: Mean Channel Gain - Opposite Walk LOS/NLOS - Tx Right Hand

		Planar Monopole			**Top Loaded Monopole**		
	Rxs	**L. Ear**	**Chest**	**R. Hip**	**L. Ear**	**Chest**	**R. Hip**
LOS	$\boldsymbol{n_{LOS}(0°)}$	1.35	1.28	1.28	0.14	1.91	1.59
	$\boldsymbol{G_0(d_{LOS}, 0°)}$ $\boldsymbol{[dB]}$	-55.03	-51.82	-51.81	-52.77	-50.12	-50.80
NLOS	$\boldsymbol{n_{NLOS}(180°)}$	0.55	0.45	0.73	0.55	0.95	0.20
	$\boldsymbol{G_0(d_{NLOS}, 180°)}$ $\boldsymbol{[dB]}$	-65.19	-71.12	-68.43	-62.47	-66.23	-67.64
	$\boldsymbol{\Delta G_0}$	10.16	19.30	16.62	9.69	16.10	16.84

Table C.3: Fast Fading Statistics - Walking - Tx on Right Hip

	Rxs	Planar Monopole					Top Loaded Monopole				
		ν	σ	K	$LCR[Hz]$	$AFD[ms]$	ν	σ	K	$LCR[Hz]$	$AFD[ms]$
LOS	Left Ear	0.0007	0.95	0	3.23	170	0.64	0.81	0.31	3.23	170
	Chest	0.97	0.51	1.81	2.74	180	0.0014	0.94	0	2.74	200
	Right Hip	0.97	0.51	1.81	2.31	220	0.0008	0.85	0	3.37	160
NLOS	Left Ear	0.0008	0.95	0	6.34	90	0.001	0.95	0	7.14	80
	Chest	0.0007	0.96	0	6.03	90	0.0003	0.97	0	5.37	100
	Right Hip	0.71	0.78	0.41	6.86	80	0.0008	0.94	0	6.69	80

Table C.4: Fast Fading Statistics - Walking - Tx on Right Hand

	RXs	Planar Monopole					Top Loaded Monopole				
		ν	σ	K	$LCR[Hz]$	$AFD[ms]$	ν	σ	K	$LCR[Hz]$	$AFD[ms]$
LOS	Left Ear	0.76	0.76	0.50	3.29	160	0.96	0.52	1.70	4.06	130
	Chest	0.99	0.49	2.04	2.34	160	0.53	0.85	0.20	4.09	130
	Right Hip	0.95	0.58	1.34	2.60	200	0.86	0.66	0.83	4.48	120
NLOS	Left Ear	0.001	0.94	0	7.43	70	0.001	0.95	0	5.63	100
	Chest	0.0029	0.93	0	8.31	70	0.0002	0.96	0	5.31	110
	Right Hip	0.001	0.93	0	8.26	70	0.56	0.85	0.22	6.91	80

Table C.5: Fast Fading Statistics - Walking - Tx on Left Thigh

	Rxs	$\boldsymbol{\nu}$	$\boldsymbol{\sigma}$	$\boldsymbol{K}$	$\boldsymbol{LCR[Hz]}$
PM	**Left Ear**	0.85	0.69	0.76	7.20
	Chest	0.91	0.63	1.04	9.15
	Right Hip	0.90	0.61	1.09	7.48
TLM	**Left Ear**	0.92	0.58	1.26	8.53
	Chest	0.99	0.39	3.22	4.75
	Right Hip	0.99	0.43	2.65	2.38

Table C.6: Fast Fading Statistics - Walking - Tx on Right Hand

	Rxs	$\boldsymbol{\nu}$	$\boldsymbol{\sigma}$	$\boldsymbol{K}$	$\boldsymbol{LCR[Hz]}$
PM	**Left Ear**	0.81	0.70	0.67	8.15
	Chest	0.94	0.38	1.31	8.62
	Right Hip	0.93	0.58	1.29	7.28
TLM	**Left Ear**	0.93	0.56	1.38	8.95
	Chest	1	0.40	3.13	5.03
	Right Hip	0.97	0.48	2.04	4.57

Bibliography

[1] M. Patel and J. Wang. Applications, challenges, and prospective in emerging body area networking technologies. *IEEE Wireless Communications*, 17(1):80–88, 2010.

[2] S. Cotton and W. Scanlon. Using Smart People to Form Future Mobile Wireless Networks. *Microwave Journal*, 54(12):24–40, December 2011.

[3] P.S. Hall and Y. Hao. *Antennas and Propagation for Body-Centric Wireless Communications, Second Edition*. Artech House antennas and propagation library. Artech House, 2012.

[4] IEEE Standard for Local and metropolitan area networks - Part 15.6: Wireless Body Area Networks. *IEEE Std 802.15.6-2012*, pages 1–271, February 2012.

[5] Channel Model for Body Area Network. Available at: https://mentor.ieee.org/802.15/documents, September 2010.

[6] R. Bashirullah. Wireless Implants. *IEEE Microwave Magazine*, 11(7):S14–S23, 2010.

[7] G.-Z. Yang and M. Yacoub. Body sensor networks. *Springer London*, 2006.

[8] R. D'Errico and L. Ouvry. A Statistical Model for On-Body Dynamic Channels. *International Journal of Wireless Information Networks*, 17:92–104, 2010.

[9] N. Vastardis and K. Yang. Mobile social networks: Architectures, social properties, and key research challenges. *IEEE Communications Surveys and Tutorials*, 15(3):1355–1371, 2013.

[10] R. Rosini, R. D'Errico, and R. Verdone. Body-to-Body communications: A measurement-based channel model at 2.45 GHz. In *2012 IEEE 23rd International Symposium on Personal Indoor and Mobile Radio Communications (PIMRC)*, pages 1763–1768, September 2012.

[11] R. Rosini and R. D'Errico. Comparing on-body dynamic channels for two antenna designs. In *2012 Loughborough Antenna and Propagation Conference (LAPC)*, November 2012.

[12] WiserBAN - Smart miniature low-power wireless microsystem for Body Area Networks. Website: http://wiserban.eu/.

[13] European Commission 7th Framework Programme FP7. Website: http://cordis.europa.eu/fp7/home_en.html/.

[14] R. Rosini, R. Verdone, and R. D'Errico. Body-to-Body Indoor Channel Modelling at 2.45 GHz. *Submitted for review to IEEE Transaction on Antenna and Propagation*, January 2014.

[15] R. Rosini and R. D'Errico. Space-time correlation for on-to-Off Body channels at 2.45 GHz. In *2013 7th European Conference on Antennas and Propagation (EuCAP)*, April 2013.

[16] M. Mackowiak, R. Rosini, R. D'Errico, and L.M. Correia. Comparing off-body dynamic channel model with real-time measurements. In *2013 7th International Symposium on Medical Information and Communication Technology (ISMICT)*, July 2013.

[17] R. Rosini and R. D'Errico. Off-Body channel modelling at 2.45 GHz for two different antennas. In *2012 6th European Conference on Antennas and Propagation (EUCAP)*, March 2012.

[18] R. Cavallari, F. Martelli, R. Rosini, C. Buratti, and R. Verdone. A Survey on Wireless Body Area Networks: Technologies and Design Challenges. *IEEE Communications Surveys and Tutorials*.

[19] R. Rosini, F. Martelli, M. Maman, R. D'Errico, C. Buratti, and R. Verdone. On-body area networks: from channel measurements to MAC layer performance evaluation. In *2012 18th European Wireless Conference (EW)*, April 2012.

[20] Won-Jae Yi and J. Saniie. Smart mobile system for body sensor network. In *2013 IEEE International Conference on Electro/Information Technology (EIT)*, pages 1–4, 2013.

[21] Huasong Cao, V. Leung, C. Chow, and H. Chan. Enabling technologies for wireless body area networks: A survey and outlook. *IEEE Communications Magazine*, 47(12):84–93, 2009.

[22] B. Latré, B. Braem, I. Moerman, C. Blondia, and P. Demeester. A Survey on Wireless Body Area Networks. *Wireless Network*, 17(1), 2011.

[23] A. Boulis, D. Smith, D. Miniutti, L. Libman, and Y. Tselishchev. Challenges in body area networks for healthcare: the MAC. *IEEE Communications Magazine*, 50(5):100–106, 2012.

[24] M. Chen, S. Gonzalez, A. Vasilakos, H. Cao, and V. C. Leung. Body Area Networks: A Survey. *Mobile Networks and Applications*, 16(2), 2011.

[25] Jie Dong and D. Smith. Cooperative body-area-communications: Enhancing coexistence without coordination between networks. In *2012 IEEE 23rd International Symposium onPersonal Indoor and Mobile Radio Communications (PIMRC)*, 2012.

[26] Lusheng Wang, C. Goursaud, N. Nikaein, L. Cottatellucci, and J. Gorce. Cooperative Scheduling for Coexisting Body Area Networks. *IEEE Transactions on Wireless Communications*, 12(1):123–133, 2013.

[27] F. Martelli. *Wireless Network for Body-centric Communications*. PhD thesis, Ph.D. Thesis, Alma Mater Studiorum - Università di Bologna.

[28] S. Mai, C. Zhang, M. Dong, and Z. Wang. A Cochlear System with Implant DSP. In *2006 IEEE International Conference on Acoustics, Speech and Signal Processing (ICAPSSP)*, volume 5, May 2006.

[29] D.B. Shire, S.K. Kelly, J. Chen, P. Doyle, M.D. Gingerich, S.F. Cogan, W.A. Drohan, O. Mendoza, L. Theogarajan, J.L. Wyatt, and J.F. Rizzo. Development and Implantation of a Minimally Invasive Wireless Subretinal Neurostimulator. *IEEE Transactions on Biomedical Engineering*, 56(10):2502–2511, October 2009.

[30] S. Ullah, P. Khan, N. Ullah, S. Saleem, H. Higgins, and K. Sup Kwak. A Review of Wireless Body Area Networks for Medical Applications. *International Journal of Communications, Network and System Sciences*, 2(8):797–803, 2009.

[31] H.Alemdar and C. Ersoy. Wireless sensor networks for healthcare: A survey . *Computer Networks*, 54(15):2688 – 2710, 2010.

[32] S. Drude. Requirements and Application Scenarios for Body Area Networks. In *16th IST Mobile and Wireless Communications Summit*, pages 1–5, July 2007.

[33] A.F. Smeaton, D. Diamond, P. Kelly, K. Moran, K.T. Lau, D. Morris, N. Moyna, N.E. O'Connor, and K. Zhang. Aggregating multiple body sensors for analysis in sports. *5th International Workshop on Wearable Micro and Nanosystems for Personalised Health*, 2008.

[34] D.K. Arvind and A. Bates. The speckled golfer. In *Proceedings of the ICST 3rd international conference on Body area networks*, page 28, 2008.

[35] F. Dijkstra. Requirements for BAN and BAN standardization from the point of view of gaming. In *7th International Conference on Body Area Networks (BodyNets)*, Sep. 2012.

[36] K. Piotrowski, A. Sojka, and P. Langendoerfer. Body area network for first responders: A case study. In *Proceedings of the 5th International ICST Conference on Body Area Networks (BodyNets)*, pages 37–40, 2011.

[37] M. Chammem, S. Berrahal, and N. Boudriga. Smart Navigation for Firefighters in Hazardous Environments: A BAN-based Approach. In *Proceedings of the 2012 International Conference on Pervasive Computing and the Networked World*, (ICPCA/SWS), pages 82–96, 2013.

[38] C.R. Baker, K. Armijo, S. Belka, M. Benhabib, V. Bhargava, N. Burkhart, A. Der Minassians, G. Dervisoglu, L. Gutnik, M.B. Haick, C. Ho, M. Koplow, J. Mangold, S. Robinson, M. Rosa, M. Schwartz, C. Sims, H. Stoffregen, A. Waterbury, E.S. Leland, T. Pering, and P.K. Wright. Wireless Sensor Networks for Home Health Care. In *2007 21st International Conference on Advanced Information Networking and Applications Workshops (AINAW)*, volume 2, pages 832–837, 2007.

[39] V. Jones. From BAN to AmI-BAN: micro and nano technologies in future Body Area Networks. In *Proceedings of Symposium on Integrated Micro Nano Systems: Convergence of Bio and Nanotechnologies*, June 2006.

[40] R.W. Hoyt. SPARNET-Spartan Data Network for Real-Time Physiological Status Monitoring. Technical report, DTIC Document, 2008.

[41] S. Schillaci. BAN in defence applications. In *2012 7th International Conference on Body Area Networks (BodyNets)*, September 2012.

[42] A. Sassi, L. Gioanola, and P. Civera. Proposal of a workers and scaffolds monitoring and risk mitigation system for building sites. In *Bridge Maintenance, Safety, Management and Life-Cycle Optimization - Proceedings of the 5th International Conference on Bridge Maintenance, Safety and Management*, pages 1656–1663, 2010.

[43] F. Petre, F. Bouwens, S. Gillijns, F. Masse, M. Engels, B. Gyselinckx, K. Vanstechelman, and C. Thomas. Wireless vibration monitoring on human machine operator. In *2010 17th IEEE Symposium on Communications and Vehicular Technology in the Benelux (SCVT)*, pages 1–6, Nov. 2010.

[44] K. Takeda. *In-Vehicle Corpus and Signal Processing for Driver Behavior*. Springer, 2009.

[45] Yao-Jen Chang, Chen-Nien Chen, Li-Der Chou, and Tsen-Yung Wang. A novel indoor wayfinding system based on passive RFID for individuals with cognitive impairments. In *2008 Second International Conference on Pervasive Computing Technologies for Healthcare (PervasiveHealth)*, pages 108–111, 2008.

[46] J.F. Debroux et al. Report about WiserBAN platform applications. WiserBAN Deliverable D1.1, November 2010.

[47] L. Brown, B. Grundlehner, and J. Penders. Towards wireless emotional valence detection from EEG. In *2011 Annual International Conference of the IEEE Engineering in Medicine and Biology Society (EMBC)*, pages 2188–2191, 2011.

[48] M.S. El-Nasr and A.V. Vasilakos. DigitalBeing - Using the Environment As an Expressive Medium for Dance. *Information Sciences*, 178(3), February, 2008.

[49] B. Zhen, M. Patel, S. Lee, E. Won, and A. Astrin. TG6 Technical Requirements Document (TRD). Available at: https://mentor.ieee.org/802.15/documents, November 2008.

[50] R. D'Errico, R. Rosini, and M. Maman. A Performance Evaluation of Cooperative Schemes for On-Body Area Networks Based on Measured Time-Variant Channels. In *2011 IEEE International Conference on Communications (ICC)*, pages 1–5, 2011.

[51] P. Ferrand, J.M. Gorce, and C. Goursaud. On the packet error rate of correlated shadowing links in body-area networks. In *Proceedings of the 5th European Conference on Antennas and Propagation (EUCAP)*, pages 3094–3098, 2011.

[52] J. Espina, H. Baldus, T. Falck, O. Garcia, and K. Klabunde. Towards easy-to-use, safe, and secure wireless medical body sensor networks. *Mobile Health Solutions for Biomedical Applications. IGI Global, ISBN*, pages 978–1, 2009.

[53] D. Singelée, B. Latré, B. Braem, M. Peeters, M. De Soete, P. De Cleyn, B. Preneel, I. Moerman, and C. Blondia. A secure cross-layer protocol for multi-hop wireless body area networks. In *Ad-hoc, Mobile and Wireless Networks*, pages 94–107. Springer, 2008.

[54] M. Guennoun, M. Zandi, and K. El-Khatib. On the use of biometrics to secure wireless biosensor networks. In *2008 3rd International Conference onInformation and Communication Technologies: From Theory to Applications (ICTTA)*, pages 1–5. IEEE, 2008.

[55] C. C Y Poon, Yuan-Ting Zhang, and Shu-Di Bao. A novel biometrics method to secure wireless body area sensor networks for telemedicine and m-health. *IEEE Communications Magazine*, 44(4):73–81, 2006.

[56] Chia-Hsien Lin, K. Saito, M. Takahashi, and K. Ito. A Compact Planar Inverted-F Antenna for 2.45 GHz On-Body Communications. *Antennas and Propagation, IEEE Transactions on*, 60(9):4422–4426, 2012.

[57] L.J. Chu. Physical Limitations of Omni-Directional Antennas. *Journal of Applied Physics*, 19(12):1163–1175, 1948.

[58] H. Giddens, D.-L. Paul, G.S. Hilton, and J.P. McGeehan. Influence of body proximity on the efficiency of a wearable textile patch antenna. In *2012 6th European Conference on Antennas and Propagation (EUCAP)*, pages 1353–1357, 2012.

[59] V.S. Mallela, V. Ilankumaran, and N. S. Rao. Trends in cardiac pacemaker batteries. *Indian pacing and electrophysiology journal*, 4(4):201, 2004.

[60] Duc Chinh Hoang, Yen Kheng Tan, Hock Beng Chng, and Sanjib Kurmar Panda. Thermal energy harvesting from human warmth for wireless body area network in medical healthcare system. In *2009 International Conference on Power Electronics and Drive Systems (PEDS)*, pages 1277–1282. IEEE, 2009.

[61] T. Von Buren, P.D. Mitcheson, T.C. Green, E.M. Yeatman, A.S. Holmes, and G. Troster. Optimization of inertial micropower generators for human walking motion. *IEEE Sensors Journal*, 6(1):28–38, 2006.

[62] Fan Zhang, Yanqing Zhang, J. Silver, Y. Shakhsheer, M. Nagaraju, A. Klinefelter, J. Pandey, J. Boley, E. Carlson, A. Shrivastava, B. Otis, and B. Calhoun. A batteryless 19uW MICS/ISM-band energy harvesting body area sensor node

SoC. In *2012 IEEE International Solid-State Circuits Conference Digest of Technical Papers (ISSCC)*, pages 298 –300, feb. 2012.

[63] V. Leonov, P. Fiorini, and R.J.M. Vullers. Theory and simulation of a thermally matched micromachined thermopile in a wearable energy harvester. *Microelectronics Journal*, 42(4):579 – 584, 2011.

[64] F. Martelli and R. Verdone. Coexistence Issues for Wireless Body Area Networks at 2.45 GHz. *2012 18th European Wireless Conference European Wireless (EW)*, pages 1 –6, april 2012.

[65] M. Hernandez and R. Kohno. Coexistence of UWB-BANs with other wireless systems. In *2009 International Symposium on Intelligent Signal Processing and Communication Systems (ISPACS)*, pages 135–137, 2009.

[66] M. Hernandez and R. Miura. Coexistence of IEEE Std 802.15.6TM-2012 UWB-PHY with other UWB systems. In *2012 IEEE International Conference on Ultra-Wideband (ICUWB)*, pages 46–50, 2012.

[67] B. de Silva, A. Natarajan, and M. Motani. Inter-user interference in body sensor networks: Preliminary investigation and an infrastructure-based solution. In *2009 Sixth International Workshop onWearable and Implantable Body Sensor Networks (BSN)*, pages 35–40, 2009.

[68] I. Khan, P.S. Hall, Y.I. Nechayev, and L. Akhoondzadeh-Asl. Multiple antenna systems for increasing on-body channel capacity and reducing BAN-to-BAN interference. In *2010 International Workshop on Antenna Technology (iWAT*, pages 1–4, 2010.

[69] Shih Heng Cheng and Ching Yao Huang. Coloring-Based Inter-WBAN Scheduling for Mobile Wireless Body Area Networks. *IEEE Transactions on Parallel and Distributed Systems*, 24(2):250–259, 2013.

[70] S.F. Heaney, W.G. Scanlon, E. Garcia-Palacios, S.L. Cotton, and A. McKernan. Characterization of inter-body interference in context aware body area networking (CABAN). In *2011 IEEE GLOBECOM Workshops*, pages 586–590, 2011.

[71] A. Augimeri, G. Fortino, M.R. Rege, V. Handziski, and A. Wolisz. A cooperative approach for handshake detection based on body sensor networks. In *2010 IEEE International Conference on Systems Man and Cybernetics (SMC)*, pages 281–288, 2010.

[72] T. Someya. *Stretchable Electronics*. Wiley, 2012.

[73] Shi Cheng and Zhigang Wu. Microfluidic stretchable RF electronics. *Lab on a Chip, Royal Society of Chemistry*, 10(23):3227–3234, 2010.

[74] Fan Cai, Zhuo Li, Joshua C. Agar, C. P. Wong, and J. Papapolymerou. Novel stretchable electrically conductive composites for tunable RF devices. In *2012 IEEE MTT-S International Microwave Symposium Digest (MTT)*, pages 1–3, 2012.

[75] T. Rai, P. Dantes, B. Bahreyni, and W.S. Kim. A Stretchable RF Antenna With Silver Nanowires. *IEEE Electron Device Letters*, 34(4):544–546, 2013.

[76] G. Dolmans. BAN and PN in Health. In *2012 7th International Conference on Body Area Networks (BODYNETS)*, Sept. 2012.

[77] D.L. Donoho. Compressed sensing. *IEEE Transactions on Information Theory*, 52(4):1289–1306, 2006.

[78] H. Mamaghanian, N. Khaled, D. Atienza, and P. Vandergheynst. Design and Exploration of Low-Power Analog to Information Conversion Based on Compressed Sensing. *IEEE Journal on Emerging and Selected Topics in Circuits and Systems*, 2(3):493–501, 2012.

[79] M. Balouchestani, K. Raahemifar, and S. Krishnan. Wireless Body Area Networks with compressed sensing theory. In *2012 ICME International Conference on Complex Medical Engineering (CME)*, pages 364–369, 2012.

[80] Guidelines for Limiting Exposure to Time-Varying Electric, Magnetic, and Electromagnetic Fields (up to 300 GHz). *Health Physics*, 74(4):494–522, 1998.

[81] Public health: electromagnetic fields. http://ec.europa.eu/health.

[82] FCC Encyclopedia - Radio Frequency Safety. http://www.fcc.gov/encyclopedia/radio-frequency-safety.

[83] I.F. Akyildiz, F. Brunetti, and C. Blázquez. Nanonetworks: A new communication paradigm. *Computer Networks*, 52(12):2260–2279, August 2008.

[84] L. Galluccio, T. Melodia, S. Palazzo, and G.E. Santagati. Challenges and implications of using ultrasonic communications in intra-body area networks. In *2012 9th Annual Conference on Wireless On-demand Network Systems and Services (WONS)*, pages 182–189, 2012.

[85] M. Seyedi, B. Kibret, D.T.H. Lai, and M. Faulkner. A Survey on Intrabody Communications for Body Area Network Applications. *IEEE Transactions on Biomedical Engineering*, 60(8):2067–2079, 2013.

[86] J. Bae, H. Cho, K. Song, H. Lee, and H.J. Yoo. The signal transmission mechanism on the surface of human body for body channel communication. *IEEE Transactions on Microwave Theory and Techniques*, 60(3):582–593, 2012.

[87] S. Gonzalez-Valenzuela, X. Liang, H. Cao, M. Chen, and V.C.M. Leung. Body Area Networks. In Daniel Filippini, editor, *Autonomous Sensor Networks*, volume 13 of *Springer Series on Chemical Sensors and Biosensors*, pages 17–37. 2013.

[88] S. Ullah, H. Higgins, B. Braem, B. Latrè, C. Blondia, I. Moerman, S. Saleem, Z. Rahman, and K.S. Kwak. A Comprehensive Survey of Wireless Body Area Networks. *Journal of Medical Systems*, 36(3):1065–1094, 2012.

[89] IEEE Standard for Information Technology - Telecommunications and Information Exchange Between Systems - Local and Metropolitan Area Networks - Specific Requirements Part 15.4: Wireless Medium Access Control (MAC) and Physical Layer (PHY) Specifications for Low-Rate Wireless Personal Area Networks (WPANs). *IEEE Std 802.15.4-2006 (Revision of IEEE Std 802.15.4-2003)*, pages 1–305, 2006.

[90] Specification of the Bluetooth System version 4.0. *Bluetooth SIG*, June 2010.

[91] A. Reichman. Standardization of body area networks. In *2009 IEEE International Conference on Microwaves, Communications, Antennas and Electronics Systems (COMCAS)*, pages 1 –4, November 2009.

[92] IEEE 802.15 WPAN Task Group 4. Website: http://www.ieee802.org/15/pub/TG4.html.

[93] Zigbee Alliance. Website: http://www.zigbee.org.

[94] IEEE Standard for Information Technology - Telecommunications and Information Exchange Between Systems - Local and Metropolitan Area Networks - Specific Requirement Part 15.4: Wireless Medium Access Control (MAC) and Physical Layer (PHY) Specifications for Low-Rate Wireless Personal Area Networks (WPANs). *IEEE Std 802.15.4a-2007 (Amendment to IEEE Std 802.15.4-2006)*, pages 1–203, 2007.

[95] IEEE Standard for Local and metropolitan area networks–Part 15.4: Low-Rate Wireless Personal Area Networks (LR-WPANs) Amendment 1: MAC sublayer. *IEEE Std 802.15.4e-2012*, pages 1–225, April 2012.

[96] M. Träskbäck. Security of bluetooth: An overview of bluetooth security. In *Helsinki University of Technology, Department of Electrical and Communications Engineering, seminar material for the course Tik-86.174 Bluetooth technology & utilization*. Citeseer, 2000.

[97] Bluetooth products. Website: http://www.bluetooth.com/Pages/Bluetooth-Smart-Devices.aspx, October 2012.

[98] ANT technology. Website: http://www.thisisant.com/, September 2013.

[99] Sensium technology. Website: http://www.toumaz.com/, October 2013.

[100] Zarlink technology. Website: http://www.microsemi.com/, July 2013.

[101] Z-Wave technology. Website: http://www.z-wave.com/, August 2013.

[102] Insteon technology. Website: http://www.insteon.com/, August 2013.

[103] Rubee technology. Website: www.rubee.com/, November 2011.

[104] M. Okoniewski and M.A. Stuchly. A study of the handset antenna and human body interaction. *IEEE Transactions on Microwave Theory and Techniques*, 44(10):1855–1864, 1996.

[105] W.G. Scanlon and N.E. Evans. Numerical analysis of bodyworn UHF antenna systems. *Electronics & communication engineering journal*, 13(2):53–64, 2001.

[106] K. Siwiak. *Radiowave Propagation and Antennas for Personal Communications, Second Edition*. Artech House, Inc., Norwood, MA, USA, 2nd edition, 1998.

[107] C. Roblin, R. D'Errico, J.M. Gorce, J.M. Laheurte, and L. Ouvry. TD(09)07054 - Propagation channel models for BANs: an Overview. In *COST Action 2100*, February 2009.

[108] T. Zasowski, F. Althaus, M. Stger, A. Wittneben, and G. Tröster. UWB for noninvasive wireless body area networks: Channel measurements and results. In *2003 IEEE Conference on Ultra Wideband Systems and Technologies (UWBST)*, November 2003.

[109] P.S. Hall, M. Ricci, and T.M. Hee. Measurements of on-body propagation characteristics. In *2002 IEEE Antennas and Propagation Society International Symposium*, volume 2, pages 310–313. IEEE, 2002.

[110] Thomas Zasowski, Gabriel Meyer, Frank Althaus, and Armin Wittneben. Propagation effects in uwb body area networks. In *2005 IEEE International Conference on Ultra-Wideband (ICU)*, pages 16–21, 2005.

[111] A. Fort, C. Desset, P. De Doncker, P. Wambacq, and L. Van Biesen. An ultra-wideband body area propagation channel Model-from statistics to implementation. *IEEE Transactions on Microwave Theory and Techniques*, 54(4), 2006.

[112] A. Fort, C. Desset, J. Ryckaert, P. De Doncker, L. Van Biesen, and P. Wambacq. Characterization of the ultra wideband body area propagation channel. In *2005 IEEE International Conference on Ultra-Wideband (ICU)*, 2005.

[113] S. Van Roy, C. Oestges, F. Horlin, and P. De Doncker. On-body propagation velocity estimation using ultra-wideband frequency-domain spatial correlation analyses. *Electronics Letters*, 43(25), 2007.

[114] P.S. Hall, Yang Hao, Y.I. Nechayev, A. Alomainy, C.C. Constantinou, C. Parini, M.R. Kamarudin, T.Z. Salim, D.T.M. Hee, R. Dubrovka, A.S. Owadally, Wei Song, A. Serra, P. Nepa, M. Gallo, and M. Bozzetti. Antennas and propagation for on-body communication systems. *IEEE Antennas and Propagation Magazine*, 49(3), 2007.

[115] S.L. Cotton and W.G. Scanlon. A Statistical Analysis of Indoor Multipath Fading for a Narrowband Wireless Body Area Network. In *2006 IEEE 17th International Symposium on Personal, Indoor and Mobile Radio Communications*, 2006.

[116] S.L. Cotton and W.G. Scanlon. Higher Order Statistics for Lognormal Small-Scale Fading in Mobile Radio Channels. *IEEE Antennas and Wireless Propagation Letters*, 6:540–543, 2007.

[117] D. Smith, L. Hanlen, D. Miniutti, Jian Zhang, D. Rodda, and B. Gilbert. Statistical characterization of the dynamic narrowband body area channel. In *2008 First International Symposium on Applied Sciences on Biomedical and Communication Technologies (ISABEL)*, 2008.

[118] K. Takizawa, T. Aoyagi, J.-i. Takada, N. Katayama, Kamya Yekeh, K.Y. Yazdandoost, and T. Kobayashi. Channel models for wireless body area networks. In *30th Annual International Conference of the IEEE Engineering in Medicine and Biology Society (EMBS)*, 2008.

[119] K. Takizawa, T. Aoyagi, Li Huan-Bang, J. Takada, T. Kobayashi, and R. Kohno. Path loss and power delay profile channel models for wireless body area networks. In *2009 IEEE Antennas and Propagation Society International Symposium (APSURSI)*, 2009.

[120] A. Fort, F. Keshmiri, G.R. Crusats, C. Craeye, and C. Oestges. A Body Area Propagation Model Derived From Fundamental Principles: Analytical Analysis and Comparison With Measurements. *IEEE Transactions on Antennas and Propagation*, 58(2):503–514, 2010.

[121] Lingfeng Liu, F. Keshmiri, P. De Doncker, C. Craeye, and C. Oestges. 3-D body scattering interference to vertically polarized on-body propagation. In *2010*

IEEE Antennas and Propagation Society International Symposium (APSURSI), pages 1–4, 2010.

[122] T. Alves, B. Poussot, and J.-M. Laheurte. Analytical Propagation Modeling of BAN Channels Based on the Creeping-Wave Theory. *IEEE Transactions on Antennas and Propagation*, 59(4):1269–1274, 2011.

[123] R. D'Errico et al. Final report on the antenna-human body interactions, around-the-body propagation. WiserBAN Deliverable D3.1, October 2010.

[124] D. Smith, D. Miniutti, T. Lamahewa, and L. Hanlen. Propagation Models for Body Area Networks: A Survey and New Outlook. *IEEE Antennas and Propagation Magazine*, December 2013.

[125] M.S. Wegmueller, A. Kuhn, J. Froehlich, M. Oberle, N. Felber, N. Kuster, and Wolfgang Fichtner. An Attempt to Model the Human Body as a Communication Channel. *IEEE Transactions on Biomedical Engineering*, 54(10), 2007.

[126] A.T. Barth, M.A. Hanson, H.C. Powell, Jr., D. Unluer, S.G. Wilson, and J. Lach. Body-coupled Communication for Body Sensor Networks. In *Proceedings of the ICST 3rd International Conference on Body Area Networks*, BodyNets '08, 2008.

[127] C. Roblin, J.M. Laheurte, R. DErrico, A. Gati, D. Lautru, T. Alvs, H. Terchoune, and F. Bouttout. Antenna design and channel modeling in the BAN context-part II: channel. *annals of telecommunications - annales des tèlècommunications*, 66(3-4), 2011.

[128] A. Alomainy, Y. Hao, C.G. Parini, and P.S. Hall. Comparison between two different antennas for UWB on-body propagation measurements. *IEEE Antennas and Wireless Propagation Letters*, 4, 2005.

[129] Y.I. Nechayev, P.S. Hall, I. Khan, and C.C. Constantinou. Wireless channels and antennas for body-area networks. In *2010 Seventh International Conference on Wireless On-demand Network Systems and Services (WONS)* , 2010.

[130] A. Takahiro, T. Junichi, and K. Minseok. TD(13)06040 - Characterization of an electrically small antenna in proximity to human body by multipole technique. In *COST Action IC1004*, February 2012.

[131] A. Fort, C. Desset, P. Wambacq, and L.V. Biesen. Indoor body-area channel model for narrowband communications. *IET Microwaves, Antennas Propagation*, 1, 2007.

[132] L. Liu, F. Keshmiri, C. Craeye, P. De Doncker, and C. Oestges. An Analytical Modeling of Polarized Time-Variant On-Body Propagation Channels with Dynamic Body Scattering. *EURASIP Journal on Wireless Communications and Networking*, 2011(1), 2011.

[133] N. Katayama, K. Takizawa, T. Aoyagi, J.-i. Takada, Huan-Bang Li, and R. Kohno. Channel model on various frequency bands for wearable Body Area Network. In *2008 First International Symposium onApplied Sciences on Biomedical and Communication Technologies (ISABEL)*, 2008.

[134] A.F. Molisch, K. Balakrishnan, D. Cassioli, Chia-Chin Chong, S. Emami, A. Fort, J. Karedal, J. Kunisch, H. Schantz, and K. Siwiak. In *2005 Global Telecommunications Conference (GLOBECOM).*

[135] A. Fort, J. Ryckaert, C. Desset, P. De Doncker, P. Wambacq, and L. Van Biesen. Ultra-wideband channel model for communication around the human body. *IEEE Journal on Selected Areas in Communications*, 24(4), 2006.

[136] A. Alomainy and Yang Hao. Radio channel models for UWB body-centric networks with compact planar antenna. In *2006, IEEE Antennas and Propagation Society International Symposium*, 2006.

[137] Y. P. Zhang, Li Bin, and Cao Qi. Characterization of on-human-body UWB radio propagation channel. *Microwave and Optical Technology Letters*, 49(6).

[138] D. Smith, L. Hanlen, A. Zhang, D. Miniutti, D. Rodda, and B. Gilbert. First and Second-Order Statistical Characterizations of the Dynamic Body-Area Propagation Channel of Various Bandwidths. *Annals of Telecommunications*, pages pp 1–17, December 2010.

[139] R. DErrico and L. Ouvry. A statistical model for on-body dynamic channels. *International journal of wireless information networks*, 17(3-4):92–104, 2010.

[140] Y.I. Nechayev, P.S. Hall, and Z.H. Hu. Characterisation of narrowband communication channels on the human body at 2.45 GHz. *IET Microwaves, Antennas Propagation*, 4(6), 2010.

[141] W.G. Scanlon and S.L. Cotton. Understanding on-body fading channels at 2.45 GHz using measurements based on user state and environment. In *2008 Loughborough Antennas and Propagation Conference (LAPC)*, pages 10–13, 2008.

[142] Y.I. Nechayev, P.S. Hall, C. Constantinou, Yang Hao, A. Alomainy, R. Dubrovka, and C.G. Parini. On-body path gain variations with changing body posture and antenna position. In *2005 IEEE Antennas and Propagation Society International Symposium*, volume 1B, pages 731–734 vol. 1B, 2005.

[143] A. Taparugssanagorn, C. Pomalaza-Raez, R. Tesi, M. Hamalainen, and J. Iinatti. Effect of body motion and the type of antenna on the measured

UWB channel characteristics in medical applications of wireless body area networks. In *2009 IEEE International Conference on Ultra-Wideband (ICUWB)*, pages 332–336, 2009.

[144] Q.H. Abbasi, A. Sani, A. Alomainy, and Yang Hao. Experimental Characterization and Statistical Analysis of the Pseudo-Dynamic Ultrawideband On-Body Radio Channel. *IEEE Antennas and Wireless Propagation Letters*, 10, 2011.

[145] S.L. Cotton and W.G. Scanlon. Characterization of the on-body channel in an outdoor environment at 2.45 GHz. In *2009 3rd European Conference on Antennas and Propagation (EuCAP)*, 2009.

[146] Statistical Property of Dynamic BAN Channel Gain at 4.5GHz. Available at: https://mentor.ieee.org/802.15/documents, September 2008.

[147] Bin Zhen, Minseok Kim, J.-i. Takada, and R. Kohno. Characterization and Modeling of Dynamic On-Body Propagation at 4.5 GHz. *IEEE Antennas and Wireless Propagation Letters*, 8, 2009.

[148] R. D'Errico and L. Ouvry. Delay dispersion of the on-body dynamic channel. In *2010 Proceedings of the Fourth European Conference on Antennas and Propagation (EuCAP)*, pages 1–5, 2010.

[149] A. Abdi and M. Kaveh. On the utility of gamma PDF in modeling shadow fading (slow fading). In *1999 IEEE 49th Vehicular Technology Conference*, volume 3, pages 2308–2312 vol.3, July 1999.

[150] M.D. Yacoub, J.E. Vargas B., and L.G. De R.Guedes. On the statistics of the Nakagami-m signal. In *Proceedings of the 1998 SBT/IEEE International-Telecommunications Symposium (ITS)*, volume 2, pages 377–382 vol.2, August 1998.

[151] D.B. Smith, D. Miniutti, L.W. Hanlen, D. Rodda, and B. Gilbert. Dynamic Narrowband Body Area Communications: Link-Margin Based Performance Analysis and Second-Order Temporal Statistics. In *2010 IEEE Wireless Communications and Networking Conference (WCNC)*, 2010.

[152] D.B. Smith, J. Zhang, L.W. Hanlen, D. Miniutti, D. Rodda, and B. Gilbert. Temporal correlation of dynamic on-body area radio channel. *Electronics Letters*, 45(24), 2009.

[153] S.L. Cotton, W.G. Scanlon, and G.A. Conway. Autocorrelation of signal facing in wireless body area networks. In *2009 2nd IET Seminar on Antennas and Propagation for Body-Centric Wireless Communications*, pages 1–5, 2009.

[154] S. Van Roy, F. Quitin, Lingfeng Liu, C. Oestges, F. Horlin, J. Dricot, and P. De Doncker. Dynamic Channel Modeling for Multi-Sensor Body Area Networks. *IEEE Transactions on Antennas and Propagation*, 61(4):2200–2208, 2013.

[155] Lingfeng Liu, P. De Doncker, and C. Oestges. Fading correlation measurement and modeling on the front side of a human body. In *2009 3rd European Conference on Antennas and Propagation (EuCAP)*, 2009.

[156] Xiao Dong Yang, Q.H. Abbasi, A. Alomainy, and Yang Hao. Spatial Correlation Analysis of On-Body Radio Channels Considering Statistical Significance. *IEEE Antennas and Wireless Propagation Letters*, 10:780–783, 2011.

[157] Picosecond Pulse Lab. Website: http://www.picosecond.com/.

[158] Tektronix. Website: http://www.tek.com/.

[159] C. Delaveaud, P. Leveque, and B. Jecko. New kind of microstrip antenna: The monopolar wire-patch antenna. *Electronics letters*, 30(1):1–2, 1994.

[160] IEC 62209-1, IEEE 1528 and CENELEC EN62209.

[161] A. Lea, P. Hui, J. Ollikainen, and R.G. Vaughan. Propagation between on-body antennas. *IEEE Transactions on Antennas and Propagation*, 57(11):3619–3627, 2009.

[162] H. Akaike. A new look at the statistical model identification. *IEEE Transactions on Automatic Control*, 19(6):716–723, 1974.

[163] P. Pasquero, R. Rosini, R. D'Errico, and C. Oestges. On-Body Channel Correlation in Various Walking Scenarios. *Accepted to the 2014 8th European Conference on Antennas and Propagation (EuCAP)*, 2014.

[164] Narrowband on body to off body channel characterization for BAN. Available at: https://mentor.ieee.org/802.15/documents, August 2008.

[165] K.I. Ziri-Castro, W.G. Scanlon, and N.E. Evans. Indoor radio channel characterization and modeling for a 5.2 GHz bodyworn receiver. *IEEE Antennas and Wireless Propagation Letters*, 3(1):219–222, 2004.

[166] K.I. Ziri-Castro, W.G. Scanlon, R. Feustle, and N.E. Evans. Indoor channel measurements for a body-worn 5.2 GHz receiver. In *2003 5th European Personal Mobile Communications Conference*, pages 191–194, 2003.

[167] K.I. Ziri-Castro, W.G. Scanlon, and N.E. Evans. Characterisation of body-shadowing effects in the indoor environment at 5.2 GHz. In *2003 High Frequency Postgraduate Student Colloquium*, pages 2–5, 2003.

[168] A.J. Ali, W.G. Scanlon, and S.L. Cotton. Pedestrian effects in indoor UWB off-body communication channels. In *2010 Loughborough Antennas and Propagation Conference (LAPC)*, pages 57–60, 2010.

[169] A.J. Ali, S.L. Cotton, and W.G. Scanlon. Spatial diversity for off-body communications in an indoor populated environment at 5.8 GHz. In *2009 Loughborough Antennas Propagation Conference (LAPC)*, pages 641–644, 2009.

[170] S.L. Cotton and W.G. Scanlon. Indoor channel characterisation for a wearable antenna array at 868 MHz. In *2006 IEEE Wireless Communications and Networking Conference (WCNC)*, volume 4, pages 1783–1788, 2006.

[171] S.L. Cotton and W.G. Scanlon. Statistical characterisation for a mobile bodyworn personal area network in an indoor multipath environment at 868 MHz. In *2006 First European Conference on Antennas and Propagation (EuCAP)*, pages 1–7, 2006.

[172] S.L. Cotton and W.G. Scanlon. Characterization and Modeling of the Indoor Radio Channel at 868 MHz for a Mobile Bodyworn Wireless Personal Area Network. *IEEEAntennas and Wireless Propagation Letters*, 6:51–55, 2007.

[173] S.L. Cotton and W.G. Scanlon. Spatial Diversity and Correlation for Off-Body Communications in Indoor Environments at 868 MHz. In *2007 IEEE 65th Vehicular Technology Conference (VTC-Spring)*, pages 372–376, 2007.

[174] S.L. Cotton and W.G. Scanlon. Measurements, Modeling and Simulation of the Off-Body Radio Channel for the Implementation of Bodyworn Antenna Diversity at 868 MHz. *IEEE Transactions on Antennas and Propagation*, 57(12):3951–3961, 2009.

[175] D. Smith, L. Hanlen, Z. Jian, D. Miniutti, D. Rodda, and B. Gilbert. Characterization of the Dynamic Narrowband On-Body to Off-Body Area Channel. In *2009 IEEE International Conference on Communications (ICC)*, pages 1–6, 2009.

[176] A. Chunsu, A. Byoungjik, K. Sunwoo, and C. Jaehoon. Experimental outage capacity analysis for off-body wireless body area network channel with transmit diversity. *IEEE Transactions on Consumer Electronics*, 58(2):274–277, 2012.

[177] S.H. Kvist, P.F. Medina, J. Thaysen, and K.B. Jakobsen. On-body and off-body 2.45 GHz MIMO communications for hearing instrument applications. In *2013 7th European Conference on Antennas and Propagation (EuCAP)*, pages 2595–2599, 2013.

[178] S.L. Cotton, A. McKernan, A.J. Ali, and W.G. Scanlon. An experimental study on the impact of human body shadowing in off-body communications channels at 2.45 GHz. In *2011 5th European Conference on Antennas and Propagation (EUCAP)*, pages 3133–3137, 2011.

[179] P. Van Torre, H. Rogier, L. Vallozzi, C. Hertleer, and M. Moeneclaey. Application of channel models to indoor off-body wireless MIMO communication with textile antennas. In *9th COST 2100 MCM*. COST 2100, 2009.

[180] P. Van Torre, L. Vallozzi, C. Hertleer, H. Rogier, M. Moeneclaey, and J. Verhaevert. Indoor Off-Body Wireless MIMO Communication With Dual Polarized Textile Antennas. *IEEE Transactions on Antennas and Propagation*, 59(2):631–642, 2011.

[181] P. Van Torre, L. Vallozzi, L. Jacobs, H. Rogier, M. Moeneclaey, and J. Verhaevert. Characterization of Measured Indoor Off-Body MIMO Channels with Correlated Fading, Correlated Shadowing and Constant Path Loss. *IEEE Transactions on Wireless Communications*, 11(2):712–721, 2012.

[182] P. Van Torre, L. Vallozzi, C. Hertleer, H. Rogier, M. Moeneclaey, and J. Verhaevert. Dynamic link performance analysis of a rescue worker's off-body communication system using integrated textile antennas. *IET Science, Measurement Technology*, 4(2):41–52, 2010.

[183] A.A. Goulianos, T.W.C. Brown, and S. Stavrou. A Novel Path-Loss Model for UWB Off-Body Propagation. In *2008 IEEE Vehicular Technology Conference (VTC-Spring)*, pages 450–454, 2008.

[184] A.A. Goulianos, T.W.C. Brown, and S. Stavrou. Ultra-wideband measurements and results for sparse off-body communication channels. In *2008 Loughborough Antennas and Propagation Conference (LAPC)*, pages 213–216, 2008.

[185] A.A. Goulianos, T.W.C. Brown, and S. Stavrou. Power delay profile modelling of the ultra wideband off-body propagation channel. *IET Microwaves, Antennas Propagation*, 4(1):62–71, 2010.

[186] A.A. Goulianos, T.W.C. Brown, B.G. Evans, and S. Stavrou. Wideband Power Modeling and Time Dispersion Analysis for UWB Indoor Off-Body Communications. *IEEE Transactions on Antennas and Propagation*, 57(7):2162–2171, 2009.

[187] P.A. Catherwood and W.G. Scanlon. Link characteristics for an off-body UWB transmitter in a hospital environment. In *2009 Loughborough Antennas Propagation Conference (LAPC)*, pages 569–572, 2009.

[188] P.A. Catherwood and W.G. Scanlon. Body-centric ultra-wideband multi-channel characterisation and spatial diversity in the indoor environment. *IET Microwaves, Antennas Propagation*, 7(1):61–70, 2013.

[189] M.M. Khan, Q.H. Abbasi, A. Alomainy, and H. Yang. Study of line of sight (LOS) and none line of sight (NLOS) ultra wideband off-body radio propagation for body centric wireless communications in indoor. In *2011 5th European Conference on Antennas and Propagation (EUCAP)*, pages 110–114, 2011.

[190] M.M. Khan, A. Alomainy, and H. Yang. Off-Body Radio Channel Characterisation Using Ultra Wideband Wireless Tags. In *2010 International Conference on Body Sensor Networks (BSN)*, pages 80–83, 2010.

[191] M.M. Khan, Q.H. Abbasi, A. Alomainy, and H. Yang. Ultra wideband wireless tags for off-body radio channel characterisation with varying subject postures. In *2011 41st European Microwave Conference (EuMC)*, pages 701–704, 2011.

[192] T. Mavridis, L. Petrillo, J. Sarrazin, D. Lautru, A. Benlarbi-Delai, and P. De Doncker. Theoretical and Experimental Investigation of a 60 GHz Off-Body Propagation Model. *IEEE Transactions on Antennas and Propagation*, (99):1–1, 2013.

[193] X.Y. Wu, Y.I. Nechayev, C.C. Constantinou, P.S. Hall, A. Brizzi, A. Pellegrini, Y. Hao, and C.G. Parini. Preliminary estimate for observability of 60 GHz wireless body area networks. In *2012 IEEE Asia-Pacific Conference on Antennas and Propagation (APCAP)*, pages 110–111, 2012.

[194] N. Chahat, C. Leduc, M. Zhadobov, and R. Sauleau. Antennas and interaction with the body for body-centric wireless communications at millimeter-waves. In *2013 7th European Conference on Antennas and Propagation (EuCAP)*, pages 772–775, 2013.

[195] S.L. Cotton and W.G. Scanlon. Channel Characterization for Single- and Multiple-Antenna Wearable Systems Used for Indoor Body-to-Body Communications. *IEEE Transactions onAntennas and Propagation*, 57(4):980–990, 2009.

[196] S.L. Cotton, W.G. Scanlon, and J. Guy. The The k-μ Distribution Applied to the Analysis of Fading in Body to Body Communication Channels for Fire and Rescue Personnel. *IEEE Antennas and Wireless Propagation Letters*, 7:66–69, 2008.

[197] Yu Wang, I.B. Bonev, J.O. Nielsen, I.Z. Kovacs, and G.F. Pedersen. Characterization of the Indoor Multiantenna Body-to-Body Radio Channel. *IEEE Transactions on Antennas and Propagation*, 57(4):972–979, 2009.

[198] G.F. Pederen, J.O. Nielsen, O. Franek, J.B. Andersen, M. Pelosi, and Yu Wang. Measurement based investigations for future communication system performance evaluation. In *2009 Loughborough Antennas Propagation Conference (LAPC)*, pages 23–30, 2009.

[199] Y. Nechayev, Zhen Hua Hu, and P. Hall. Fading of the transmission channel between two wireless body area networks in an office at 2.45 GHz and 5.8 GHz. In *2010 LoughboroughAntennas and Propagation Conference (LAPC)*, pages 489–492, 2010.

[200] S.L. Cotton, A. McKernan, and W.G. Scanlon. Received signal characteristics of outdoor body-to-body communications channels at 2.45 GHz. In *2011 Loughborough Antennas and Propagation Conference (LAPC)*, pages 1–4, 2011.

[201] S.F. Heaney, W.G. Scanlon, and E. Garcia-Palacios. Effect of environmental multipath on line of sight body to body communication at 2.45 GHz. In *2012 Loughborough Antennas and Propagation Conference (LAPC)*, pages 1–4, 2012.

[202] T.S.P. See, J.Y. Hee, C.T. Ong, L.C. Ong, and Zhi Ning Chen. Inter-body channel model for UWB communications. In *2009 3rd European Conference onAntennas and Propagation (EuCAP)*, pages 3519–3522, 2009.

[203] L. Hanlen, D. Miniutti, D. Smith, D. Rodda, and B. Gilbert. Co-channel Interference in Body Area Networks with Indoor Measurements at 2.4 GHz: Distance-to-interferer is a poor estimate of received interference power. *International Journal of Wireless Information Networks, Springer*, 17(3-4):113–125, August 2010.

[204] L.W. Hanlen, D. Miniutti, D. Rodda, and B. Gilbert. Interference in body area networks: Distance does not dominate. In *2009 IEEE 20th International Symposium on Personal, Indoor and Mobile Radio Communications*, pages 281–285, 2009.

[205] B. de Silva, A. Natarajan, and M. Motani. Inter-User Interference in Body Sensor Networks: Preliminary Investigation and an Infrastructure-Based Solution. In *2009 Sixth International Workshop on Wearable and Implantable Body Sensor Networks (BSN)*, pages 35–40, 2009.

[206] K. Ghanem, H. Al Qowaiee, I. Khan, and P. Hall. Effect of Antenna Type on the Capacity of Body-to-Body Capacity When Using Uniform Power Allocation. In *2012 IEEE Vehicular Technology Conference (VTC-Fall)*, pages 1–5, 2012.

[207] Rohde&Schwarz. Website: http://www.rohde-schwarz.com/.

[208] C. Buratti, R. D'Errico, M. Maman, F. Martelli, R Rosini, and R. Verdone. Design of a body area network for medical applications: the WiserBAN project. In *Proceedings of the 4th International Symposium on Applied Sciences in Biomedical and Communication Technologies*, October 2011.

[209] H. Hashemi. The indoor radio propagation channel. *Proceedings of the IEEE*, 81(7):943–968, 1993.

[210] S.L. Cotton and W.G. Scanlon. Channel Characterization for Single- and Multiple-Antenna Wearable Systems Used for Indoor Body-to-Body Communications. *IEEE Transactions on Antennas and Propagation*, 57(4):980 –990, April 2009.

[211] G. McLachlan and D. Peel. *Finite mixture models*. Wiley-Interscience, 2004.

[212] M. Mackowiak and L.M. Correia. A Statistical Model for the Influence of Body Dynamics on the Gain Pattern of Wearable Antennas in Off-Body Radio Channels. *Wireless Personal Communications*, pages 1–19, 2013.

[213] P.K. Tiwary, Woon-Sung Baek, Dong-Min Kim, and Jae-Young Pyun. A study on ultra low power MAC protocols over Wireless Body Area Network. In *2012 IEEE Region 10 Conference (TENCON)*, pages 1–6, 2012.

[214] S.A. Gopalan and Jong-Tae Park. Energy-efficient MAC protocols for wireless body area networks: Survey. In *2010 International Congress on Ultra Modern Telecommunications and Control Systems and Workshops (ICUMT)*, pages 739–744, 2010.

[215] N. Javaid, I. Israr, M.A. Khan, A. Javaid, S.H. Bouk, and Z.A. Khan. Analyzing Medium Access Techniques in Wireless Body Area Networks. *CoRR*, abs/1304.1047, 2013.

[216] S.A. Gopalan, Dong-Hyun Kim, Jae-Wook Nah, and Jong-Tae Park. A survey on power-efficient MAC protocols for wireless body area networks. In *2010 3rd IEEE International Conference on Broadband Network and Multimedia Technology (IC-BNMT)*, pages 1230–1234, 2010.

[217] S. Ullah, B. Shen, S. M. Riazul Islam, P. Khan, S. Saleem, and K. S. Kwak. A Study of Medium Access Control Protocols for Wireless Body Area Networks. *ArXiv e-prints*, April 2010.

[218] T. Van Dam and K. Langendoen. An Adaptive Energy-efficient MAC Protocol for Wireless Sensor Networks. In *Proceedings of the 1st International Conference on Embedded Networked Sensor Systems*, SenSys '03, pages 171–180. ACM, 2003.

[219] J. Polastre, J. Hill, and D. Culler. Versatile Low Power Media Access for Wireless Sensor Networks. In *Proceedings of the 2nd International Conference on Embedded Networked Sensor Systems*, SenSys '04, pages 95–107. ACM, 2004.

[220] Wei Ye, J. Heidemann, and D. Estrin. An energy-efficient MAC protocol for wireless sensor networks. In *2002 Twenty-First IEEE Annual Joint Conference of the IEEE Computer and Communications Societies (INFOCOM)*, volume 3, pages 1567–1576, 2002.

[221] S. Mijovic, A. Stajkic, R. Cavallari, and C. Buratti. Experimental Characterization of Low Power Listening in BAN. In *2013 IEEE International Conference on e-Health Networking, Applications and Services (Healthcomm)*, pages 2101–2105, 2013.

[222] A. El-Hoiydi and J.D. Decotignie. WiseMAC: An Ultra Low Power MAC Protocol for Multi-hop Wireless Sensor Networks. In *Algorithmic Aspects of Wireless Sensor Networks*, volume 3121 of *Lecture Notes in Computer Science*, pages 18–31. Springer Berlin Heidelberg, 2004.

[223] M. Patel and D. Wang. Energy Efficient Methods of Encoding Destination Address to Address Overhearing Problem in BAN. In *IEEE PIMRC 2010 International Workshop on Body Area Networks - Enabling Technologies for Wearable and Implanable Body Sensors*, September 2010.

[224] S. Marinkovic, C. Spagnol, and E. Popovici. Energy-Efficient TDMA-Based MAC Protocol for Wireless Body Area Networks. In *2009 Third International Conference on Sensor Technologies and Applications (SENSORCOMM)*, pages 604–609, 2009.

[225] Li Changle, W. Lingling, L. Jiandong, Z. Bin, Li Huan-Bang, and R. Kohno. Scalable and robust medium access control protocol in wireless body area networks. In *2009 IEEE 20th International Symposium on Personal, Indoor and Mobile Radio Communications*, pages 2127–2131, 2009.

[226] M.M. Alam, O. Berder, D. Menard, and O. Sentieys. TAD-MAC: Traffic-Aware Dynamic MAC Protocol for Wireless Body Area Sensor Networks. *IEEE Journal on Emerging and Selected Topics in Circuits and Systems*, 2(1):109–119, March 2012.

[227] O.C. Omeni, O. Eljamaly, and A.J. Burdett. Energy Efficient Medium Access Protocol for Wireless Medical Body Area Sensor Networks. In *2007 4th IEEE/EMBS International Summer School and Symposium on Medical Devices and Biosensors (ISSS-MDBS)*, pages 29–32, 2007.

[228] M.A. Ameen, N. Ullah, and Kyungsup Kwak. Design and analysis of a MAC protocol for wireless body area network using wakeup radio. In *2011 11th International Symposium on Communications and Information Technologies (ISCIT)*, pages 148–153, 2011.

[229] N. Golmie, D. Cypher, and O. Rebala. Performance analysis of low rate wireless technologies for medical applications. *Computer Communications*, 28(10):1266–1275, 2005.

[230] S. Ullah and K.S. Kwak. An Ultra Low-power and Traffic-adaptive Medium Access Control Protocol for Wireless Body Area Network. *Journal of Medical Systems*, 36(3):1021–1030, June 2012.

[231] F. Gengfa and E. Dutkiewicz. BodyMAC: Energy efficient TDMA-based MAC protocol for Wireless Body Area Networks. In *2009 9th International Symposium on Communications and Information Technology (ISCIT)*, pages 1455–1459, 2009.

[232] N.F. Timmons and W.G. Scanlon. An adaptive energy efficient MAC protocol for the medical body area network. In *2009 1st International Conference on Wireless Communication, Vehicular Technology, Information Theory and Aerospace Electronic Systems Technology (Wireless VITAE)*, pages 587–593, 2009.

[233] F. Martelli, R. Verdone, and C. Buratti. Link Adaptation in IEEE 802.15.4-based Wireless Body Area Networks. In *2010 IEEE 21st International Symposium on Personal, Indoor and Mobile Radio Communications Workshops (PIMRC Workshops)*, pages 117–121, 2010.

[234] S. Ullah and L. Kwak. Performance Study of Low-power MAC Protocols for Wireless Body Area Networks. In *IEEE PIMRC 2010 International Workshop on Body Area Networks - Enabling Technologies for Wearable and Implanable Body Sensors*, pages 111–115, September 2010.

[235] H. Li and J. Tan. An Ultra-low-power Medium Access Control Protocol for Body Sensor Network. In *2005 27th Annual International Conference of the Engineering in Medicine and Biology Society (IEEE-EMBS)*, pages 2451–2454, 2005.

[236] D.Yun, S.-E. Yoo, D. Kim, and D. Kim. OD-MAC: An On-Demand MAC Protocol for Body Sensor Networks Based on IEEE 802.15.4. In *2008 4th IEEE International Conference on Embedded and Real-Time Computing Systems and Applications (RTCSA)*, pages 413–420, August 2008.

[237] B. Latrè, B. Braem, I. Moerman, C. Blondia, E. Reusens, W. Joseph, and P. Demeester. A Low-delay Protocol for Multihop Wireless Body Area Networks. In *2007 Fourth Annual International Conference on Mobile and Ubiquitous Systems: Networking Services (MobiQuitous)*, pages 1–8, 2007.

[238] Huaming Li and Jindong Tan. Heartbeat-Driven Medium-Access Control for Body Sensor Networks. *IEEE Transactions on Information Technology in Biomedicine*, 14(1):44–51, 2010.

[239] M. Maman and L. Ouvry. BATMAC: An adaptive TDMA MAC for body area networks performed with a space-time dependent channel model. In *2011 IEEE International Symposium on Medical Information and Communication Technology (ISMICT)*, pages 1–5, March 2011.

[240] Lee Cheolhyo, Kim Jaehwan, Lee Hyung-Soo, and Kim Jaeyoung. Physical layer designs for WBAN systems in IEEE 802.15.6 proposals. In *9th International Symposium on Communications and Information Technology (ISCIT)*, pages 841–844, 2009.

[241] Li Miaoxin and Z. Mingjie. An overview of Physical layers on wireless body area network. In *2012 International Conference on Anti-Counterfeiting, Security and Identification (ASID)*, pages 1–5, 2012.

[242] N. Bradai, S. Belhaj, L. Chaari, and L. Kamoun. Study of medium access mechanisms under IEEE 802.15.6 standard. In *2011 4th Joint IFIP Wireless and Mobile Networking Conference (WMNC)*, pages 1–6, October 2011.

[243] S. Ullah and K.S. Kwak. Throughput and delay limits of IEEE 802.15.6. In *2011 IEEE Wireless Communications and Networking Conference (WCNC)*, pages 174–178, March 2011.

[244] S. Ullah, M. Chen, and K.S. Kwak. Throughput and Delay Analysis of IEEE 802.15.6-based CSMA/CA Protocol. *Journal of Medical Systems*, 36:3875–3891, 2012.

[245] C. Tachtatzis, F. Di Franco, D.C. Tracey, N.F. Timmons, and J. Morrison. An energy analysis of IEEE 802.15.6 scheduled access modes. In *2010 IEEE GLOBECOM Workshops*, pages 1270–1275, December 2010.

[246] S. Rashwand, J. Misic, and H. Khazaei. IEEE 802.15.6 under saturation: Some problems to be expected. *Journal of Communications and Networks*, 13(2):142–148, April 2011.

[247] B.H. Jung, R.U. Akbar, and D.K. Sung. Throughput, Energy Consumption, and Energy Efficiency of IEEE 802.15.6 Body Area Network (BAN) MAC Protocol. In *2012 IEEE 23nd International Symposium on Personal Indoor and Mobile Radio Communications (PIMRC)*, pages 600–605, September 2012.

[248] F. Martelli, C. Buratti, and R. Verdone. On the performance of an IEEE 802.15.6 Wireless Body Area Network. In *11th European Wireless Conference 2011 - Sustainable Wireless Technologies (EW)*, pages 1–6, 2011.

[249] E. Ben Hamida, G. Chelius, and J.M. Gorce. Impact of the Physical Layer Modeling on the Accuracy and Scalability of Wireless Network Simulation. *Simulation*, 85(9):574–588, September 2009.

[250] S. Rashwand, J. Misic, and V. Misic. MAC performance modeling of IEEE 802.15.6-based WBANs over Rician-faded channels. In *2012 IEEE International Conference on Communications (ICC)*, pages 5462–5467, 2012.

[251] M. Maman, F. Dehmas, R. D'Errico, and L. Ouvry. Evaluating a TDMA MAC for body area networks using a space-time dependent channel model. In *2009 IEEE 20th International Symposium on Personal, Indoor and Mobile Radio Communications*, pages 2101–2105, 2009.

[252] E. Ben Hamida, M. Maman, B. Denis, and L. Ouvry. Localization performance in Wireless Body Sensor Networks with beacon enabled MAC and space-time

dependent channel model. In *2010 IEEE 21st International Symposium on Personal, Indoor and Mobile Radio Communications Workshops (PIMRC Workshops)*, pages 128–133, 2010.

[253] L. Ouvry et al. BAN Upper Layers, Base Band and DSP Architecture Specification. WiserBAN Deliverable D4.1, September 2011.

[254] M. Goyal, S. Prakash, W. Xie, Y. Bashir, H. Hosseini, and A. Durresi. Evaluating the Impact of Signal to Noise Ratio on IEEE 802.15.4 PHY-Level Packet Loss Rate. In *13th International Conference on Network-Based Information Systems (NBiS)*, pages 279–284, September 2010.

[255] C. Gezer, C Buratti, and R. Verdone. Capture Effect in IEEE 802.15.4 Networks: Modelling and Experimentation. In *2010 IEEE International Symposium on Wireless Pervasive Computing (ISWCP)*, pages 204–209, May 2010.

[256] M. Maman, F. Dehmas, R. D'Errico, and L. Ouvry. Evaluating a TDMA MAC for body area networks using a space-time dependent channel model. In *2009 IEEE 20th International Symposium on Personal, Indoor and Mobile Radio Communications*, pages 2101–2105, September 2009.

[257] A. Alomainy, Y. Hao, Y. Yuan, and Y. Liu. Modelling and Characterisation of Radio Propagation from Wireless Implants at Different Frequencies. In *2006 The 9th European Conference on Wireless Technology*, pages 119–122, 2006.

[258] Texas Instruments. Website: http://www.ti.com/product/cc2530.

[259] O. Helgason, S.T. Kouyoumdjieva, and G. Karlsson. Does mobility matter? In *2010 Seventh International Conference on Wireless On-demand Network Systems and Services (WONS)*, pages 9–16, 2010.

[260] J. Lessmann and S. Lutters. An Integrated Node Behavior Model for Office Scenarios. In *2008 41st Annual Simulation Symposium (ANSS)*, pages 298–307, 2008.

[261] Qunwei Zheng, Xiaoyan Hong, and Jun Liu. An agenda based mobility model. In *2006 39th Annual Simulation Symposium*, pages 8 pp.–, 2006.

[262] M. Musolesi and C. Mascolo. A Community Based Mobility Model for Ad Hoc Network Research. In *Proceedings of the 2nd International Workshop on Multi-hop Ad Hoc Networks: From Theory to Reality*, REALMAN '06, pages 31–38, 2006.

[263] K. Wei, X. Liang, and K. Xu. A Survey of Social-Aware Routing Protocols in Delay Tolerant Networks: Applications, Taxonomy and Design-Related Issues. Number 99, pages 1–23, 2013.

[264] Ying Zhu, Bin Xu, Xinghua Shi, and Yu Wang. A Survey of Social-Based Routing in Delay Tolerant Networks: Positive and Negative Social Effects. *IEEE Communications Surveys Tutorials*, 15(1):387–401, 2013.

[265] R. Injong, S. Minsu, H. Seongik, L. Kyunghan, J.K. Seong, and C. Song. On the Levy-Walk Nature of Human Mobility. *IEEE/ACM Transactions on Networking*, 19(3):630–643, 2011.

[266] D. Brockmann, L. Hufnagel, and T. Geisel. The scaling laws of human travel. *Nature*, 439(7075):462–465, 2006.

[267] D. Karamshuk, C. Boldrini, M. Conti, and A. Passarella. Human mobility models for opportunistic networks. *IEEE Communications Magazine*, 49(12):157–165, 2011.

[268] B. Oztas, T. Kurt, and E. Anarim. A survey of social based mobility models for ad hoc networks. In *2011 2nd International Conference on Wireless Communication, Vehicular Technology, Information Theory and Aerospace Electronic Systems Technology (Wireless VITAE)*, pages 1–5, 2011.

[269] Tai Suk Kim, Jae Kyun Kwon, and Dan Keun Sung. Mobility modeling and traffic analysis in three-dimensional high-rise building environments. *IEEE Transactions on Vehicular Technology*, 49(5):1633–1640, 2000.

[270] C. Papageorgiou, K. Birkos, T. Dagiuklas, and S. Kotsopoulos. An obstacle-aware human mobility model for ad hoc networks. In *2009 IEEE International Symposium on Modeling, Analysis Simulation of Computer and Telecommunication Systems (MASCOTS)*, pages 1–9, 2009.

[271] G. Lu, G. Manson, and D. Belis. Mobility modeling in mobile ad hoc networks with environment-aware. *Journal of Networks*, 1(1):54–63, 2006.

[272] A. Jardosh, E.M. Belding-Royer, K.C. Almeroth, and S. Suri. Towards Realistic Mobility Models for Mobile Ad Hoc Networks. In *Proceedings of the 9th Annual International Conference on Mobile Computing and Networking*, MobiCom '03, pages 217–229, 2003.

[273] A.P. Jardosh, E.M. Belding-Royer, K.C. Almeroth, and S. Suri. Real-world environment models for mobile network evaluation. *IEEE Journal on Selected Areas in Communications*, 23(3):622–632, 2005.

[274] C. Gustafson and F. Tufvesson. Characterization of 60 GHz shadowing by human bodies and simple phantoms. In *2012 6th European Conference on Antennas and Propagation (EUCAP)*, pages 473–477, 2012.

[275] J. Kunisch and J. Pamp. Ultra-wideband double vertical knife-edge model for obstruction of a ray by a person. In *2008 IEEE International Conference on Ultra-Wideband (ICUWB)*, volume 2, pages 17–20, September 2008.

[276] Z. Zhaoyang, W. Honggang, W. Chonggang, and F. Hua. Interference Mitigation for Cyber-Physical Wireless Body Area Network System Using Social Networks. *IEEE Transactions on Emerging Topics in Computing*, 1(1):121–132, 2013.

[277] Shih Heng Cheng and Ching Yao Huang. Coloring-Based Inter-WBAN Scheduling for Mobile Wireless Body Area Networks. *IEEE Transactions on Parallel and Distributed Systems*, 24(2):250–259, 2013.

[278] V. Gabale, B. Raman, P. Dutta, S. Kalyanraman, B. Raman, P. Dutta, and S. Kalyanraman. A Classification Framework for Scheduling Algorithms in Wireless Mesh Networks. *IEEE Communications Surveys Tutorials*, 15(1):199–222, 2013.

[279] A. Asadi and V. Mancuso. A Survey on Opportunistic Scheduling in Wireless Communications. *IEEE Communications Surveys Tutorials*, 15(4):1671–1688, 2013.

[280] H. Fattah and C. Leung. An overview of scheduling algorithms in wireless multimedia networks. *IEEE Wireless Communications*, 9(5):76–83, 2002.

[281] K. Seungku, K. Seokhwan, K. Jin-Woo, and E. Doo-Seop. Flexible beacon scheduling scheme for interference mitigation in body sensor networks. In *2012 9th Annual IEEE Communications Society Conference on Sensor, Mesh and Ad Hoc Communications and Networks (SECON)*, pages 157–164, 2012.

[282] F. Gengfa, E. Dutkiewicz, Yu Kegen, R. Vesilo, and Yu Yiwei. Distributed Inter-Network Interference Coordination for Wireless Body Area Networks. In

2010 IEEE Global Telecommunications Conference (GLOBECOM), pages 1–5, 2010.

[283] R. Kazemi, R. Vesilo, E. Dutkiewicz, and F. Gengfa. Inter-network interference mitigation in Wireless Body Area Networks using power control games. In *2010 International Symposium on Communications and Information Technologies (ISCIT)*, pages 81–86, 2010.

[284] M. Maman, A. Di Paolo, R. Rosini, and R. D'Errico. Dynamic management of cooperative communications in Body Area Networks. In *2012 Future Network Mobile Summit (FutureNetw)*, July 2012.

Publications and Awards

Besides WiserBAN (see Sec.), this Ph.D. activity was performed in the framework of the COST Actions 2100 (Pervasive Mobile and Ambient Wireless Communications) and IC1004 (Cooperative Radio Communications for Green Smart Environments).

The work described in this thesis has led to the following publications to Journals:

- R.Rosini, R.D'Errico, R.Verdone; "Body-to-Body Indoor Channel Modelling at 2.45 GHz"; Submitted for review to *"IEEE Transaction on Antenna and Propagation"*; August 2013.

- R.Cavallari, F.Martelli, R.Rosini, C.Buratti, R.Verdone; "A Survey on Wireless Body Area Networks: Technologies and Design Challenges"; *"IEEE Communications Surveys and Tutorials"*; March 2014.

and to the following papers presented to International Conferences, some of them describing the results obtained through fruitful collaboration with the Technical University of Lisbon (IST/INOV-INESC) [16], the ICTEAM - Universitè Catholique de Louvain (UCL) [163] and other research groups at CEA-Leti Grenoble [284]:

- O.P.Pasquero, R.Rosini, R.D'Errico, C.Oestges; "On-Body Channel Correlation in Various Walking Scenarios"; Accepted to *European Conference on Antennas and Propagation (EuCAP) 2014, The Hague (NL)*; October 2014 [also TD(13)07021 presented at the VII Management Committee Meeting of Cost IC1004, Ilmenau (D), May 2013].

- R.Rosini, R.D'Errico; "Space-Time Correlation for On-to-Off Body Channels at 2.45 GHz"; *European Conference on Antennas and Propagation (EuCAP) 2013, Gotheborg (S)*; April 2013 [also TD(13)06061 presented at the VI Management Committee Meeting of Cost IC1004, Malaga (E), February 2013].

- M.Mackowiak, R.Rosini, R.D'Errico, L.M.Correia; "Comparing Off-Body Dynamic Channel Model with Real-Time Measurements"; *7th International Symposium on Medical Information and Communication Technology (ISMICT) 2013, Tokyo (J)*; March 2013.

- R.Rosini, R.D'Errico; "Comparing On-Body Dynamic Channels for Two Antenna Designs"; *Loughborough Antenna and Propagation Conference (LAPC) 2012, Loughborough (UK)*; November 2012 [also TD(12)05081 presented at the V Management Committee Meeting of Cost IC1004, Bristol (UK), September 2012].

- R.Rosini, R.D'Errico, R.Verdone; "Body-to-Body Communications: a Measurement-based Channel Model at 2.45 GHz"; *IEEE International Symposium on Personal, Indoor and Mobile Radio Communications (PIMRC) 2012, Sydney (AUS)*; September 2012 [also TD(12)04026 presented at the IV Management Committee Meeting of Cost IC1004, Lyon (F), May 2012].

- M.Maman, A.Di Paolo, R.Rosini, R.Verdone, R.D'Errico; "Dynamic management of cooperative mechanisms in on-body area networks"; *Future Network & Mobile Summit (FuNeMs) 2013, Berlino (D)*; July 2012 [also TD(11)02071 presented at the II Management Committee Meeting of Cost IC1004, Lisbon (P), October 2011].

- R.Rosini, F.Martelli, M.Maman, R.D'Errico, C.Buratti, R.Verdone; "On-Body Area Networks: from Channel Measurements to MAC Layer Performance Evaluation"; *European Wireless 2012, Poznan (PL)*; April 2012 also TD(12)03060 presented at the III Management Committee Meeting of Cost IC1004, Barcelona (E), February 2012].

- R.Rosini, R.D'Errico; "Off-Body Channel Modelling at 2.45 GHz for Two Different Antennas"; *European Conference on Antennas and Propagation (EuCAP) 2012, Praga (CZ)*; March 2012 [also TD(11)02043 presented at the II Management Committee Meeting of Cost IC1004, Lisbon (P), October 2011].

- C.Buratti, R.D'Errico, M.Maman, F.Martelli, R.Rosini, R.Verdone, S.Huettinger; "Design of a Body Area Network for Medical Applications: the WiserBAN Project"; *ACM ISABEL 2011, Barcellona (E)*; October 2011.

- R.D'Errico, R.Rosini, M.Maman; "A Performance Evaluation of Cooperative Schemes for On-Body Area Networks based on Measured Time-variant Channels"; *IEEE International Conference on Communications (ICC) 25011, Kyoto (J)*; June 2011 [also TD(10)11083 presented at the XI Management Committee Meeting of Cost 2100, Aalborg (DK), May 2010].

Other Temporary Documents (TD) presented at COST Action IC1004 Meetings follow:

- R.Rosini, R.Verdone, R.D'Errico; "Body Shadowing in Body-to-Body Indoor Channel Model"; TD(13)08055 presented at the VIII Management Committee Meeting of Cost IC1004, Ghent (B), September 2013.

- R.Rosini, R.D'Errico, R.Verdone; "A General Heuristic Approach for Channel Modeling in Body-Centric Communications"; TD(13)07044 presented at the VII Management Committee Meeting of Cost IC1004, Ilmenau (D), May 2013.

- R.Rosini, R.D'Errico, R.Verdone; "A General Heuristic Approach for Channel Modeling in Body-Centric Communications"; TD(13)07044 presented at the VII Management Committee Meeting of Cost IC1004, Ilmenau (D), May 2013.

- R.Rosini, F.Martelli, M.Maman, R.D'Errico, R.Verdone; "Radio Channel Requirements for BAN Performance Evaluation"; TD(12)03063 presented at the III Management Committee Meeting of Cost IC1004, Barcelona (E), February 2012.

Paper [11] was awarded with the *"Best Student Paper Award"* at the Loughborough Antenna and Propagation Conference (LAPC) in November 2012, while paper [10] deserved the assigning of a *"Student Travel Grant"* to the IEEE International Symposium on Personal, Indoor and Mobile Radio Communications (PIMRC) in September 2012.

As for the WiserBAN project, contributions to the following deliverables were given:

- D1.1 – "Report about WiserBAN platform applications", edited by Jean-Francois Debroux, November 2010.
- D3.1 – "Final report on the antenna-human body interactions, around-the-body propagation", edited by Raffaele D'Errico, October 2011.
- D4.2 – "Characterization and Validation of the first Base-Band version", edited by Laurent Ouvry, February 2012.

Acknowledgements

"Dove sono gli amici, là sono le ricchezze." [Plauto]

Molto oltre le formalità di rito, la mia riconoscenza ed il mio grazie più sincero vanno ai miei supervisori, Prof. Roberto Verdone ed Dr. Raffaele D'Errico. Con stili, tempi e modalità molto diverse tra loro, entrambi avete saputo essere guide di un cammino che non sempre è stato facile, e che spesso ha messo in luce le mie fragilità. Quella che vedo come la mia crescita professionale dipende largamente dal tempo e dal sostegno che mi avete dato, mostrandomi come la passione e la dedizione per il proprio lavoro vengano sempre ripagati dalla stima e dalla fiducia dei propri collaboratori.

Un ringraziamento sentito ai revisori di questa tesi, Dr. Simon Cotton e Prof. Jean-Marie Gorce, i cui commenti precisi e attenti hanno contribuito a migliorare questo lavoro e ad aprire nuovi spunti di riflessione e di studio.

Andrea, Chiara, Danilo, Riccardo, Stefan; il suono delle risate che spesso si sentono uscire dalla porta del nostro laboratorio non hanno riempito solo i corridoi del dipartimento, ma anche le mie malinconie e le mie difficoltà al rientro da Grenoble. Chi con la sua risata contagiosa, chi con la sua discreta ma attenta presenza, chi con la sua straripante simpatia e "bellezza", chi con la sua caustica ironia, chi con la sua curiosità e attenzione; tutti avete reso l'ambiente di lavoro un posto dove si incontrano non solo dei colleghi, ma anche degli amici. Flavia, un grazie speciale va anche a te, da compagne di scrivania ad amiche il salto è stato breve, ma non scontato. Grazie per le chiacchere, i viaggi e le serate da adolescenti, e per aver condiviso con me un percorso ben più bello del solo dottorato.

Grazie anche a Silvia, una delle persone più dirette e sincere che conosca. Nonostante i pochi mesi di lavoro assieme, la tua presenza è stata molto più che un semplice aiuto per districarsi nei meandri della burocrazia universitaria. Tanti altri volti sono passati dalle scrivanie del DEI(S): Giorgia, Raffa, Cengiz, Davide, Gaia, Anto, Francesca; il mio grazie è anche per voi.

Grazie anche a tutti i colleghi del CEA, in particolare Mickael, per aver accolto l'ennesima stagista italiana con la voce acuta e strillante, e per averle fatto trovare un posto in cui crescere non solo professionalmente.

Vale, eccoti ancora qui tra le righe dei miei ringraziamenti, come qualche anno fa eri tra quelli della mia tesi. Sono sicura che ti ritroverò anche tra quelle che fra quarant'anni daranno vita ai racconti che faremo ai nostri nipotini. Magari gli racconteremo dei primi anni di unversità, degli esami fatti assieme, delle ansie e delle gioie, delle lacrime e dei sorrisi, delle cose belle delle vita, ma anche di quelle che ci hanno fatto soffrire e che comunque siamo riuscite a condividere. Magari gli racconteremo tutte queste cose sedute nel giardino di una casina da mare, in un pomeriggio assolato di agosto.

Alice, Carlo, Chiara, Clio, Conni, Cus, Gan, Giada, Giò, Giova, Kawtar, Lia, Lorenzo, Radek, Ricky, Vera, insomma la mia famiglia d'oltralpe. Ogni volta che torno a Grenoble è sempre come ritrovare un po' di casa. Non la casa in cui nasci e cresci, ma quella in cui ti trovi forse un po' per caso e che poi cresce con te. Grenoble per me ha significato tanto, e voi con lei. Grazie.

Le mie cocche, Fra & Paro, grazie perchè ci siete, perchè chiaccherare con voi dal "nostro" Marretti è proprio bello, perchè dopo pi di dieci anni che ci conosciamo c'è sempre qualcosa per cui mi capita di pensare: "Questa devo proprio dirla alle mie cocche!". Perchè con voi è sempre facile ridere di noi.

Doc, quanta strada da quel pomeriggio giocando a pallavolo, quando sei diventato "caustica" (almeno sulla rubrica telefonica!) Che pazienza che ci vuole con me, e per fortuna che tu ne hai tanta. Grazie per questo, e perchè hai sempre l'orecchio attento ed il cuore grande, come solo i veri amici hanno.

Ale, l'amica dei viaggi e delle birre (le tue), quella che sa guidare mentre io so parcheggiare, quella che c'è e che ci sarà, quella che mi affiderà una parte importante di sè. Grazie, perchè hai sempre avuto fiducia in me. E con te ci sono anche gli altri amici di sempre: Laura, Massimo, Monica, Mirko, Rita, senza scordare Zuccherino. Quelli che nonostante i tanti chilometri di distanza sono sempre stati lí, magari dall'altro

capo del telefono, ma comunque presenti. Il mio grazie è per la presenza e la pazienza, e perchè mi ricordate sempre che la vera amicizia va oltre la vicinanza.

Grazie ai tanti compagni di viaggio, e non solo metaforico. Grazie ai ragazzi del team che conta, ed alle ragazze di un altro team che mi hanno accolto con un pallone da basket in mano! Grazie ai miei coinquilini: Chiara, Michele e Riccardo. Abitare con me in questi mesi non deve essere stato divertente, ma per fortuna che ci pensano gli Osti's! Un aphoyo matek al "gruppo africano", e chi a Gulu ancora c'è rimasto. E a "carincretino", perchè ho amato.

Ciao Marta, più di un pensiero tra queste pagine è per te. Non scorderò mai la nostra ultima chiacchereta al telefono.

Il mio ultimo grazie è per mamma e papà, senza i quali questi ringarziamenti non avrebbero senso. Grazie perchè mi avete lasciato seguire le mie passioni, anche se non le condividevate. Grazie perchè avete sempre rispettato le mie decisioni, anche se non eravate d'accordo. Grazie perchè mi avete dato la possibilità di inseguire i miei sogni, anche se non erano i vostri. Grazie perchè mi avete insegnato che amare significa lasciare liberi, ed io mi sono sempre sentita libera. Vi voglio bene. Grazie.